Characterization of pathogenic immune mechanisms in oligoarticular juvenile idiopathic arthritis applying single-cell transcriptomics and proteomics

Mireia López Corbeto

Universitat Autònoma de Barcelona

Doctoral Thesis

Characterization of pathogenic immune mechanisms in oligoarticular juvenile idiopathic arthritis applying single-cell transcriptomics and proteomics

Doctoral thesis presented by Mireia López Corbeto

Directors of the Doctoral Thesis

Prof. Sara Marsal Barril, MD PhD

Antonio Julià Cano, PhD

Tutor of the Doctoral Thesis

Prof. Albert Selva O'Callahan, MD PhD

Doctoral Program in Medicine, Department of Medicine

Universitat Autònoma de Barcelona

Barcelona, 2023

Acknowledgments

Completing this dissertation represents the culmination of an intensive predoctoral period and marks the beginning of a new phase in my career.
I am grateful to have had the opportunity to undertake this project, and I recognize that it would not have been possible without the support and trust of a large group of people. I dedicate this work to them as a well-deserved tribute.

I am deeply grateful to my supervisor, Prof. Sara Marsal, for her invaluable guidance, encouragement, and constant support throughout my doctoral studies. From the very beginning of my journey in rheumatology, Prof. Marsal has placed her trust in me, pushing me to provide the best possible care for our patients and challenging me to continuously improve. Her unwavering dedication to the field and her humanistic approach have inspired me, shaping my professional values and guiding my career trajectory. It has been an honor to have her as my mentor, and I am grateful for the opportunity to learn from her and to work alongside her.

I sincerely appreciate my supervisor, Dr. Toni Julià, whose knowledge, insightful feedback, and support in this research. I am deeply grateful for his dedication to guiding me throughout this project. Dr. Julià's remarkable patience and trust in me have motivated me, and it has been a privilege to learn from him.

Many thanks to Dr. Guillen for her invaluable and generous help throughout the project. Her attention and support in carrying out the difficult task of bioinformatics and many hours dedicated to this project have been essential.

I would like to thank the IMID Biobank team, Dr. Núria Palau and Dr. Raül Tortosa, who taught me how to process the samples. Without the rigor of their work, this project would not have been possible.

Also, many thanks to the Centre Nacional d'Analàsi Genòmic (CNAG) team, led by Dr. Holger Heyn, and Laura Jiménez involved in the scRNA-seq step of the project. Their expertise has been essential in ensuring the success of this project.

I would also like to thank Dr. Michael Liu for all the help he has given me in fine-tuning the CyTOF technique and the many hours of work this has entailed.

I sincerely thank all the members of the Rheumatology Department, past and present, for their contributions, support, and cherished friendship.

In particular, I would like to express my deep appreciation to Dr. Estefanía Moreno and Dr. Laia Martínez for being incredible team members who have consistently gone above and beyond in their contributions to this project.

I would also like to extend my thanks to Dr. Maria Lopez and Dr. Andrea Pluma for their moral support and encouragement throughout this doctoral thesis.

To Elena Granell, for her tireless efforts in coordinating the logistics and providing her support at every step of the way.

My deepest gratitude is to the patients and their families participating in this project. Thier willingness to collaborate has been invaluable and has contributed greatly to the success of this project. Their are the driving force that makes us work and for which I want to improve every day.

Finally, I would like to express my deep appreciation to my family and friends for their love, encouragement, and understanding. Your support has been a constant source of motivation throughout my PhD.

Abbreviations

ACR	American College of Rheumatology
ADA	Adenosine Deaminase
ADGRG1	Adhesion G protein-coupled receptor G1
AES	Acción Estratégica en Salud
AHA	Anti-Histone Antibodies
ANA	Antinuclear Antibodies
ANG	Angiogenin
ANGPT2	Angiopoietin 2
APCA	Anti-Citrullinated Protein Antibodies
APCs	Activated Antigen-Presenting Cells
ARG1	Arginase 1
ARTN	Artemin
B2M	Beta-2-Microglobulin
bDMARDs	Biological Disease-Modifying Antirheumatic Drugs
C2	Complement component 2
CARRA	Childhood Arthritis and Rheumatology Research Alliance
CASP8	Caspase 8
cDMARDs	Conventional Disease-Modifying Antirheumatic Drugs
CCA17	C-C Motif Chemokine Ligand 17
CCA18	C-C Motif Chemokine Ligand 18
CD6	Cluster of Differentiation 6
CD70	Cluster of Differentiation 70
CCL3	Chemokine C-C motif Ligand 3
CCL4	C-C Motif Chemokine Ligand 4
CCL5	Chemokine C-C motif Ligand 5
CCL11	C-C Motif Chemokine Ligand 11
CCL17	C-C Motif Chemokine Ligand 17
CCL18	C-C Motif Chemokine Ligand 18
CCL20	C-C Motif Chemokine Ligand 20
CD6	Cluster of Differentiation 6
CD70	Cluster of Differentiation 70
CDR3	Complementary Determining Region 3
CFHR5	Complement Factor H-Related Protein 5
CLR	Centered Log Ratio
COMP	Cartilage Oligomeric Matrix Protein
CR2	Complement Receptor 2
CRP	C-Reactive Protein
CSUR	Centros, Servicios y Unidades de Referencia del Sistema Nacional de Salud
CTLA-4	Cytotoxic T-Lymphocyte Antigen 4
CXCL9	Chemokine C-X-C motif Ligand 9

CXCL13	C-X-C Motif Chemokine Ligand 13
CXCR6	C-X-C Motif Chemokine Receptor 6
DEA	Differential gene Expression Analysis
DPBS	Dulbecco's Phosphate Buffered Saline
EBV	Epstein-Barr Virus
EC	Endothelial Cells
ECR	Enhanced Centroid Ratio
ECV	Extracellular Vesicle
ELISA	Enzyme-Linked Immunosorbent Assay
ELS	Ectopic Lymphoid Structures
EMA	European Medicines Agency
ESR	Erythrocyte Sedimentation Rate
FcRn	Neonatal Fc Receptor
FOXP3	Forkhead Box P3
G6PI	Glucose-6-Phosphate Isomerase
GATA3	GATA Binding Protein 3
G-CSF	Granulocyte-Colony Stimulating Factor
GITR	Glucocorticoid-Induced TNFR Family Related Gene
HCs	Healthy Controls
HGF	Hepatocyte Growth Factor
HLA	Human Leukocyte Antigen
HRQoL	Health-Related Quality of Life
HTB	Human Tumor Biopsy
IBD	Inflammatory Bowel Disease
IF	Immunofluorescence
Ig	Immunoglobulin
IL-1	Interleukin-1
IL-1RA	Interleukin-1 Receptor Antagonist
IL-2	Interleukin-2
IL-4	Interleukin-4
IL-6	Interleukin-6
IL-7	Interleukin-7
IL-8	Interleukin-8
IL-10	Interleukin-10
IL-12	Interleukin-12
IL-13	Interleukin-13
IL-15	Interleukin-15
IL-17	Interleukin-17
IL-18	Interleukin-18
IL-21	Interleukin-21
IL-22	Interleukin-22
IL-23	Interleukin-23
IL-33	Interleukin-33
IL-37	Interleukin-37

IL-38	Interleukin-38
IFN	Interferon
IFN-γ	Interferon Gamma
IFNAR	Interferon Alpha/Beta Receptor
IFN-λ	Interferon Lambda
IGF-1	Insulin-Like Growth Factor 1
IgG	Immunoglobulin G
IgM	Immunoglobulin M
IR	Immunoreceptor
ITGA4	Integrin Subunit Alpha 4
ITGB7	Integrin Subunit Beta 7
JAK	Janus Kinase
JIA	Juvenile Idiopathic Arthritis
JNK	c-Jun N-Terminal Kinase
LFA-1	Lymphocyte Function-Associated Antigen 1
LPS	Lipopolysaccharide
MAPK	Mitogen-Activated Protein Kinase
MBL	Mannose-Binding Lectin
M-CSF	Macrophage-Colony Stimulating Factor
MFI	Mean Fluorescence Intensity
MHC	Major Histocompatibility Complex
MIF	Migration Inhibitory Factor
MMP	Matrix Metalloproteinase
MOG	Myelin Oligodendrocyte Glycoprotein
mRNA	Messenger RNA
MS	Multiple Sclerosis
MRI	Magnetic Resonance Imaging
mTOR	Mammalian Target of Rapamycin
NLRP3	NOD-Like Receptor Pyrin Domain Containing 3
NMO	Neuromyelitis Optica
OA	Osteoarthritis
OPG	Osteoprotegerin
PADI4	Peptidyl Arginine Deiminase 4
PBMCs	Peripheral Blood Mononuclear Cells
PD-1	Programmed Cell Death Protein 1
PD-L1	Programmed Death-Ligand 1
PDE4	Phosphodiesterase 4
PI3K	Phosphatidylinositol 3-Kinase
PTPN22	Protein Tyrosine Phosphatase Non-Receptor Type 22
RA	Rheumatoid Arthritis
RANK	Receptor Activator of Nuclear Factor Kappa-B
RANKL	Receptor Activator of Nuclear Factor Kappa-B Ligand
RF	Rheumatoid Factor
RISC	RNA-Induced Silencing Complex

ROS	Reactive Oxygen Species
SLE	Systemic Lupus Erythematosus
SNP	Single Nucleotide Polymorphism
SSc	Systemic Sclerosis
STAT	Signal Transducer and Activator of Transcription
TACI	Transmembrane Activator and Calcium-Modulating Cyclophilin Ligand Interactor
TCR	T Cell Receptor
TGF-β	Transforming Growth Factor Beta
Th	T Helper
TLR	Toll-Like Receptor
TNF	Tumor Necrosis Factor
TNFRSF	Tumor Necrosis Factor Receptor Superfamily
Treg	Regulatory T Cell
VCAM-1	Vascular Cell Adhesion Molecule 1
VEGF	Vascular Endothelial Growth Factor

Index

Abstract

Juvenile idiopathic arthritis (JIA) is a prevalent rheumatic disease in children, comprising seven distinct subtypes.

The most common subtype is oligoarticular JIA (oJIA), which accounts for 30-60% of all cases depending on the series studied. oJIA patients typically experience asymmetrical arthritis and have an elevated risk of developing uveitis (oJIA-U), a severe and unique phenotype rarely seen in adult arthritis. The main cells of the immune system that lead to synovial inflammation or uveitis production is not well understood. While studies on T cells in oJIA have mainly focused on $CD4^+$ T cells due to their strong association with major histocompatibility class II alleles, research on the role of $CD8^+$ T cells in oJIA has been limited. Although $CD8^+$ T cells have been described in the synovium of rheumatoid arthritis (RA) and have been implicated in germinal center formation, their role in oJIA remains understudied. In addition, the contribution of members of the innate immune system in the pathogenesis of oJIA is increasingly recognized.

To characterize which pathogenic cells of the immune system are involved in the development of oJIA, we performed scRNA-Seq and TCR sequencing analysis, examining 132,824 peripheral blood (PB) and synovial fluid (SF) mononuclear cells (MCs) from three patients with newly diagnosed oJIA. We also analyzed PBMCs from four patients with oJIA-U and four healthy controls (HCs) at the single-cell level. Using single-cell mRNA sequencing encapsulated in Chromium 10x Genomics beads (scRNA-seq), we elucidated different cellular clusters not previously identified in this entity, difference in abundance in different pathogenic cells in both oJIA and oJIA-U and determined the clonal architecture of alpha-/beta-paired T-cell receptor strands in SF and PB. After identification of the most significant cell types, a validation study was initiated on an independent dataset using mass cytometry with the CyTOF platform.
In a second stage, we characterized the proteomic profile of plasma from patients with newly diagnosed oJIA, oJIA-U, HCs, and individuals with other conditions related to treatment, disease activity, and diseases such as RA. We analyzed 235 proteins using the proximity extension assay (PEA).

Our findings revealed the presence of intermediate monocytes, regulatory T cells, activated $CD8^+$ T cells and $NKG2C^+$ effector memory $CD8^+$ T cells in the SF of oJIA patients, cells not expected in normal conditions. Conversely, these cell populations showed reduced levels in the PB of oJIA patients compared to controls. This observation suggests the active recruitment of these cell types from blood into the inflamed synovium of oJIA patients and their importance in the pathology. We observed significant transcriptional differences in activated effector memory $CD8^+$ T cells and $NKG2C^+$ effector memory $CD8^+$ T cells from FS and PB of oJIA patients compared to HCs, showing overexpression of CCL5, GMZA, GZMK, CXCL13, CXCR6, S100A6 and S100A11 genes.

In patients with oJIA-U, we observed a higher presence of circulating dendritic cells of types 1 and 4, as well as mature NK cells, compared to both oJIA patients without uveitis and healthy controls. At the transcriptional level, the more abundant cells in PB from oJIA-U patients showed a marked up-regulation of type I and III interferon signaling pathway and antigen processing and peptide antigen presentation through MHC class I. Specifically, $CD56^+$ dim mature NKs from patients with oJIA-U compared to patients without uveitis and HCs overexpress PRF1, FECR1G, CCL4 (MIP-1β), and B2M.

Analysis of plasma proteins by PEA assay revealed increased levels of crucial innate immune system proteins such as FGF-23, TRAIL, C2, IL-18R1 and IL-6 in oJIAs compared to HCs. Interestingly, elevated levels of GZH and MMP-1 were found in the most severe oJIA-U patients. The observed protein expression profile is consistent with the involvement of innate immune system cells such as NKs in oJIA-U or intermediate monocytes in oJIA. Patients on anti-TNF alpha therapy had increased levels of TNF alpha.

This study represents the first single-cell atlas of its kind and provide valuable insights into the cellular dynamics and potential cellular drivers in the context of oJIA and oJIA-U. The next steps of this research will be to validate the results obtained in this work using the CyTOF technique as well as to perform different in vitro assays that will characterize these pathogenic cells. Investigation of these cell populations may

contribute to a better understanding of the underlying mechanisms and, ultimately, to the improvement of therapeutic strategies for these conditions.

Resumen

La artritis idiopática juvenil (AIJ) es una enfermedad reumática prevalente en niños, que comprende siete subtipos distintos.

El subtipo más frecuente es la AIJ oligoarticular (AIJo), que representa entre el 30 y el 60% de todos los casos en función de las series estudiadas. Los pacientes con AIJo suelen presentar una artritis asimétrica y tienen un riesgo elevado de desarrollar uveítis (AIJo-U), un fenotipo grave y único que rara vez se observa en la artritis del adulto. No se conocen bien las principales células del sistema inmunitario que provocan la inflamación sinovial o la producción de uveítis. Mientras que los estudios sobre las células T en la AIJo se han centrado principalmente en las células T $CD4^+$ debido a su fuerte asociación con los alelos mayores de histocompatibilidad de clase II, la investigación sobre el papel de las células T $CD8^+$ en la oJIA ha sido limitada. Aunque las células T $CD8^+$ se han descrito en la sinovial de la artritis reumatoide (AR) y se han implicado en la formación de centros germinales, su papel en la oJIA sigue sin estudiarse. Además, cada vez se reconoce más la contribución de los miembros del sistema inmunitario innato en la patogénesis de la AIJo.

Para caracterizar qué células patógenas del sistema inmunitario están implicadas en el desarrollo de la oJIA, realizamos análisis de secuenciación de scRNA-Seq y TCR, examinando 132,824 células mononucleares (CM) de sangre periférica (SP) y líquido sinovial (LS) de tres pacientes con oJIA recién diagnosticada. También analizamos PBMC de cuatro pacientes con AIJo-U y cuatro controles sanos (CS) a nivel unicelular. Mediante la secuenciación de ARNm unicelular encapsulado en perlas Chromium 10x Genomics (scRNA-seq), dilucidamos diferentes agrupaciones celulares no identificadas previamente en esta entidad, diferencias en la abundancia en diferentes células patogénicas tanto en oJIA como en oJIA-U y determinamos la arquitectura clonal de las cadenas de receptores de células T alfa-/beta-pareadas en LS y SP. Tras la identificación de los tipos celulares más significativos, se inició un estudio de validación en un conjunto de datos independiente utilizando citometría de masas con la plataforma CyTOF.

En una segunda etapa, caracterizamos el perfil proteómico del plasma de pacientes con AIJo-U recién diagnosticada, AIJo-U, CS e individuos con otras afecciones relacionadas con el tratamiento, la actividad de la enfermedad y enfermedades como la AR. Analizamos 235 proteínas mediante el ensayo de extensión de proximidad (PEA).

Nuestros hallazgos revelaron la presencia de monocitos intermedios, células T reguladoras, células T $CD8^+$ activadas y células T $CD8^+$ de memoria efectoras $NKG2C^+$ en el LS de pacientes con AIJo, células no esperadas en el líquido sinovial en condiciones normales. Por el contrario, estas poblaciones celulares mostraron niveles reducidos en la SP de pacientes con AIJo en comparación con los controles. Esta observación sugiere el reclutamiento activo de estos tipos celulares desde la sangre a la sinovial inflamada de los pacientes con AIJo y su importancia en la patología. Se observaron diferencias transcripcionales significativas en las células T $CD8^+$ de memoria efectoras activadas y en las células T $CD8^+$ de memoria efectoras $NKG2C^+$ del LS y la SP de los pacientes con AIJo en comparación con los CS, mostrando una sobreexpresión de los genes CCL5, GMZA, GZMK, CXCL13, CXCR6, S100A6 y S100A11.

En los pacientes con AIJo-U, observamos una mayor presencia de células dendríticas circulantes de los tipos 1 y 4, así como de células NK maduras, en comparación tanto con los pacientes con AIJo sin uveítis como con los controles sanos. A nivel transcripcional, las células más abundantes en la SP de los pacientes con AIJo-U mostraron una marcada regulación al alza de la vía de señalización del interferón de tipo I y III y del procesamiento de antígenos y presentación de antígenos peptídicos a través del MHC de clase I. En concreto, las NK maduras $CD56^+$ dim de los pacientes con AIJo-U en comparación con los pacientes sin uveítis y los CS sobreexpresan PRF1, FECR1G, CCL4 (MIP-1β) y B2M.

El análisis de las proteínas plasmáticas mediante el ensayo PEA reveló un aumento de los niveles de proteínas cruciales del sistema inmunitario innato como FGF-23, TRAIL, C2, IL-18R1 e IL-6 en los AIJo en comparación con los CS. Se encontraron niveles elevados de GZMH y MMP-1 en los pacientes con AIJo-U más graves. El perfil de expresión proteica observado es coherente con la implicación de células del

sistema inmunitario innato, como las NK en la AIJo-U o los monocitos intermedios en la AIJo. Los pacientes en tratamiento con anti-TNF alfa presentaban mayores niveles de TNF alfa.

Este estudio representa el primer atlas unicelular de este tipo y proporciona información valiosa sobre la dinámica celular y los posibles impulsores celulares en el contexto de la AIJo y la AIJo-U. Los próximos pasos de esta investigación serán validar los resultados obtenidos en este trabajo mediante la técnica CyTOF, así como realizar diferentes ensayos in vitro que caractericen estas células patógenas. La investigación de estas poblaciones celulares puede contribuir a una mejor comprensión de los mecanismos subyacentes y, en última instancia, a la mejora de las estrategias terapéuticas para estas afecciones.

1. Introduction

1.1. Juvenile idiopathic arthritis

1.1.1. Concept and epidemiology

Juvenile idiopathic arthritis (JIA) represents a heterogeneous group of autoimmune diseases, and it is the most prevalent chronic rheumatic condition in childhood. As in other chronic diseases, confronting JIA involves physical, social, emotional, and psychological challenges for the child and the family [1].

JIA was defined by the International League of Associations for Rheumatology (ILAR) at the Edmonton conference in 2001 as an arthritis of unknown etiology with onset before the age of 16, with more than 6 weeks of evolution, and which requires ruling out other possible causes before making this diagnosis [2]. Nevertheless, an experienced clinician can establish the diagnosis in the first weeks of disease without applying many diagnostic techniques to exclude other etiologies.

The incidence and prevalence of JIA have been estimated in different settings.
In developed countries, the annual incidence rate for all forms of JIA varies from 1.6 to 23/100,000 children, and the prevalence ranges from 3.8 to 400/100,000 children [3]. A study performed between 2004 and 2006 in Catalonia, and the only epidemiological study carried out in southern Europe, estimated an incidence rate of 6.9 and a prevalence rate of 39.2/100,000 children <16 years [4].

The incidence and prevalence of the different ILAR categories are unequal among the population. The most common JIA category is oligoarthritis (oJIA), with an annual estimated pooled incidence and prevalence of 3.7 and 17 cases per 100,000 children, respectively. Less common JIA categories include systemic JIA (sJIA), enthesitis-related arthritis (ERA), and psoriatic arthritis (PsA), with pooled annual incidences of 0.6, 2.0, and 0.5 cases per 100,000 children, respectively [3].

Studies have shown a biphasic peak in age at onset in some categories, including peaks in children from 2–4 years of age in oligoarthritis, psoriatic JIA, and RF-negative

JIA [5]. JIA is more common in females than in males (ratio 2:1), although the distribution varies across the ILAR categories [3]. Systemic JIA is thought to occur equally in both genders, whereas ERA and psoriatic JIA are more common in males than in females [3].

The socio-economic impact of direct healthcare costs of the disease in European countries has been estimated at around 11,068 to 22,138 € per patient/year, between 7,837 to 14,155 € per patient/year of non-healthcare costs [6].

1.1.2. Current classification and future perspective

Under the umbrella of JIA, the current ILAR classification identifies seven categories defined based on the clinical presentation within 6 months of developing signs and symptoms of JIA [2]. All categories are mutually exclusive, and each subtype has a list of common inclusion and exclusion criteria.

Table 1. ILAR Classification and category definition.

Systemic juvenile idiopathic arthritis
Enthesitis-related arthritis
Rheumatoid factor-positive polyarthritis
Rheumatoid factor-negative polyarthritis
Psoriatic arthritis
Oligoarthritis - Persistent oligoarthritis - Extended oligoarthritis
Undifferentiated arthritis

Adapted from [7].

In each category, any of the clinical or laboratory characteristics that will later be used as exclusion criteria can be present and are presented below [1]:

a. Psoriasis or a history of psoriasis in the patient or first-degree relative
b. Arthritis in an HLA-B27 positive male beginning after the sixth birthday
c. Ankylosing spondylitis, enthesitis-related arthritis, sacroiliitis with inflammatory bowel disease, Reiter syndrome or acute anterior uveitis, or a history of one of these disorders in a first-degree relative
d. The presence of IgM rheumatoid factor on at least two occasions at least 3 months apart
e. The presence of systemic juvenile idiopathic arthritis in the patient

The inclusion and exclusion criteria for each category are set out as follows:

- **Systemic JIA.** Arthritis in one or more joints with fever or preceded by fever for at least 2 weeks that is documented to be daily for at least 3 days and accompanied by one or more of the following: evanescent erythematous rash, generalized lymph node enlargement, hepatomegaly and/or splenomegaly, serositis. Exclusions: a, b, c, d.

- **Enthesitis-related arthritis.** Arthritis and enthesitis, or arthritis or enthesitis with at least two of the following: a history of sacroiliac joint tenderness and/or inflammatory lumbosacral pain. The presence of HLA-B27 antigen, the onset of arthritis in a male >6 years of age, acute (symptomatic) anterior uveitis, history of ankylosing spondylitis, enthesitis-related arthritis, sacroiliitis with inflammatory bowel disease, Reiter syndrome, or acute anterior uveitis in a first-degree relative. Exclusions: a, d, e.

- **Rheumatoid factor-positive polyarthritis.** Arthritis that affects five or more joints during the first 6 months of disease; two or more positive tests for rheumatoid factor at least 3 months apart during the first 6 months of disease. Exclusions: a, b, c, e.

- **Rheumatoid factor-negative polyarthritis.** Arthritis that affects five or more joints during the first 6 months of disease; test for rheumatoid factor is negative.

Exclusions: a, b, c, d, e.

- **Psoriatic arthritis.** Arthritis and psoriasis or arthritis, and at least two of the following: dactylitis, nail pitting or onycholysis, and psoriasis in a first-degree relative. Exclusions: b, c, d, e.

- **Oligoarthritis.** Arthritis affects one to four joints during the first 6 months of the disease; two subcategories are recognized.
  • Persistent oligoarthritis: affecting not more than four joints throughout the disease course.
  • Extended oligoarthritis: affecting more than four joints after the first 6 months of disease.
  Exclusions: a, b, c, d, e.

- **Undifferentiated arthritis.** Arthritis fulfills criteria in no category or two or more of the other categories.

The ILAR classification has led to a series of advances in the knowledge of JIA, facilitating understanding among clinicians worldwide. It has also helped to support the development of research organizations specialized in pediatric rheumatology, such as the Paediatric Rheumatology Collaborative Study Group (PRINTO) or the Childhood Arthritis and Rheumatology Research Alliance (CARRA), as well as organizations for parents of children with JIA. These organizations have collectively achieved funding for pediatric rheumatology research, moving forward into understanding JIA's pathogenic mechanisms. In addition, it has helped to emphasize the particularities of the children's joints, which are highly vulnerable to injury by systemic inflammation or the need to establish periodic screenings to rule out complications such as chronic uveitis [8].

However, several aspects of this classification have been challenged since the early 2000s, and many have been debated since basic research has progressed [9,10].
Firstly, the cut-off at the age of 16 years does not correspond to the legal divide between children and adults, which is in most countries at 18 years. This division in the classification system does not distinguish those JIA subtypes that

occur in children and adults from those that may be specifically for children, an important issue not just for the transition process from childhood to adult care, but also to speed up new drug approvals [11].
Indeed, if the disease is the same in children and adults, there will be no necessity to prove the efficacy of a new drug in children if it has been approved for its use in adults. Moreover, any other specialty has been found useful to distinguish a disease between adult or pediatric onset, understanding diseases or conditions as a continuum rather than compartmentalized.

Currently, huge efforts are aimed at revising the JIA classification to distinguish those forms of arthritis that overlap in children and adults from those unique to children [10]. In this regard, it has to be pointed out the presence of a juvenile-only form of arthritis, named oligoarthritis, which has no counterpart in adult-onset arthritis, with a higher positivity for anti-nuclear antibodies (ANA) and confers a higher risk of developing chronic anterior uveitis. PRINTO has proposed a form for the “early-onset ANA-positive JIA.” Nevertheless, there is still much research to be done as data supporting the existence of a unique form of arthritis are not yet conclusive [7,12].

From a practical point of view, the current classification has other difficulties, such as the complex defined inclusion and exclusion criteria described previously or the lack of up-to-date in the inclusion of anti-citrullinated protein antibodies (ACPA) in RF-positive JIA. Moreover, many patients with systemic JIA are excluded from this category at disease onset because they don’t present arthritis, even though with early treatment, some patients escape joint synovitis [13].

Other difficulties are related to oligoarticular JIA and its differentiation from polyarticular JIA. Establishing the cut-off point of 4 affected joints during the first 6 months of the onset of the disease can be complicated by the limitation in inter-examiner reproducibility or missing inflamed joints by not applying an imaging technique for evaluation [14]. Furthermore, the division between oligo and polyarticular JIA introduces the assumption that the number of joints reflects disease type rather than disease severity [9]. These limitations highlight the emerging need to rethink or re-study the current ILAR classification based on disease biology.

Currently, two models have been proposed that incorporate biological data into the definition of different subtypes: the PRINTO model and the four-cluster model (Figure 1) [15].

In December 2015, an international conference was convened by researchers at the PRINTO headquarters to reach a consensus on the new JIA classification criteria. The consensus panel proposed the following distinct 6 JIA categories: sJIA, RF-positive JIA, enthesitis/spondylitis-related JIA, early-onset ANA JIA, other JIA (fits the criteria for no definition), and unclassified JIA (fits the criteria for more than one definition). Psoriatic JIA was omitted because a consensus was not reached [10]. These definitions are still considered preliminary, and an ongoing project of a prospective cohort of 1,000 JIA patients evaluated at onset and at 4-time points since disease onset will provide great value information about different categories.

In a parallel effort, the four-cluster model has been proposed for arthritis in adults and children based on genetic risk loci shared between seropositive and seronegative arthritis [16]. This classification, which lacks inclusion and exclusion criteria, is represented by a Venn diagram, points out the overlap of some subtypes, and enhances the group of early-onset JIA inside the seronegative arthritis category. Strengths of the four-cluster model are its pathophysiological basis and the fact that it encompasses both children and adults, as it serves as a new way to classify arthritis globally.

Figure 1. The PRINTO model and the four-cluster model.

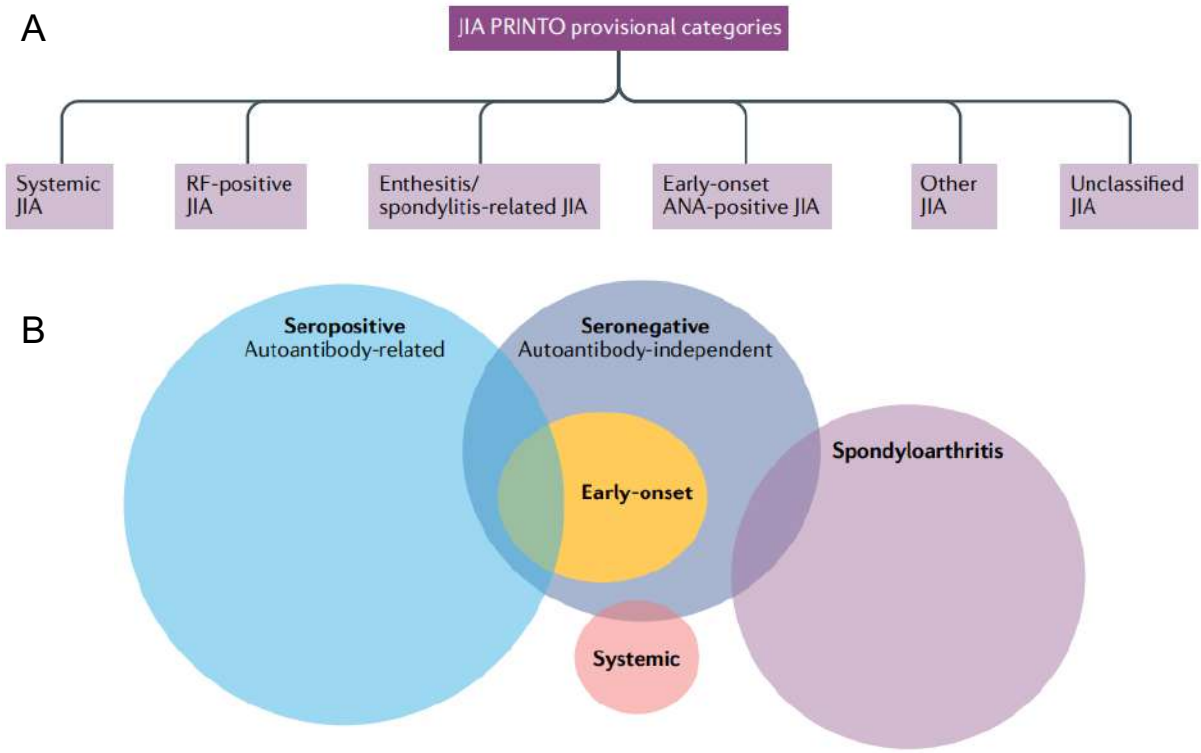

Extracted from [15]. A) The provisional Paediatric Rheumatology International Trials Organization (PRINTO) juvenile idiopathic arthritis categories for childhood-onset arthritis. B) The four-cluster model defining mechanistic subgroups within arthritis across the age spectrum.

1.1.3. Oligoarthritis: articular manifestations and uveitis

Oligoarticular JIA (oJIA) is the most common of the 7 subtypes of JIA, with an incidence of 3.5-8.4/100,000 children/year. In the epidemiological study conducted in Spain, oJIA accounted for 51% of all JIA cases [4]. After sJIA, oJIA is the second JIA regarding health care costs per patient, estimated at €12,000 per patient/year [6]. However, given its high prevalence, oJIA represents a much higher health expenditure, up to three times the cost of sJIA in public health systems such as the Spanish.

As mentioned above, this form is typical of children and does not occur in adults, and is characterized by asymmetric arthritis, early onset (before 6 years of age), and a female predilection [17]. The course is insidious and frequently affects the lower

extremities (knees and ankles), causing irreversible damage to the growth plate without treatment [18]. Acute-phase reactants are often normal or moderately increased, although in some instances, erythrocyte sedimentation rate (ESR) can be moderately high. ANAs are detected in substantial titers in about 70 - 80% of patients.

The ILAR classification distinguishes two categories in the oligoarthritis subtype: persistent oligoarthritis, in which the disease is confined to four or fewer joints, and extended oligoarthritis, in which arthritis extends to more than four joints after the first 6 months of disease. Up to 50% of oJIA children will develop an extended oligoarticular form throughout the evolution of the disease, and 30% will do so during the first two years [19]. However, ANA-positive patients belonging to these two categories have been reported to be homogeneous in several clinical features, including age at onset, sex ratio, asymmetry of joint involvement, and frequency of uveitis, suggesting that extended oligoarthritis is the same disease as persistent oligoarthritis [19].

One of the most significant complications associated with JIA is chronic anterior uveitis. JIA-associated uveitis (JIA-U) is manifested by inflammation of the iris and the ciliary body, and is, therefore, referred to as iritis or iridocyclitis [20]. Classification has been defined in terms of the anatomy and time course of the disease according to the Standardisation of Uveitis Nomenclature (SUN) International Working Group [21]. Uveitis may develop in the absence of active arthritis and the onset is frequently insidious, initially asymptomatic, and requires regular eye evaluations to establish an early diagnosis. Without prompt recognition and treatment, chronic JIA-U can lead to synechiae, band keratopathy, and, ultimately, blindness [22].

In patients already known to have JIA, estimates of the prevalence of uveitis range from 11 to 30%, and it is most frequently associated with oJIA and RF-negative polyarticular JIA [23,24]. A younger age, female gender, ANA, HLA-DRB1*11, HLA-DRB1*13 and HLA-B27 positivity are other risk factors apart from the JIA subtype related to JIA-U [23,25]. Uveitis may precede arthritis in 3 - 7% of children with JIA but it is more frequent to develop JIA-U during the disease [26].
A study of 52 children with JIA-U conducted in Atlanta, USA, found that 22% of children with JIA developed uveitis within the first year of JIA diagnosis [24]. Another study has

found that the mean time from the onset of JIA to the onset of JIA-U was 1.8 years [22]. In our experience, this manifestation should be carefully monitored over time.

1.1.4. Clinical outcome measures and monitoring

The objectives of the management of JIA are to ameliorate patient symptoms, improve health-related quality of life (HRQL) and prevent comorbidities. Numerous outcome measures have been developed and validated for use in JIA patients, including methods for scoring disease activity, therapeutic response, and questionnaires to address HRQL. Furthermore, recent interest has been focused on including parent and children-reported outcomes as they capture the perception of the disease state [27].

Regularly measuring disease activity levels is essential to monitor the disease course over time and allows the assessment of the efficacy of therapeutic regimens. Composite scores are suitable as unique items may be insufficient to evaluate a complex disease such as JIA.

1.1.4.1. Disease activity evaluation

To evaluate the clinical status of a patient with JIA, the variables that we must have noted down in each consultation to apply the activity indices are:

- Physician's global assessment of disease activity (PGA): measured on a 0-10 visual analog scale (VAS) where 0 = no activity and 10 = maximum activity.
- Parent global well-being assessment: measured on a 0-10 VAS where 0 = very well and 10 = very poor.
- Count of joints with active disease: the number of joints that on physical examination, are painful and/or swollen.
- Count of limited joints: the number of joints that in the physical examination have a smaller amplitude in their range of motion than the normal.
- Acute phase reactants: we measure ESR quantified in mm/hour and C-reactive protein (CRP) in mg/dl.

The Juvenile Arthritis Disease Activity Score (JADAS) was the first composite disease activity score developed for JIA and includes PGA, parent global assessment, ESR normalized to a 0 to 10 scale, and a count of joints with active disease [28]. Three different versions of the JADAS were developed, each one differing in the active joint count incorporated: JADAS 71, JADAS 10, and JADAS 27, being this last one a good surrogate for the whole joint count in JIA. It considers the cervical spine, elbows, wrists, metacarpophalangeal joints, proximal interphalangeal joints, hips, knees, and ankles [29].

The JADAS is calculated as the simple sum of the scores of its four components and is designed to follow the disease course of JIA over time. There have been established cutoff values for oJIA and polyarticular JIA that discriminate between inactive, low, moderate, and high disease activity (Table 2).

Table 2. JADAS 27 cutoffs for disease activity states for oligoarticular and polyarticular JIA.

	JADAS 27
Oligoarthritis	
Inactive disease	⩽1
Low disease activity	1.1 - 2
Moderate disease activity	2.1 - 4.2
High disease activity	> 4.2
Polyarthritis	
Inactive disease	⩽1
Low disease activity	1.1 - 3.8
Moderate disease activity	3.9 - 8.5
High disease activity	> 8.5

Adapted from [27].

A different approach to defining disease activity states based on the use of a core set of multiple criteria is Wallace's preliminary criteria for clinically inactive disease and remission in JIA developed in 2004 [30].

A patient is defined as having inactive disease if he or she has no joints with active disease, no systemic manifestations attributable to JIA, duration of morning stiffness less than 15 minutes, no active uveitis, normal levels of acute phase reactants and PGA of disease activity indicating no disease activity.

If all these criteria are met for six consecutive months while the patient is on treatment, the patient is in clinical remission with medication. If the patient is not receiving treatment, these criteria must be present for one year [31].

1.1.4.2. Ocular disease activity evaluation

Monitoring children with JIA for uveitis includes age-appropriate visual acuity testing, intraocular pressure measurement, and slit lamp examination. The diagnosis of uveitis is based on signs of inflammation in the slit-lamp examination, including cells and flare from protein leakage into the anterior chamber due to a breakdown in the blood-aqueous humor barrier [32].

Intraocular inflammation is graded according to the SUN criteria, which consider the number of cells in the anterior chamber, flare, vitreous cells, and vitreous haze or debris. SUN also provides definitions for improvement or worsening of the condition, being a score that is reproducible and helps to monitor JIA-U patients (Table 3) [21,33]. Follow-up must be performed regularly at intervals depending on the risk stratification defined by the JIA subtype, the positivity of ANA, and the time from the onset of JIA disease [34].

Table 3. Measures of activity for uveitis.

Grading scheme for anterior chamber cells	
0	< 1 cell in field
0.5+	1 - 5 cells in field
1+	6 - 15 cells in field
2+	16 - 25 cells in field
3+	25 - 50 cells in field
4+	> 50 cells in field
Grading scheme for anterior chamber flare	
0	None
1+	Faint
2+	Moderate
3+	Marked
4+	Intense
Activity of uveitis terminology	
Inactive	Grade 0 cells
Worsening activity	Two-step increase in the level of inflammation or increase from grade 3+ to grade 4+

Grading scheme for anterior chamber cells	
Improved activity	Two-step decrease in the level of inflammation or decrease to grade 0
Remission	Inactive disease for > 3 months after discontinuing all treatments for eye disease

Adapted from [21].

1.1.4.3. Response to treatment

As the number of treatments available for JIA has increased and their efficacy has improved, it has also become necessary to quantify the change in disease activity. In 1997, the American College of Rheumatology (ACR) developed a core set of outcomes for JIA consisting of PGA, parent/patient global assessment, functional ability, number of joints with active arthritis, number of joints with limitation of movement, and ESR [35].

An ACR Pedi 30 response is at least a 30% improvement from baseline in three of six variables with no more than one remaining variable worsening by >30%.

These criteria are accepted by both the US Food and Drug Administration and the European Medicines Agency for all phase III trials in JIA seeking drug registration [36]. Although they have not been formally validated, other pediatric ACR indices such as the ACR Pedi 20, 50, 70, and 90 have also been used to evaluate the clinical response in JIA in clinical trials. The JADAS index adequately discriminates between the ACR Pedi 30, 50, and 70 response rates [37].

For JIA-associated uveitis, effective treatment aims to achieve 0 cells in the anterior chamber evaluation of both eyes [33].

Some scientific societies, including ours, have developed practical management algorithms for systematized control and treatment strategies according to clinical characteristics and disease severity in children with JIA-related uveitis [34].

1.1.5. Treatment

The treatment of patients with JIA needs to be multidisciplinary. The team must be confirmed by pediatric rheumatologists, ophthalmologists, nurses, therapists, and psychologists, with the patient and her/his family maximum implication.

The development of new treatments has improved dramatically since the early 2000s with the approval of the first biological disease-modifying antirheumatic drugs (bDMARDs), first investigated in randomized control trials on adults, and the implementation of specific legislation for the development of pediatric medicines in the European Union and the United States.

Furthermore, two large international not-for-profit networks, the Pediatric Rheumatology Collaborative Study Group (PRCSG) and the PRINTO have helped to conduct these clinical trials in pediatric rheumatic patients [36].

1.1.5.1. Pharmacological treatment

The classic JIA therapeutic approach has been based on a step-up strategy considering the JIA subtype and the level of disease activity.
However, in recent years, the paradigm of starting treatment has changed to apply a faster and better control of disease activity by adjusting pharmacological drugs in a treat-to-target approach (T2T) instead of a step-up strategy (Figure 2).

In the first instance, the pharmacological armamentarium involves the use of non-steroidal anti-inflammatory drugs (NSAIDs) mainly for pain control and glucocorticosteroids (GC) for controlling systemic inflammation or polyarticular forms. GC injections, preferably triamcinolone hexacetonide, are particularly useful in oJIA [38].

Children with oligo or polyarticular courses who do not respond to NSAIDs or GC should promptly start conventional disease-modifying antirheumatic drugs (cDMARDs) such as methotrexate (MTX), leflunomide, or sulfasalazine.

Methotrexate is the first drug of choice for patients with oligo and polyarticular JIA when a second-line treatment is needed. It is normally well tolerated and has been extensively studied with folic acid to avoid side effects such as nausea or mild transaminase elevation [39].

However, data suggests that approximately 30-50% of patients do not respond to conventional disease-modifying antirheumatic drugs (cDMARDs). In such cases, the utilization of biological DMARDs (bDMARDs) or targeted synthetic DMARDs (tsDMARDs), such as Janus kinase inhibitors, becomes necessary.

When it comes to bDMARDs, specifically anti-TNFα agents, three drugs have demonstrated effectiveness in controlled trials and have been approved for use in treating JIA: etanercept, adalimumab, and golimumab [40–42]. Although infliximab is not officially approved, it is sometimes employed off-label, while certolizumab is currently being tested for its effectiveness in polyarticular JIA. Furthermore, tocilizumab (anti-IL-6) and abatacept (anti-CTLA4) have been approved for polyarticular JIA [43,44].

Another promising category of tsDMARDs comprises JAK inhibitors, which function by interrupting the transmission of extracellular pro-inflammatory signals into the nucleus [45]. Recent approval has been granted based on the outcomes of a randomized phase 3 multicenter, double-blind controlled trial that demonstrated the safety and efficacy of tofacitinib for children over 2 years old with polyarticular JIA [46].

JIA-associated uveitis's first-line treatment is topical GC. The indication for cDMARDs is the failure to adequately control inflammations after 3 months of topical treatment, especially if more than 3 drops of GC are needed.
Methotrexate is the most used second-line treatment for this complication, and if, after three months on it, there are still cells in the anterior chamber, a bDMARD is recommended [22].

Previously derived from cohort studies and more recently from a clinical trial, the greatest evidence relies on adalimumab to efficiently control JIA-U [47]. Infliximab has similar effects to adalimumab, and both are superior to etanercept,

which is not recommended as several studies have reported new onset uveitis while on this drug [47].
Recently, evidence has pointed out the efficacy of tocilizumab for treating JIA-U. A multicenter, single-arm phase II trial, APTITUDE, recently assessed the safety and efficacy of tocilizumab in children with JIA-associated uveitis refractory to MTX and adalimumab [48].

In addition to anti-TNF or anti-IL-6 treatments, other treatments have been or are being tested in patients with JIA-U, such as anti-CTLA4, which is approved for the treatment of JIA patients with a polyarticular course, also appears to be effective in some patients with chronic uveitis. However, no controlled trial has been performed [49]. Data on rituximab and IL-1 inhibitors are even more limited. JAK inhibitors are also being investigated in an ongoing clinical trial.

Figure 2. Simplified treatment algorithms for JIA.

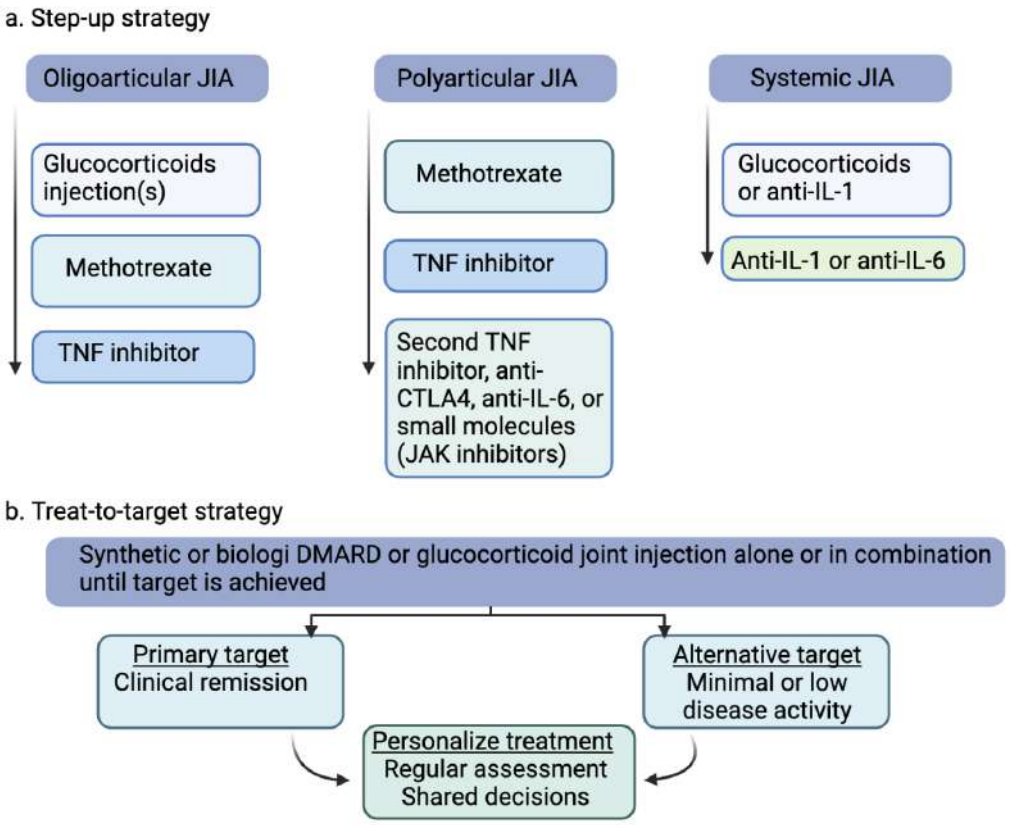

Adapted from [7]. (a) Step-up strategy: increasing the level of the drug progressively for the treatment of different forms of JIA. (b). Treat-to-target strategy: use all drugs available based on the level of disease activity.

1.1.5.2. Non-pharmacological treatment

Although cDMARDs and bDMARDS have drastically changed the prognosis of JIA, it is crucial to recognize the importance of normal psychosocial and social development of the child and to accompany the family throughout the process to facilitate relationships with health professionals. Participation in social events and school attendance should be encouraged, as well as the continuation of sports activities [50]. Appropriate attention to psychosocial issues, if needed, can positively impact the child's well-being.

Physiotherapy and occupational therapy may be needed at some point during the disease to help achieve a normal range of joint movement [51].

Despite the decreasing need for orthotic devices, they may still be useful in treating flexion contractures, particularly in oJIA. Surgical approaches such as arthroscopic synovectomy or irreversible joint contractures are becoming less necessary.

1.1.6. Prognosis

Long-term outcomes in JIA depend on the subtype, disease activity, and prompt recognition and initiation of treatment. Studies conducted in early adulthood have shown that 30% of patients suffer from some form of disability, and the remission rate is not achieved in 40% of patients. [52].

The functional disability may be due to structural damage or comorbidities the patient may develop over time, such as pubertal delay, height retardation, leg discrepancies, or increased cardiovascular burden due to ongoing inflammation.

The prognosis of JIA-U is also a result of both disease activity and treatment. Despite apparent improvements, more than 20% of JIA-U patients still develop complications in long-term follow-up. In addition, about 50% of JIA-U patients continue to have active uveitis into adulthood.
Therefore, JIA-U is still associated with a high risk of late sequelae, including loss of visual acuity, functional and structural damage to the eye, and impaired quality of life [53].

1.2. Etiopathogenesis of juvenile idiopathic arthritis

1.2.1. Environmental risk factors

It is postulated that JIA, like other autoimmune diseases, has a multifactorial origin. In a genetically susceptible individual, following an environmental trigger, a pathological immune response would be activated, leading to dysregulation of the innate and adaptive immune systems, and once activated, this pathological response would be self-sustaining, causing tissue damage.
Environmental risk factors are not strictly the cause of the disease but act as triggers. Several studies have attempted to identify the environmental factors that increase the risk of developing JIA.

Prenatal and early-life exposures have received much attention, although the results have been inconsistent between studies. Breastfeeding has been one of the factors studied in JIA and has been reported to be potentially protective. A population-based birth cohort study in Sweden, which prospectively collected information on early feeding practices before the onset of JIA, found that children who developed JIA were significantly less likely to have been breastfed for more than 4-6 months, after adjustment for multiple factors such as parental education and tobacco exposure [54].

Infections have long been postulated to contribute to JIA. The clustering of JIA incidence in certain seasons may support this hypothesis. In this sense, an Israeli study of 558 children with different types of JIA found a pattern of incidence peaks from late autumn and winter compared to the general population [61].
Already at birth, children born by elective cesarean section correlate with lower microbial diversity and less bifidobacterium benefit. In JIA, two large population-based studies from northern countries showed a small but significantly increased risk of JIA in children born by cesarean section [55,56].

As for the involvement of infectious agents, viruses such as parvovirus B19 and Epstein-Barr virus (EBV) are well-known candidates to explain the pathogenesis of JIA. However, several studies have yielded contradictory results.

In the case of parvovirus B19, Lehmann *et al*. described the presence of anti-parvovirus B19 IgG and IgM and viral DNA in 5 JIA patients. All patients showed persistent B19 infection [57].
These results are in agreement with those published by von Landenberg *et al*. who found that 24 out of 88 patients with various forms of JIA positive for anti-parvovirus IgG, which appeared to elicit an autoimmune reaction partly mediated by anti-phospholipid autoantibodies [58].
Gonzalez *et al.* investigated the presence of parvovirus B19 infection in 50 JIA patients and 39 healthy controls. IgM antibodies were found in 20% of cases and viral DNA in 10%, but none in controls. On the other hand, they observed IgG antibodies in 32% of JIA patients and 44% of controls: the percentage of parvovirus B19 IgG positivity was not significantly higher in the disease subgroups compared to healthy controls [59].

The role of EBV in the pathogenesis of oJIA was investigated by Massa et al. by analyzing 17 patients with active oJIA, all with serological evidence of previous EBV infection, and 20 healthy children with serologically confirmed previous EBV infection. The authors found homologies between oJIA HLA class II alleles and EBV proteins, and a cytotoxic response to EBV-derived peptides was demonstrated in both patients and controls. In addition, the expansion of EBV-specific T cells led to the generation of self-HLA-directed cross-reactive responses. These data support the hypothesis that EBV antigens may induce an autoimmune response through the induction of autoreactive cells against HLA-derived peptides [60].

The role of bacteria in the pathogenesis of JIA has been extensively studied, and different sites of origin in the body have been considered, including mucosal surfaces, the respiratory tract, and the gut. Bacterial agents such as Salmonella spp, Shigella spp, Campylobacter spp, M. tuberculosis, and Chlamydia trachomatis, among others, have been described with inconclusive results linking infection to disease.

In addition to infectious agents, imbalances in the microbiota caused by indiscriminate use of antibiotics have been postulated as risk factors for developing JIA. For example, some children with newly diagnosed JIA have higher Bacteroidetes, a bacterium found after antibiotic exposure.
However, most studies published in this area are observational and cannot rule out bias and confounding unmeasured factors.

Finally, pollutants such as sulfur dioxide, ozone, and carbon monoxide, among others, may contribute to oxidative stress and perpetuate inflammation in JIA.
Two North American studies have examined the association between inhaled particulate matter and JIA.
In a Utah population-based study of 338 children diagnosed with JIA, elevated particulate matter concentrations in the previous 14 years were associated with an increased risk of JIA-onset in children younger than 5.5 years, with an RR of 1.6 per 10 μg/m3 (95% CI: 1.00 to 2.54). However, the results were imprecise when all age groups were included in the analysis (RR: 1.11; 95% CI: 0.85-1.45) [61]. The results were not replicated when studying a broader population in America and Canada with systemic-onset JIA.

There are many difficulties in interpreting studies of environmental exposures in JIA, including the synergistic effect of different exposures with genetic factors, or the fact that there are probably environmental factors that are not yet known.

1.2.2. Genetic factors

JIA is a complex disease influenced by genetic traits and environmental factors [62]. A genetic contribution has been demonstrated in family and twin studies, where the inherited susceptibility to JIA in siblings and probands is 15 to 30 times higher than in the general population. A recent heritability study based on SNP-h2 estimated that the heritability of JIA is 0.73 among the most highly heritable pediatric autoimmune diseases (Li et al., 2015b). However, there are no evidences of highly penetrants mutations.

Over the past decades, numerous studies have attempted to investigate potential susceptibility loci for JIA, including all JIA subtypes or just the most common ones, such as oJIA and RF-negative polyarticular. JIA.Genome-wide association studies (GWAS) have the characteristic of covering the whole genome so that associations of genotypes with phenotypes can be established by testing for differences in allele frequencies of genetic variants between ancestrally similar but phenotypically different individuals. GWAS can consider copy-number variants or sequence variations in the human genome, although the most studied genetic variants in GWAS are single-nucleotide polymorphisms (SNPs). Standardized GWAS protocols require researchers to replicate findings and impose a stringent significance threshold ($P \leq 5 \times 10\text{-}8$) due to the large number of simultaneously analyzed polymorphisms [63].

GWAS have facilitated the identification of new genes some of which have shown to be shared across multiple autoimmune diseases, resulting in emerging common pathways that have helped the understanding of biological basis of these conditions. The complexity of JIA has also been investigated using the GWAS approach [64].

HLA associations in oligoarticular and polyarticular RF-negative JIA

The human leukocyte antigen (HLA) genes are located on chromosome 6 and are essential to the immune system. HLA genes are highly polymorphic and associated with many autoimmune diseases such as rheumatoid arthritis (RA) or type 1 diabetes [65,66].

The first study in JIA to elucidate this association was performed in 2010 by Hollenbach and colleagues. In this study, they peformed high-resolution typing of class I and II loci in 820 children with JIA and 273 healthy controls [67]. HLA-DRB1:11:03/11:04 alleles were found to be associated with oJIA and with younger patients with polyarticular RF-negative JIA. Instead, HLA-DRB1:15:01 was found to be protective to these diseases. In addition to HLA-DRB1 associations, a modest association was observed between HLA-DPB1:02:01 allele and JIA [68].

Based on the major implications of the HLA region and its contribution to other autoimmune diseases, in 2013, Hinks *et al.* applied the custom Illumina Infinium genotyping array designed by the Immunochip Consortium, which covers the extended HLA region and 186 non-HLA regions that have shown genome-wide evidence of association with one or more of 12 autoimmune diseases, to 2,816 oJIA and polyarticular RF-negative patients and 13,056 controls [69]. The most significant associations in this study were observed within the MHC region, with HLA-DQB1 and HLA-DQA2 SNP rs7775055 provided the strongest evidence of association with JIA (odds ratio (OR) = 6.01; $P = 3.14 \times 10^{-174}$) [70].
A few years later, the same Immunochip was applied to fine-map the MHC locus in a larger cohort of 5,043 JIA patients and 14,390 controls. The authors identified for the first time that oJIA and polyarticular RF-negative JIA are genetically similar in their HLA associations, with the strongest one for amino acid at position 13 in the HLA-DRB1 gene [71].

Regarding JIA-associated uveitis, just a single genome-wide study has been performed that distinguish JIA without uveitis from JIA with uveitis. Recently, Haanoot *et al.* performed GWAS in 192 patients with JIA-U and 330 JIA patients without uveitis and 394 controls. The only significant signal observed in

patients with uveitis compared to patients without uveitis was the presence of serine and aspartic acid amino acid changes at positions 11 and 13 of the HLA-DRB1 gene, respectively (OR 2.59, $P = 4.80 \times 10^{-10}$) [72].

Non-HLA associations in oligoarticular and polyarticular RF-negative JIA

The first GWAS studies in oJIA and RF-negative polyarticular JIA identified risk SNPs in the genomic loci for genes Protein Tyrosine Phosphatase Non-Receptor Type 22 (PTPN22), the Protein Tyrosine Phosphatase Non-Receptor Type 2 (PTPN2), the Signal Transducer and Activator of Transcription 4 (STAT) and Interleukin 2 Receptor Alpha (IL2RA) [73,74].

These confirmed JIA risk loci have clear roles in immune regulation and function. In the years after that, the Immunochip confirmed the implication of previously found risk loci such as STAT4, Interleukin 2-Interleukin 21 (IL2-IL21), and Interleukin 2 Receptor Alpha (IL2RA), and provided evidence for new regions such as Ankyrin Repeat Domain 55 (ANKRD55), Tyrosine Kinase 2 (TYK2), SH2B Adaptor Protein 3-Ataxin 2 (SH2B3-ATXN2), Runt-Related Transcription Factor 1 (RUNX1), among others [70]. These risk loci were previously reported in RA and other autoimmune diseases with pediatric onset [75].

More recently, the largest JIA cohort analyzed on genome-wide platforms to date, (2,751 patients with oJIA or RF-negative polyarticular JIA and 15,886 controls) identified 9 new risk loci that include Janus Kinase 1 (JAK1), Proline-Rich 9 - Leucine Rich (PRR9_LOR), Parathyroid Hormone 1 Receptor (PTH1R), Immunoglobulin-Like Domain Containing Receptor 1 - Cluster of Differentiation 86 (ILDR1_CD86), and Ring Finger Protein 215 (RNF215) (Figure 3). Some of these loci have been associated with other autoimmune diseases such as celiac disease, multiple sclerosis, or systemic lupus erythematosus [76–78]. These findings strongly support the existence of a genetic landscape of overlapping diseases and, consequently, a shared heritability among several autoimmune diseases.

Figure 3. Manhattan plot of genome-wide genetic association statistics for oJIA and RF-negative polyarticular JIA risk loci.

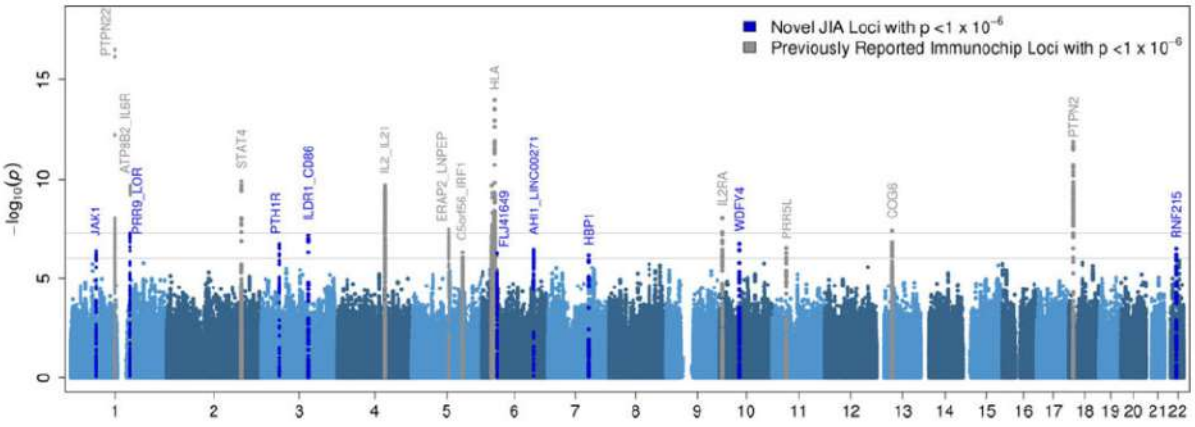

Extracted from [79]. The upper gray line indicates the threshold of genome-wide significance ($P < 5 \times 10^{-8}$). The lower gray line indicates the threshold of suggestive association (P < 1 × 10-6). Loci reaching this threshold and individual SNPs mapping these loci are shown in dark blue. Loci in gray have been reported for the association by Hinks *et al.* [70].

In addition, other groups have identified new JIA susceptibility variants by pooling all JIA supotypes to increase the power of the results and identify new-shared susceptibility loci. Lopez-Isaac *et al.* conducted a GWAS JIA study involving 3,305 cases and 9,196 healthy controls. The combined analysis of all available JIA cases identified five novel genome-wide significant association loci lead bySNP rs497523 (p=7.12 x 10-9), which is intronic to CCDC101 (16p11.2), also known as SGF29, and followed by AHI1 (rs2614258) (p=9.17 x 10-8), CCR3 (rs79815064) (p=7.61 x 10-8), TNFSF11 (rs12430303) (p=3.61 x 10-6), and FOXP1 (rs7647909) (p=4.56 x 10-6). Furthermore, the authors also performed and enrichment analysus identifying the key transcription factors v-Rel Avian Reticuloendotheliosis Viral Oncogen Homolog A (RELA) and Early B-Cell Factor 1 (EBF1), related to the regulation of Treg-induced tolerance and B cell functioning [80].

Studies in non-HLA genes associated with JIA-U are scarce and have shown conflicting results. An investigation of 17 non-HLA variants associated with JIA-U in a multicenter cohort of Nordic countries that included 282 JIA patients with and without uveitis identified a polymorphism in the gene encoding the V-set domain-containing T cell activation inhibitor-1 (VTCN1) (rs2358820) associated with uveitis (OR 3.5, p= 0.029). VTCN1, also known as B7-H4, is a inhibitor of T-cell function, including

proliferation, cytokine production, and development of cytotoxicity, and may play a role in the pathogenesis of rheumaotid arthritis (RA) [81,82].

Although there are fewer studies with JIA subtypes other than oligo- and polyarticular RF-negative, it is relevant to know the genetic mechanisms underlying these subtypes to understand their differences and similarities at the genetic level. The HLA and non-HLA loci associations in the remaining subtypes are grouped below.

HLA and non-HLA associations in polyarticular RF-positive JIA

This subtype is strongly associated with HLA variants like other JIA categories and RA. Based on the observation in RA that different HLA-DR molecules share some common amino acid motifs (shared epitopes, SE), several studies have demonstrated the association of SE encoding HLA-DRB1, particularly DRB1 04:01/04:04 alleles, in RF-positive polyarticular JIA. In contrast to the JIA and RF-negative polyarticular JIA, non-HLA risk loci associated with this subtype are rare due to the low prevalence of this subtype, but similar to those in RA [83].

HLA and non-HLA associations in systemic JIA

The distinctive clinical features of sJIA indicate that it differs from other types of JIA. Consequently, some proponents assert that sJIA should be classified separately from other forms of JIA and designated as an autoinflammatory disease. The most notable work done in this regard is that of Ombrello *et al.* who conducted a genome-wide association study of 770 children with JIA collected from nine countries. The association of SNPs with JIA was tested, and weighted genetic risk scores were used to compare the genetic architecture of sJIA with other JIA subtypes [84]. The strongest sJIA risk locus identified by this study was the HLA locus. None of the SNPs, HLA alleles and HLA haplotypes described in sJIA were shared across other subtypes like oJIA. Beyond the MHC locus, they identified a novel sJIA susceptibility locus on the short arm of chromosome 1 (1p36.32) (rs72632736) ($p= 2.5 \times 10\text{-}8$), nearest to an uncharacterised long non-coding RNA gene. More recently it has been described the association of a mutation in the Laccase Domain Containing 1 (LACC1) gene in a family form of systemic onset JIA [85].

Other non-HLA associations have demonstrated the involvement of genes encoding pro-inflammatory cytokines such as Interleukin 6 (IL-6) and Interleukin 1 (IL-1) [86].

Other non-HLA related associations have demonstrated the involvement of genes encoding pro-inflammatory cytokines such as interleukin-6 (IL-6) and interleukin-1 (IL-1), a discovery of great impact with important therapeutic implications as the use of IL-6 and IL-1 inhibitors as first-line therapeutic drugs in JIA has significantly improved the prognosis of this subtype of JIA.

HLA and non-HLA associations in ERA and psoriatic JIA

There is a well-described association between class I HLA-B27 and ERA. Patients with ERA who are HLA-B27 positive are more likely to have a chronic course and to develop an axial involvement. Class II HLA alleles like HLA DRB1:01, DQA1:01:01 and DQB1:05 have also been associated with ERA, but these results have been extracted from studies involving this subtype of JIA in very few patients. [87].

In addition to HLA genes, non-HLA polymorphisms have also been described. In 2011, Hinks et al genotyped SNPs in the ERAP1 gene in 1,054 JIA cases including 74 ERA and 5,200 controls and found a strong association between this gene and the ERA subtype. ERAP1 encodes a multifunctional aminopeptidase, but its role in the pathogenesis in any of the associated diseases has yet to be determined. It may play a role in trimming peptides, in the endoplasmic reticulum, for binding to HLA class I molecules where they are transported to the cell surface for presentation to T cells.
As well, polymorphisms in the MEFV Innate Immunity Regulatory Pyrin gene (MEFV), implicated in the pathogenesis of Mediterranean familial fever, an autoinflammatory disease, have been related to ERA [88].

Similar to ERA, the prevalence of HLA-B27 in psoriatic JIA was 11% in children with this subgroup. Some authors have suggested that psoriatic JIA has many of the features of the autoinflammatory disease, so variants such as NOD-like receptor family pyrin domain containing 3 (NLRP3), Nucleotide-binding oligomerization domain containing 2 (NOD2), and MEFV have been investigated.
In a study of 950 children with JIA and 728 healthy controls, Dey *et al.* investigated 41 SNPs at NLPR3, NOD2, MEFV, and Proline-Serine-Threonine Phosphatase Interacting Protein 1 (PSTPIP1) loci. After correcting for multiple testing, two genetic associations remained significant in the psoriatic JIA group, including the MEFV SNP rs224204 ($p= 0.025$) and the NLRP3 SNP rs3806265 ($p= 0.04$) [89].

1.2.3. Immune pathogenesis

Numerous changes in the immune system have been described in oJIA, which may partly explain the aetiopathogenesis of this subtype of JIA. The following is a review of the current knowledge of the described changes in the immune system components in patients with oJIA and uveitis-related JIA.

1.2.3.1. Cellular landscape in the pathogenesis of oJIA and uveitis

Synovial inflammation in oJIA involves a complex set of interactions between immune and non-immune cellular subsets. However, the most studied feature of the immune response is produced by adaptive immunity, with effector T cells being one of the most important components in the pathogenesis of oJIA. This is in accordance with the strong genetic risk associations between JIA (or oJIA) and MHC class II alleles. The $CD4^+$ T effector cell population comprises several T helper (Th) subsets that develop after the TCR in naïve $CD4^+$ T cells recognises an antigen preseted by the HLA-II in activated antigen-presenting cells (APCs).

The discovery of other T helper subsets different from the original Th1 and Th2 paradigm, such as Th17, Th9, and T follicular helper (Tfh) cells, has helped to understand the pathogenesis of JIA. Specifically, in oJIA, a mixed Th17/Th1 phenotype is found in inflamed joints, capable of producing both IL-17 and interferon-gamma (IFNγ) [90]. Th17, characterized by their environmental plasticity and in contact with pro-inflammatory cytokines such as TNFα or IL-12, acquires a shift towards the production of IFN-γ. Targeting IL-17 with IL-17 inhibitors is providing promising results in the treatment of children with psoriatic JIA and ERA. The role of IL-17 is also described in other forms of JIA, including sJIA. Therefore, IL-17 blockade may be extended in the future to other subtypes of JIA [91].
Both Th1 and Th17 cells have been identified in the eyes of mice with experimental autoimmune uveoretinitis. Specifically, activated retinal antigen-specific Th1 or Th17 cells can pass the blood-retina-barrier, and secrete cytokines and chemokines to

attract additional inflammatory cells, including macrophages, monocytes, and non-specific lymphocytes that will conduct the tissue damage in the eye (Figure 4) [92].

Figure 4. Pathophysiology of experimental animal models of uveitis.

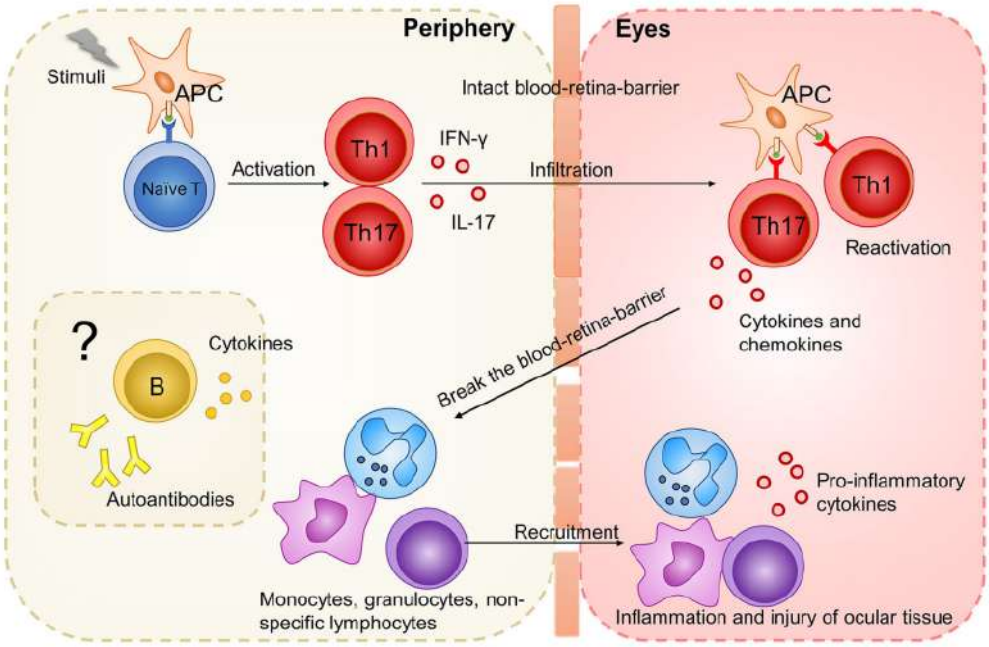

Extracted from [93]. APC: antigen-presenting cell; Th1: T helper cell type 1; Th17: T helper cell type 17; IFN-γ: interferon-gamma.

Regulatory T cells (Tregs) are a subset of $CD4^+$ T-cells with antiinflamatory properties, characterized by the expression of CD25 (IL-2 receptor α) and transcription factor FOXP3. Different Treg phenotypes are described based on the expression of functional markers such as inducible costimulator (ICOS) and Cytotoxic T-Lymphocyte Antigen 4 (CTLA-4) observed in effector Tregs ($FOXP3^{high}$, $CD25^{high}$, $ICOS^+$, $CTLA\text{-}4^+$) [94]. They have attracted considerable attention as they have been found within the joints of oJIA patients as well [95].

The instability of Tregs defined by loss of FOXP3 expression and of their suppressive function is still a matter of debate in the pathogenesis of oJIA. Data support differences in Treg stability depending on whether they are found in peripheral blood or influenced by the pro-inflammatory synovial fluid environment [96]. In the SF the Treg/Th17 balance seems to be lost, either through FOXP3 lineage instability or the incapacity of Treg to regulate conventional T cells at the inflammation site [97].

$CD8^+$ T-cells, although not as extensively studied as $CD4^+$ T-cells in oJIA, contribute to its pathogenesis with their cytolytic capacity and proinflammatory cytokine production. Also described to be present in the SF of oJIA patients [98], $CD8^+$ T-cells have been found to express the negative costimulatory marker programmed death-1 (PD-1). However, far from being functionally exhausted, infiltrating $PD1^+$ $CD8^+$ T cells seem to maintain their effector function. Furthermore, these $PD\text{-}1^+$ $CD8^+$ T-cells in SF were shown to be enriched for a tissue-resident memory T-cell (Trm) transcriptomic profile compared to the $PD\text{-}1^-$ $CD8^+$ counterparts [99,100]. The hypothesis drawn from these results is that the $PD\text{-}1^+$ $CD8^+$ T-cells found in SF may come from inflamed synovial tissue, although how they are related to Trm cells is still unknown.

In addition to T cells, B cells have an important role in the pathogenesis of JIA as they contribute to ANAs and RF production detected oJIA and RF-positive polyarticular JIA patients. ANAs are IgG antibodies recognizing nuclear antigens whereas RF refers to a group of antibodies of various classes whose antigen binding sites are specific to the Fc portion of IgG molecules. Although the exact targets of these ANA are yet to be defined, their presence provides strong evidence that B cell tolerance is also altered in both oligoarticular and RF-negative polyarticular JIA. Moreover, it has been demonstrated a positive correlation between ANAs and synovial tissue plasma cells infiltrations [101].
The participation of B cells in JIA-associated uveitis has been demonstrated by identifying plasma cells comprising focal aggregates of CD20-positive cells in the ocular tissue using immunohistochemical studies [102]. Elevated amounts of immunoglobulin (Ig) have been observed in the vitreous fluid and the anterior chamber, supporting the local production of antibodies in uveitis and transcriptomic analysis also pointed out the role of B cells in oJIA-U identifying different components of Igs [103,104].

Much less studied than the adaptive immune system, the innate immune system has been also implicated in oJIA pathogenesis. Several types of innate cells, including dendritic cells, natural killer cells, neutrophils, and macrophages, have been described, frequently accumulating in inflamed tissue.

Specifically, recent advances in the study of the synovial membrane in RA have identified macrophages and monocytes as the pivotal cells upon which numerous cellular interactions occur in inflamed tissue. The healthy normal synovium is a membrane that consists of a thin lining composed mainly of macrophage-derived synoviocytes, and fibroblasts and a sublining composed of macrophages, fibroblasts, and other cells such as adipocytes, blood vessels, and lymphocytes [96]. Under homeostatic conditions, the synovial tissue is an immunologically challenging environment that constantly prevents synovial inflammation in response to synovial fluid-derived danger signals like alarmins or damage-associated molecular patterns accumulated due to mechanical stress. The synovial membrane produces the syonvial fluid, whose function is to reduce friction between articular cartilages during movement and help to absorb mechanical impact. The composition of SF changes during an individual's lifetime due to changes in mechanical loading and its closer contact with the synovial membrane makes it a good surrogate of tissue turnover and state [105].

Based on the hypothesis that circulating monocytes migrate to synovium and influence tissue-resident monocytes to produce cytokines, Schmidt *et al.* studied 13 patients with untreated oJIA collecting paired SF, PB, and synovial biopsies (n=3). Monocytes were analyzed for polarization markers by flow cytometry and real time PCR (qPCR). Effector function was analyzed by phagocytosis assay, and monocyte distribution and mRNA expression were investigated in biopsies by immunohistochemistry, immunofluorescence, and in situ hybridization.
The distribution of monocyte subsets was different between SF and PB, observing an increased frequency of intermediate ($CD14^{++}CD16^{+}$) monocytes in SF compared to PB. Moreover, SF monocytes displayed mixed M1/M2 (IL-4) phenotypes with the expression of CD40, CD80, and CD206 compared to patients' circulating monocytes. Functionally, these cells were found to have reduced phagocytosis compared to circulating monocytes. In tissue, macrophages were identified in both the lining and sublining region of the synovial [106].

Finally, neutrophils have been also found in significant quantities in the SF of oJIA patients. Arve-Butler *et al.* recently characterized the phenotype of SF neutrophils from 17 oJIA patients and function (n=13) by flow cytometry. They found that SF neutrophils

have an active phenotype characterized by increased CD66b and CD11b levels. An impaired phagocytosis capacity of these SF neutrophils compared to their PB counterparts was observed, which can play a role in sustaining joint inflammation if neutrophils are not able to exercise their effector capacities [107].

Currently, due to high invasiveness of obtaining synovial tissue samples, especially in pediatric patients, most JIA cell data comes from peripheral blood and synovial fluid. However, significant progress is being made in the study of synovial tissue using high-throughput technology in diseases such as rheumatoid arthritis, which will be discussed below.

1.2.3.2. Sequencing of the TCR repertoire in oligoarticular juvenile idiopathic arthritis

The adaptative immune system is implicated in oJIA's pathogenesis evidenced by the oligoclonality of certain T cell receptor (TCR) subsets in immune pathogenic populations.

Two different protein chains comprise TCRs. The vast majority of TCRs are composed by an alpha and beta chains, while a small percentage of T cells (gamma delta T cels) express a TCR composed of gamma and delta chains [108].

Essentially, studies have focused on alpha and beta TCR and the wide possible combinations that explain TCR variability. The genes encoding alpha (TCRA) and beta (TCRB) chains are comprised of multiple gene segments, which include variable (V), diversity (D), and joining (J) segments for TCRB gene and variable (V) and joining (J) for TCRA gene [109].
The huge number of random combinations of germline segments as well as the addition/deletion on the junction site of the segments contribute to its enormous diversity.
The sequence encoded by the V(D)J junction is the complementary determining region 3 or CDR3. This sequence is characterized by disposing of the highest variability and gives the ability of a T cell to recognize a huge divesity of antigen peptides presented by the class I and II HLA genes [110].

Finally, the ultimate level of diversity is provided by the pairing of alpha and beta chains with different CDR3 sequences, leading to an estimated total of 10^{18} possible TCR combinations [111].

Studying T cell response through the analysis of TCRs provides information about how antigen-driven clonal expansion is produced, and longitudinal clonal dynamics of the T cell that can be correlated with treatment response or clinically relevant changes [112].

The first TCR sequencing studies applied in oJIA focused on the analysis of pathogenic $CD4^+$ T cells and their migration from peripheral blood PB to SF. Spreafico *et al.* identified a pathogenic subset of activated memory T cells $CD45RA^-$, $CD69^+$, $HLA\text{-}DR^+$ with exhaustion markers ($PD1^+$, $CTLA4^+$) and cytokine production markers ($CCR5^+$, $CCR6^+$) in PB from active oJIA patients with similar transcriptomic profile as their SF counterparts and clonally expanded especially in those patients who did not respond to MTX [113].
Subsequently, the same group focused on the analysis of the Treg compartment since they are found in greater proportion in SF compared to PB in oJIA patients. Here they found that a subset of Tregs cells defined by HLA-DR migrates from PB to SF and a partial overlap in TCR repertoire was found between Tregs and the pathogenic circulating activated memory T cells described previously [114].

Further insights have been gained lately thanks to the combinatory analysis of TCRs and single-cell RNA-Sequencing (scRNA-seq).
Julé *et al.* analyzed scRNA-Seq and TCR repertoire on sorted Tregs and T effector cells from the SF of 2 oJIA patients. They found five different clusters of Tregs and seven clusters of T effector cells. The authors also defined a highly expanded Treg subset with an upregulation of interferon-induced genes [115].

More recently, $CD8^+$ T cells have gained increasing attention as progressively described in inflamed tissues or associated with poor prognosis in many rheumatoid diseases including RA and systemic lupus erythematosus (SLE) [116,117]. Maschmeyer *et al.* identified pathogenic $CD4^+$ and $CD8^+$ T cells in chronically inflamed joints and PB of seven patients with oJIA patients utilizing scRNA-seq combined with

TCR analysis. Of particular interest is the presence of a PD-1$^+$ TOX$^+$ EOMES$^+$ population of CD4$^+$ and CD8$^+$ effector T cells clonally expanded, terminally differentiated, and non-proliferating but very active with the potential to attract myeloid cells to SF but also expressing IL-10. These cells were also found in PB and might have the capacity to limitate systemic inflammation [118]. In summary, dissecting synovial and peripheral blood effector and Tregs compartments using single-cell transcriptomics and TCR sequencing has revealed a previously unexplained heterogeneity and plasticity of these cells.

1.2.3.3. Insights from transcriptomic studies in oligoarticular juvenile idiopathic arthritis and uveitis

The term transcriptomics refers to using several technologies for the high-throughput identification of ribonucleic acid (RNA) species. Genome-wide gene expression profiling using RNA sequencing (RNA-seq) has been widely used to study rheumatic diseases and has provided insights into gene function and gene expression signatures [119]. Transcriptomics analyzes the expression of different genes under various conditions, such as at different time points or between normal/diseased tissues or cells. Differential expression (DE) analysis between conditions produces gene signatures characteristic of the condition or disease being studied. For more than 20 years, DNA microarray studies have been used to measure transcript abundance. However, microarrays cannot detect novel transcripts or splice variants due to their low sensitivity. RNA-seq, on the other hand, can detect both coding and noncoding novel transcripts and has higher sensitivity and reproducibility between biological replicates [120]. Several companies offer different NGS platforms based on different methodologies, including sequencing-by-synthesis technology, with a DNA polymerase or ligase as the key component. Regardless of the technology of choice, a classical RNA-seq workflow includes RNA isolation, library preparation, sequencing, and data analysis (Figure 5).

Figure 5. RNA-seq workflow.

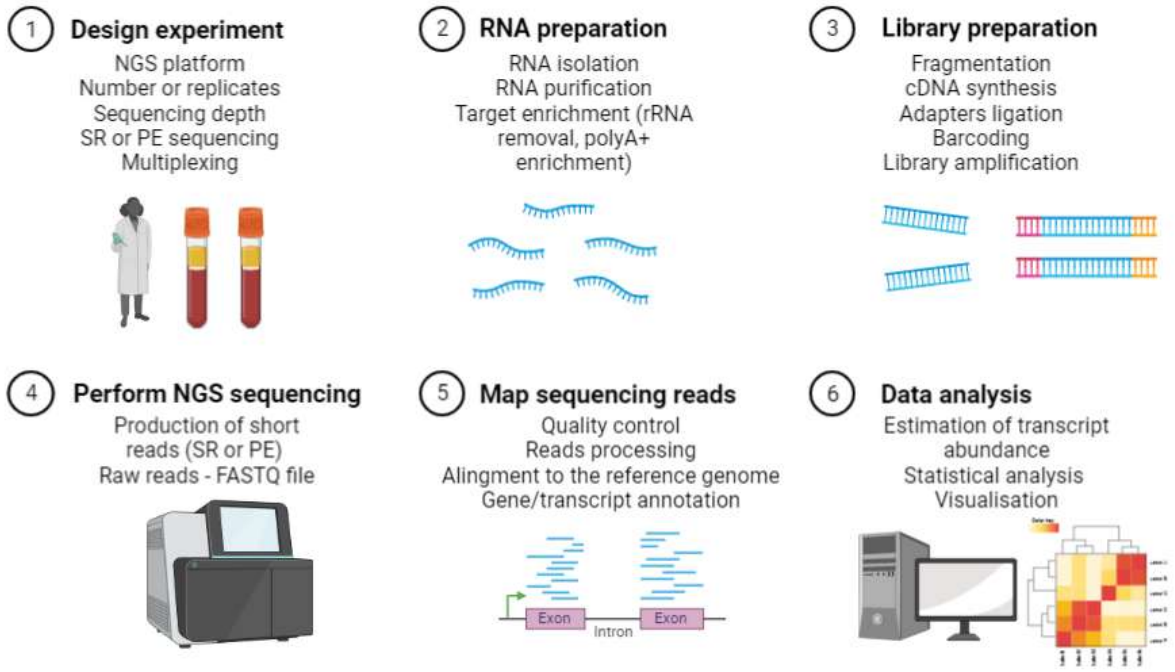

Adapted from [119]. NGS: next-generation sequencing; RNA: ribonucleic acid; rRNA: ribosomal RNA; cDNA: complementary deoxyribonucleic acid; SR: single-read; PE: paired-end read.

RNA-seq transcriptomic analysis in JIA has aided in the identification and characterization of dysregulated pathways and cellular subsets implicated in disease pathogenesis.

In non-systemic JIA, studies have focused on the adaptive immune system in both SF and PB and on transcriptomic profile changes during treatment.

Peeters *et al.* applied RNA-seq to study autophagy, a lysosomal degradation pathway involved in T cell activation, differentiation, and survival to 13 oJIA patients with an active disease either untreated or treated with MTX or anti-TNFα and 32 healthy controls. Isolated $CD4^+$ $CD45RO^+$ T cells from PB and SF were analyzed demonstrating an up-regulation of autophagy genes in JIA PB compared to healthy controls and in SF-derived $CD4^+$ T cells compared to paired PB-derived $CD4^+$ T cells. As autophagy was increased in cells derived from the SF, the investigators aimed to determine whether inflammatory mediators in SF could induce autophagy. However, culturing healthy controls and oJIA's T cells in the presence of SF did not induce autophagy [121]. It was hence postulated that the increase in autophagy may

have occurred to cope with the greater metabolic demand of inflamed and dysregulated T cells.

Other studies have sought to determine biological and genetic predictors of response to MTX in oJIA. Moncrieffe *et al.* studied 47 children with oligoarticular and polyarticular RF-negative JIA at two-time points, prior to and 2 months later being into MTX, and 14 age-matched controls. Peripheral blood mononuclear cells (PBMCs) were isolated and RNA-seq was performed to characterize molecular heterogeneity related to MTX responsiveness. Six significant DE genes were identified comparing MTX responders and non-responders [122]. When all JIA patients' samples pre-treatment were compared with healthy controls, significant differences in gene expression levels were detected identifying 99 DE genes. Unsupervised clustering of all samples using these 99 genes formed three distinct clusters: cluster I - healthy controls, cluster II - MTX responders, and cluster III - MTX non-responders. Then, transcriptional profiles from the human Gene Atlas dataset for purified B cells, CD4, CD8 T cells, and monocytes were used to identify possible cellular origins contributing to this differential expression signature driving into clusters. Interestingly, cluster III was correlated to the monocyte profile being CXCL8 (IL-8), a chemokine implicated in neutrophil migration from peripheral blood to tissues, the most significant up-regulated gene [123].

The study of JIA-U at the transcriptomic level presents an additional difficulty due to the availability of tissue samples. Previous immunohistochemical studies of iris biopsies in end-stage JIA-U showed a predominance of B cells in the intraocular inflammatory infiltrate and increased levels of immunoglobulins in the vitreous fluid [20,124]. Wildschütz et al. analyzed iris samples from 30 oJIA-U patients, 18 adult patients with different autoimmune-related diseases, and 20 adult patients with primary open-angle glaucoma (POAG). By RNA-seq they identified 136 DE genes among all samples. Regarding B cells, the expression of several immunoglobulin-related genes such as the Immunoglobulin Heavy Constant Gamma 4 gene (IGHG4) was statistically differentially up-regulated in JIA-U compared to PAOG (log2 fold change = 3.44, P = 2.44^{-32})[104].

Recently, Wennink *et al.* studied in more depth the transcriptome profile of B cells in JIA-U. Purified $CD19^{+}$ B cells purified by flow cytometry from PB were collected from 14 children with JIA-U, 13 JIA patients without uveitis, and 5 healthy controls, and

whole-transcriptome RNA sequencing was performed. The DE analysis between JIA-U and JIA without uveitis just revealed only 6 differentially expressed genes which suggest that these differences are unlikely to be robust but included genes such as TXNIP – related to B cell-associated germinal centers in peripheral lymphoid organs (31) and MN1, linked to the colony-forming activity of B cells [125–127].
Further studies are needed beyond the B-cell subsets using other, more novel techniques, and at different time points.

Despite considerable progress, there have been studies that have encountered serious difficulties in defining molecular signatures when analyzing gene expression patterns in PBMCs from patients with JIA and JIA-U at different stages of the disease [128]. Although PBMCs are easy to obtain, their high heterogeneity is a major drawback. Technical advances have been made by introducing techniques such as scRNA-Seq, which will be discussed below.

1.2.3.4. Proteomic studies in in oligoarticular juvenile idiopathic arthritis and uveitis

Proteomics refers to the large-scale characterization of the proteins of a cell, tissue, or organism. Its complexity resides in the enormous varieties of proteins due to their post-translational modifications, temporarily distinct structures, functions, and protein interactions [129]. Proteomics can technically be classified into three types although they are interrelated: structural proteomics, functional and expression proteomics. The latter, which from the rheumatologist perspective has more utility, is crucial to determine which proteins are significantly altered in specific pathological processes and help to define biomarkers.

Advances in methods and technology now enable the construction of a comprehensive biomarker pipeline from candidate protein discovery to biomarker validation and commercialization [130]. For this purpose, different proteomic strategies are used such as mass spectrometry (MS) methods and immunoassays (Figure 6).

Figure 6. Proteomic biomarker strategies pipeline.

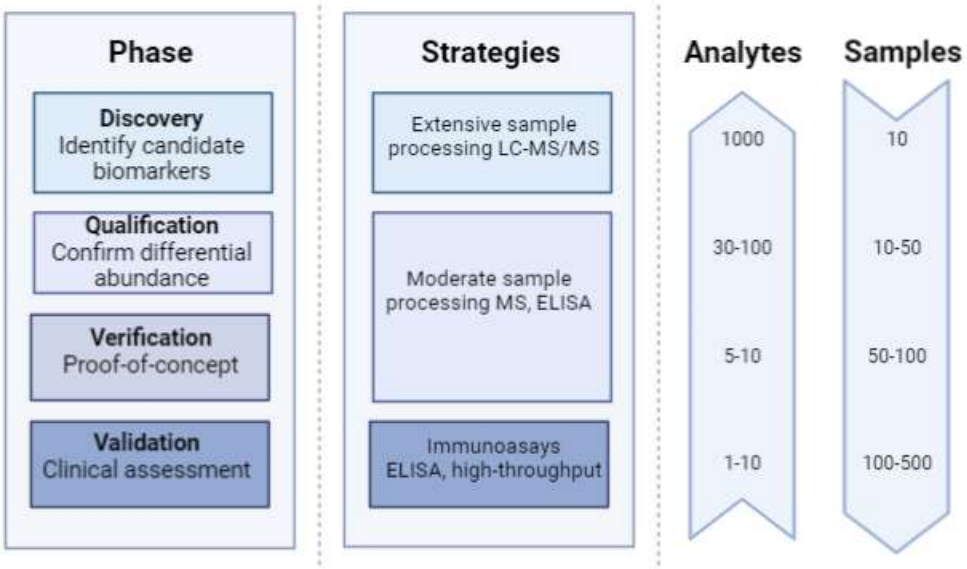

Adapted from [130]. LC-MS: liquid chromatography mass-spectrometry; MS: mass-spectrometry; ELISA: enzyme-linked immunosorbent assay.

MS strategies are suitable for multiplex biomarker discovery. For validations proposals, it is convenient to use enzyme-linked immunosorbent assays (ELISA) as it is generally more sensitive than MS. ELISA is based on enzyme immunoassay (EIA) to detect the presence of a target antigen using specific antibodies. In pediatric rheumatic diseases, this technology has been used to analyze cytokines, chemokines, and other pathogenic antibodies [131].

However, conventional ELISA can miss other biomarkers of importance in autoimmune diseases such as JIA as it is a lower-throughput technique than other novel techniques. Multiplex immunoassay (MIA) panels confer advanced measurement techniques to analyze multiple proteins in a single patient sample. Current multiplex immunoassays can be divided into two formats: planar assays and microbead-based assays [132].

Briefly, MIAs are conducted by incubating microbeads or microarrays with a biological sample, followed by adding a mixture of detection antibodies. These techniques are not exempt of limitations. Cross-reactivity between antibodies can reduce the limit of detection, and thus increasing the probability of misrepresentative results.

Since 2013, a technology combining NGS with fundamentals of ELISA, called Proximity Extension Assay (PEA) (Olink®), is currently available. PEA technology is an antibody-based immunoassay that combines a polymerase chain reaction (PCR) and is read out using NGS or qPCR. At present, the PEA assay is capable of quantifying the levels ~3000 proteins at a time [133,134].

Proteins studied in JIA are related to both innate and adaptive immune system activation. Basically, soluble factors are identified to be of importance in JIA, mainly cytokines, chemokines, and damage-associated molecular pattern molecules (DAMPs) [135].

Gibson *et al*. studied the SF proteome by MS of ten de novo oJIA, five extended oJIA, and seven polyarticular RF-negative JIA objectifying that the expression levels of a set of 40 proteins segregated the different forms of JIA studied. Amongs the most relevant proteins, apolipoproteins AI and AII were overexpressed in polyarticular JIA when compared to both groups of oJIA (p= 0.08). Vitamin D binding protein and complement component C3 were overexpressed in polyarticular JIA compared to oJIA (p= 0.019 and 0.033, respectively) [136].

Another study used MIA to analyze 30 soluble mediators in SF and PB of 30 oJIA patients, 15 polyarticular RF-negative JIA, 20 systemic JIA, and 9 disease control patients found statistically significant differences in plasma mediators comparing JIA (all subtypes) to controls with higher levels of tumor necrosis factor α (TNFα), chemokine (C-C motif) ligand 3 (CCL3), chemokine (C-X-C motif) ligand 9 (CXCL9) and macrophage inhibitory factor (MIF) among others. Of relevance, one particular cytokine, interleukin-17 (IL-17), was increased in the plasma of patients with both oligo- and poly-JIA but not in patients with systemic JIA [137].

More recently, data from the Inception Cohort of Newly diagnosed patients with JIA (the ICON-JIA study) described the association of baseline serum biomarkers within the 12-month outcome of 266 active JIA patients (all subtypes) to identify biomarkers related to disease extension. Particularly in oJIA, granulocyte colony-stimulating factor (G-CSF), interleukin-18 (IL-18), and tumor necrosis factor ligand superfamily member

12 (TWEAK) were higher at baseline in patients with persistent oJIA at 12 months compared to extended oJIA [138].

As for the therapeutic response, different protein biomarkers have been described in oJIA in both SF and PB. Cattalini *et al.* studied the protein composition of SF at the time of intra-articular GC injection of oJIA de novo patients and correlated them with the clinical outcome at 6 and 12 months. Higher levels at baseline of IL-6 predicted a shorter time to relapse whereas higher levels of IL-10 correlated with a longer duration of GC response. IL-6 and IL-10 are pro-inflammatory and anti-inflammatory cytokines respectively. It can be argued that IL-10 high levels reflect a suppressive response to a state of active inflammation, to which the addition of the GC a synergistic anti-inflammatory effect [139].

Apart from IL-6 and IL-10, different research groups have evaluated the therapeutic response by determining the biomarkers called calgranulins, the most familiar S100 myeloid-related proteins. They include S100A8, S100A9, and S100A12; the first two can dimerize in the heterocomplex S100A8/A9, also known as MRP8/14 or calprotectin.

Engagingly, Monchieffe *et. al* demonstrated that non-systemic JIA patients with higher calprotectin levels before initiating MTX had a better response at a 6-month follow-up [140]. Similarly, it has been demonstrated that calgranulins also work well in predicting flares after therapeutic withdrawal. Very recently, the multicenter trial PREVENT-JIA has demonstrated that pharmacological withdrawal based on S100A12 determination results in lower relapse rates compared to standard clinical practice [141].
S100A8/A9 and S100A12 levels have been found to be elevated in patients with active uveitis and inactive joint disease [142].
Conversely, in the previously mentioned ICON-JIA study, elevated S100A12 levels were not associated with the risk of uveitis, perhaps due to the influence of concurrent anti-inflammatory treatment [138].

Finally, JIA-U represents a condition that, because it is usually asymptomatic and can occur even when the arthritis is inactive, in which the availability of biomarkers for its detection and monitoring is a priority [143].
For many years, the association between JIA-U and ANA positivity has been known [24,144]. Anti-histone antibodies (AHA) have also been detected in JIA patients, increasing the sensitivity for JIA-U detection if ordered together with ANAs [25]. Inflammatory biomarkers such as ESR also seem to be a predictor for the occurrence of uveitis in JIA but the threshold to define a high risk for uveitis has not been clearly defined [145] [146].

However, larger studies are needed to establish the real utility of these biomarkers in clinical practice. As far as eye fluid is concerned, pilot studies investigating aqueous humor (AH) have found the presence of anti-parvovirus B19 antibodies even though no viral DNA was detected [147]. Transthyretin has also been linked to ocular inflammation, but it is not clear to be specific from JIA-U [148].
Many other pro-inflammatory cytokines and chemokines have been found to be elevated in the AH of patients with clinically inactive JIA-U compared to other non-inflammatory eye conditions such as glaucoma [149] (Table 4).
Nevertheless, obtaining AH samples is not commonly feasible, and current efforts are focused on the analysis of tears for the identification of biomarkers.
Recently, Angeles-Han *et al.* collected tears using Schirmer strips from children with JIA-U (n = 20) and pediatric controls (n = 20). Calgranulins and several cytokines were measured by ELISA and Luminex assays and compared between active and inactive JIA-U and controls. Interestingly, active JIA-U had significantly increased levels of S100A12, IL-8, and soluble intercellular adhesion molecule 1 (sICAM-1) compared to inactive JIA-U [150].

Table 4. Principal biomarkers for prediction JIA-U.

Biomarker	Direction of trend	Sample	Clinical relevance	Reference
ANA	Positivity	PB	Predicts uveitis development	[24,144]
AHA	Positivity	PB	Predicts uveitis development	[25]
ESR	Increased	PB	Predicts uveitis development	[145,146]
Calgranulins	Increased	PB	Predicts uveitis development	[138,142]
Anti-parvovirus B19 antibodies	Present	AH	Correlates with the presence of uveitis	[147]
Transthyretin	Increased	AH	Correlates with the presence of uveitis (non-specific)	[148]
IL-8, MMP-2, MMP-3, MMP-9, TGFβ-1, TGFβ-2, TGFβ-3, SAA, TNFα	Increased	AH	Correlates with the presence of uveitis	[149]
IL-8, sICAM-1, S100A12	Increased	Tears	Correlates with active uveitis	[150]

Adapted from [151]. ANA: antinuclear antibodies; AHA: anti-histone antibodies; PB: peripheral blood; ESR: erythrocyte sedimentation rate; AH: aqueous humor; IL-8: interleukin 8; MMP-2: matrix metalloproteinase 2; MMP-3: matrix metalloproteinase 3; MMP-9: matrix metalloproteinase 9; MMP-9; TGFβ-1 transforming growth factor β 1; TGFβ-2: transforming growth factor β 2; TGFβ-3: transforming growth factor β 3; SAA: serum amyloid A; TNFα: tumor necrosis factor α; sICAM-1: soluble intercellular adhesion molecule 1.

1.3. High dimensional single-cell resolution profiling in juvenile idiopathic arthritis

The immunological landscape of JIA is complex and heterogeneous. As a result, it is difficult to study high-dimensional inputs at the signaling cell level using conventional technologies.
The development of single-cell technologies has the potential to provide an unprecedented amount of information that can help in understanding disease mechanisms and identifying predictive biomarkers. Mass cytometry has significantly expanded the analytical depth of cytometric assays, allowing to characterize the immune cell composition at a very high level of detail. Compared to scRNA-Seq, however, this technology is limited since the set of proteins to be measured has to be predetermined. ScRNA-seq represents an unbiased definition of single-cell expression profiles and allows for the discovery of novel transcriptional regulatory networks. The combination of these two technologies has the potential to provide predictive insights into disease mechanisms in JIA.

1.3.1. Fundamentals of mass cytometry

For many years, immunological research has relied on flow cytometry, immunohistochemistry, or immunofluorescence imaging techniques to study cellular heterogeneity. The low number of parameters that could be analyzed with these methods restricted the possibility to disentangle heterogeneous cell populations. In flow cytometry, the development of novel fluorophores, and laser systems have increased the capacity to discover new immune cell subtypes. However, technical limitations like spectral overlap or autofluorescence reduce the number of parameters to determine.

One solution to this problem was substituting the fluorescence-based probes for non-biological elemental isotopes (heavy metals) via covalent conjugation. These heavy metals, many of them from the lanthanide family, have non-overlapping masses, and

if present, minor sources of overlap (usually <1%) are isotopic impurities in the metal stocks and metal oxidation. This lack of nonspecific signal facilitates the designs of panels of up to 60 antibodies in mass cytometry (Table 5). Cells are also stained with rhodium or iridium-conjugated DNA intercalators that provide information about DNA content [152].

Table 5. Comparison of flow cytometry and mass cytometry

Characteristic	Flow cytometry	Mass cytometry
Measurement basis	Fluorescent probes	Stable mass isotopes
Sources of nonspecific signal	Spectral overlap (10-50%) Autofluorescence (5-10%) Fluorophore degradation (5-10%)	Isotopic impurity Spectral overlap and oxidation (all <5%)
Maximum number of markers	20	60
Sampling efficiency	>95%	50%
Number of cells measured per second	500 - 40,0000	50 - 1,000

After staining with the desirable antibodies, single-cell suspensions are introduced into the CyTOF analyzer where they are first nebulized into droplets and subsequently introduced into an inductively coupled plasma mass spectrometry-based readout that vaporizes, atomizes, and ionizes the sample. The resulting ion cloud is then filtered by mass to remove biologically abundant, low-mass ion species and finally analyzed by time-of-flight (TOF) mass spectrometry to quantify the abundance of all the isotopic reporter masses, which enables the quantification of bound antibodies and therefore the expression of the markers of interest [153].

The output data from the machine is in the form of a Flow Cytometry Standard file (FCS file; fcs). The FCS file structure is a standardized array with columns representing channels and rows representing events. This is used for downstream data analysis through programming languages (e.g., R) or FCS file-processing platforms (e.g. Cytobank®, FlowJo®) [154].

Firstly, data output has to be corrected by normalization, to correct machine signal variation. The two algorithms for normalization are MATLAB® based bead normalization shown by Finck *et al.* and Fluidigm's bead identification and normalization [155]. This procedure helps to remove doublets since they are a source of unwanted confounders.

Subsequently, as samples have been previously barcoded with a unique identifier and mixed in a tube before data acquisition, "debarcoding" has to be done. This means splitting the output data from each barcode into its own FCS file. In this process (which can be done manually or by using an algorithm such as CATALYST in R), it is defined which channels are positive and negative for each cell, being many unassigned events, cell-cell doublets or debris.

After normalization and debarcoding, compensation is the final data-processing step. In flow cytometry, compensation subtracts the percentage of fluorophore's spillover from the measured signal in that channel. In CyTOF, as spillover is minimal, this step is a straightforward process that can be done with the CATALYST algorithm as well [156].

The next step is data clustering based on similarities between cells. As some clusters might represent the same population with slightly different marker expressions it is important to carefully study and compare these markers within each cluster. Many clustering algorithms have been created for this purpose such as FlowSOM, X-Shift, and PhenoGraph [157].

To visualize and represent this amount of multidimensional data, dimensionality reduction algorithms can be applied to visualize the information in two dimensions. Principal component analysis (PCA), a mathematical algorithm that reduces dimensionality, and t-distributed stochastic neighbor embedding (t-SNE) are common sources of data representation. Uniform manifold approximation and projection (UMAP) is a viable alternative that overcomes some limitations of PCA and t-SNE as it preserves global structures and the pseudo-temporal ordering of cells [158]. Once clusters have been visualized and characterized, they can be annotated in R.

1.3.2. Fundamentals of single-cell RNA sequencing

Understanding and treating complex diseases such as JIA, in which the immune system is the main actor, requires an in-depth understanding of its heterogeneity and behavior. Considering that all cells in our body share an identical genotype, the differences in their gene expression allow us to study the differential activity between apparently homogeneous cells.

ScRNA-seq technology can analyze RNA molecules in individual cells with high resolution and on a genomic scale. Since the first scRNA-seq study was published in 2009, there has been an exponential increase in studies using this technology, allowing disentangling and understanding very complex cellular systems like the immune system (Figure 7).

For example, scRNA-Seq has been applied to dissect heterogeneous cell populations such as the intestine, spleen, lung, or brain as it detects underlying groups of cells in an unsupervised manner [159]. Furthermore, it can add information regarding cellular transitions between different states and reveal cell trajectories based on their transcriptome profile [160].

Also, scRNA-seq has helped to describe the process of cellular transcription, showing that it occurs in short bursts of activity, a phenomenon known as “transcriptional bursting”, rather than being a continuous process. These periods of "on" and "off" transcription are also a source of gene heterogeneity between cells [161]. Finally, this variability can be used to infer gene regulatory networks in which genes are grouped in modules of expression profile similarity [162].

Figure 7. Applications of single-cell RNA sequencing.

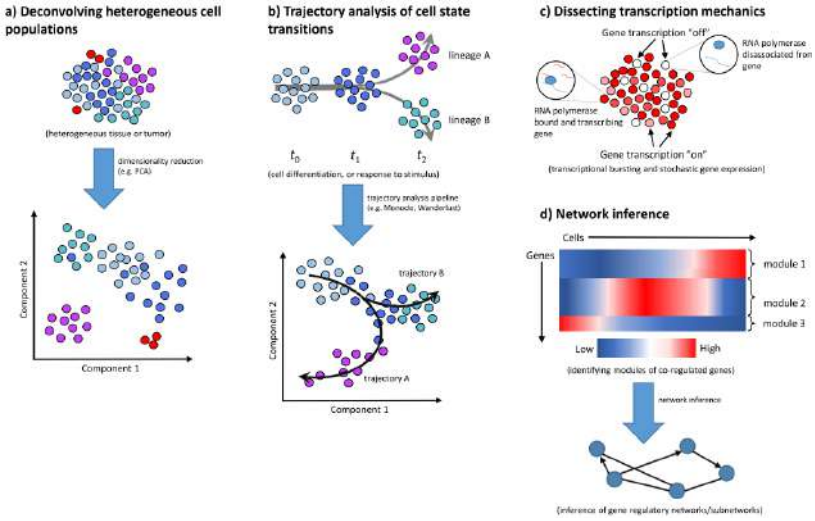

Extracted from [163]. a) Deconvolving heterogeneous cell populations. PCA: principal component analysis. b) Trajectory analysis of cell state transitions. c) Dissecting transcription mechanics. d) Network inference.

The first step in a scRNA-seq study is isolating viable, single cells from the tissue of interest. Micromanipulation techniques such as micropipetting or laser capture microdissection have been used for tissues with a low number of cells, being time-consuming techniques. Suspended cells can be sorted into individual wells using fluorescence-activated cell sorting (FACS) or microfluidics platforms such as the Fluidigm C1 robot and, more recently, droplet-based platforms (e.g., Chromium from 10x Genomics, InDrop from 1CellBio) that allow a fast assessment of many thousands of cells at a time.

Droplet-based instruments can encapsulate single cells with all the necessary reagents for cell lysis, reverse transcription, and molecular tagging in reaction vesicles called Gel Beads in emulsion, or GEMS [164].

Some tagging strategies include targeting epitopes of interest with oligonucleotide-labeled antibodies that will allow its tracking after scRNA-seq library preparation and sequencing. This technique is called Cell Hashing (Hashtag oligonucleotide, HTO) and enables a robust sample multiplexing, identification, and discrimination of low-quality cells.

Next, isolated individual cells are lysed to allow the capture of as many RNA molecules as possible. PolydT-primers are commonly used to select polyadenylated mRNA molecules instead of ribosomal RNA or transfer RNA. After capture, mRNA molecules are reverse-transcribed into stable complementary DNA (cDNA). Random-nucleotide-sequences are added to the polydT oligonucleotides in each mRNA molecule during reverse transcription serving as unique molecular identifiers (UMI) to reduce amplification biases and technical noise. UMIs also help to identify transcripts' cellular origins and quantification. cDNA can then be amplified by PCR or in vitro transcription, followed by another round of reverse transcription. Then, amplified and tagged cDNA from every cell is pooled and sequenced by NGS using library preparation protocols, similar to bulk samples.

Single-cell transcriptome coverage can be done through full-length transcript analysis or by digital counting of 3' or 5' transcript ends. The choice of sequencing should be established based on the experiment's goals. The digital counting strategy is more affordable and allows the introduction of UMIs. Regarding digital 3' or 5'-end transcript sequencing, the two assays are similar but capture different ends of the polyadenylated transcript in the final library. Both solutions use polydT primer for reverse transcription, although in the 3' assay, the polydT sequence is located on the gel bead oligo, while in the 5' assay, the polydT is supplied as an RT primer. A template switching oligo (TSO) is used in both workflows to reverse transcribe the full-length transcript.

After amplifying the cDNA, the molecules are randomly fragmented under conditions that favor 300-400 bp length fragments. Downstream of fragmentation, only transcripts containing a 10x Barcode and an Illumina Read 2 adaptor, which is ligated onto the cDNA after fragmentation, will be amplified. This results in final 10x libraries that either represent the 3' end of the transcript (as the 10x Barcode is adjacent to the polyA tail on the 3' end of the transcript) or the 5' end of the transcript (as the 10x Barcode is adjacent to the TSO and the 5' end of the transcript).

Data processing includes all the necessary steps to convert raw sequencing reads into gene expression matrices. After FASTQ files have been generated and their quality

checked, the next important step is de-multiplexing the reads using cell barcodes. Then, the reads are mapped to the reference genome with alignment tools like STAR or TopHat (171,172). In the final step, mapped reads are quantified to create a transcript expression matrix.

The analysis and interpretation of the data represent a computational challenge in constant development. Quality control checks represent a major step as poor-quality data from single cells, poor cell viability at lysis, poor mRNA recovery, and low-efficiency cDNA production should be excluded from subsequent analysis. For example, in the FACS sorting step, information about live/dead cells must be revised. Despite no consensus on exact filtering strategies, the most used criteria include relative library size, number of detected genes, and the fraction of read mapping to mitochondrial-encoded genes or synthetic spike-in RNAs that interrogate technical variability [165,166].
Furthermore, other important points must be considered, such as the correct isolation of single cells or if two or more cells (duplicates) have been captured in a particular sample by mistake.

Once the scRNA-seq data has been cleaned, novel cell types from a heterogeneous composition of cells by clustering them by their transcriptional similarity can be indentifyed. As in CyTOF, dimensionality reduction algorithms like PCA, t-SNE, and UMAP are used to represent cell distribution in two dimensions.
Several bioinformatic tools have been described to help unsupervised clustering such as Seurat, and PAGODA, among many others [167]. Differential gene expression analysis (DGE) of clusters can identify marker genes that discriminate subpopulations. Other computational algorithms are being created to analyze cell relationships and infer trajectories or intermediate cell states (Monocle2, TSCAN) [168].

Finally, to make data publicly available, most researchers share the raw data and more processed formats to repositories like The Gene Expression Omnibus (GEO) or make their computational pipelines public through databases such as GitHub [169] [170].

1.3.3. High-dimensional single-cell profiling discoveries in rheumatoid arthritis

Important discoveries using scRNA-seq and CyTOF have taken place in the study of chronic inflammatory arthritis. Because of their clinical and genetic similarity to oJIA, the most recent advances in applying these technologies to RA are discussed below (Figure 8). Various joint cell types are important in RA joint inflammation, including synovial fibroblast, macrophages, lymphocytes, and many other cells.

The first study using scRNA-seq to decode synovial tissue heterogeneity in RA was published in 2018 by Stephenson *et al.* [171]. By sequencing 20,387 single cells isolated from the joints of five RA patients, they identified two major subsets of fibroblasts characterized by the expression of DAF (CD55) and Thy-1 cell surface antigen (THY1), the latter being a promoter of inflammatory stimuli in response to an increased endothelial NOTCH3 signaling.

Later, Mizoguchi *et al.* confirmed these findings with the same technique. They examined the heterogeneity of synovial fibroblasts by collecting tissue from joint replacement surgery of patients with RA and osteoarthritis. ScRNA-seq unbiased analysis identified three major fibroblast subsets and its location in the synovial membrane: $CD34^-$ $THY1^-$ (lining membrane), $CD34^-$ $THY1^+$ (sublining, perivascular zone), and $CD34^+$ (lining and sublining membrane). Compared to osteoarthritis, $CD34^-$ $THY1^+$ fibroblasts were significantly increased in RA. The gene set enrichment analysis (GSEA) revealed significant enrichment of mitotic and proliferative genes and actively proliferated states with genes implicated in fibroblast migratory response and matrix cartilage invasiveness [172].

In addition to synovial fibroblast, the study of Zhan *et al.* described other cell populations involved in synovial inflammation performing scRNA-seq in combination with CyTOF and bulk RNA-seq [173]. They recruited 36 patients with RA and 15 patients with osteoarthritis and obtained synovial tissues from ultrasound-guided biopsies or joint replacements. 362,190 viable cells were obtained, of which 5,265 scRNA-seq profiles passed quality control, including 1,142 B cells, 1,844 fibroblasts,

750 monocytes, and 1,529 T cells. Compared to synovial osteoarthritis, the enriched populations in RA were the previously described THY1^{+} HLA-DRA^{hi} sublining fibroblasts, and IL1B^{+} pro-inflammatory monocytes, ITGAX^{+}TBX21^{+} autoimmune-associated B cells, PDCD1^{+} peripheral helper T (Tph) cells and Tfh cells. Finally, they defined distinct subsets of CD8^{+} T cells characterized by GZMK^{+}, GZMB^{+}, and GNLY^{+} phenotypes.

Subsequently, Alivernini *et al.* sought to describe the role of synovial tissue macrophages that reside in the lining layer as the key drivers of joint homeostasis. Probably differentiated from blood-derived monocytes, synovial macrophages are the main source of TNF. Using scRNA-seq, multiparameter flow cytometry, and immunofluorescent staging, they characterized changes in synovial tissue macrophage subpopulations in 45 treatment-naive active RA patients, 31 treatment-resistant active RA, 36 sustained clinical and ultrasound remission RA and 10 healthy control donors were studied. Two macrophage subpopulations (MerTK^{-} / MerTK^{+}), showed gene expression signatures enriched in negative regulators of inflammation. These macrophages abundantly produce inflammation-resolving lipid mediators and induce tissue repair mechanisms in synovial fibroblasts in vitro.
RA patients in remission with a low percentage of MerTK^{+} had an increased risk of flare, indicating that subpopulations could represent a potential treatment strategy for RA [174].

Like the previous study, Orange D *et al.* wanted to elucidate the molecular mechanisms behind a RA flare. Through the analysis of a prospectively home collection of the blood of patients with RA, they identified transcripts differentially expressed before flares. They compared these with data from synovial scRNA-seq. Consistent changes were observed in blood transcriptional profiles 1 to 2 weeks before a flare. They found that B-cell activation was followed by expansion of circulating CD45^{-} CD31^{-} PDPN^{+} preinflammatory mesenchymal cells (PRIME cells), which show transcriptional features reminiscent of inflammatory synovial sublining fibroblasts [175].
Taken together, these observations suggest a model in which sequential activation of B cells activates PRIME cells just before flares, opening the possibility to study many

other inflammatory autoimmune diseases characterized by flare/remission states like JIA.

Figure 8. Applications of high-dimensional single-cell RNA seq profiling technology in rheumatoid arthritis.

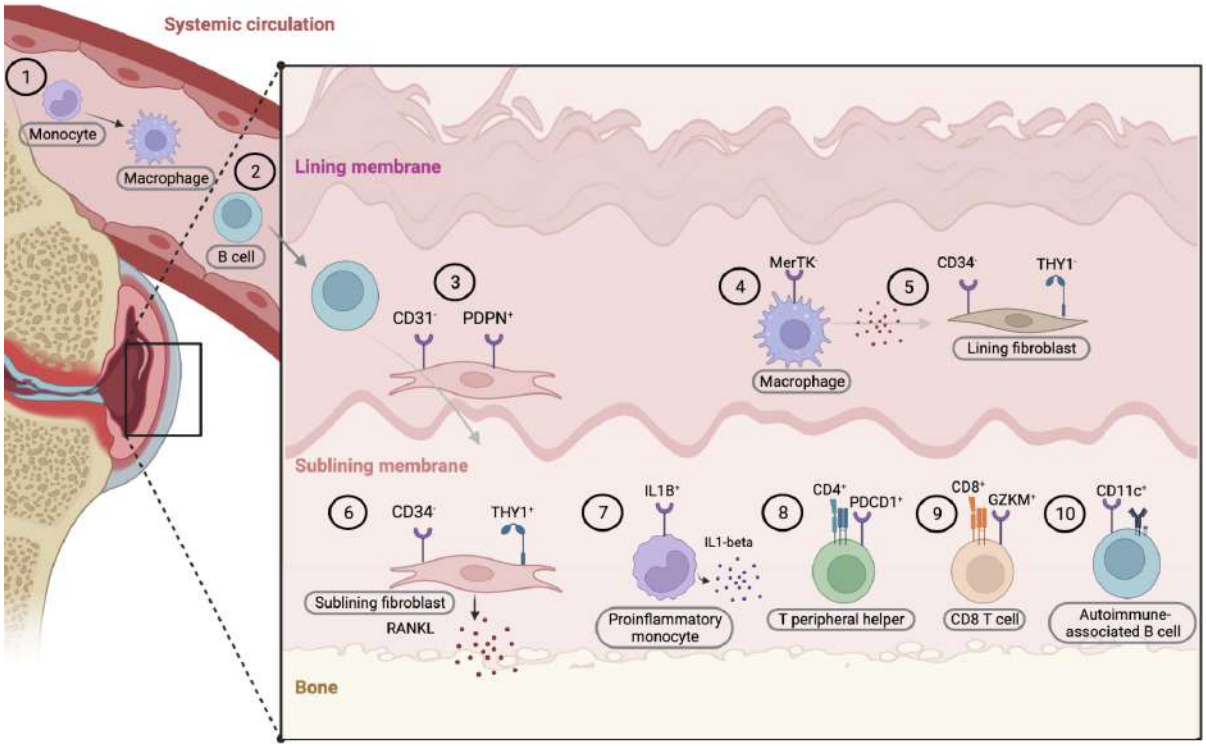

Original. Data extracted from (188-192). 1) Monocyte that differentiates into macrophages in circulation, active macrophages MerTK^{+}. 2) Naive B cells differentiate into activated B cells and contribute to the expansion of 3) circulating CD45^{-} CD31^{-} PDPN^{+} preinflammatory mesenchymal cells. 4) MerTK^{-} in higher proportion contributes to RA flare secreting proinflammatory cytokines, which activate 5) lining fibroblast CD34^{-} THY1^{-}.
6) Sublining fibroblasts CD34^{-} THY1^{+} locate in the perivascular zone and secrete proinflammatory cytokines like RANKL. 7) Proinflammatory monocytes IL1B^{+} secrete IL-1beta. 8) T peripheral helper cells PDCD1^{+} are highly abundant in RA. 9) CD8 T-cells with activated effector functions and expressing cytotoxicity markers. 10) Autoimmune-associated B cells expressing CD11c are abundant in synovial RA.
THY1: Thy-1 cell surface antigen; RANKL: Receptor Activator for Nuclear Factor κ B Ligand; PDCD1: Programmed Cell Death Protein 1; GZMK: Granzyme K; CD11c: integrin αx.

1.3.4. High-dimensional single-cell profiling discoveries in juvenile idiopathic arthritis

Following the discoveries made in RA, few studies have been published in JIA, specifically in oJIA, applying scRNA-seq in synovial tissue or synovial fluid to identify different pathogenic cell types.

The first scRNA-seq study to decipher SF heterogeneity in oJIA was uploaded to an open-access preprint repository in 2018 [176]. While it has not yet been published in a peer-review journal, the results are of interest. In this study, Velasco-Herrera *et al.* isolated 45,715 cells from the SF of inflamed knees of two treatment-naive oJIA patients and paired-peripheral blood. They identified a population of synovial innate lymphoid cells (ILCs) common to all patients, with a unique transcriptional profile compared to canonical ILC subtypes [176]. JIA ILCs were distinguished by the expression of genes associated with extracellular matrix remodeling, indicating a possible contribution of synovial ILCs to tissue homeostasis, and genes related to antigen presentation and leukocyte activation. Next, they investigated whether synovial ILCs were a universal feature of the cellular landscape of inflamed joints or a specific-JIA cell by analyzing the SF from 32 children at diagnosis or relapse following treatment, with different JIA subtypes. Flow cytometry assessment of the SF revealed significant enrichment of these cells in oJIA and polyarticular RF-negative JIA compared to the other subtypes.

Later in 2021, based on the well-known Treg/Th17 imbalance theory in oJIA SF, Julé AM *et al.* sought to determine the immunophenotype of joint infiltrating CD4+ T cells in SF and Treg stability. 36 oJIA patients provided SF, PB, and PB from 8 healthy children and 10 healthy adult controls.
First, flow cytometry revealed a higher proportion of CD8+ and CD4+ memory T cells expressing the Th1 cytokine INFγ in SF compared to PB of oJIA patients.
Bulk RNA-seq analysis of SF Tregs and Teffs revealed upregulation of IFNG and CXCR3, markers of the Th1 transcriptomic signature.

To gain insight into the heterogeneity of these Th1-skewed CD4+ T cells, scRNA-seq and TCR repertoire analysis was performed on 1,882 Tregs and 4,308 Teffs from the SF of two patients with oJIA.
High-dimensional analysis revealed 5 clusters of Tregs and 7 clusters of Teffs, and TCR repertoire analysis showed that highly expanded Teffs (> 3 clones) were concentrated in the Tph cluster. In conclusion, the results of this group show that oJIA SF is characterized by a Th1 polarization [115].

In line with the previous authors, Maschmeyer *et al.* analyzed the transcriptional and clonal heterogeneity of SF T lymphocytes in JIA by scRNA-seq combined with TCR repertoire profiling on the same cells. Cells were isolated from SF and PB of seven patients with oJIA by FACS before scRNA-seq and TCR repertoire analysis. They identified clonally expanded subpopulations of T lymphocytes expressing genes reflecting recent activation by antigen in situ. A PD-1$^+$ TOX$^+$ EOMES$^+$ population of CD4$^+$ T cells expressed immunoregulatory genes and chemoattractant genes for myeloid cells but also expressed IL-10 with the potential to downregulate the immune response. These cells were also found in the circulation and may have the potential to limit the systemic spread of inflammation by killing myeloid cells and activated cells with granzymes. Two other populations of interest were PD-1$^+$ TOX$^+$ BHLHE40$^+$ CD4$^+$ T cells and a mirror population of CD8$^+$ T cells, which were thought to support extrafollicular B cell activation and myeloid cell activation [118].

Finally, Imbach K *et al.* recently published a proof-of-principle study using scRNA-seq to analyze the effect of PBMC activation by 24-hour TNF exposure ex vivo, comparing six newly diagnosed oJIA patients with two HC.
Although the amount of TNF present in SF is not predictive of patient response to TNF inhibition, it may be possible to identify a subset of responders based on the differential transcriptional response to TNF stimulation. 45,943 cells were analyzed, identifying 17 cell clusters grouped into nine T cell populations, three NK cell types, naive and memory B cells, monocytes, macrophages, and monocyte-derived dendritic cells. Following TNF stimulation, the abundance of many cell types was significantly affected, increasing memory CD8$^+$ T cells and NK cells, but a down-regulation of naïve B cell proportions. Significant differential expression responses to TNF stimulus were

also characterized, with monocytes showing more transcriptional shifts than T-lymphocyte subsets, while the B-cell response was more limited.

2. Hypothesis

Juvenile idiopathic oligoarticular arthritis (oJIA) is the most common form of childhood arthritis. A subset of patients with JIAoA is at risk of developing uveitis, which can be sight threatening and therefore carries a considerable risk of morbidity in these patients. However, its etiology is still not fully understood, especially in comparison to other less common forms of JIA.

Recently, single-cell RNA sequencing (scRNA-seq) has emerged as a powerful tool in the field of next-generation sequencing. This technology has the potential to transform our understanding of the pathogenic basis of many diseases, enabling the identification of previously undetectable cellular subtypes.

This project aims to test the hypothesis that a detailed and individualized characterization of the immune landscape and proteome profile of oJIA patients using scRNA-seq and proteomics can identify specific pathogenic cell populations, which will be later replicate by CyTOF, and biomarkers associated with the disease and with the development of uveitis.

I will determine the association between the pathogenic cells found in both oJIA and uveitis, a fact that will have a high translational potential and could ultimately contribute to significantly improve the treatment of this childhood disease.

3. Objectives

3.1. Primary objective

The main aim of this study is to identify the different biological mechanisms associated with oligoarticular juvenile idiopathic arthritis and to identify and compare the abundance of different cell types in oJIA with healthy controls and other diseases.

3.2. Secondary objectives

1. - To describe the first single-cell RNA seq atlas of blood and synovial fluid from patients with oligoarticular juvenile idiopathic arthritis.

2. - To determine the usefulness of the probably pathogenic cellular populations as biomarkers for the diagnosis of oJIA and oJIA uveitis.

3. - To identify and compare the abundance of different proteins that can serve as biomarkers in the diagnosis, the presence of uveitis and the response to treatment of patients with oligoarticular juvenile idiopathic arthritis.

4. Material and Methods

4.1. Origins of pediatric rheumatology research at the hospital

The Pediatric Rheumatology Unit (PRU) is currently staffed by two paediatric rheumatologists, Drs. Estefanía Moreno and Mireia Lopez, and a paediatrician, Dr. Laia Martínez.
Th PRU has been a national reference and a center of excellence in diagnosing, treating, and researching rheumatic diseases in children for more than 25 years.

In the research field, the PRU is part of the Grup de Recerca de Reumatologia (GRR-VHIR), a research group led by Prof. S Marsal that specializes in the study of immune-mediated inflammatory diseases (IMIDs). The GRR is a reference translational research group in this area with publications in leading journals. The group's research includes a line of precision medicine for IMIDs, focusing on studying prevalent diseases with significant socioeconomic impact such as RA, PsA, SLE, Crohn's disease, Ulcerative Colitis, and JIA using various genomic approaches. The group performed the first GWAS in Spain, and other genomic approaches such as metabolomics, methylomics, and transcriptomics on relevant immune system cells have been incorporated [177–180].

In the context of the GRR-VHIR, the PRU has led several research studies, including the "Epidemiological Study of Juvenile Idiopathic Arthritis" in Catalonia conducted by Dr. Consuelo Modesto, funded by the Fundació Marató TV3. This study is one of the few epidemiological investigations conducted in southern Europe and the only one in Spain [4]. Another area of utmost relevance for the PRU is the investigation of immunological differences in JIA concerning the response to anti-TNF treatment (Instituto Carlos III, PI Prof. Sara Marsal PI13/00857, PhD student Dr. Estefanía Quesada). This study integrates clinical data, cytometry, and ultrasound data to determine complex response patterns to biologics [181].

Dr. Moreno and Lopez involved at the national level in the first multicenter registry of JIA patients in the transition period (JUVENSER), led by the Spanish Society of

Rheumatology, and actively collaborates with various working groups of the Spanish Society of Pediatric Rheumatology [182].

Dr. Moreno, Mitjana and Lopez participate in various international studies led by PRINTO and the PRCSG. It is an active collaborator in the European Pharmachild project on pharmacovigilance, which is funded by the European Economic Community [183].

However, the need to implement a quality training program in pediatric rheumatology has become increasingly evident in recent years. To address this need, the Instituto Carlos III, the managing body for the activities of the Acción Estratégica en Salud (AES) included in the State Plan for Scientific, Technical, and Innovation Research, has implemented the State Program for the Promotion of Talent and its Employability in R+D+I, through the Río Hortega subprogram. In the 2018 call, Prof. Sara Marsal presented a training program in this medical subspecialty, allowing the doctoral student, Dr. Mireia Lopez, to receive training and carry out translational research in an area of high impact and great relevance in the pediatric population. The favorable result of the call (CM18/00012) has enabled the execution of the training program and the development of this doctoral thesis project on juvenile idiopathic arthritis.

Always working to give patient-centered care, the PRU currently offers a daily assistance activity of highly specialized clinical care in JIA, including assistance in pediatric hospitalization and pediatric day hospital, working closely with pediatric ophthalmology specialists for the diagnosis and follow-up of JIA-associated uveitis, as well as with other pediatric specialists when needed.

Patients included in this research project were prospectively recruited from the PRU outpatient clinic, pediatric ophthalmology outpatient clinic, and the inflammatory arthritis unit (Unitat d'Artritis Inflamatòries - UAI) in the Rheumatology Department of the Vall Hebron University Hospital.

4.2. Study design and subjects

The present prospective observational study includes two stages of patient recruitment (Figure 9).

In the first stage, the objective was to capture the best representation of the pathological cell subsets in peripheral blood and synovial fluid from oJIA patients with new onset of the disease.
For this purpose, samples were obtained from children with oJIA who hadn't ever received any treatment, whose diagnosis was made in accordance with the ILAR classification criteria for JIA. All the patients were admitted for an articular aspiration from the knee at the pediatric rheumatology unit at Vall d'Hebron Barcelona Hospital Campus.
Blood samples from JIA-U patients with a flare under treatment were obtained from the pediatric ophthalmology department.
Peripheral blood samples were taken from age- and sex-matched healthy children, relatives of patients with other non-immune related diseases.

In the second stage, the objective was to validate the pathological cell subsets found at the first stage as well as to determine different protein markers that could be found in greater abundance in each of the conditions.
For this purpose, a prospective validation cohort of patients with different conditions have been recruited:

1. Group 1: patients with oJIA onset who hadn't ever received any treatment. Peripheral blood samples were extracted, and SF samples when fluid aspiration was productive.
2. Group 2: patients with oJIA who initiate an anti-TNF therapy have been obtained at two-time points, just before its initiation (week 0) and at week 12 of treatment. Peripheral blood samples were extracted.
3. Group 3: patients with oJIA under treatment with a cDMARD in clinical remission. Peripheral blood samples were extracted.

4. Group 4: patients with oJIA who present a uveitis flare. Peripheral blood samples were extracted.
5. Group 5: patients with polyarticular JIA with a de novo onset who hadn't ever received any treatment. Peripheral blood samples were extracted.
6. Group 6: patients with rheumatoid arthritis with a de novo onset who hadn't ever received any treatment. Peripheral blood samples were extracted.
7. Group 7: healthy children matched by age and sex were recruited. Peripheral blood samples were extracted.

Figure 9. The two phases of the study are represented graphically.

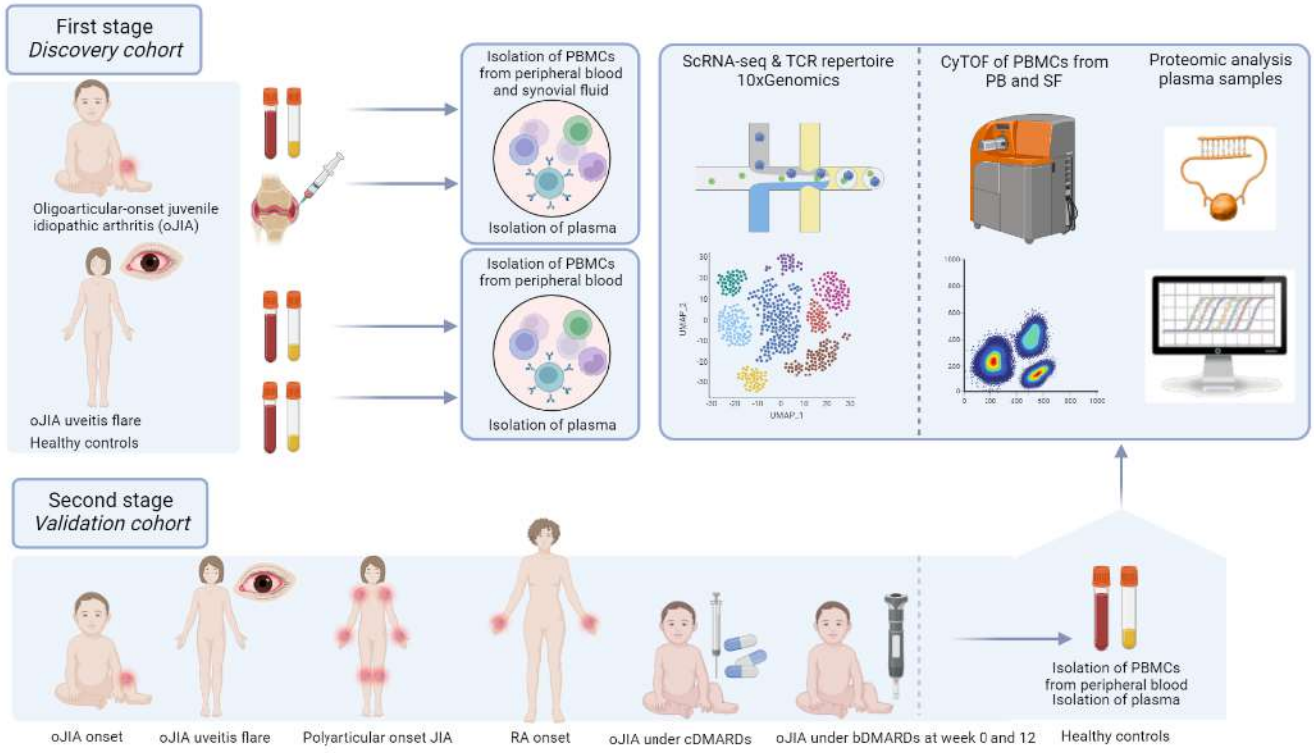

This figure graphically represents the two stages of the project. On the one hand, in the discovery stage, SF and PB samples have been obtained from patients with debut oJIA and patients with uveitis outbreak, and the study has been carried out using scRNA-seq. In the second stage of the study, PB samples have been collected from patients with different conditions, a proteomic study has been performed, and CyTOF will perform a validation of the pathogenic cells found in the first stage.
oJIA: Oligoarticular juvenile idiopathic arthritis; PBMCs: Peripheral blood mononuclear cells; PB: peripheral blood; SF: synovial fluid; RA: rheumatoid arthritis; cDMARDS: conventional disease-modifying antirheumatic drugs; bDMARDs: biological disease-modifying antirheumatic drugs.

4.2.1. Inclusion and exclusion criteria

First stage: discovery cohort

Oligoarticular-onset JIA

a) Inclusion criteria:

- Children less than 16 years old with arthritis that affects one to four joints for at least 6 weeks.
- Have never received glucocorticosteroids or immunosuppressants (oral or injected). Treatment with AINEs is allowed.

b) Exclusion criteria:

- Psoriasis or a history of psoriasis in the patient or first-degree relative.
- Arthritis in an HLA-B27 positive male beginning after 5 years of age.
- Ankylosing spondylitis, enthesitis-related arthritis, sacroiliitis with inflammatory bowel disease, Reiter syndrome or acute anterior uveitis, or a history of one of these disorders in a first-degree relative.
- The presence of IgM rheumatoid factor on at least two occasions at least 3 months apart.
- The presence of systemic juvenile idiopathic arthritis in the patient.
- Differential diagnosis different from oJIA (i.e. septic arthritis, reactive arthritis).

Oligoarticular JIA with a uveitis flare

a) Inclusion criteria:

- Children less than 16 years old with an oligoarticular JIA and having a uveitis flare defined by SUN criteria [33].
- Being controlled at the PRU and pediatric ophthalmology department at the Vall d'Hebron Barcelona Hospital Campus.
- Treatment with cDMARDs and bDMARDs is allowed.

b) Exclusion criteria:

- Differential diagnosis different from oJIA uveitis flare (i.e., infectious uveitis).

Healthy control children

c) Inclusion criteria:

- Children less than 16 years old.
- No previous chronic autoimmune inflammatory disease.

d) Exclusion criteria:

- Active infection at recruitment.

Second stage: validation cohort

Group 1. Oligoarticular-onset JIA

Same inclusion and exclusion criteria as the patients in the first stage.

Group 2. Patients with oJIA who initiate an anti-TNF therapy

a) Inclusion criteria:

- Children less than 16 years old with oJIA with active disease defined by JADAS27 between 2.1 and 4.2 points.
- Being controlled at the PRU at the Vall d'Hebron Barcelona Hospital Campus.
- Treatment with cDMARDs is allowed.

b) Exclusion criteria:

- Same exclusion criteria related to the diagnosis of oJIA.
- Have never received treatment with anti-TNF therapy.
- Unable to commit to follow-up in the unit at week 12 of treatment.

Group 3. Patients with oJIA under treatment with a cDMARD in clinical remission

a) Inclusion criteria:

- Children less than 16 years old with oJIA with inactive disease defined by JADAS27 less than 1 under treatment with cDMARDs.
- Being controlled at the PRU at the Vall d'Hebron Barcelona Hospital Campus.

b) Exclusion criteria:

- Same exclusion criteria related to the diagnosis of oJIA.
- Have never received treatment with anti-TNF therapy.

Group 4. Patients with oJIA who present a uveitis flare

Same inclusion and exclusion criteria as the patients in the first stage.

Group 5. Patients with polyarticular FR-negative JIA onset

a) Inclusion criteria:

- Children less than 16 years old with arthritis that affects five or more joints for at least 6 weeks with active disease defined by JADAS27 higher than 3.9 points. The test for rheumatoid factor is negative.
- Have never received glucocorticosteroids or immunosuppressants (oral or injected). Treatment with AINEs is allowed.

b) Exclusion criteria:

- Psoriasis or a history of psoriasis in the patient or first-degree relative.
- Arthritis in an HLA-B27 positive male beginning after 5 years of age..
- Ankylosing spondylitis, enthesitis-related arthritis, sacroiliitis with inflammatory bowel disease, Reiter syndrome or acute anterior uveitis, or a history of one of these disorders in a first-degree relative.
- The presence of IgM rheumatoid factor on at least two occasions at least 3 months apart.
- The presence of systemic juvenile idiopathic arthritis in the patient.
- Differential diagnosis different from polyarticular FR-negative JIA (i.e. septic arthritis, reactive arthritis).

Group 6. Rheumatoid arthritis onset

a) Inclusion criteria:

- Adults older than 18 years old who fulfill the EULAR/ACR classification criteria for RA [184].
- Have never received glucocorticosteroids or immunosuppressants (oral or injected). Treatment with AINEs is allowed.

b) Exclusion criteria:

- Active infection at recruitment.

Group 7. Healthy control children

c) Inclusion criteria:

- Children less than 16 years old
- No previous chronic autoimmune inflammatory disease

d) Exclusion criteria:

- Active infection at recruitment

4.2.2. Study protocol

The study protocol for the discovery cohort included a visit at the time of diagnosis of oJIA to assess whether the patient met the inclusion criteria and none of the exclusion criteria, and to obtain informed consent.
A second visit, at a maximum interval of 1 to 2 weeks, was performed to collect synovial fluid and peripheral blood. Synovial fluid aspiration from the affected knee was performed in all cases with appropriate sedation and under aseptic conditions in the Paediatric Multidisciplinary Cabinet of the Vall d'Hebron Barcelona Hospital Campus. All aspirations were performed by the PhD student. Peripheral blood samples were taken by trained personnel.

In the case of patients with uveitis, all patients with oJIA were followed in the paediatric ophthalmology unit. If a relapse of uveitis was detected at any of the follow-up visits, the treating ophthalmologist contacted the doctoral student who had seen the patient on the same day and assessed whether the patient met the inclusion and exclusion criteria. Informed consent was obtained, and a peripheral blood sample was taken by trained staff.

The study protocol for the validation cohort was the same as for the discovery cohort, except that patients with first-onset rheumatoid arthritis were seen at the UAI in the Rheumatology Department of Vall Hebron University Hospital.
The treating rheumatologist notified the PhD student who saw the patient within a maximum of 5 days and assessed whether the patient met the inclusion and exclusion criteria. Informed consent was obtained, and a peripheral blood sample was taken by trained staff.

Afterward, an exhaustive anamnesis was made to the participants to record the following clinical and laboratory variables:

4.2.2.1. Epidemiological variables

- Age
- Gender

4.2.2.2. Disease-related variables

- Date of oJIA diagnosis
- Date of onset of ocular involvement
- Concomitant treatment with cDMARDs or bDMARDs

4.2.2.3. Disease activity and presence of uveitis

- Physical general exploration
- In the case of oJIA, oJIA-U, and poly RF-negative JIA, JADAS 27 which includes:
    - PGA: measured on a 0-10 VAS where 0 = no activity and 10 = maximum activity
    - Parent global assessment of well-being: measured on a 0-10 VAS where 0 = very well and 10 = very poor
    - Count of 27 joints with active disease (cervical spine, elbows, carpals, metacarpophalangeal joints of the first to third fingers, proximal interphalangeal joints of the hands, hips, knees, and ankles): the number of joints that are painful and/or swollen
    - ESR normalized to a 0 to 10 scale
- In the case of RA, DAS28 was measured:
    - Number of swollen joints
    - Number of painful joints
    - ESR (mm/h)
    - PGA
- SUN activity index for oJIA-U flares [21]:
    - Grade of flare
    - Grade of cellularity
- ANA: positivity if a titer greater than 1:160
- ESR (mm/h)
- CRP (mg/dl)

4.3. Data collection

The annotation of the clinical and epidemiological data obtained from each individual was registered in a database developed at the GRR-VHIR. This lab has more than 20 years of experience in coordinating data collection for different studies. The database was hosted on the 10 terabyte server in Dr Marsal's laboratory. This database also stored the scRNA-seq data (first stage, discovery cohort), the proteomic data (second stage, validation cohort), and will store de CyTOF data (second stage, validation cohort).

4.4. Biological sample collection

Obtaining biological samples from pediatric patients is challenging due to the small amount of blood per kg of body weight that can be collected for each test.
In addition, due to the patient's size, the amount of synovial fluid produced is usually less than in adults.
For these reasons, a specific protocol has been developed to obtain PBMCs and plasma using the smallest possible blood volume. A specific protocol has also been established to isolate PMBCs from synovial fluid.
All samples have been stored in the IMID biobank with maximum preservation guarantees, allowing us to use these samples in future research projects.
The full protocols for obtaining biological samples from JIA and RA patients and healthy individuals are described below.

4.4.1. Procedure to isolate plasma mononuclear cells from blood and synovial fluid

4.4.1.1. Scope of application

The described procedure has been carried out in a class II biosafety cabinet at the GRR-VHIR laboratory always following the laboratory work standards. The persons in charge of carrying out this task were the qualified personnel of the GRR-VHIR laboratory and the PhD candidate.

4.4.1.2. Material

Biological material

Blood 20 ml: 12 ml in two ACD tubes from which the Peripheral Blood Mononuclear Cells (PBMCs) isolation has been performed and 8 ml from an EDTA tube, from which the plasma and buffy coat fraction have been separated.

Synovial fluid: variable volume depending on the quantity extracted and obtained in Heparin tubes. Used to the isolation of Synovial Fluid Mononuclear Cells (SFMCs).

Reagents

- 70% alcohol
- Ficoll-Paque PLUS (GE-Healthcare, 17-1440-82)
- Sterile Dulbecco's Phosphate Buffered Saline (DPBS) (Gibco, 14190)
- RPMI 1640 Medium (4.5 g/L D-glucose, 1.5 g/L Sodium Bicarbonate, 1 mM Sodium Pyruvate, 10 mM HEPES and 300 mg/L L-glutamine) (Gibco, A10491)
- Hyaluronidase (2.5 mg/ml) (Sigma, H3506).
- Fetal Bovine Serum, heat-inactivated (Sigma, 4135-500ML)
- Sterile dimethylsulfoxide (DMSO) (Sigma, D2650)
- Penicillin 10.000 - Streptomycin 10.000 (Mixture) (Lonza,17-602F)
- Trypan Blue cell counting (Sigma, T8154)
- Freezing media: RPMI 1640 with 15% heat-inactivated fetal bovine serum, 10% DMSO and penicillin-streptomycin 1:1000

Consumables

- BD Vacutainer ACD Solution B, 6mL (BD, 367756)
- BD Vacutainer K2 (EDTA), 10mL (BD, 367525)
- LH Lithium Heparin, 9ml (Vacuette, 455084)
- Sterile Pasteur pipettes.
- Sterile graduated serological pipettes
- Sterile tips with filter for P1000 and P100 micropipette
- Sterile 50 ml and 15 ml Falcon conical tubes with screw cap
- Sterile Eppendorf tubes

Equipment

- Class II biosafety cabinet
- Mechanical pipette controller
- P1000 and P100 micropipette
- Centrifuge with swing-out rotor
- Water Bath
- Neubauer chamber
- Phase contrast microscope (common services PCB)
- Cryo Freezing Container (Mr. Frosty, Nalgene)
- -80ºC Ultra-freezer
- Phase liquid nitrogen tank

4.4.1.3. Procedure

MCs isolation from peripheral blood

1. Once whole blood samples were obtained by peripheral venipuncture, the ACD tubes were sent immediately to the GRR-VHIR laboratory and processed in less than 2 hours after blood extraction.

2. Blood from ACD tubes was poured into a 50 ml Falcon tube and an equal volume of RPMI culture medium was added.

3. The mixture of blood and RPMI medium was homogenized for 15 min in a roll homogenizer at room temperature (RT).

4. The amount of Ficoll needed (3:4 ratio Ficoll: blood and RPMI mix) was added to a new 50 ml Falcon tube with a serological pipette.

5. The blood-RPMI culture medium mix was pipetted, very slowly, with a serological pipette onto the Ficoll.

6. A slow centrifugation at 1200 rpm for 30 minutes at RT was performed, without acceleration or deceleration, to get the PBMCs layer formed.

7. The PBMCs layer was carefully aspirated with a Pasteur pipette and transferred into a 50 ml Falcon tube with 10 ml of RPMI. More RPMI was added up to 20 ml.

8. A centrifuge at 400×g for 15 minutes at RT was performed and the supernatant was discarded.

9. The pellet was resuspended in 10 ml of RPMI and centrifuged again at 400×g for 10 minutes at RT.

10. Following a second washing step with 10 ml of medium and 10-minute centrifugation at 400×g, PBMCs were resuspended in 4 aliquots of freezing media.

11. 25 ul of the cell suspension were mixed with an equal amount of Trypan Blue, (marker for viable cells), and counted in a Neubauer chamber.

12. PBMCs aliquots were gradually frozen using a Cryo Freezing Container (Mr. Frosty, Nalgene) at −80°C for 24 h and then stored in a vapor-phase liquid nitrogen tank at −150 °C.

Plasma and buffy coat separation from blood

1. Once whole blood samples were obtained by peripheral venipuncture, the EDTA tube was sent immediately to the GRR-VHIR laboratory and processed in less than 2 hours after blood extraction.

2. In the laboratory, blood in the EDTA tube was centrifuged for 10 min, at 1500×g and RT.

3. The resulting plasma layer (upper interface) was gently aspirated with a Pasteur pipette, transferred to a 15 ml Falcon tube, and centrifuged again for 5 min, at 2500×g, to eliminate platelets.

4. The clean plasma supernatant was then aliquoted and stored at -80ºC.

5. The rest of the blood (with the buffy coat layer) was vortexed for 10 seconds to homogenize, aliquoted and stored also at -80ºC.

MCs isolation from synovial fluid

1. SF was extracted by arthrocentesis under aseptic conditions. A variable volume of SF was obtained for each patient.

The heparin tube with SF was immediately sent to the GRR-VHIR laboratory and processed in less than 2 hours.

2. SF from heparin tube was poured into a 15 ml Falcon tube and hyaluronidase enzyme was added (0.2 ml of hyaluronidase / 6 ml of SF). The mix was incubated for 30 min in a water bath at 37ºC.

3. After incubation, twice the volume of RPMI medium was added to the mix of SF and hyaluronidase.

4. A 50 ml Falcon tube was prepared with the amount of Ficoll needed (3:4 ratio Ficoll: SF and RPMI mix). Then, the mix of SF and RPMI was pipetted very slowly with a serological pipette onto the Ficoll.

5. A slow centrifugation at 580×g for 20 minutes at RT, without acceleration or deceleration, was performed.

6. The layer of SFMCs was carefully aspirated with a Pasteur pipette and transferred to a 50 ml Falcon with 10 ml of RPMI medium. More RPMI was added up to 20 ml.

7. A centrifuge at 400×g for 15 minutes at RT was performed and the supernatant was discarded.

8. SFMCs were resuspended in 4 aliquots of freezing media.

9. 25 ul of the cell suspension were mixed with an equal amount of Trypan Blue and counted in a Neubauer chamber.

10. SFMCs aliquots were gradually frozen using a Cryo Freezing Container (Mr. Frosty, Nalgene) at −80°C for 24 h and then stored in a vapor-phase liquid nitrogen tank at −150 °C.

4.5. Droplet-based single-cell RNA sequencing

Paired cryopreserved PBMCs and SF samples from oJIA patients and PBMCs from matched healthy individuals, as well as cryopreserved PBMCs from patients with JIA-U and matched healthy individuals, were rapidly thawed in a 37ºC water bath and transferred to 15 ml Falcon tubes containing pre-warmed thawing medium (Hibernate-E supplemented with 10% FBS).
Samples were centrifuged at 500 x g for 10 min at room temperature, washed once, and resuspended in PBS + 0.05% BSA. Cell number and viability were verified using a TC20™ automated cell counter (Bio Rad).

Samples were stained with DAPI and FACS sorted using a FACSAria™ Fusion Flow Cytometer (BD Biosciences) to isolate live cells and remove dead cells, red blood cells, platelets, and cell debris. The sorted cells were counted, centrifuged, and resuspended with an appropriate volume of Cell Staining Buffer (BioLegend, Cat# 420201). Cell hashing was performed using TotalSeqTM™ C antibodies (BioLegend) according to the manufacturer's instructions.

Specifically, in the case of paired PBMCs and synovial fluid samples, synovial fluid cells were labeled with TotalSeqTM C anti-human hashtag 1, while PBMCs were split into three tubes to which TotalSeqTM C anti-human hashtags 2, 3, and 4 were added to label cells.

For unpaired PBMC samples, cells were split into four tubes and labeled with TotalSeqTM C anti-human hashtag 1-4. After hashing, cells from paired PBMCs and synovial fluid were pooled in a 3:1 ratio, filtered through a 40 µm strainer, and loaded into the Chromium Controller (10X Genomics) to achieve a theoretical target recovery of 25K total cells per case. Similarly, in the case of unpaired PBMCs, cells from the four tubes were pooled, and filtered through a 40 µm strainer, and 25 K target cells were encapsulated.

Single-cell sequencing libraries were prepared using the Chromium Next GEM Single Cell V(D)J Reagent Kits v1.1 with Feature Barcode technology for Cell Surface Protein (10X Genomics, Cat. No. 1000165) according to the manufacturer's instructions. Briefly, after GEM-RT clean-up, cDNA was amplified for 13 cycles, and a SPRI selection clean-up was performed to separate the amplified cDNA molecules for 5' gene expression and the HTO cDNA. cDNA quantification was performed on an Agilent Bioanalyzer High Sensitivity chip (Agilent Technologies).

TCR genes were enriched by targeted amplification and 50 ng of the enriched cDNA obtained was used to prepare TCR-enriched libraries. 1-25 ng of mRNA-derived cDNA was used for GEX library construction, while 5 µl of hashtag-derived cDNA was used to amplify the corresponding library. GEX and TCR libraries were indexed by PCR using PN-2000240 Single Index Plate T Set A, while HTO libraries were indexed using PN-3000427 Single Index Plate N Set A.

Size distribution and library concentration was determined using a Bioanalyzer High Sensitivity chip (Agilent Technologies).
Finally, the libraries obtained were sequenced on an Illumina NovaSeq 6000 sequencer to obtain approximately 40,000 read pairs per cell in the case of the 5'GEX library and a minimum of 5,000 read pairs per cell for the TCR and HTO libraries.

4.6. Proteomic analysis

Based on the scRNA-seq study results in the discovery cohort, which analyzed cellular proportions and differential gene expression, and considering the existing findings in the published literature, several noteworthy proteins were identified.
To further explore these findings, three precision proteomic panels were utilized: cardiometabolic, immuno-oncology, and inflammation.
Collectively, these panels allowed for the simultaneous investigation of 276 biomarkers. Notably, 235 of these biomarkers were unique to specific panels, providing a comprehensive and diverse set of proteins for analysis. For a detailed account of all the biomarkers that were examined, please refer to Supplementary Table 1.

The proximity extension assay (PEA; Olink Bioscience) was performed on plasma samples from the discovery and validation cohorts at the Olink Bioscience Center in Uppsala, Sweden. One µl of plasma was used for each measurement, and triplicates were run for each sample according to the manufacturer's instructions [185].
The three core steps of the technology are based on a first incubation step in which the panel of antibodies selected overnight (16-22 hours) and labeled with DNA oligonucleotides bind to their respective protein in the samples.
This is followed by a 2-hour extension and amplification step in which the oligonucleotides are hybridized and extended using a DNA polymerase.
This newly created piece of DNA barcode is amplified by PCR.
Finally, during the 4.5-hour detection step, the amount of each DNA barcode is quantified by microfluidic qPCR.

4.7. CyTOF panel design, antibody labeling, titration, and staining

4.7.1. Antibody Panel design

As in conventional flow cytometry, antibody panel design is key to CyTOF experiments. In our study, marker selection was determined by combining biological knowledge from the literature and relevant biological information obtained in the first stage of scRNA-seq application regarding cellular proportions and differential expression analysis of genes in these overrepresented cells.

As cells are atomized and ionized in the mass cytometer, the data lack the side scatter (SSC) and forward scatter (FSC) parameters obtained in conventional flow cytometry. Therefore, CyTOF relies on the use of a DNA intercalator to provide information on correct cell staining. Another key marker is cisplatin, which gives us information about cell viability. Cisplatin is a chemotherapeutic drug that functions by binding to DNA and inducing cross-links, leading to DNA damage and cell death. In the context of cell viability assessment in CyTOF, cisplatin is used at a sublethal concentration. It is added to the cell suspension and allowed to incubate briefly, preferentially labeling cells that have compromised plasma membranes, such as dead or dying cells[154].

The next step in panel design is to pair an antibody with a metal isotope that will provide optimal signal intensity with minimal overlap. Many reference resources are available to support mass cytometry panel design. For this project, we relied on Fluidigm's Maxpar® Panel Designer, an interactive web-based application that simplifies and optimizes panel design. It allows users to build a panel using antibodies from the Fluidigm® catalog and custom conjugates. The tool calculates and visualizes the predicted signal overlap for each panel, which is the main source of noise due to isotopic contamination, oxide formation, and abundance sensitivity. Maxpar Panel Designer quantifies the predicted background signal in all channels of the panel and provides a signal and tolerance number for signal overlap within its channel.
A final panel of 32 target antibodies was selected (Table 6, Figure 10). The selection of markers was established based on the literature review and the results of scRNA-seq of the first stage.

In other to characterize in-depth CD8 effector memory T cells, NKs, and monocytes, we selected the following markers:

- *For CD8 T cells:*
    - CD3: is a transmembrane subunit of the TCR complex and plays a role in antigen recognition, signal transduction, and T cell activation.
    - CD4: is a transmembrane glycoprotein expressed on the helper subset of T cells, on immature T cells in the thymus, and weakly on monocytes and dendritic cells.
    - CD8a: is found on the majority of thymocytes and NK cells. CD8 acts as a co-receptor with MHC class I-restricted T cell receptors in antigen recognition.
    - CD45: also known as leukocyte common antigen (LCA), is expressed on the plasma membrane of all hematopoietic cells except mature red blood cells, platelets, and some plasma cells. It is a positive marker for effector memory CD8 T cells.
    - CD45RA: is a specific splice variant of the transmembrane tyrosine phosphatase CD45. The CD45RA isoform is most highly expressed in resting/naive T cells. It is negative in most activated and effector memory T cells.
    - CD45RO: is a splice variant of CD45, expressed on activated memory T cells. It is a negative marker for NK and B cells.
    - CD27: also known as S152 and T14, binds to CD70 and plays a key role in regulating B cell activation and immunoglobulin synthesis. It is a negative marker for effector memory CD8 T cells.
    - CCL5: marker differentially expressed in activated effector memory CD8 T cells from scRNA-seq data. It is an intracellular marker that has to be previously stimulated.
    - CX3CR1: is a G protein-coupled receptor with 7 transmembrane regions. CX3CR1 is expressed by M2-polarized macrophages, a subset of monocytes, dendritic cells, mast cells, natural killer (NK) cells, and subsets of memory T cells. Bound to its ligand CX3CL1 (fractalkine), CX3CR1 mediates leukocyte recruitment during inflammation and is involved in cell adhesion and extravasation from blood vessels.

- CXCR6 (CD186): CXCR6 is a 39 kDa, G protein-coupled chemokine receptor with 7 transmembrane-spanning regions, also known as CD186. It is expressed on activated and memory T cells and is involved in the recruitment of cells during the inflammatory response. It is also a marker of tissue residency.
- GZMA: marker DEG in activated effector memory CD8 T cells from scRNA-seq data. It is an intracellular marker that has to be previously stimulated.
- CCR7, also known as CD197, binds CCL19 and CCL21. These two cytokines are expressed on lymph nodes and guide the homing of naive and central memory T cells (both expressing CCR7). Activated and effector memory T cells egress from the lymph nodes by downregulating this cytokine receptor.

  CCR7 and its ligands link innate and adaptive immunity through their effects on interactions between T cells and dendritic cells. Both memory ($CD45RO^+$) and naïve ($CD45RA^+$) $CD4^+$ and $CD8^+$ T cells express the CCR7 receptor. Within the memory T cell population, CCR7 expression discriminates between T cells with effector function that can migrate to inflamed tissues ($CCR7^-$) vs. T cells that require a secondary stimulus prior to displaying effector functions ($CCR7^+$)[186].

- *For NKs:*
  - CD16: also known as low-affinity Fc IgG receptor III, is a polypeptide-anchored transmembrane protein that binds to IgG1 and IgG3 antibodies. CD16 is low expressed for bright NKs and positive or high for dim NKs.
  - CD56: also known as neural cell adhesion molecule (NCAM), is expressed in NK cells, NK-T cells, neural lineages, and in some cancers. CD56 is a cell adhesion molecule that exists in two isoforms: CD56dim and CD56bright.
  - CD57: is a cell surface glycoprotein and is expressed on NKs and indicates its matureness. Low for bright and transitional NK; positive for dim NKs.

- CD7: a marker that helps to differentiate between NK and monocytes. Expressed in NK cells.
- FceRI: human high-affinity Fc receptor for IgE. This receptor plays a key role in the IgE-mediated allergic immune response. Marker differentially expressed in terminal and mature NK from scRNA-seq data.
- MIP-1β (macrophage inflammatory protein-1β), also known as CCL4, is a cysteine-cysteine chemokine. It is a chemoattractant for natural killer cells, monocytes, and a variety of other immune cells. Marker DEG in mature NK from scRNA-seq data. It is an intracellular marker that has to be previously stimulated.
- CD62L: also known as L-selectin, is involved in immune cell homing and is expressed on naive T cells, most B cells, most thymocytes, and subsets of memory T cells, NK cells, monocytes, and granulocytes. Is a marker of NK immaturity. Low for mature and terminal NK; positive for bright and intermediate NK.
- CD335: also known as NKp46, triggers cytotoxicity in NK cells. It is a conserved activating NK receptor.
- CD161: also known as KLRB1 and NKR-P1A, is a type II transmembrane glycoprotein expressed as a homodimer on a majority of NK cells.
- CD314: also known as NKG2D, is an activation receptor found in NK cells. It is a conserved activating NK receptor.
- CD159a: also known as NKG2A, is an inhibitory natural killer cell receptor. Low in terminal NK and positive in intermediate and bright NK.
- B2M: binds specifically to β2-microglobulin, a 12 kDa nonpolymorphic Ig-like protein. Marker DEG in mature NK cells from our scRNA-seq data.
- CD94: up-regulation of CD94 expression appears to correlate with NK cell activation. Low in terminal and positive in intermediate and bright NK cells.
- Perforin: a 70 kDa cytolytic protein, is found in the granules of cytotoxic T lymphocytes and NKs. Marker DEG in mature NK of our scRNA-seq data. It is an intracellular marker that has to be previously stimulated.

- *For monocytes:*
    - CD14: is a positive marker for monocytes.
    - HLA-DR, or human leukocyte antigen DR, is an MHC class II cell surface receptor that is expressed on B cells, activated T cells, monocytes/macrophages, dendritic cells, and other nonprofessional APCs.
    - CD33: a negative marker for NK, positive for monocytes and macrophages. Helps to differentiate between NKs and monocytes.
- *Other markers:*
    - CD19: also known as B4, is expressed on B cells, B cell progenitors, and follicular dendritic cells.
    - Ki-67 protein is a nuclear protein that is associated with cellular proliferation. It is an intracellular marker reliable of cell proliferation.
    - Cisplatin is commonly applied for live-dead discrimination because it binds covalently to cellular proteins within cells and stains cell membranes of viability-compromised cells to a much greater extent than live cells.
    - Intercalator is commonly applied to discriminate single nucleated cells from doublets. Intercalators are molecules that can bind to DNA by inserting themselves between the base pairs, resulting in fluorescence emission upon excitation. When cells are labeled with metal-tagged intercalators and run through the CyTOF instrument, the signals from the intercalators provide information about the DNA content of the cells. During data analysis, singlet events are identified based on the DNA content signal. Singlet cells are expected to have a consistent DNA content, while doublet events will show an increased DNA content due to the presence of two sets of DNA [154].

Table 6. Panel design of target antibodies.

Target	Label	Clone	Signal	Tolerance	Activation	Surface/IC	Pre-conjugated	Source
CD45	089Y	HI30	195	49	No	Surface	Yes	Fluidigm
CD8a	114Cd	RPA-T8	100	20	No	Surface	No	Biolegend
CD19	116Cd	HIB19	100	20	No	Surface	No	Biolegend
CD3	141Pr	UCHT1	153	30	No	Surface	Yes	Fluidigm
CD57	142Nd	HCD57	1000	200	No	Surface	Yes	Fluidigm
CD45RA	143Nd	HI100	130	26	No	Surface	Yes	Fluidigm
CD4	145Nd	RPA-T4	308	62	No	Surface	Yes	Fluidigm
CD7	147Sm	CD7-6B7	244	49	No	Surface	Yes	Fluidigm
FceRI	148Nd	AER-37 [CRA-1]	400	100	No	Surface	No	Biolegend
CD45RO	149Sm	UCHL1	60	12	No	Surface	Yes	Fluidigm
MIP-1beta (CCL4)	150Nd	D21-1351	243	49	Yes	Intracellular	Yes	Fluidigm
CD14	151Eu	M5E2	62	12	No	Surface	Yes	Fluidigm
CD62L (L-selectin)	153Eu	DREG-56	26	5	No	Surface	Yes	Fluidigm
CD27	155Gd	L128	136	27	No	Surface	Yes	Fluidigm
CD33	158Gd	WM53	176	35	No	Surface	Yes	Fluidigm
CCL5	159Tb	VL1	30	6	No	Intracellular	No	Biolegend
CXCR6 (CD186)	160Gd	K041E5	26	5	No	Surface	Yes	Fluidigm
GzmA	161Dy	CB9	50	10	No	Intracellular	No	Biolegend
CD335 (NKp46)	162Dy	BAB281	14	3	No	Surface	Yes	Fluidigm
CD161	164Dy	HP-3G10	67	13	No	Surface	Yes	Fluidigm
CD314 (NKG2D)	166Er	ON72	60	12	No	Surface	Yes	Fluidigm
CD197 (CCR7)	167Er	G043H7	201	40	No	Surface	Yes	Fluidigm
Ki67	168Er	B56	100	20	Yes	Intracellular	Yes	Fluidigm
CD159a (NKG2A)	169Tm	Z199	76	15	No	Surface	Yes	Fluidigm
B2M	170Er	2M2	800	150	No	Surface	Yes	Fluidigm
CX3CR1	172Yb	2A9-1	30	6	No	Surface	No	Biolegend
HLA-DR	173Yb	L243	168	34	No	Surface	Yes	Fluidigm

CD94	174Yb	HP-3D9	86	17	No	Surface	Yes	Fluidigm
Perforin	175Lu	B-D48	533	107	No	Intracellular	Yes	Fluidigm
CD56 (NCAM)	176Yb	NCAM16.2	91	18	No	Surface	Yes	Fluidigm
CD16	209Bi	3G8	259	52	No	Surface	Yes	Fluidigm
Cell-ID Cisplatin	195Pt	n/a	n/a	n/a	n/a	n/a	Yes	Fluidigm
Intercalator	191Ir	n/a	n/a	n/a	n/a	n/a	Yes	Fluidigm

Bi: Bismuth; Cd: Cadmium; Dy: Dyrosium; Er: Erbium; Eu: Europium; Gd: Gadolinium; Lu: Lutetium; Nd: Neodymium; Pr: Praseodyum; Sm: Samarium; Tb: Terbium; Tm:Thulium; Y: Yttrium; Yb: Ytterbium; n/a: not available; IC: intracellular.

Figure 10. Panel wheel design strategy used to optimize the combination and selection of metal-labeled antibodies.

Elaborated with Fluidigm's Maxpar® Panel Designer. Each channel tile is arrayed counterclockwise on the wheel in order of ascending tolerance values within four tolerance zones. The channel tile height is proportional to the sensitivity of the channel. The tile is heat-mapped to indicate the signal overlap into the channel, expressed as a percentage of the tolerance value for the target in that channel.

4.7.2. Antibody labeling

Although many antibodies are available pre-conjugated, our panel required in-house conjugations with their isotopes in the case of CD8a, CD19, CCL5, GZMA, CX3CR1 and FceRI. The full list of materials required is given in Supplementary Table 2. Several considerations need to be considered when labeling antibodies. Firstly, two different guidelines were followed, the Maxpar® MCP9 Antibody Labeling Kit for labeling CD8a-114Cd and CD19-116Cd and the Maxpar X8 Antibody Labeling Kit for labeling CCL5-159Tb, FceRI-148Nd, GzmA-161Dy and CXCR1-172Yb. The reason for using different protocols and different conjugations is that, due to the ion optics of the CyTOF, the low mass Cd metal isotopes are detected with lower relative sensitivity than metal isotopes in the 153-176 Da range. Therefore, ideal antibody candidates for Cd labeling should consist of antibody clones with high antigen expression and high antibody sensitivity.

Briefly, the Maxpar® MCP9 Antibody Labeling Kit protocol consists of loading the Maxpar metal-chelating polymer with Cd metal solution and partial reduction of the antibody. Similarly, the Maxpar® X8 Labelling Kit protocol consists of loading the polymer with an Ln metal solution and also partial reduction of the antibody (Figure 11).

Figure 11. Maxpar® MCP9 Antibody Labeling Kit protocol and Maxpar® X8 Labeling Kit protocol

1)

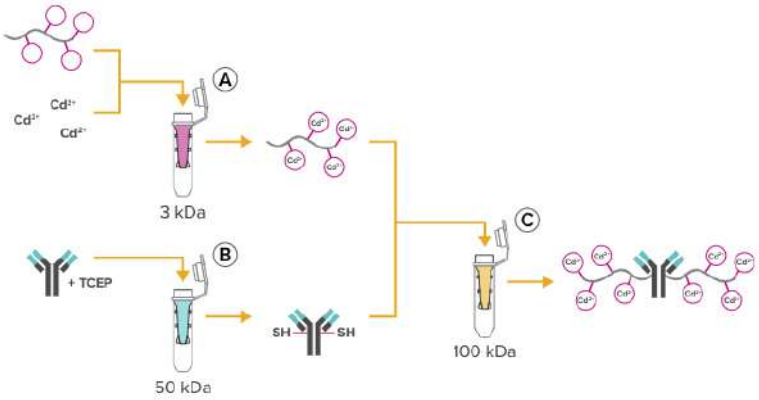

2)

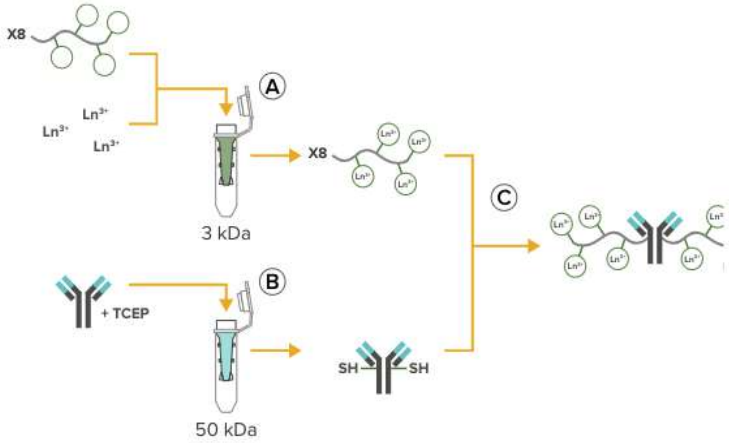

1) This procedure involves first loading the MCP9 polymer with Cd metal solution (A) and partially reducing the antibody (B), then conjugating the antibody with the Cd-loaded polymer (C).
2) This procedure involves first loading the X8 polymer with Ln metal solution (A) and partially reducing the antibody (B), then conjugating the antibody with the Ln-loaded polymer (C).

The two protocols were performed on separate days because of differences in materials and procedures between the kits, which could lead to user error or procedural delays. In addition, only 2 antibody conjugations were performed at a time to avoid procedural delays. The ultimate Maxpar antibody labeling protocol is available on request.

4.7.3. Titration and sample staining

The next critical steps are to titrate all the antibodies and run a test without the samples of interest in our study. To get the best signal-to-noise ratio and reduce non-specific antibody binding spillover, it's important to find the appropriate antibody concentration before titrating the samples [187]. Antibody titers are determined by calculating the staining index, a method very similar to that used in conventional flow cytometry [188]. The first antibody concentration assay was performed in a five-day protocol where cells were divided between unstimulated and stimulated protocols.

Stimulation of the cells was needed to titrate and stain intranuclear markers that are visible just under stimuli such as Ki67 and MIP-1beta.

Protocol for stimulated cells

On day 1, $25x10^6$ cells were thawed and $2x10^6$/ml cells were stimulated with 10 µg/ml of phytohemagglutinin (PHA) for 3 days. PHA helps to stimulate lymphocytes while killing monocytes.

On day 3, 6-24 hours before the end of the simulation, Brefeldin A and monesin were added in order to stop protein transport in order to keep MIP-1beta in the cell. On day 4, at the end of stimulation, cells were stored at 4ºC.

On day 5, harvest cells were washed and counted, obtaining $7.38x10^5$ cells per mL (live $5.67x10^5$ /dead$1.71x10^5$). Then, the cisplatin viability staining protocol was followed, and resuspended cells in 50µg/ml of RPMI and using 50 µg/ml of cisplatin (final concentration 2 µM). Different concentration tubes were labeled (1:50, 1:100, 1:200, 1:400, 1:800, and 1:1600) and $3x10^6$ cells were transferred to each tube. After washing and spinning steps, cells were resuspended in 45 µl of Cell Staining Buffer and 5 µl of Human TruStain FcX™. This product is specially formulated for blocking the FcR-involved unwanted staining without interfering with antibody-mediated specific staining of human cells. An extra 100 µl of Cell Staining Buffer was added to each tube. Maxplar Nuclear Antigen Staining protocol was followed to stain cells with nuclear antibodies such as Ki67 and MIP-1beta are intracellular antibodies. Lastly, we followed the protocol up to Stain Cells with Cell-ID Intercalator-Ir previously titrated (400 nM) (supplementary figure 1). Tubes were stored at -80ºC before acquisition.

Protocol for unstimulated cells

For markers that do not need to be pre-stimulated, a specific titration strategy has been designed due to the high number of markers. Although signal overlap is minimal, constant, and predictable in CyTOF, an algorithm was designed to assign metals with less than 0.3% signal overlap to the same titration group. A metal compatibility matrix was created from the output of the algorithm that helps to design the best strategy and distribute the different metals in each titration tube (Supplementary Figure 1). It is recommended to titrate surface antibodies separate from the intracellular antibodies and label different concentrations of each tube (1:50, 1:100, 1:200, 1:400, 1:800, and 1:1600).

On day 4, cells were thawed, and $2x10^6$/ml cells were cultured with Brefeldin A and monesin during 6 hours. At the end of the culture, cells were stored at 4ºC.

On day 5, harvest cells were washed and counted.

Then, the cisplatin viability staining protocol was followed, and resuspended cells in 50µg/ml of RPMI and using 50 µg/ml of cisplatin (final concentration 2 µM). Different concentration tubes were labeled (A to D and different concentrations: 1:50, 1:100, 1:200, 1:400, 1:800, 1:1600) and $3x10^6$ cells were transferred to each tube. An extra tube of unstimulated and unstained cells (negative control) was added in which 45 µL of Cell Staining Buffer was resuspended with 5µL of Human TruStain FcX to block any interaction of the constant fragment with an antibody that with create a false positive signal.

As we had many antibodies to titrate, surface cocktails were grouped into 4 groups and 4.8µL of each one was added to the corresponding tube (A-D):

A: CD45, CD57, CD14, CD27, B2M, CX3CR1, CD56.

B: CD19, FceRI, CXCR6, CD335, CD197.

C: CD8a, CD45RA, CD45RO, CD62L, CD33, CD314, CD159a, HLA-DR.

D: CD3, CD4, CD7, CD161, CD94, CD16.

For the 5 dilution tubes (1:100, 1:200,1:400, 1:800, 1:1600), 60 µL of Cell Staining Buffer was added. In the 1:50 dilution tube, 30 µL of the 4X cocktails A-D was placed. To the unstained cells, we added 350 µL of Cell Staining Buffer. Subsequently, we followed the protocol to Stain Cell with Nuclear Antibodies (steps 4 and 5).

The intracellular antibodies were grouped into 2 groups, and 4.8µL of each one was added to the corresponding tube (A-B):

A: CCL5/RANTES, Granzyme A.

B: Perforin.

The same protocol was followed as described for surface unstimulated antibodies.

In the end, we followed the protocol up to Stain Cells with Cell-ID Intercalator-Ir previously titrated (400 nM). Tubes were stored at -80ºC before acquisition.

Tubes were listed as follows:

- Unstimulated: 1) A, 2) B, 3) C, 4) D, 5) 1:50, 6) 1:100, 7) 1:200, 8) 1:400, 9) 1:800, 10) 1:1600
- Stimulated: 11) D, 12) 1:50, 13) 1:100, 14) 1:200, 15) 1:400, 16) 1:800, 17) 1:1600

Samples were analyzed on a Helios instrument (Fluidigm) after antibody staining and fixation.

4.8. Advanced analytics

4.8.1. Single-cell RNA sequencing

4.8.1.1. Sample pre-processing and demultiplexing

We processed sequencing reads with the 10X Genomics Inc. software package CellRanger (v.5.0.1) against the human GRCh38 reference genome and VDJ reference provided by 10X with v5 release. To simultaneously profile the transcriptomic profile and the TCR repertoire, and to specify the HTO libraries, we followed the “cellranger multi” pipeline. We set the --chemistry to “SC5P-R2” and the --expect-cells to “20000”, with an exception for the non-multiplexed library which was set to “6000”.

We demultiplexed cell hashtags as described in Stoeckius *et al.* for each library separately [189]. Briefly, we normalized HTO counts using a centered log ratio (CLR), where counts were divided by the geometric mean of an HTO across cells and log-transformed and run “HTODemux” function from Seurat package with the default parameters. Each barcode was classified to its origin sample, and multiplets (barcodes

assigned to more than one condition) or negatives (barcodes not assigned to any condition) were discarded.

4.8.1.2. Quality control and normalization of scRNA-seq

We performed quality control (QC) and normalization considering all 11 libraries together after ensuring there were no remarkable differences in the three main QC metrics: the number of reads per barcode (read depth), the number of genes per barcode, and the fraction of reads from mitochondrial genes per barcode. This QC was performed among the different donors and tissues, as described in the guidelines from Luecken *et al* [190].
We filtered out low-quality barcodes by removing those ones with a deficient number of UMI (< 225) and genes per barcode (< 100) or with a percentage of expression from mitochondrial expression higher than 20% as it is indicative of lysed cells. We also considered removing barcodes with a large library size and complexity (> 7.000 UMIs and > 2.000 genes). We cleaned out genes that were detected in less than 5 cells. Finally, the data was normalized, and log was transformed.

4.8.1.3. Single-cell transcriptome combined analysis

To achieve a successful cell-type annotation combining data from all 11 patients it is needed to remove the batch effect associated with the confounder variable (library/donor). To do so, we followed Seurat's standard integration pipeline [191]. This harmonization approach is based on the identification of “anchor” correspondences between pairs of datasets. Prior to integration, we obtained donor-specific highly variable features; only 3,000 features common among all libraries were used to compute the integration anchors, thereby reducing noise. To speed up the anchor identification, we used the alternative reciprocal PCA (RPCA) as suggested by the authors. To explore our data in a two-dimensional embedding we applied the UMAP algorithm.

After integration, we used the first 20 Principal Components to create a k-nearest neighbors’ graph with the “FindNeighbors” function followed by the cell clustering using the Louvain clustering algorithm with the “FindClusters” function and setting the

resolution parameter to 0.5. We performed a DEA for all clusters to determine their marker genes using the normalized RNA counts instead of the integrated data slot. The clusters were annotated by expression of canonical markers of immune cell types, compared with the results of the DEA analysis, and grouped into major cell groups (CD4+, CD8+ and Unconventional T, NK, Lymphoid B, Myeloid, Proliferative, and dead cells).

Cells annotated as dead showed low counts, low features, and high mitochondrial percentages, and were automatically removed. Subsequently, each cell group was independently re-processed following the previously described steps (different integration for lineages with very few cells, and independent resolution depending on the lineage) to obtain a fine-grained resolution of clusters and to annotate them into specific cell types and states. Manual annotation was performed using a collection of gene markers and it was compared with the annotation of the same clusters produced by Celltypist, a semi-automated annotation algorithm [192].
Cell compositional differences in blood were tested for different compared groups using a t-test. Also, a paired test was performed to compare cell proportions between blood and synovial from the same donor.

4.8.1.4. Single-cell TCR repertoire profiling

Clonotypes were defined by donor origin, the V(D)J genes, and the CDR3 annotations for both the TCR alpha and beta chain. Clonotype expansion was characterized per each cell type and defined by the total number of clones. The Gini-coefficient parameter was computed for each cell subpopulation and donor (blood and synovial fluid) to compare the inequality in clonotype size across cell subpopulations and samples [193]. Following Yost et al. [194], T-cells with at least 10% of the TCR sequenced were reclustered and TCR expansion was analyzed. Clonotypes were categorized as expanded (≥2 clones) or not expanded, and a 4-sample test for equality of proportions without continuity correction was performed.

4.8.1.5. Differential expression analysis

To define disease-specific signatures, we performed a Wilcoxon signed-rank test to test for differential expression for each gene using the Seurat function “FindMarkers”, and comparing oJIA and oJIA-U patients against all healthy donors. In contrast, to define tissue-specific signatures from oJIA paired samples (SF and PBMC), we used a generalized linear model (MAST package) considering “donor” as a covariate. MAST uses a model to account for dropout while modeling changes in gene expression depends upon the condition and technical covariates. To increase specificity, we only considered the genes with Log2FC > |0.25|, present in at least 10% of cells, and with a p.adj.value < 0.001.

4.8.1.6. Gene Ontology (GO) enrichment analysis

Gene-level analysis methods often produce long lists of candidate genes that are difficult to interpret. To facilitate the interpretation of these results and unravel biological processes enriched in specific-disease (oJIA and oJIA-U vs healthy controls) or tissue conditions (SF vs PBMC), we carried out a GO enrichment analysis against the “GO_Biological_Processes_2021” database using the “EnrichR” package.

4.8.1.7. Gene Set Enrichment Analysis

Using well-defined gene sets from the Molecular Signatures Database v6.2, Broad Institute, for Human Phenotype Ontology (HPO) named “HP_JUVENILE_RHEUMATOID_ARTHRITIS” and disease-relevant hallmarks such as [ADD hallmark names!], we computed a signature-specific score using the “AddMoleculeScore” function from Seurat. To test for statistical differences between conditions, we performed a Wilcoxon signed-rank test between the means.

4.8.1.8. Code and data availability

All analyses were carried out using R version 4 (4.0.1/4.0.5) and Python (v3.8). Single-cell transcriptomic data was analyzed using the Seurat package (v4.0.0) whereas single-cell V(D)J data was analyzed using Scirpy and scRepertoire package [195].

4.8.2. CyTOF analytics

Although the integrated analysis of all samples has not yet been performed and we are still finalizing the refinement of all selected markers, we have made progress in the first phase of the statistical analysis, which concerns understanding the parameters and measurements as well as the strategies used to clean the data and unwanted events.

Flow cytometers, whether fluorescence-based or metal-based, often require elimination of undesired events prior to analysis. To achieve this, most flow cytometers are equipped with internal circuitry or logic that can ignore signal-derived pulses that are partially formed or abnormally long.
Unlike flow cytometry, mass cytometry utilizes an atomization process to create clouds of positively charged ions from particles, which are then analyzed. Consequently, pulse processing capabilities of mass cytometry are mainly focused on detecting and eliminating coincident ion clouds or poorly formed pulses. Additionally, mass cytometry incorporates DNA intercalators that can help eliminate debris and some true aggregates.

Briefly, the ions enter the TOF chamber via a narrow slit. Every 13 µs, a high-voltage pulse provides equal energy to all ions that have accumulated in the chamber during the interval, accelerating them across the TOF chamber and onto the detector. This high-voltage pulse is a push (Figure 12A). As the energy provided to the ions is uniform, velocity varies by mass and ions with greater mass require longer times to reach the detector. Once these ions hit the detector, they generate an electronic pulse which when plotted and mathematically smoothened takes the shape of a bell curve (Gaussian distribution) from which the Gaussian discrimination parameters (center, offset, and width) are extracted (Figure 12B). These Gaussian parameters can be

leveraged by gating or modeling analysis strategies to eliminate unwanted non-Gaussian pulses (Supplementary Figure 2) [196] .

Figure 12. Event detection and parametrics of Gaussian Data Cleanup.

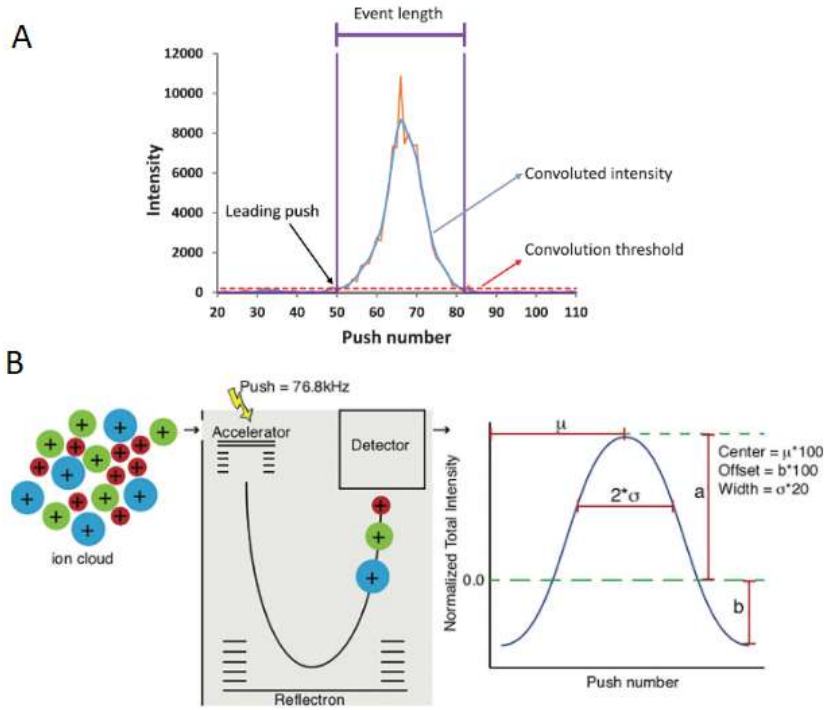

A) The total current or intensity pulse is first smoothed with a convoluted Gaussian smoothing routine to eliminate unwanted noise. An event begins when smoothed intensities are higher than an internal threshold for at least 10 but no more than 150 consecutive pushes or digitizations. B) Gaussian parameters (center, offset, width).

4.8.3. Olink proteomics

Firstly, an inter-plate normalization was carried out by standardizing the data for each plate using the included Olink Control Sample. Subsequently, an inverse log transformation was applied to facilitate analysis. The results are reported in the unit of Normalized Protein eXpression, representing relative quantification. All measurements falling within the measurable range based on the Olink antibody panel were included and were further adjusted for plate layout using residualization techniques.

Later, a comprehensive quality control screening of the data was conducted.

Additionally, the reproducibility of protein duplicates across panels was assessed, with 39 of them following a linear relationship. However, IL1-alpha, IL-13, IL-2, IL-33, and CSF exhibited deviations from this pattern indicating a poor replication capacity.

PCA was employed to evaluate all variables encompassing all patients, and no major outliers were detected.
Subsequently, PCA analysis specifically focusing on children revealed a PC1 value of 25.8% for oJIA debut patients, which was associated with the younger age at onset in these cases (Supplementary Figure 3).
To account for the influence of age, appropriate adjustments were made for subsequent analyses.

4.9. Ethical aspects

The current project has been presented and approved by the Ethical Committee for Clinical Research of the Vall d'Hebron Barcelona Hospital Campus. It has been approved and assigned the project code PR(AMI)234/2018. The study has been developed in accordance with the principles of the Declaration of Helsinki.

The PhD student adequately informed the patients and their parents in the case of minors, and healthy controls about the purpose and details of the project included in the information document prepared for this project. If the subject agreed to participate in the research, the informed consent was in triplicate, one for the patients and their parents, one for the clinical records, and one for the IMID-Biobank's registry.

4.10. Work plan

This project has been developed in the following phases:

Figure 13. Gantt chart representing the phases of the doctoral thesis project.

*The stages affected by the COVID-19 pandemic are marked with an asterisk.

This PhD project was significantly affected by the COVID-19 pandemic. Several phases of the project were interrupted, from patient recruitment due to the decrease in the number of new JIA diagnoses, to reduced patient contact with the hospital. In addition, both the GRR laboratory and the CNAG laboratory, where the scRNA-seq analysis was performed, limited the number of samples to be processed.

Furthermore, from March 2020 to around August 2020, the PhD student's support activity was focused on responding to the hospital's request for support against the pandemic, with a gradual resumption of research activity.

5. Results

5.1. Analysis of the characteristics of the subjects and samples

This section presents the results on the demographic, clinical, treatment-related characteristics and variables related to the sample acquisition of all patients with juvenile idiopathic arthritis and rheumatoid arthritis included in each phase of the study.

The presentation of the results has been divided into two phases of the study (the first stage and the second stage).

Clinical, disease-related variables, laboratory variables related to the sample acquisition and characteristics of the biological samples are described.

Table 7 schematically shows all the available samples and the analyses carried out specifically on each.

Table 7. Summary of all available samples for each stage and experiment.

ID	Condition	Tissue	Sc-RNAseq	CyTOF	Proteomics
oJIA1	oJIA debut	Blood, SF	First stage	Yes	Yes
oJIA2	oJIA debut	Blood, SF	First stage	Yes	Yes
oJIA3	oJIA debut	Blood, SF	First stage, not recovered	No	No
oJIA4	oJIA debut	Blood, SF	No, not recovered	No	Yes
oJIA5	oJIA debut	Blood	No	Yes	Yes
oJIA6	oJIA debut	Blood	No	Yes	Yes
oJIA7	oJIA debut	Blood, SF	No	Yes	Yes
oJIA8	oJIA debut	Blood	No	Yes	Yes
oJIA9	oJIA debut	Blood, SF	No	Yes	Yes
UV1	Uveitis flare	Blood	First stage	Yes	No
UV2	Uveitis flare	Blood	First stage	Yes	No
UV3	Uveitis flare	Blood	First stage	Yes	Yes
UV4	Uveitis flare	Blood	First stage, not recovered	No	Yes
UV5	Uveitis flare	Blood	No	Yes	Yes
UV6	Uveitis flare	Blood	No	Yes	Yes
UV7	Uveitis flare	Blood	No	Yes	Yes
UV8	Uveitis flare	Blood	No	Yes	Yes
UV9	Uveitis flare	Blood	No	Yes	Yes
oJIAcDMARD1	oJIA_cDMARD	Blood	No	Yes	Yes
oJIAcDMARD2	oJIA_cDMARD	Blood	No	Yes	Yes
oJIAcDMARD3	oJIA_cDMARD	Blood	No	Yes	Yes
oJIATNFW0_1	oJIA_W0_TNF	Blood	No	Yes	Yes
oJIATNFW0_2	oJIA_W0_TNF	Blood	No	Yes	Yes
oJIATNFW0_3	oJIA_W0_TNF	Blood	No	Yes	Yes
oJIATNFW12_1	oJIA_W12_TNF	Blood	No	Yes	Yes
oJIATNFW12_2	oJIA_W12_TNF	Blood	No	Yes	Yes
oJIATNFW12_3	oJIA_W12_TNF	Blood	No	Yes	Yes
pJIA1	pJIA	Blood	No	Yes	Yes
RA1	RA_onset	Blood	No	Yes	Yes
RA2	RA_onset	Blood	No	Yes	Yes
RA3	RA_onset	Blood	No	Yes	Yes
RA4	RA_onset	Blood	No	Yes	Yes
RA5	RA_onset	Blood	No	Yes	Yes
HC1	Healthy control	Blood	First stage	Yes	Yes
HC2	Healthy control	Blood	First stage	Yes	Yes
HC3	Healthy control	Blood	First stage, not recovered	No	Yes
HC4	Healthy control	Blood	First stage, not recovered	No	Yes
HC5	Healthy control	Blood	No	Yes	Yes
HC6	Healthy control	Blood	No	Yes	Yes
HC7	Healthy control	Blood	No	Yes	Yes
HC8	Healthy control	Blood	No	Yes	Yes

CyTOF: mass cytometry; HC: healthy control; ID: identification; oJIA: oligoarticular juvenile idiopathic arthritis; oJIAcDMARD: oligoarticular juvenile idiopathic arthritis under conventional disease-modifying antirheumatic drugs; oJIATNFW0: oligoarticular juvenile idiopathic arthritis under anti-TNF therapy at week 0; oJIATNFW12: oligoarticular juvenile idiopathic arthritis under anti-TNF therapy at week 12; pJIA: polyarticular rheumatoid factor-

negative juvenile idiopathic arthritis; RA: rheumatoid arthritis; scRNA-seq: single-cell RNA sequencing; SF: synovial fluid; UV: uveitis-related oligoarticular juvenile idiopathic arthritis.

Technical problems with sample processing

The boxes marked in red correspond to those patients whose samples were not valid for any of the project phases due to the technical problems discussed below. The following statistical analyses do not consider failed samples at each stage.

Here is a comprehensive breakdown of the technical issues faced at every stage:

- For patient oJIA3, isolated mononuclear cells from peripheral blood and synovial fluid couldn't be recovered from the scRNA-seq first stage. Therefore, the data of this patient is not further considered for the CyTOF second stage. Due to a technical problem at the IMID biobank lab, plasma couldn't be obtained. Therefore, the data of this patient is not further considered for the proteomics second stage.

- For patient oJIA4, the peripheral blood and synovial fluid samples could not be processed correctly. There was a problem during sample pre-processing and hashing at CNAG wet lab in the scRNA-seq first stage. This meant that the libraries could not be generated properly. The samples could not be recovered, so no more mononuclear cell aliquots were available for the second stage of mass cytometry. Although, as plasma was available, this patient was included in the proteomics second stage.

- For patients UV1 and UV2, plasma couldn't be obtained due to a technical problem at the IMID biobank wet lab. Therefore, the data of these patients were not further considered for the proteomics second stage.

- UV4 patient PBMCs couldn't be recovered from the first stage scRNA-seq step, so no more mononuclear cell aliquots were available for the second stage of mass cytometry. Although, as plasma was available, this patient was included in the proteomics second stage.

- Finally, HC3 and HC4, as well as in oJIA3 patient, isolated mononuclear cells from peripheral blood couldn't be recovered from the scRNA-seq first stage. Therefore, the data of this patient was not further considered for the CyTOF second stage. These patients were included in the proteomics second stage as plasma was available.

5.1.1. First stage: discovery cohort with single-cell RNA sequencing

From our pediatric rheumatology unit, three patients with oligoarticular JIA new onset disease were recruited. In conjunction with the pediatric ophthalmology department, four patients with oJIA and a uveitis flare were recruited, as well as 4 gender and age-matched healthy controls.

Epidemiological and clinical variables of first-stage patients are presented in Table 8, and variables related to sample acquisition are presented in Table 9.

Table 8. Epidemiological and clinical variables of first-stage patients.

ID	Condition	Gen	Age	Years JIA	Years JIAU	ANA	CRP	ESR	JADAS27	SUN cells	SUN flare	Active joints	cDMARD	bDMARD
oJIA1	oJIA debut	M	9	0	NA	P	0.27	29	11.9	NA	NA	Yes	NA	NA
oJIA2	oJIA debut	F	4	0	NA	P	0.42	60	12	NA	NA	Yes	NA	NA
oJIA3	oJIA debut	F	3	0	NA	P	9.19	113	21.3	NA	NA	Yes	NA	NA
UV1	Uveitis flare	F	14	12	3	P	0.09	26	4.6	0.5+	0	No	MTX	ADA
UV2	Uveitis flare	F	14	8	7	P	0.02	17	5	0.5+	0	No	MTX	ADA
UV3	Uveitis flare	F	12	10	7	P	0.02	5	0	0.5+	0	No	LFN	ADA
UV4	Uveitis flare	F	15	14	12	P	0.05	3	0	2+	1	No	MTX	ADA
HC1	HC	F	3	NA	NA	NA	NA	NA	NA	NA	NA	NA	NA	NA
HC2	HC	F	15	NA	NA	NA	NA	NA	NA	NA	NA	NA	NA	NA
HC3	HC	M	12	NA	NA	NA	NA	NA	NA	NA	NA	NA	NA	NA
HC4	HC	F	15	NA	NA	NA	NA	NA	NA	NA	NA	NA	NA	NA

ADA: adalimumab; ANA: antinuclear antibodies; bDMARDs: biologic disease-modifying antirheumatic drugs; cDMARDs: conventional disease-modifying antirheumatic drugs; CRP: c-reactive protein (mg/dl); ESR: erythrocyte sedimentation rate (mm/hour); F: female; Gen: Gender; HC: healthy control; ID: identification; JADAS27: composite juvenile idiopathic disease activity measure, 27 joints evaluated; LFN: leflunomide; M: male; MTX: methotrexate; NA: not applicable; oJIA: oligoarticular juvenile idiopathic arthritis; P: positive; SUN: Standardization of Uveitis Nomenclature; UV: uveitis-related oligoarticular juvenile idiopathic arthritis.

Oligoarticular juvenile idiopathic patients

In total, two females and one male were included. The mean age in this group was 5.33 ± 3.21 years. All were ANA positive and had active joints at sampling. Mean JADAS27 was 15.07 ± 5.40, indicating a high disease activity. The mean ESR was 67.33 ± 42.48 mm/h, and CRP was 3.29 ± 5.11mg/dl.

Oligoarticular juvenile idiopathic patients with a uveitis flare

In this group, four patients were included, all females with a mean age of 13.75 ± 1.26 years. The time of evolution of JIA was 11 ± 2.58 years on average, and the time of evolution of oJIA-related uveitis was 7.25 ± 3.68 years. All patients had JIA previous to the uveitis manifestation and were ANA positive. Mean JADAS27 was 2.4 ± 2.77, indicating moderate disease activity. The mean ESR was 12.75 ± 10.78 mm/h, and CRP was 0.05 ± 0.03 mg/dl. 3 patients scored 0.5+ cells in the SUN classification, and 1 had a 2+ SUN cell. Just one patient had a score of 1 in SUN flare. All patients were receiving cDMARDs (3 methotrexate; 1 leflunomide), and all were on the bDMARD adalimumab for more than a year at sampling.

Healthy controls

A total of 4 controls were included, 3 females and 1 male, with a mean age of 11.25 ± 5.68 years.

Table 9. Variables related to sample acquisition of first-stage patients.

ID	Condition	Tissue	Vol. Blood/SF	Minutes procedure	Number PBMCs	Efficiency PBMCs	Number MCs SF	Efficiency MCs SF
oJIA1	oJIA debut	Blood, SF	12/8	60	2.40E+06	1.60E+06	5.12E+06	2.56E+06
oJIA2	oJIA debut	Blood, SF	6/8	40	1.00E+06	1.33E+06	1.70E+06	8.50E+05
oJIA3	oJIA debut	Blood, SF	8/8	60	3.70E+06	3.29E+06	1.58E+06	1.05E+06
UV1	Uveitis flare	Blood	9	60	3.60E+06	3.20E+06	NA	NA
UV2	Uveitis flare	Blood	9	37	3.52E+06	3.13E+06	NA	NA
UV3	Uveitis flare	Blood	12	50	2.34E+06	1.56E+06	NA	NA
UV4	Uveitis flare	Blood	7,6	60	1.14E+06	3.80E+05	NA	NA
HC1	HC	Blood	15	75	3.45E+06	1.38E+06	NA	NA
HC2	HC	Blood	12	60	1.15E+06	7.67E+05	NA	NA
HC3	HC	Blood	6	120	1.95E+06	6.50E+05	NA	NA
HC4	HC	Blood	12	60	1.90E+06	1.27E+06	NA	NA

HC: healthy control; ID: identification; MCs: mononuclear cells; oJIA: oligoarticular juvenile idiopathic arthritis; PBMCs: peripheral blood mononuclear cells; SF: synovial fluid; UV: uveitis-related oligoarticular juvenile idiopathic arthritis; Vol.: volume.

Peripheral blood was extracted from all samples, and synovial fluid was obtained for oligoarticular juvenile idiopathic arthritis onset patients. The mean volume of peripheral

blood extracted was 9.87 ± 2.91 cc, and the mean volume of SF was 8 cc. Samples were immediately transferred to the laboratory with a mean delay of 62 ± 21 minutes, and the PhD candidate extracted mononuclear cells from peripheral blood and synovial fluid. The mean number of PBMCs obtained per aliquot (1mL) was 2.38E+06 ± 1.05E+06 cells, with an efficiency of 1.69E+06 ± 1.05E+06. Finally, the mean number of mononuclear cells obtained from synovial fluid was 2.80E+06 ± 2.01E+06 cells, with an efficiency of 1.49E+06 ± 9.35E+05.

5.1.2. Second stage: validation cohort with CyTOF and proteomics

To validate the results obtained in the single cell analysis, in this second stage, a cohort of patients with different conditions were collected.
We included more patients with oJIA de novo and uveitis flares, patients with oligoarticular with different treatments, patients with polyarticular JIA, rheumatoid arthritis patients and a larger number of healthy controls.

Epidemiological and clinical variables of second-stage patients are presented in Table 10, and separately in Table 11 are presented the variables related to sample acquisition.

5.1.2.1. CyTOF analysis

In this second stage, we recruited a total of 7 patients with oligoarticular JIA new-onset disease, 3 patients with oJIA under cDMARDs treatment, 3 patients with oJIA at week 0 and week 12 after starting a bDMARD therapy, 1 patient with a new-onset pJIA and 5 patients with new-onset RA. A total of 6 healthy children were included (Table 10).

Table 10. Epidemiological and clinical variables of stage 2 patients - CyTOF.

ID	Condition	Gen	Age	Years JIA	Years JIAU	ANA	CRP	ESR	JADAS27	DAS28	SUN cells	SUN flare	Active joints	cDMARD	bDMARD
oJIA1	oJIA debut	M	9	0	NA	1	0.27	2	11.9	NA	NA	NA	1	NA	NA
oJIA2	oJIA debut	F	4	0	NA	1	0.42	60	12	NA	NA	NA	1	NA	NA
oJIA5	oJIA debut	F	12	0	NA	0	0.10	21	3	NA	NA	NA	1	NA	NA
oJIA6	oJIA debut	F	14	0	NA	0	0.03	26	4.6	NA	NA	NA	1	NA	NA
oJIA7	oJIA debut	M	3	0	NA	1	0.03	4	6	NA	NA	NA	1	NA	NA
oJIA8	oJIA debut	F	6	0	NA	1	0.27	25	11.5	NA	NA	NA	1	NA	NA
oJIA9	oJIA debut	M	2	0	NA	0	1.5	45	7.5	NA	NA	NA	1	NA	NA
UV1	Uveitis flare	F	14	12	3	1	0.09	26	4.6	NA	0.5+	0	0	MTX	ADA
UV2	Uveitis flare	F	14	8	7	1	0.02	17	5	NA	0.5+	0	0	MTX	ADA
UV3	Uveitis flare	F	12	10	7	1	0.02	5	0	NA	0.5+	0	0	LFN	ADA
UV5	Uveitis flare	F	15	12	3	1	0.58	13	0	NA	2+	1	0	MTX	ADA
UV6	Uveitis flare	F	11	7	7	1	0.11	19	0	NA	2+	2	0	MTX	NA
UV7	Uveitis flare	F	8	4	2	1	0.04	10	0	NA	1+	0	0	MTX	ADA
UV8	Uveitis flare	F	7	3	0	1	0.03	18	0	NA	2+	1	0	NA	NA
UV9	Uveitis flare	F	15	14	13	1	0.08	16	0	NA	2+	1	0	LFN	ADA
HC1	HC	F	3	NA	NA	NA	NA	NA	NA	NA	NA	NA	NA	NA	NA
HC2	HC	F	15	NA	NA	NA	NA	NA	NA	NA	NA	NA	NA	NA	NA
HC5	HC	F	8	NA	NA	NA	NA	NA	NA	NA	NA	NA	NA	NA	NA
HC6	HC	M	4	NA	NA	NA	NA	NA	NA	NA	NA	NA	NA	NA	NA
HC7	HC	F	3	NA	NA	NA	NA	NA	NA	NA	NA	NA	NA	NA	NA
HC8	HC	M	9	NA	NA	NA	NA	NA	NA	NA	NA	NA	NA	NA	NA
oJIAD1	oJIA DMARD	F	11	9	NA	1	0.05	6	0	NA	NA	NA	0	MTX	NA
oJIAD2	oJIA DMARD	F	2	0	NA	1	0.07	35	1.5	NA	NA	NA	0	MTX	NA
oJIAD3	oJIA DMARD	F	7	0	NA	1	0.23	33	1.3	NA	NA	NA	0	MTX	NA
oJIAT W0_1	oJIA_W0 TNF	F	14	0	NA	1	10.15	82	17.2	NA	NA	NA	1	Any	NA
oJIAT W0_2	oJIA_W0 TNF	M	10	0	NA	1	0.3	10	10	NA	NA	NA	1	MTX	NA
oJIAT W0_3	oJIA_W0 TNF	F	12	10	NA	1	0.02	21	4	NA	NA	NA	1	LFN	NA
oJIAT W12_1	oJIA_W12 TNF	F	14	0	NA	1	0.81	24	0.4	NA	NA	NA	0	Any	ETN
oJIAT W12_2	oJIA_W12 TNF	M	10	0	NA	1	0.05	9	0	NA	NA	NA	0	MTX	ETN
oJIAT W12_3	oJIA_W12 TNF	F	12	10	NA	1	0.02	22	0	NA	NA	NA	0	LFN	ADA
pJIA1	Poly JIA	F	13	0	NA	0	0.58	47	27	NA	NA	NA	1	NA	NA
RA1	RA onset	M	68	0	NA	0	7.47	113	NA	6.27	NA	NA	1	NA	NA
RA2	RA onset	F	41	0	NA	0	5.46	53	NA	5.25	NA	NA	0	NA	NA
RA3	RA onset	F	39	0	NA	0	0.24	120	NA	7.26	NA	NA	1	NA	NA
RA4	RA onset	F	32	0	NA	0	0.33	50	NA	4.06	NA	NA	1	NA	NA
RA5	RA onset	F	52	0	NA	0	0.16	34	NA	4.89	NA	NA	1	NA	NA

ADA: adalimumab; ANA: antinuclear antibodies; bDMARDs: biologic disease-modifying antirheumatic drugs; cDMARDs: conventional disease-modifying antirheumatic drugs; CRP: c-reactive protein (mg/dl); DAS28: disease activity score 28-joint counts; ESR: erythrocyte sedimentation rate (mm/hour); ETN: etanercept; F: female; Gen:

gender; HC: healthy control; ID: identification; JADAS27: composite juvenile idiopathic disease activity measure, 27 joints evaluated; LFN: leflunomide; M: male; MTX: methotrexate; NA: not applicable; oJIA: oligoarticular juvenile idiopathic arthritis; oJIA cDMARD: oligoarticular juvenile idiopathic arthritis under conventional disease-modifying antirheumatic drugs; oJIATNFW0: oligoarticular juvenile idiopathic arthritis under anti-TNF therapy at week 0; oJIATNFW12: oligoarticular juvenile idiopathic arthritis under anti-TNF therapy at week 12; P: positive; pJIA: polyarticular rheumatoid factor-negative juvenile idiopathic arthritis; RA: rheumatoid arthritis; SF: synovial fluid; SUN: Standardization of Uveitis Nomenclature; UV: uveitis-related oligoarticular juvenile idiopathic arthritis.

Oligoarticular juvenile idiopathic patients

In total, four females and three males were included. The mean age in this group was 7.14 ± 4.36 years. All patients were ANA positive and had active joints at sampling. Mean JADAS27 was 8 ± 4, indicating a high disease activity. The mean ESR was 30 ± 17.9 mm/h, and CRP was 0.37 ± 0.51 mg/dl.

Oligoarticular juvenile idiopathic patients with a uveitis flare

In this group, eight patients were included, all females with a mean age of 12 ± 3.11 years. The time of evolution of JIA was 9 ± 3.95 on average and the time of evolution of JIA-related uveitis was 5 ± 4. All patients had JIA before the uveitis manifestation and were ANA positive. Mean JADAS27 was 1 ± 2, indicating low disease activity. The mean ESR was 15.5 ± 6.3 mm/h, and CRP was 0.12 ± 0.12 mg/dl. 4 patients scored 2+ in the SUN cell classification, 3 patients scored 0.5+ cells, and 1 patient had a 1+ SUN cell. 3 patients scored 1 in SUN flare, and 1 had a score of 2. Seven patients received cDMARDs (5 methotrexate; 2 leflunomide), and 6 were on adalimumab for over a year at sampling.

Oligoarticular juvenile idiopathic patients under cDMARDs in remission

A total of three patients were included, all females with a mean age of 6.6 ± 4.5 years. The time of evolution of JIA was 3 ± 4.5 years, and any patient had developed uveitis. Mean JADAS27 was 1, indicating low disease activity. The mean ESR was 26.6 ± 16.63 mm/h, and CRP was 0.12 ± 0.09 mg/dl. All patients were receiving methotrexate at sampling.

Oligoarticular juvenile idiopathic patients at week 0 and week 12 after starting a bDMARD treatment

Two females and one male at week 0 before the initiation of anti-TNF therapy and followed at week 12 were included. The mean age was 12 ± 2 years. The time of

evolution of JIA was 3 ± 5.7 years, and any patient had developed uveitis. Mean JADAS27 at week 0 was 10 ± 7, indicating high disease activity, even though 2 had been treated with cDMARDs (1 methotrexate, 1 leflunomide). The mean ESR was 37.67 ± 38.78 mm/h, and CRP was 3.49 ± 5.76 mg/dl.

At week 12, 2 patients were treated with etanercept and 1 with adalimumab. The treatment with cDMARDs didn't change. JADAS27 was reduced to 0 in all patients. The mean ESR was 18.33 ± 8.14 mm/h, and CRP was 0.29 ± 0.44 mg/dl.

Rheumatoid arthritis

In this group, 5 patients newly diagnosed with RA were included, 4 females and 1 male with a mean age of 46.4 ± 14.04 years. DAS28 was high with a mean of 6 ± 1, ESR mean was 74 ± 39.57 mm/h and CRP mean was 2.73 ± 3.48 mg/dl.

Healthy controls

Gender-matched healthy control children were recruited. A total of 6 controls were included, 4 females and 2 males, with a mean age of 7 ± 4.69 years.

Table 11. Variables related to sample acquisition of stage 2 patients - CyTOF.

ID	Condition	Tissue	Vol.	Minutes procedure	Number PBMCs blood	Efficiency PBMCs blood	Number PBMCs SF	Efficiency PBMCs SF
oJIA1	oJIA debut	Blood, SF	12	60	240E+06	1.60E+06	5.12E+06	2.56E+06
oJIA2	oJIA debut	Blood, SF	6	40	1.00E+06	1.33E+06	1.70E+06	8.50E+05
oJIA5	oJIA debut	Blood	12	150	**	**	NA	NA
oJIA6	oJIA debut	Blood	12	150	1.95E+06	1.30E+06	NA	NA
oJIA7	oJIA debut	Blood, SF	8	111	6.50E+05	3.47E+05	7.00E+04	1.75E+05
oJIA8	oJIA debut	Blood	12	180	1.25E+06	8.33E+05	NA	NA
oJIA9	oJIA debut	Blood, SF	7,5	90	1.81E+06	6.03E+05	2.86E+06	9.53E+05
UV1	Uveitis flare	Blood	9	60	3.60E+06	3.20E+06	NA	NA
UV2	Uveitis flare	Blood	9	37	3.52E+06	3.13E+06	NA	NA
UV3	Uveitis flare	Blood	12	50	2.34E+06	1.56E+06	NA	NA
UV5	Uveitis flare	Blood	12	190	1.25E+06	8.33E+05	NA	NA
UV6	Uveitis flare	Blood	8,5	166	1.35E+06	9.00E+05	NA	NA
UV7	Uveitis flare	Blood	12	120	1.55E+06	1.03E+06	NA	NA
UV8	Uveitis flare	Blood	12	25	2.86E+06	1.63E+06	NA	NA
UV9	Uveitis flare	Blood	12	91	1.85E+06	6.17E+05	NA	NA
HC1	HC	Blood	15	75	3.45E+06	1.38E+06	NA	NA
HC2	HC	Blood	12	60	1.15E+06	7.67E+05	NA	NA
HC5	HC	Blood	12	60	1.05E+06	7.00E+05	NA	NA
HC6	HC	Blood	3	90	9.50E+05	6.33E+05	NA	NA
HC7	HC	Blood	4	105	9.50E+05	9.50E+05	NA	NA
HC8	HC	Blood	6	180	**	**	NA	NA
oJIAD1	oJIA DMARD	Blood	12	270	**	**	NA	NA
oJIAD2	oJIA DMARD	Blood	5,5	270	2.30E+06	1.67E+06	NA	NA
oJIAD3	oJIA DMARD	Blood	10	150	2.05E+06	1.64E+06	NA	NA
oJIAT W0_1	oJIA_W0 TNF	Blood	10	120	1.10E+06	7.33E+05	NA	NA
oJIAT W0_2	oJIA_W0 TNF	Blood	12	210	1.45E+06	9.67E+05	NA	NA
oJIAT W0_3	oJIA_W0 TNF	Blood	10	120	1.10E+06	7.33E+05	NA	NA
oJIAT W12_1	oJIA_W12 TNF	Blood	12	60	1.30E+06	8.67E+05	NA	NA
oJIAT W12_2	oJIA_W12 TNF	Blood	12	120	1.40E+06	9.33E+05	NA	NA
oJIAT W12_3	oJIA_W12 TNF	Blood	12	45	1.40E+06	9.33E+05	NA	NA
pJIA1	Poly JIA	Blood	12	25	2.04E+06	1.36E+06	NA	NA
RA1	RA onset	Blood	12	30	2.10E+06	7.00E+05	NA	NA
RA2	RA onset	Blood	12	45	7.00E+05	3.50E+05	NA	NA
RA3	RA onset	Blood	12	45	1.00E+06	6.67E+05	NA	NA
RA4	RA onset	Blood	12	50	2.84E+06	1.89E+06	NA	NA
RA5	RA onset	Blood	15	81	1.95E+06	5.20E+05	NA	NA

HC: healthy control; ID: identification; MCs: mononuclear cells; NA: not applicable; oJIA cDMARD: oligoarticular juvenile idiopathic arthritis under conventional disease-modifying antirheumatic drugs; oJIA: oligoarticular juvenile idiopathic arthritis; oJIATNFW0: oligoarticular juvenile idiopathic arthritis under anti-TNF therapy at week 0; oJIATNFW12: oligoarticular juvenile idiopathic arthritis under anti-TNF therapy at week 12; PBMCs: peripheral blood mononuclear cells; pJIA: polyarticular rheumatoid factor-negative juvenile idiopathic arthritis; RA: rheumatoid

arthritis; SF: synovial fluid; UV: uveitis-related oligoarticular juvenile idiopathic arthritis. Vol.: volume. ** PMBCs could not be counted due to a technical problem.

The mean volume of blood extracted was 10.51 ± 2.8 cc. Samples were immediately transferred to the laboratory with a mean delay of 103 ± 66 minutes, and PBMCs were extracted in the same way as in stage one. The mean number of PBMCs obtained from blood and per aliquots (1mL) was 1.75E+06 ± 8.14E+05 cells, with an efficiency of 1.13E+06 ± 6.69E+05. Finally, the mean number of PBMCs obtained from synovial fluid was 2.44E+06 ± 1.40E+06 cells, with an efficiency of 1.13E+06 ± 4.23E+05.

5.1.2.2. Proteomic analysis cohort

In this section, we investigated the proteomic profile of the patients in the second stage. The tables summarizing the clinical and laboratory characteristics (Table 12) and the sample-related variables (Table 13) are presented separately.

Table 12. Epidemiological and clinical variables of stage 2 patients - Proteomics.

ID	Condition	Gen	Age	Years JIA	Years JIAU	ANA	CRP	ESR	JADAS27	DAS28	SUN cells	SUN flare	Active joints	cDMARD	bDMARD
oJIA1	oJIA debut	M	9	0	NA	1	0.27	29	11.9	NA	NA	NA	1	NA	NA
oJIA2	oJIA debut	F	4	0	NA	1	0.42	60	12	NA	NA	NA	1	NA	NA
oJIA4	oJIA debut	M	11	0	NA	1	45	12	5.67	NA	NA	NA	1	NA	NA
oJIA5	oJIA debut	F	12	0	NA	0	0.10	21	3	NA	NA	NA	1	NA	NA
oJIA6	oJIA debut	F	14	0	NA	0	0.03	26	4.6	NA	NA	NA	1	NA	NA
oJIA7	oJIA debut	M	3	0	NA	1	0.03	4	6	NA	NA	NA	1	NA	NA
oJIA8	oJIA debut	F	6	0	NA	1	0.27	25	11.5	NA	NA	NA	1	NA	NA
oJIA9	oJIA debut	M	2	0	NA	0	1.50	45	7.5	NA	NA	NA	1	NA	NA
UV3	Uveitis flare	F	12	10	7	1	0.02	5	0	NA	0.5+	0	0	LFN	ADA
UV4	Uveitis flare	F	15	14	12	1	0.05	3	0	NA	2+	1	0	MTX	ADA
UV5	Uveitis flare	F	15	12	3	1	0.58	13	0	NA	2+	1	0	MTX	ADA
UV6	Uveitis flare	F	11	7	7	1	0.11	19	0	NA	2+	2	0	MTX	NA
UV7	Uveitis flare	F	8	4	2	1	0.04	10	0	NA	1+	0	0	MTX	ADA
UV8	Uveitis flare	F	7	3	0	1	0.03	18	0	NA	2+	1	0	NA	NA
UV9	Uveitis flare	F	15	14	13	1	0.08	16	0	NA	2+	1	0	LFN	ADA
HC1	HC	F	3	NA	NA	NA	NA	NA	NA	NA	NA	NA	NA	NA	NA
HC2	HC	F	15	NA	NA	NA	NA	NA	NA	NA	NA	NA	NA	NA	NA
HC3	HC	M	12	NA	NA	NA	NA	NA	NA	NA	NA	NA	NA	NA	NA
HC4	HC	F	15	NA	NA	NA	NA	NA	NA	NA	NA	NA	NA	NA	NA
HC5	HC	F	8	NA	NA	NA	NA	NA	NA	NA	NA	NA	NA	NA	NA
HC6	HC	M	4	NA	NA	NA	NA	NA	NA	NA	NA	NA	NA	NA	NA
HC7	HC	F	3	NA	NA	NA	NA	NA	NA	NA	NA	NA	NA	NA	NA
HC8	HCl	M	9	NA	NA	NA	NA	NA	NA	NA	NA	NA	NA	NA	NA
oJIAD1	oJIA DMARD	F	11	9	NA	1	0.05	6	0	NA	NA	NA	0	MTX	NA
oJIAD2	oJIA DMARD	F	2	0	NA	1	0.07	35	1.5	NA	NA	NA	0	MTX	NA
oJIAD3	oJIA DMARD	F	7	0	NA	1	0.23	33	1.3	NA	NA	NA	0	MTX	NA
oJIAT W0_1	oJIA_W0 TNF	F	14	0	NA	1	10.15	82	17.2	NA	NA	NA	1	Any	NA
oJIAT W0_2	oJIA_W0 TNF	M	10	0	NA	1	0.3	10	10	NA	NA	NA	1	MTX	NA
oJIAT W0_3	oJIA_W0 TNF	F	12	10	NA	1	0.02	21	4	NA	NA	NA	1	LFN	NA
oJIAT W12_1	oJIA_W12 TNF	F	14	0	NA	1	0.81	24	0.4	NA	NA	NA	0	Any	ETN
oJIAT W12_2	oJIA_W12 TNF	M	10	0	NA	1	0.05	9	0	NA	NA	NA	0	MTX	ETN
oJIAT W12_3	oJIA_W12 TNF	F	12	10	NA	1	0.02	22	0	NA	NA	NA	0	LFN	ADA
pJIA1	pJIA	F	13	0	NA	0	0.58	47	27	NA	NA	NA	1	NA	NA
RA1	RA onset	M	68	0	NA	0	7.47	113	NA	6.27	NA	NA	1	NA	NA
RA2	RA onset	F	41	0	NA	0	5.46	53	NA	5.25	NA	NA	0	NA	NA
RA3	RA onset	F	39	0	NA	0	0.24	120	NA	7.26	NA	NA	1	NA	NA
RA4	RA onset	F	32	0	NA	0	0.33	50	NA	4.06	NA	NA	1	NA	NA
RA5	RA onset	F	52	0	NA	0	0.16	34	NA	4.89	NA	NA	1	NA	NA

ADA: adalimumab; ANA: antinuclear antibodies; bDMARDs: biologic disease-modifying antirheumatic drugs; cDMARDs: conventional disease-modifying antirheumatic drugs; CRP: c-reactive protein (mg/dl); DAS28: disease activity score 28-joint counts; ESR: erythrocyte sedimentation rate (mm/hour); ETN: etanercept; F: female; Gen: gender; HC: healthy control; ID: identification; JADAS27: composite juvenile idiopathic disease activity measure, 27 joints evaluated; LFN: leflunomide; M: male; MTX: methotrexate; NA: not applicable; oJIA: oligoarticular juvenile idiopathic arthritis; oJIA cDMARD: oligoarticular juvenile idiopathic arthritis under conventional disease-modifying antirheumatic drugs; oJIATNFW0: oligoarticular juvenile idiopathic arthritis under anti-TNF therapy at week 0; oJIATNFW12: oligoarticular juvenile idiopathic arthritis under anti-TNF therapy at week 12; P: positive; pJIA: polyarticular rheumatoid factor-negative juvenile idiopathic arthritis; RA: rheumatoid arthritis; SF: synovial fluid; SUN: Standardization of Uveitis Nomenclature; UV: uveitis-related oligoarticular juvenile idiopathic arthritis.

Oligoarticular juvenile idiopathic patients

8 patients were included, 4 females and 4 males. The mean age in this group was 7.62 ± 4.5 years. 5 patients were ANA positive, and all had active joints at sampling. Mean JADAS27 was 7.77 ± 3.6, indicating a high disease activity. The mean ESR was 27.75 ± 18 mm/h, and CRP was 0.89 ± 1.5 mg/dl.

Oligoarticular juvenile idiopathic patients with a uveitis flare

In this group, 7 patients were included, all females with a mean age of 11.85 ± 3.38 years. The time of evolution of JIA was 9 ± 4.56 on average and the time of evolution of JIA-related uveitis was 6.28 ± 4.95. All patients had JIA before the uveitis manifestation and were ANA positive. Mean JADAS27 was 0, indicating low disease activity. The mean ESR was 12 ± 6.27 mm/h, and CRP was 0.13 ± 0.2 mg/dl. 5 patients had a score of 2+ in the SUN cell classification, 1 patient had a 1+ SUN cell, and 1 patient had a score of 0.5+ cells. Six patients received cDMARDs (4 methotrexate; 2 leflunomide) and 5 were on adalimumab for over a year at sampling.

Healthy controls

Age- and gender-matched healthy control volunteers were recruited. A total of 8 controls were included, 5 females and 3 males with a mean age of 8.62 ± 5.04 years.

For the remaining groups (oJIA cDMARDs, week 0-12 anti-TNF, RA, and polyarticular JIA), as patients are the same as previously described in the CyTOF analysis, please refer to the previous section.

Table 13. Variables related to sample acquisition of stage 2 patients – Proteomics.

ID	Condition	Tissue	Vol.	Minutes procedure	Number plasma al.	Number PBMCs blood	Efficiency PBMCs blood	Number PBMCs SF	Efficiency PBMCs SF
oligoJIA1	oJIA debut	Blood, SF	12	60	16	2.40E+06	1.60E+06	5.12E+06	2.56E+06
oligoJIA2	oJIA debut	Blood, SF	6	40	2	1.00E+06	1.33E+06	1.70E+06	8.50E+05
oligoJIA4	oJIA debut	Blood, SF	12	106	15	1.10E+06	3.67E+05	7.80E+06	4.46E+06
oligoJIA5	oJIA debut	Blood	12	150	16	**	**	NA	NA
oligoJIA6	oJIA debut	Blood	12	150	15	1.95E+06	1.30E+06	NA	NA
oligoJIA7	oJIA debut	Blood, SF	8	111	7	6.50E+05	3.47E+05	7.00E+04	1.75E+05
oligoJIA8	oJIA debut	Blood	12	180	15	1.25E+06	8.33E+05	NA	NA
oligoJIA9	oJIA debut	Blood,SF	7.5	90	4	1.81E+06	6.03E+05	2.86E+06	9.53E+05
UV3	Uveitis flare	Blood	12	50	16	2.34E+06	1.56E+06	NA	NA
UV4	Uveitis flare	Blood	7.6	60	13	1.14E+06	3.80E+05	NA	NA
UV5	Uveitis flare	Blood	12	190	14	1.25E+06	8.33E+05	NA	NA
UV6	Uveitis flare	Blood	8.5	166	16	1.35E+06	9.00E+05	NA	NA
UV7	Uveitis flare	Blood	12	120	15	1.55E+06	1.03E+06	NA	NA
UV8	Uveitis flare	Blood	12	25	4	2.86E+06	1.63E+06	NA	NA
UV9	Uveitis flare	Blood	12	91	14	1.85E+06	6.17E+05	NA	NA
HC1	HC	Blood	15	75	4	3.45E+06	1.38E+06	NA	NA
HC2	HC	Blood	12	60	4	1.15E+06	7.67E+05	NA	NA
HC3	HC	Blood	6	120	6	1.95E+06	6.50E+05	NA	NA
HC4	HC	Blood	12	60	14	1.90E+06	1.27E+06	NA	NA
HC5	HC	Blood	12	60	24	1.05E+06	7.00E+05	NA	NA
HC6	HC	Blood	3	90	9	9.50E+05	6.33E+05	NA	NA
HC7	HCl	Blood	4	105	2	9.50E+05	9.50E+05	NA	NA
HC8	HC	Blood	6	180	7	**	**	NA	NA
oJIAD1	oJIA DMARD	Blood	12	270	1	**	**	NA	NA
oJIAD2	oJIA DMARD	Blood	5.5	270	15	2.30E+06	1.67E+06	NA	NA
oJIAD3	oJIA DMARD	Blood	10	150	9	2.05E+06	1.64E+06	NA	NA
oJIAT W0_1	oJIA_W0 TNF	Blood	10	120	16	1.10E+06	7.33E+05	NA	NA
oJIAT W0_2	oJIA_W0 TNF	Blood	12	210	16	1.45E+06	9.67E+05	NA	NA
oJIAT W0_3	oJIA_W0 TNF	Blood	10	120	14	1.10E+06	7.33E+05	NA	NA
oJIAT W12_1	oJIA_W12 TNF	Blood	12	60	7	1.30E+06	8.67E+05	NA	NA
oJIAT W12_2	oJIA_W12 TNF	Blood	12	120	16	1.40E+06	9.33E+05	NA	NA
oJIAT W12_3	oJIA_W12 TNF	Blood	12	45	16	1.40E+06	9.33E+05	NA	NA
pJIA1	pJIA	Blood	12	25	12	2.04E+06	1.36E+06	NA	NA
RA1	RA onset	Blood	12	30	12	2.10E+06	7.00E+05	NA	NA
RA2	RA onset	Blood	12	45	14	7.00E+05	3.50E+05	NA	NA
RA3	RA onset	Blood	12	45	16	1.00E+06	6.67E+05	NA	NA
RA4	RA onset	Blood	12	50	10	2.84E+06	1.89E+06	NA	NA
RA5	RA onset	Blood	15	81	15	1.95E+06	5.20E+05	NA	NA

HC: healthy control; ID: identification; MCs: mononuclear cells; NA: not applicable; oJIA cDMARD: oligoarticular juvenile idiopathic arthritis under conventional disease-modifying antirheumatic drugs; oJIA: oligoarticular juvenile idiopathic arthritis; oJIATNFW0: oligoarticular juvenile idiopathic arthritis under anti-TNF therapy at week 0; oJIATNFW12: oligoarticular juvenile idiopathic arthritis under anti-TNF therapy at week 12; PBMCs: peripheral blood mononuclear cells; pJIA: polyarticular rheumatoid factor-negative juvenile idiopathic arthritis; RA: rheumatoid arthritis; SF: synovial fluid; UV: uveitis-related oligoarticular juvenile idiopathic arthritis; Vol.: volume
** PMBCs could not be counted due to a technical problem.

Plasma was extracted from blood as previously described. The mean volume of blood extracted was 10.48 ± 2.87 cc. Samples were immediately transferred to the laboratory with a mean delay of 104.74 ± 63.39 minutes, and PBMCs and plasma were extracted by the Ph.D. candidate. The mean number of plasma aliquots obtained was 11.6 ± 5.37. The mean number of PBMCs obtained from blood and per aliquots (1mL) was 1.62E+06 ± 6.57E+05 cells, with an efficiency of 9.61E+05 ± 4.28E+05. Finally, the mean number of PBMCs obtained from synovial fluid was 3.51E+06 ± 3.02E+06 cells, with an efficiency of 1.80E+06 ± 1.73E+05.

5.2. Single-cell RNA sequencing analysis

5.2.1. Quality control

Raw read expression data were processed into counts matrices using CellRanger v5.0.1 and demultiplexing using the Seurat HTO Demux function (see Methods). Quality control and normalization were performed considering all 11 libraries together. For each library, the estimated number of recovered cells (before quality control) and the mean number of reads per cell, among other important library features, are indicated (Table 14).
This information is also given for T-cell receptor sequencing (Table 15).

Table 14. CellRanger quality control metrics.

ID	Number of reads	Estimated number of recovered cells	Fraction of reads in cells	Mean reads per cell	Fraction of reads mapped to exonic reads	Median genes per cell
oJIA1	729.59M	19,708	89.7%	37,020	55.1%	405
oJIA2	824.85M	24,263	89.3%	33,996	54.9%	373
oJIA3	799.84M	21,916	90%	36,495	47.9%	253
UV1	554.13M	14,945	87.5%	37,077	36.1%	312
UV2	426.50M	10,006	86.5%	42,624	40.3%	590
UV3	758.30M	20,161	85.7%	37,612	40.3%	304
UV4	275.98M	4,033	81.4%	68,430	33.3%	335
HC1	804.49M	28,092	93.7%	28,637	53.4%	321
HC2	297.97M	8,489	93.7%	35,100	44.7%	396
HC3	753.34M	18,537	93.4%	40,640	40.8%	324
HC4	605.17M	14,128	94.3%	42,834	40.8%	385

HC: healthy control; ID: identification; oJIA: oligoarticular juvenile idiopathic arthritis; UV: uveitis-related oligoarticular juvenile idiopathic arthritis.

Table 15. CellRanger quality control metrics for T-cell receptor sequencing.

ID	Number of reads	Estimated number of recovered cells	Fraction of reads in cells	Mean reads per cell	Fraction of reads mapped to any VDJ gene	Cells with product V-J spanning pair
oJIA1	140.92M	3,449	42.7%	40,859	62.1%	2,504
oJIA2	68.62M	3,389	34.5%	20,246	61.4%	1,682
oJIA3	86.33M	2,024	31%	42,653	65.3%	1,225
UV1	48.28M	380	14.2%	127,045	40%	221
UV2	35.67M	2,354	42%	15,151	54.5%	1,757
UV3	44.03M	566	17%	77,785	46.6%	260
UV4	25.23M	304	31.1%	83,006	63.4%	249
HC1	110.66M	2,632	32.1%	42,042	59.3%	1,292
HC2	42.42M	2,629	51.3%	16,134	59.1%	1,874
HC3	46.17M	1,608	29.8%	28,710	55.2%	740
HC4	42.36M	6,662	54.4%	6,358	55.7%	2,282

HC: healthy control; ID: identification; oJIA: oligoarticular juvenile idiopathic arthritis; UV: uveitis-related oligoarticular juvenile idiopathic arthritis.

Hashing efficacy is the percentage of valid reads in the HTO library. For each sample, the final number of total cells, singlets, doublets, negative cells, and percentage of reads with HTO, UMI, and cell barcode is indicated (Table 16).

Table 16. Hashing demultiplexing quality control data.

ID	Total cells	Singlets		Doublets		Negative		Reads with Ab-barcode + UMI + cell-barcode
		Cells	Fraction	Cells	Fraction	Cells	Fraction	
oJIA1	19,708	15,734	79.8%	3,411	17.3%	563	2.9%	60.1%
oJIA2	24,263	16,837	69.4%	4,232	17.4%	3,194	13.2%	60.6%
oJIA3	21,916	15,254	69.6%	3,584	16.4%	3,078	14%	20.9%
UV1	14,945	10,265	68.7%	3,170	21.2%	1,510	10.1%	42%
UV2	10,006	6,711	67.1%	1,579	15.8%	1,716	17.1%	25.1%
UV3	20,161	13,069	64.8%	4,488	22.3%	2,604	12.9%	38.9%
UV4	4,033	3,333	82.6%	397	9.8%	303	7.5%	13.4%
HC1	28,092	21,375	76.1%	5,504	19.6%	1,213	4.3%	68.4%
HC2	4,023	3,343	83%	443	9.9%	404	8.5%	12.5%
HC3	18,537	14,290	77.1%	3,241	17.5%	1,006	5.4%	39.1%
HC4	14,128	10,158	71.9%	1,679	11.9%	2,291	16.2%	29.1%

Ab-barcode: antibody-based barcode; HC: healthy control; ID: identification; oJIA: oligoarticular juvenile idiopathic arthritis; UV: uveitis-related oligoarticular juvenile idiopathic arthritis; UMI: unique molecular identifier.

We performed QC and normalization considering all 11 libraries together after ensuring no remarkable differences in the main QC metrics (Figure 14).

We filtered out low-quality barcodes by removing those with a deficient number of UMI (< 225) and genes per barcode (< 100) or with a percentage of expression from mitochondrial expression higher than 20%, as it is indicative of lysed cells. We also considered removing barcodes with a large library size and complexity (> 7,000 UMIs and > 2,000 genes). Red lines indicate the exclusion criteria. Finally, the data was normalized and log transformed.

Figure 14. Library quality control figures.

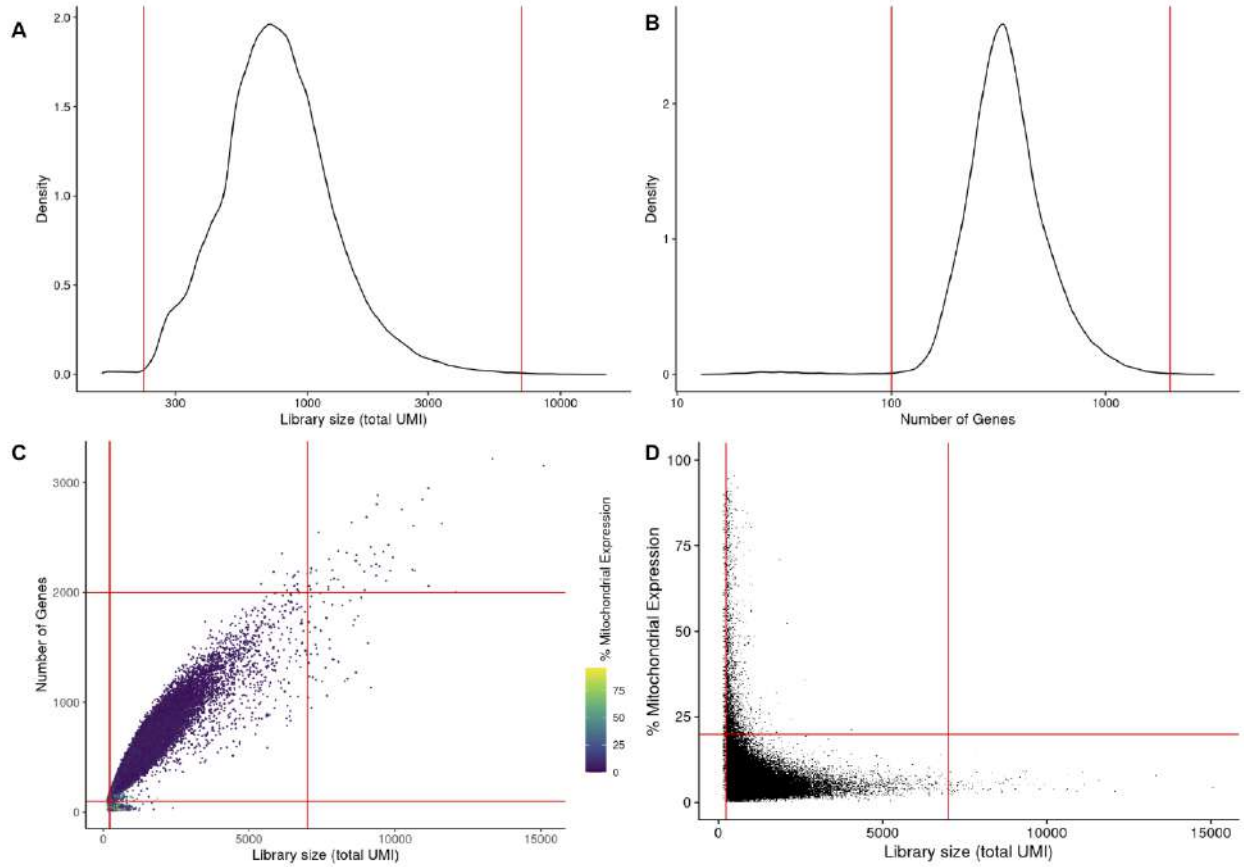

A) QC for library size. Red vertical lines delimitate the smaller and bigger library size permitted. **B)** QC for the number of genes. **C)** QC for complexity considering the number of UMIs and genes. **D)** QC for mitochondrial expression. Red lines indicate the exclusion criteria.

5.2.2. Cluster annotation

To describe the cellular and transcriptional landscape of oJIA in peripheral blood and synovial fluid at the very onset of the disease, and the transcriptional landscape in the peripheral blood of oJIA-UV at flare, the transcriptome of 132,824 cells were analyzed together.

A feature selection of the 3,000 most variable genes was applied to perform the clustering, and dimensionality was reduced by applying PC analysis (Figure 15).

Figure 15. Feature selection and dimensionality reduction.

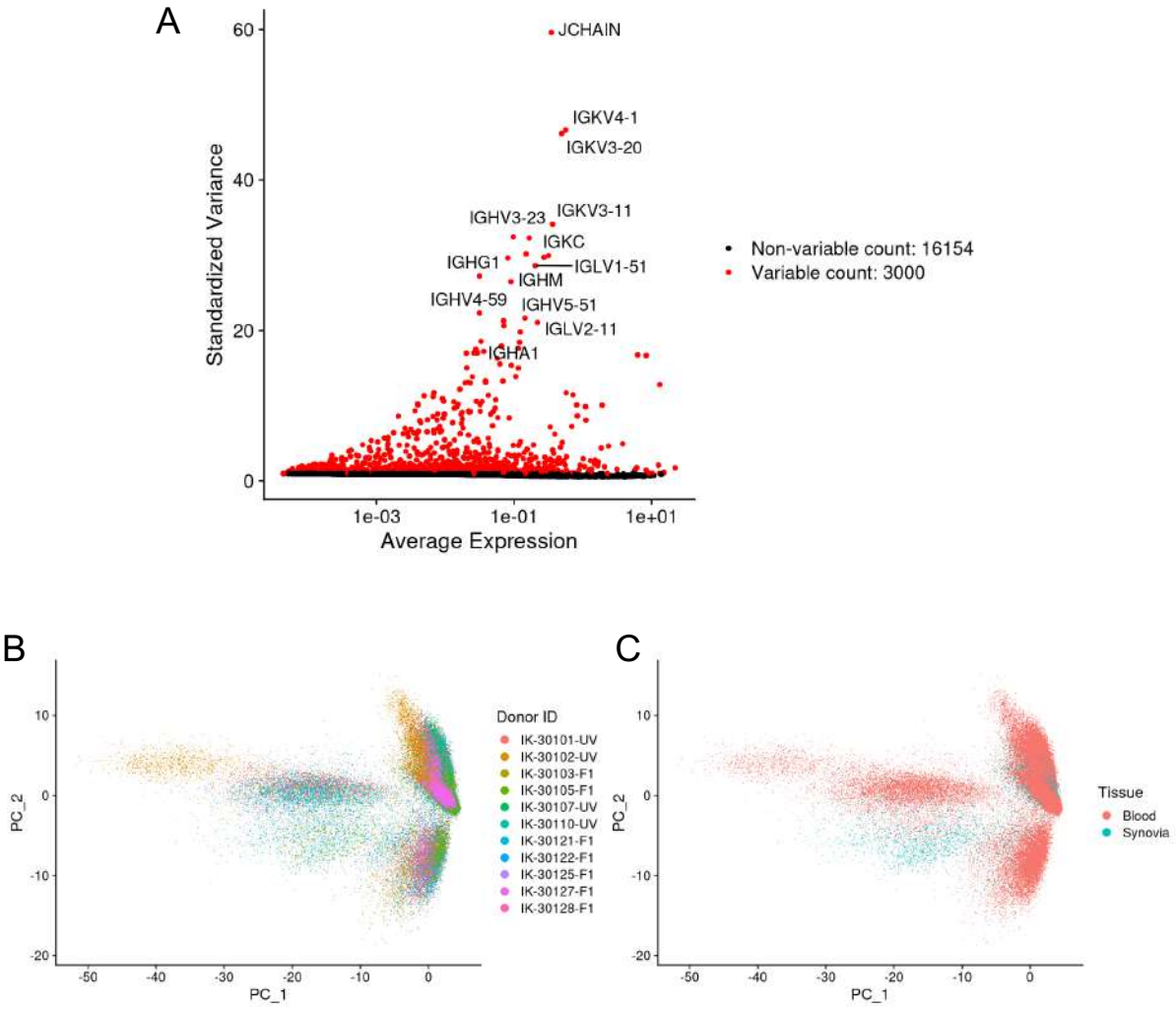

A) Top variant genes selections. Genes are shown based on their Standard Variance and their Average Expression. The 3.000 most variable genes selected for the downstream analyses are shown in red. **B)** PC dimensionality reduction for a donor. **C)** PC dimensionality reduction for tissue.

We corrected the PCs by libraries using Harmony and Seurat methods to integrate the libraries. To assess whether clusters of cells are well-mixed across some categorical variable (e.g. batch, technology, donor), Korsunsky, I. *et al.* provided an algorithm for computing a Local Inverse Simpson's Index (LISI) [197]. This resulted in an optimal integration, as reflected by the LISI score of 5.0 with both Harmony and Seurat packages.

Using the elbow rule, we selected the first 20 Harmony-integrated PCs to represent the dataset. These 20 PCs were used to compute a two-dimensional representation

of the dataset with UMAP, which is a dimensionality reduction algorithm that depicts the cell expression patterns using only two dimensions.
The 20 PCs were also used to find cell clusters by applying the Louvain clustering algorithm with the “FindClusters” function and setting the resolution parameter to 0.5 (see Methods).

5.2.2.1. Global cell lineages

Counting all together the cells from different source origins and conditions, we identified five global clusters (Figure 16). We annotated the cell types composing each cluster based on the expression of the canonical markers and the absence of markers of other lineages explained hereafter. Cluster 1 represents B cells (n=11,822), cluster 2 myeloid cells (n=11,239), cluster 3 T-NK cells (n=104,594) and proliferative cells cluster 4 (n=764). Cluster 5 was composed of death cells/low-quality cells (4,406 cells) that were not analyzed further.

Figure 16. Global cell lineages.

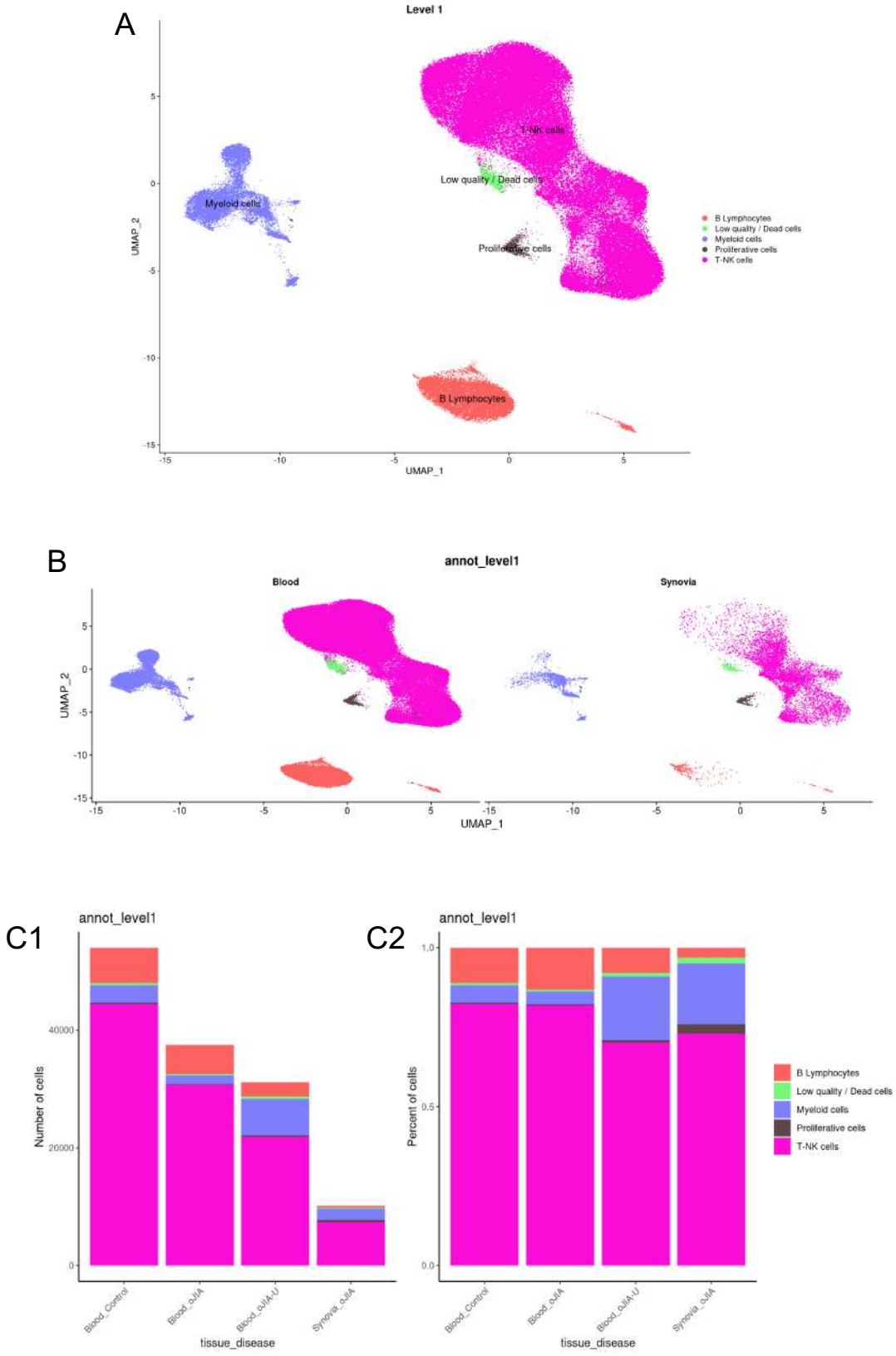

A) UMAP plot representing all the cells from different tissue sources and conditions, 5 clusters are obtained. **B)** UMAP plot representing the 5 clusters described at a level based on different tissue (blood and SF). **C)** Bar plot representing the 5 clusters based on different tissue, **C1)** number of cells and **C2)** proportion.

The cellular composition of each tissue and condition was different. As noted in Figure C1, synovial fluid was composed of a total of 10.150 cells, cluster 3 being the most abundant (n= 7,404 cells, 72.95%), followed by cluster 2 (n= 1,623 cells, 15.99%), and finally the two clusters less abundant, cluster 4 (n= 308, 3.03%) and cluster 5 (n= 815, 8.03%). Blood from HCs and oJIA patients had a similar composition of major clusters. In contrast, oJIA-U blood had a distinct profile with a higher frequency of cluster 2 (n= 5,745, 18.42%) compared to cluster 2 from oJIA and HC (n= 1,303, 3.48%; n= 2,568, 4.75%, respectively).

Cell clusters can be defined at multiple resolution levels, depending on the level of granularity the researcher is interested in. In this case, we have decided to keep clusters defined at different resolution levels for downstream analyses. We used a second and a third high-resolution level to identify specific cell populations and to study differences in terms of cell composition between tissues and conditions. The level with the highest definition of each cluster is shown below.

5.2.2.2. B cells

At level 3 and resolution 0.5, B cell clusters can be further grouped into 7 clusters based on expressed markers (Figure 17).
Cluster 0 corresponds to naive B cells (IGHD^{+}, CD27^{-}, MS4A1).
Cluster 1 corresponds to switched memory B cells. As these cells do not express IgD and have undergone class-switching, they are characterized by being IgD^{-}, CD27^{+}, CD19^{+}, and do not express the gene markers CXCR3, FAS, and CXCR5.
Clusters 2, 5, and 7 are formed by the CD69^{+} activated naive B cells.
Cluster 3 is formed by non-switched memory B cells (CD20^{+}, CD27^{+}, IgD^{+}) characterized by the expression of gene markers IGHD, CD27, IGHM, and FAS.
Cluster 4 is composed of ABCs-like (age-associated B cells) memory B cells (CD19^{high}, CD11c^{+}). Gene markers expressed in this cluster are CD19, ITAGX, CR2, and TBX21.
Cluster 6 comprises plasma B cells (JCHAIN, MZB1, CD27, IGKC), and cluster 7 comprises plasmablasts (H2AFZ, STMN1, ACTG1).

Figure 17. B cell cluster.

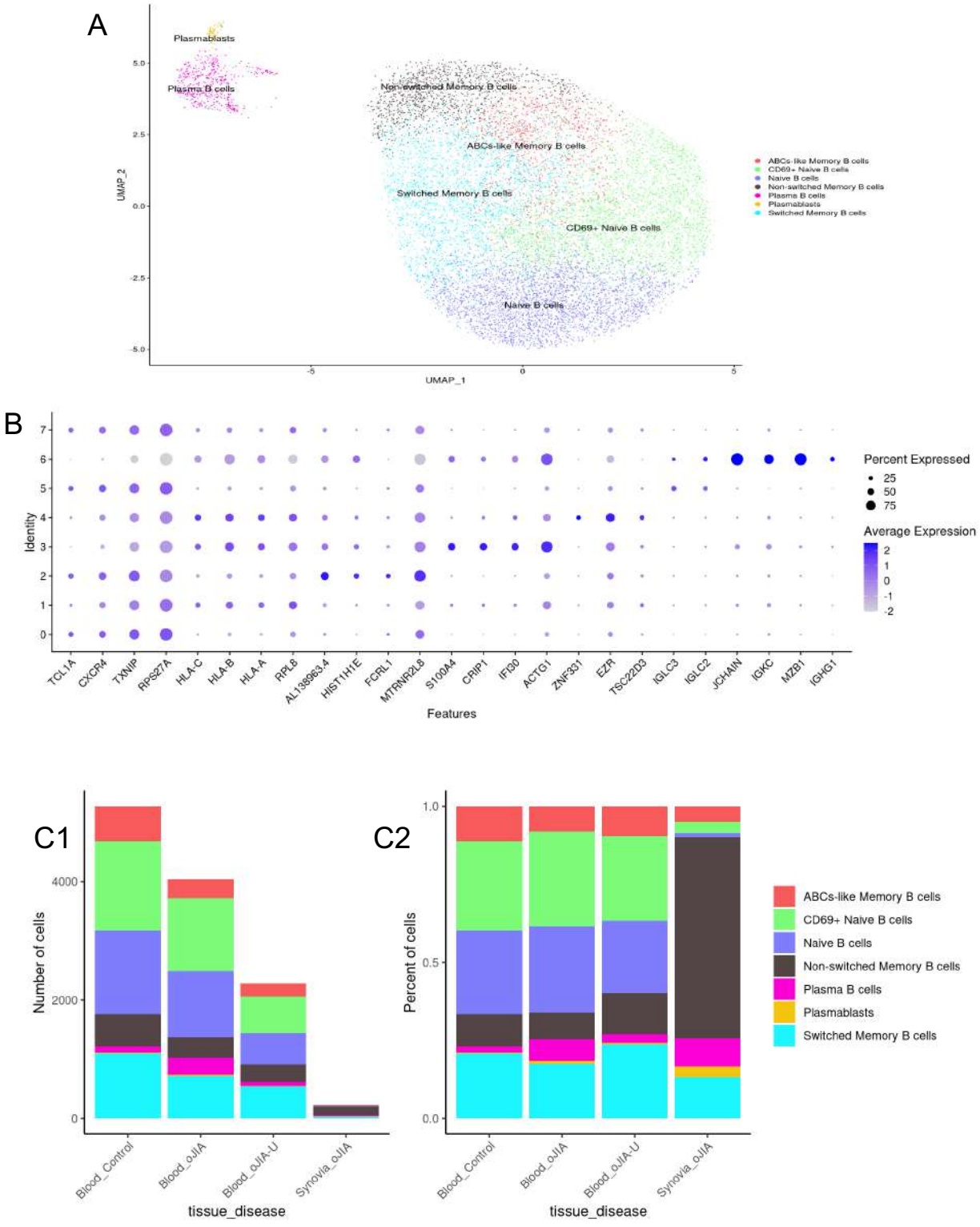

A) UMAP plot showing the identified clusters and their annotation. **B)** Dot plot representing the expression of top marker genes for cluster identification. Color is proportional to the average expression level in each cluster and size is proportional to the percentage of expressing cells. **C)** Bar plot representing the 7 clusters based on different tissue, **C1)** the frequency of cells, and **C2)** the proportion of cells.

SF has the lower total number of B cells, almost represented by non-switched memory B cells. No great differences in cell number or percentages are observed in blood from oJIA, oJIA-U, or healthy controls. Cellular frequencies and proportions are available in annexes (Supplementary Table 3).

5.2.2.3. Myeloid cells

At level 3 and resolution 0.25, the myeloid cluster is then divided into 9 subclusters (Figure 18). Cluster 0 corresponds to classical monocytes (S100A9, CD14, VCAN). Cluster 1 corresponds to dendritic cells type 4 (FCG3A, LST1), cluster 2 dendritic cells type 2 (CD1C, FCER1A, CLEC10A), cluster 4 dendritic cells type 1 (CLEC9A), cluster 5 plasmacytoid dendritic cells (GZMB, JCHAIN), cluster 6 intermediate monocytes (CSTB), cluster 7 activated dendritic cells (CCR7, CD83), and cluster 8 non-classical monocyte (PPBP).

Cluster 3, which corresponds to doublets, and cluster 9, which corresponds to proliferative myeloid cells analyzed further, are not considered for differential proportion analysis.

Figure 18. Myeloid cluster.

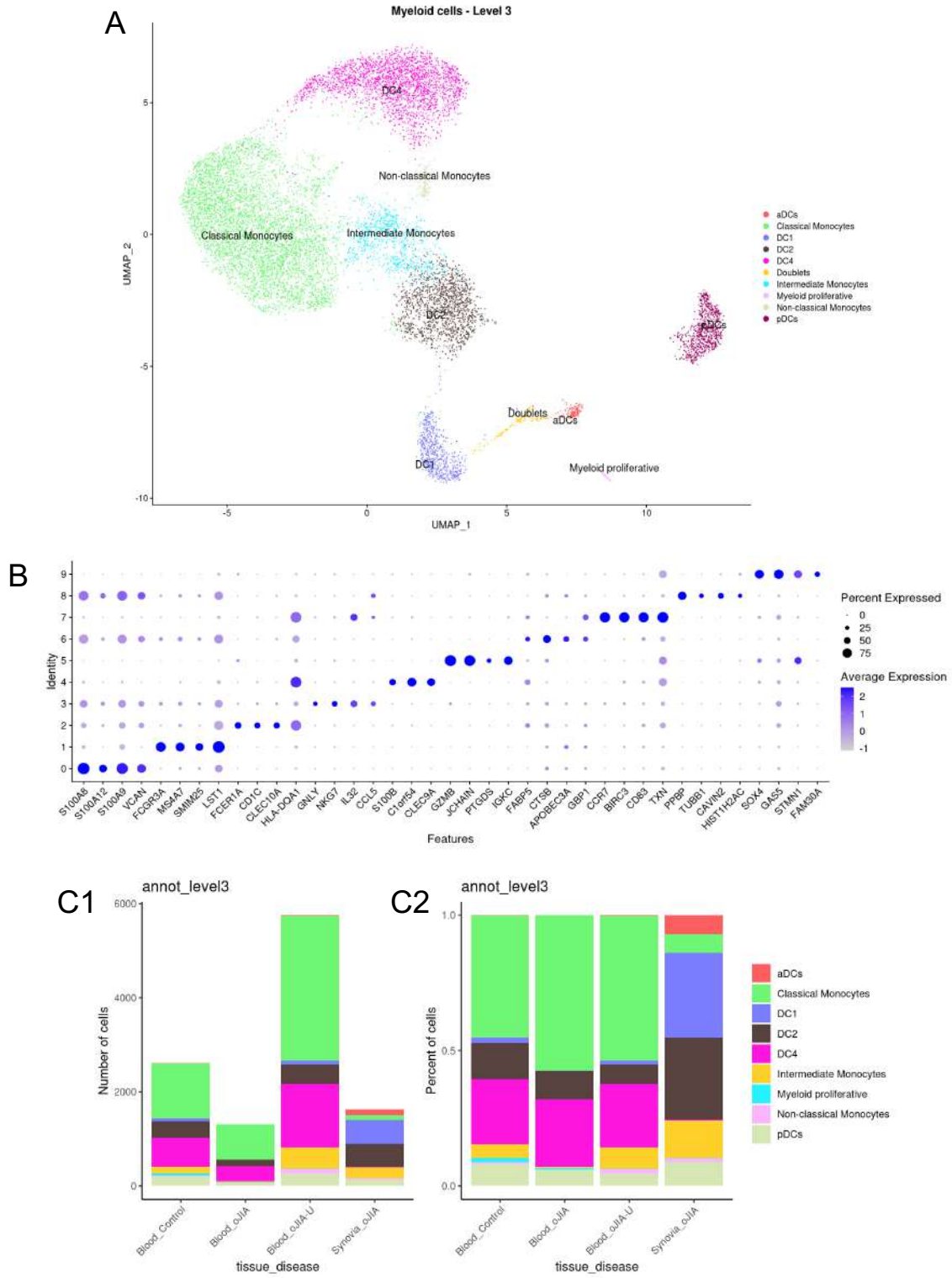

A) UMAP plot showing the 9 identified clusters and their annotation. **B)** Dot plot representing the expression of top marker genes for cluster identification. Color is proportional to the average expression level in each cluster, and size is proportional to the percentage of expressing cells. **C)** Bar plot representing the 9 clusters based on different tissue, **C1)** the frequency of cells, and **C2)** the proportion of cells.

The bar plot shows that the group oJIA-U has the largest number of myeloid cells compared to oJIA, controls, and synovial fluid. SF is more heterogeneous and is composed of a higher percentage of type 1 and type 2 dendritic cells, and intermediate monocytes than blood. Compared to oJIA without uveitis, oJIA-U has a higher percentage of dendritic cells type 1, intermediate monocytes, and non-classical monocytes. Cellular frequencies and proportions are available in annexes (Supplementary Table 4).

5.2.2.4. T-NK cells

Due to the large number of cells present in this group and their complexity, a first analysis has been performed at resolution 1.3 identifying 10 clusters, shown in Figure 19.
Subsequently, a sub-clustering has been applied with different resolution parameters allowing to focus on more detailed substructures in the dataset to identify finer cell states.

Figure 19. T-NK cluster.

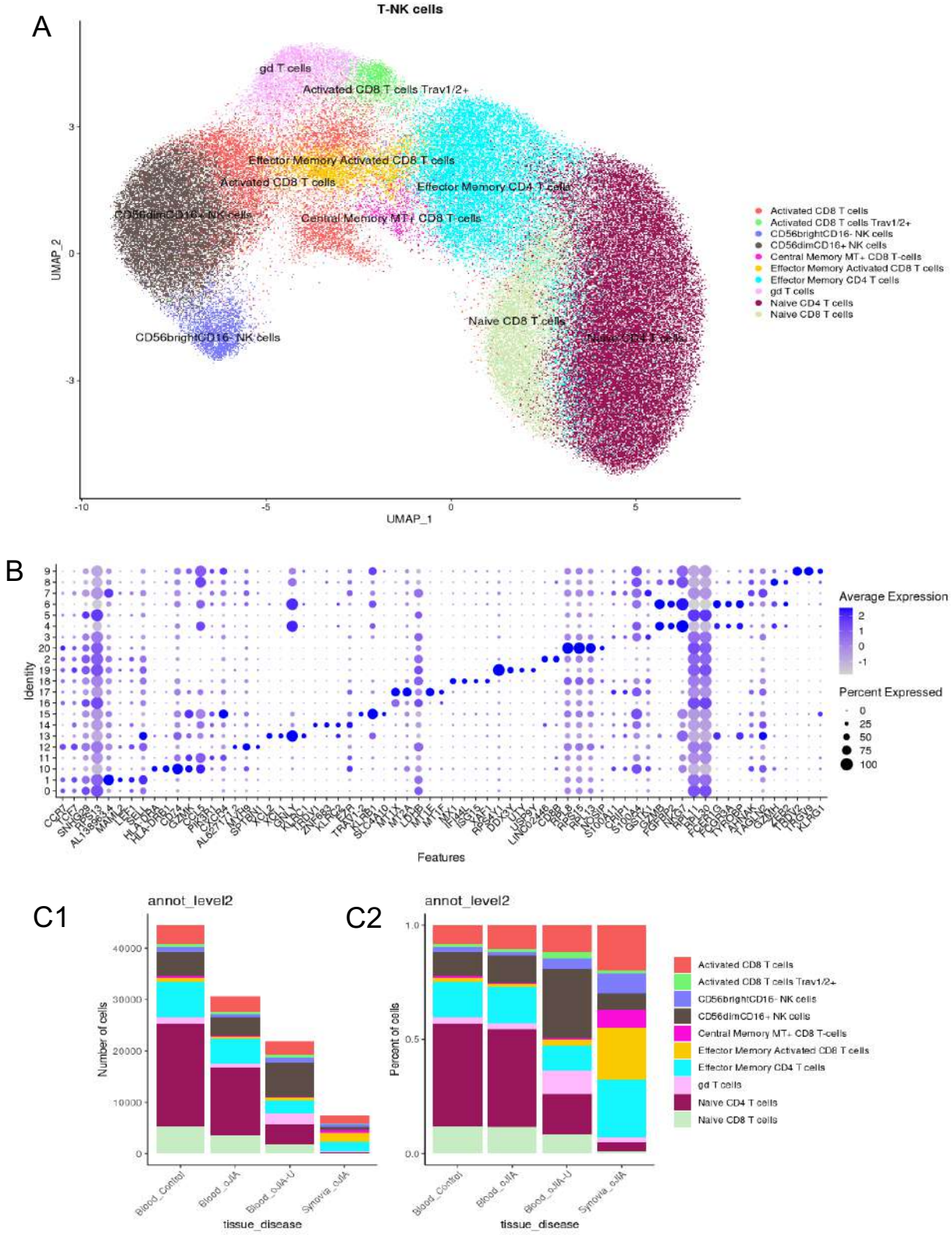

A) UMAP plot showing the 10 identified clusters: activated CD8$^+$ T cells, activated CD8$^+$ T cells Trav1/2, CD56$^+$ bright NK cells, CD56$^+$ dim NK cells, central memory CD8$^+$ T cells, activated effector memory CD8$^+$ T cell, effector memory CD4$^+$ T cells, gd T cells, naive CD4$^+$ T cells, and naive CD8$^+$ T cells. **B)** Dot plot representing the expression of top marker genes for cluster identification. **C)** Bar plot representing the 10 clusters based on different tissue, **C1)** the frequency of cells, and **C2)** the proportion of cells.

As visualized, SF composition is more heterogeneous than blood, with a higher proportion of effector memory $CD4^+$ and $CD8^+$ T cells. This heterogeneity is also seen in oJIA-U peripheral blood with a higher percentage of NK cells than blood from oJIA and HC.

5.2.2.4.1. CD8 T cells

To gain more insight into the $CD8^+$ T cell cluster, a subclustering analysis was performed exclusively for this population. Using resolution level 0.5, four different clusters were identified. Cluster 0 is composed of effector memory $CD8^+$ T cells (expressing high levels of GNLY, GZMB, PRF1), cluster 1 composed by activated effector memory $CD8^+$ T cells (HLA-DPA1, HLA-DRB1, GZMK, CCL5), cluster 2 formed by $NKG2C^+$ effector memory $CD8^+$ T cells (NKG2C, KLRC2, Hobit) and cluster 3 formed by central memory $CD8^+$ T cells (KLRC2, IFITM3, ZNF683, CCR7, CD62L) (Figure 20).

Figure 20. CD8 cluster.

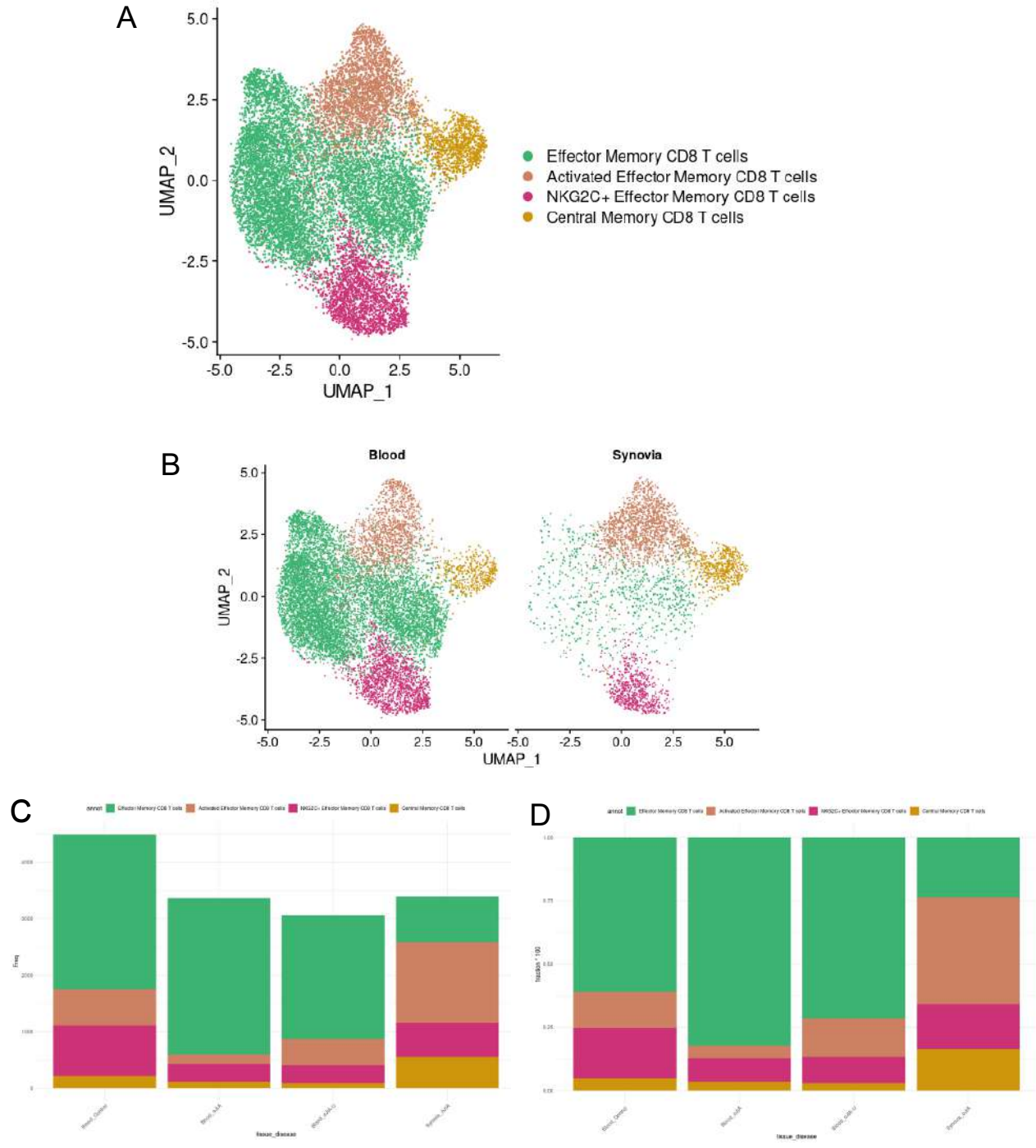

A) UMAP plot showing the 4 identified clusters for $CD8^+$ T cells. **B)** UMAP plot representing the 4 different clusters according to different tissues. **C)** Bar plot representing the frequency of the 4 clusters according to different conditions and tissue and **D)** Bar plot representing the proportions of the 4 clusters according to different conditions and tissue.

The SF is represented by a higher number and percentage of activated effector memory, NKG2C$^+$ effector memory, and central memory CD8$^+$ T cells than blood from oJIA, oJIA-U and HCs. Cellular frequencies and proportions are available in annexes (Supplementary Table 5).

5.2.2.4.2. NK cells

NK cells were also analyzed at a lower level of resolution to gain more granularity. At 0.5 level of resolution, five clusters were identified.
Cluster 0 consists of immature CD56$^+$dim CD16$^+$ NK cells (NKG7, GZMA), cluster 1 of mature CD56$^+$dim CD16$^+$ NK cells (GMZA, ACTB), cluster 2 of terminal CD56$^+$dim CD16$^+$ NK cells (ZEB2, CX3CR1), cluster 3 of CD56$^+$ bright NK cells (CD62L/SELL, GZMK), and cluster 5 of NK-like CD8$^+$ T cells (Figure 21).

Figure 21. NK cluster.

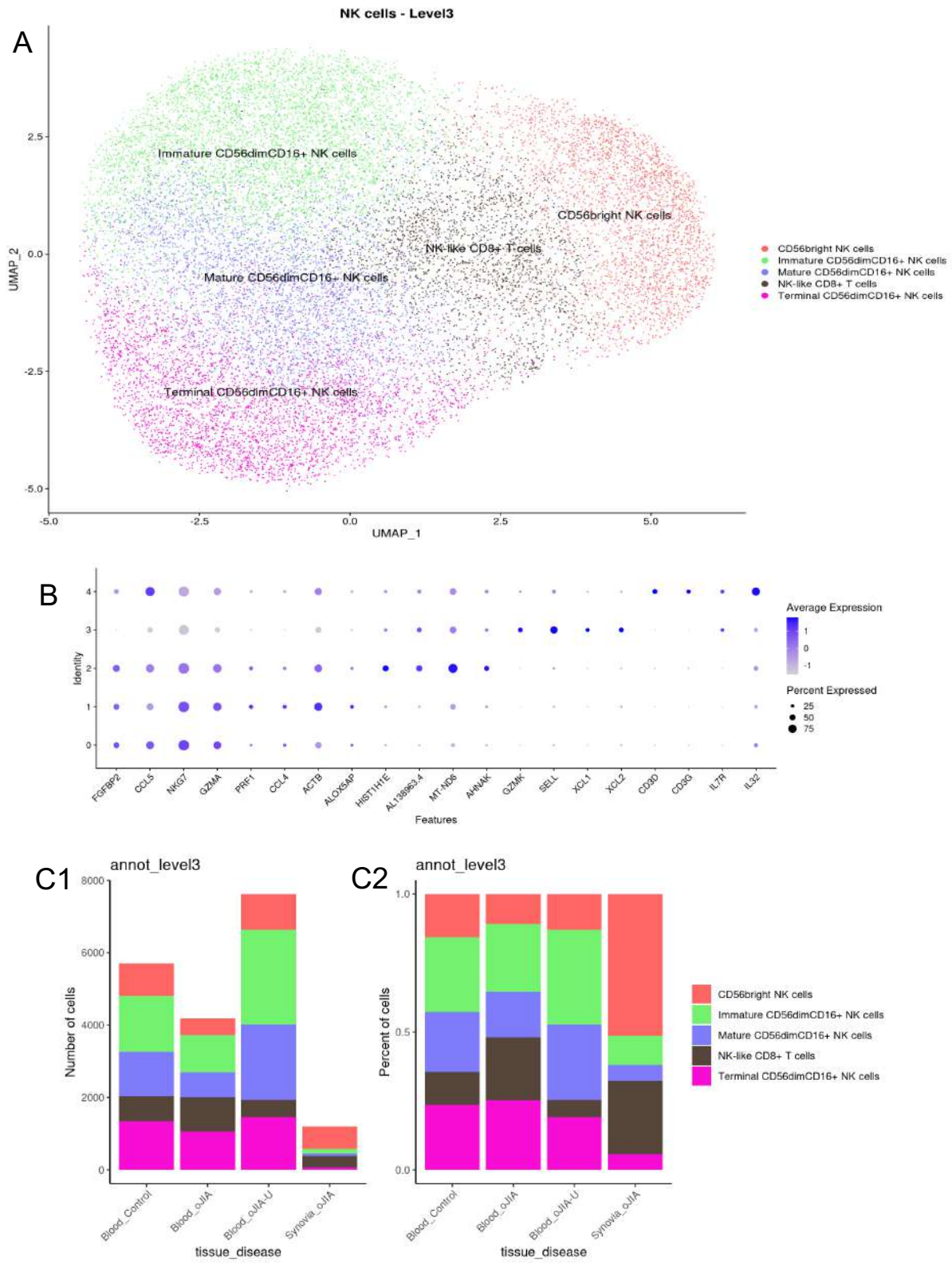

A) UMAP plot showing the 5 identified clusters **B)** Dot plot representing the expression of top marker genes for cluster identification. **C)** Bar plot representing the 10 clusters based on different tissue, **C1)** the number of cells, and **C2)** the frequency.

As visualized, SF composition has a higher percentage of $CD56^+$ bright NK cells. A higher number of NK cells is found in oJIA-U patients, predominantly mature and immature $CD56^+$dim $CD16^+$ NK cells, compared to HCs and oJIA patients without uveitis.
Cellular frequencies and proportions of NK cells are available in annexes (Supplementary Table 6).

5.2.2.4.3. CD4 and other T cells

Starting from T-NK cell cluster 3 (level 2, resolution 1.3), we analyzed in depth those clusters that were neither naive cells (analyzed below) nor NKs (Figure 21).
At level 3, resolution 0.5, we obtain different $CD4^+$ T-cell clusters and other less abundant subpopulations (Figure 22).

Figure 22. CD4 and other T cell lineages.

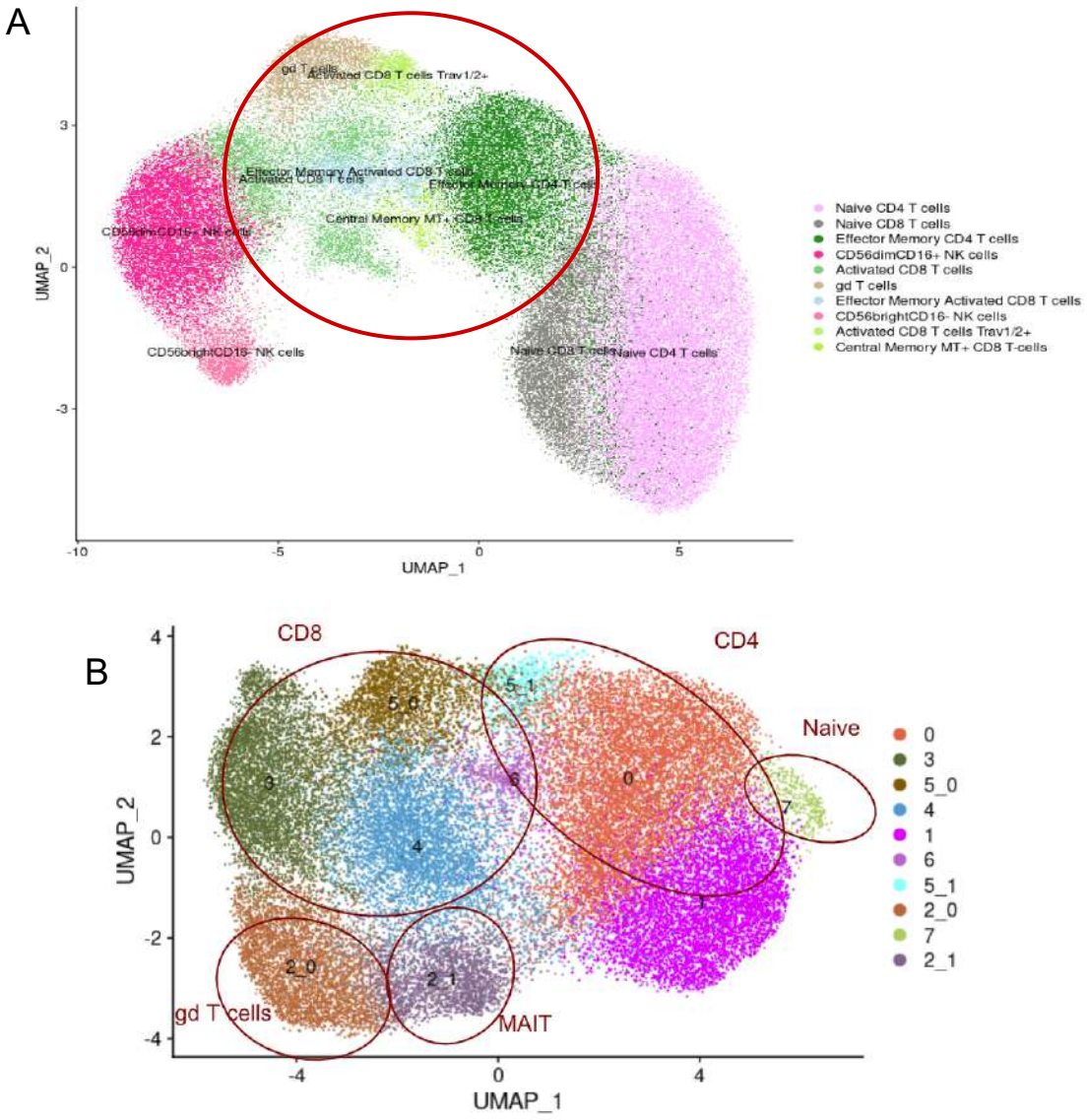

A) UMAP plot showing T-NK cluster with the 10 identified clusters. **B)** UMAP plot representing the clusters depicting the T cell pools with NK cells and naive cells removed. CD8 T cells have been analyzed in major detail.

Subsequently, we found the cluster formed by mucosal-associated invariant T (MAIT) cells, which typically express TRAV1-2^{+}. On the other hand, we found the γdT cells cluster, characterized by the expression of TRGV9 (Figure 23).

Figure 23. Mucosal-associated invariant T and γdT cells cluster.

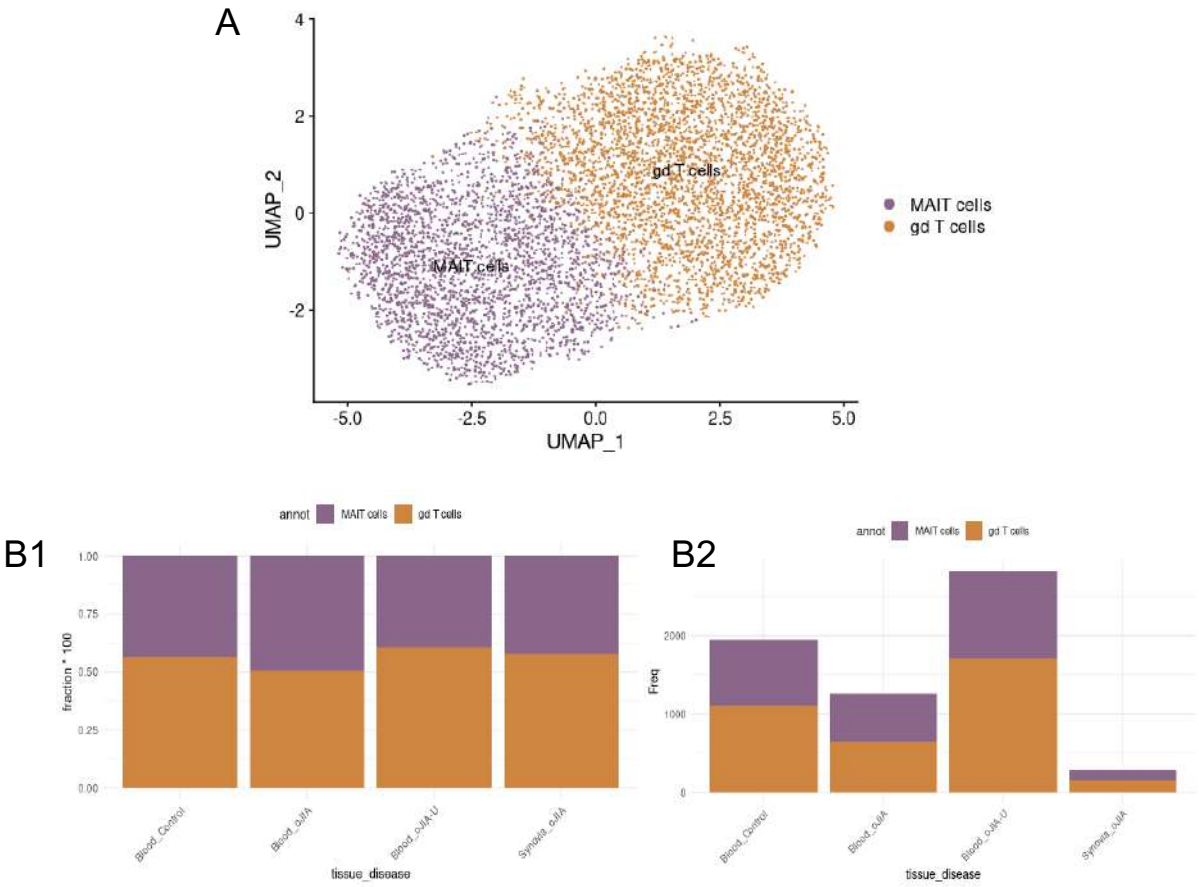

A) UMAP plot showing MAIT γdT cell clusters. **B)** Bar plots representing the 2 clusters based on different tissue, **B1)** the number of cells, and **B2)** the frequency.

Finally, we identified double-negative (DN) T cells ($CD4^-$, $CD8^-$), T regs (CTLA4, FOXP3, TIGIT), effector memory $CD4^+$ T cells (GZMK, NKG7, GNLY, GZMA), central memory $CD4^+$ T cells (CCR7, KLRB1, KLRG1) and naive CD4 T cells which are further explained hereunder (Figure 24).

Figure 24. Other CD4 T cells cluster.

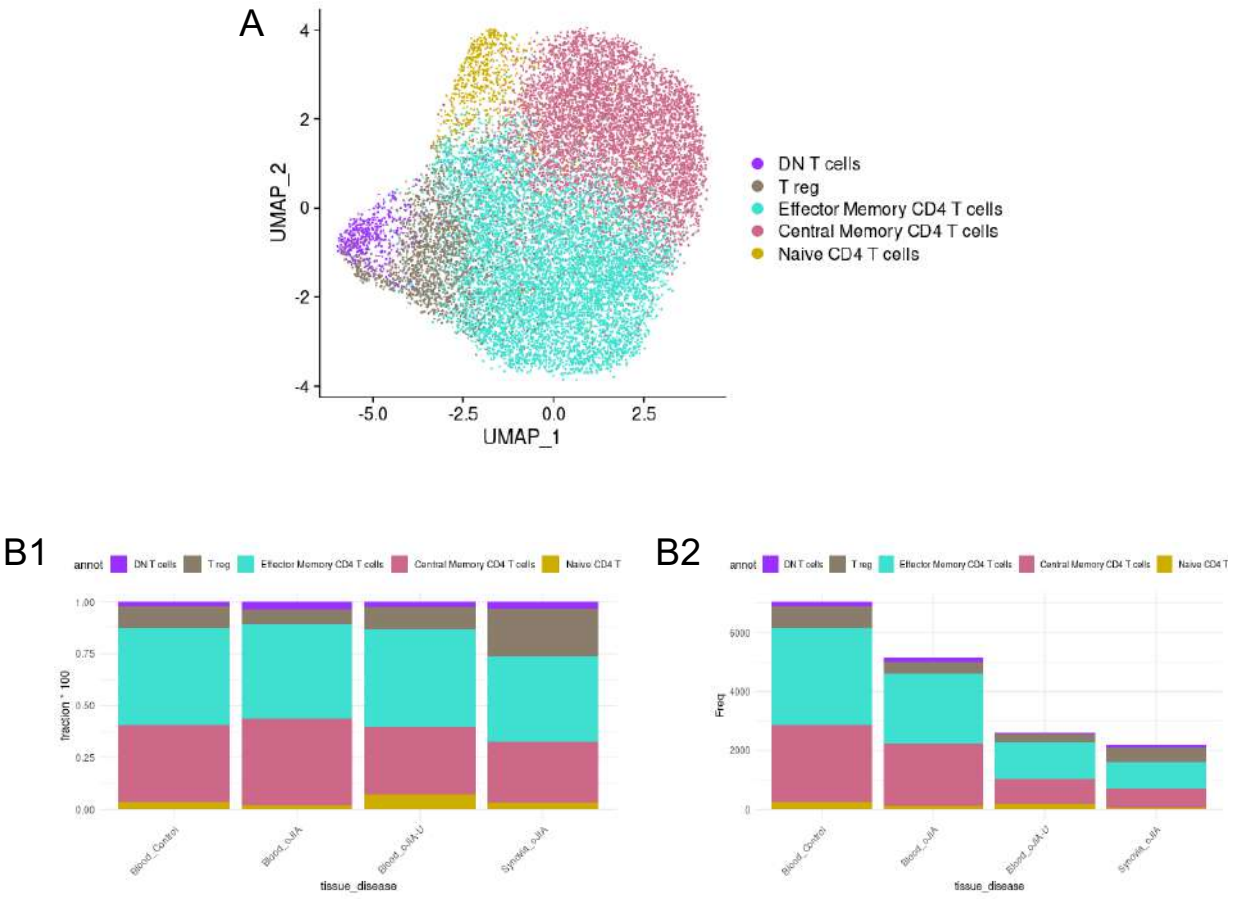

A) UMAP plot showing other CD4 T cell clusters. **B)** Bar plots representing the 2 clusters based on different tissue, **B1)** the number of cells, and **B2)** the frequency.

5.2.2.4.4. Naive T cells

At level 3, resolution 0.5, the naive T cell cluster (CCR7, SELL) is represented by two subclusters: naive CD4⁺ T cells and naive CD8⁺ T cells (Figure 25).

Figure 25. Naive T cell cluster.

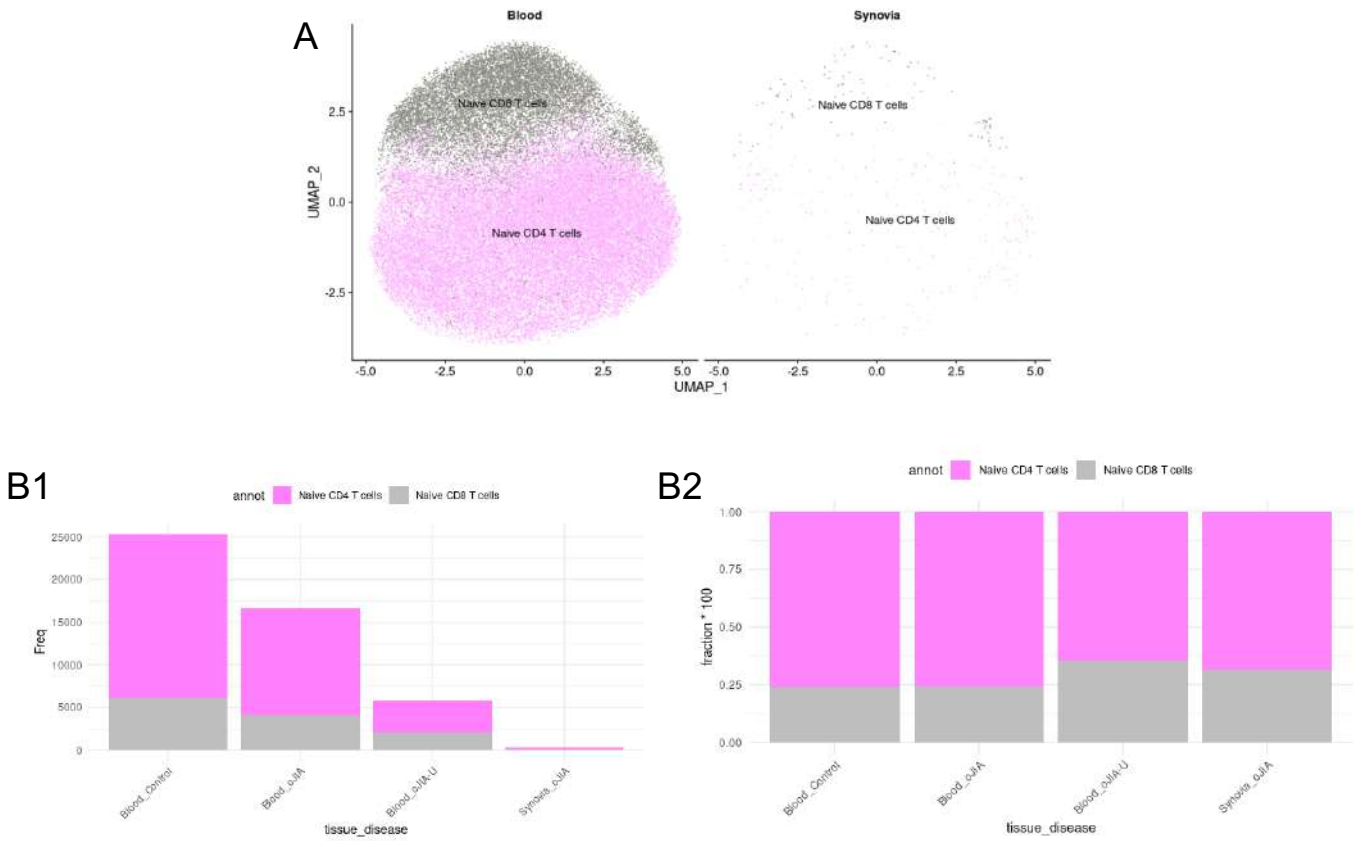

A) UMAP plot representing naive T cell cluster. **B)** Bar plots representing the 2 clusters based on different tissue, **B1)** the number of cells, and **B2)** the frequency.

As noted, naive T cells are scarcely represented in SF. Naive T cells are more abundant in peripheral blood from HC, followed by oJIA patients.

Cellular frequencies and proportions of CD4⁺ T cells, other less abundant T cell populations, and naive T cells are available in annexes (Supplementary Table 7).

5.2.2.5. Proliferative cells

Cluster 4 (level 2; resolution 1.) comprises proliferative cells based on cell cycle markers for S, G2, and M stages. Seven different clusters are distinguished.
Clusters 0, 2, 3, 5, correspond to proliferative T cells (PRDX1, IL32, CD3G, CD52, RPS26, RPL30, RP53A, RPS13, GZMK, CD27), clusters 1 and 4 to proliferative NK cells (FCER1G, GNLY, TYROBP, GZMB, RPS26, RPL30, RP53A, RPS13), and cluster 6 to proliferative myeloid cells (LYZ, IFI30, HLA-DRA, HLA-DPB) (Figure 26).

Figure 26. Proliferative cells.

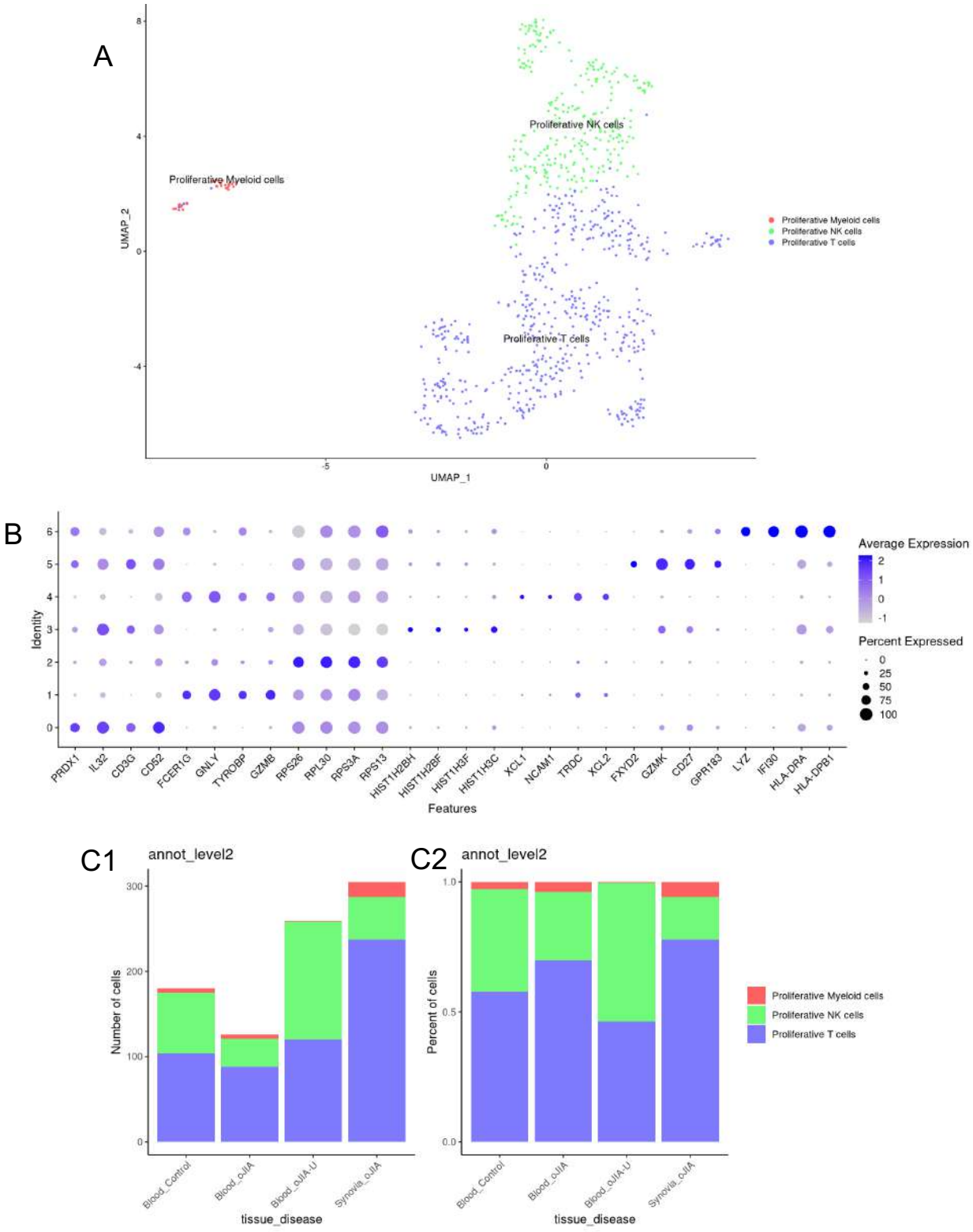

A) UMAP plot representing proliferative cell clusters and **B)** Dot plot representing the expression of top marker genes for cluster identification. **C)** Bar plot representing the **C1)** frequency of cells and **C2)** the proportion of cells in each tissue and condition.

SF is represented by a higher percentage of myeloid proliferative cells compared to blood (all conditions). Remarkably, NK proliferative cells are more abundant in blood from oJIA-U patients. Cellular frequencies and proportions of proliferative cells are available in annexes (Supplementary Table 8).

5.2.3. Differences in cell type abundances

Once the annotation of all cell clusters was completed, we investigated the cell type abundances in each tissue and condition, and we tested for significant differences in cell composition among different groups (Figure 27).

Figure 27. Cell type abundances per tissue and condition.

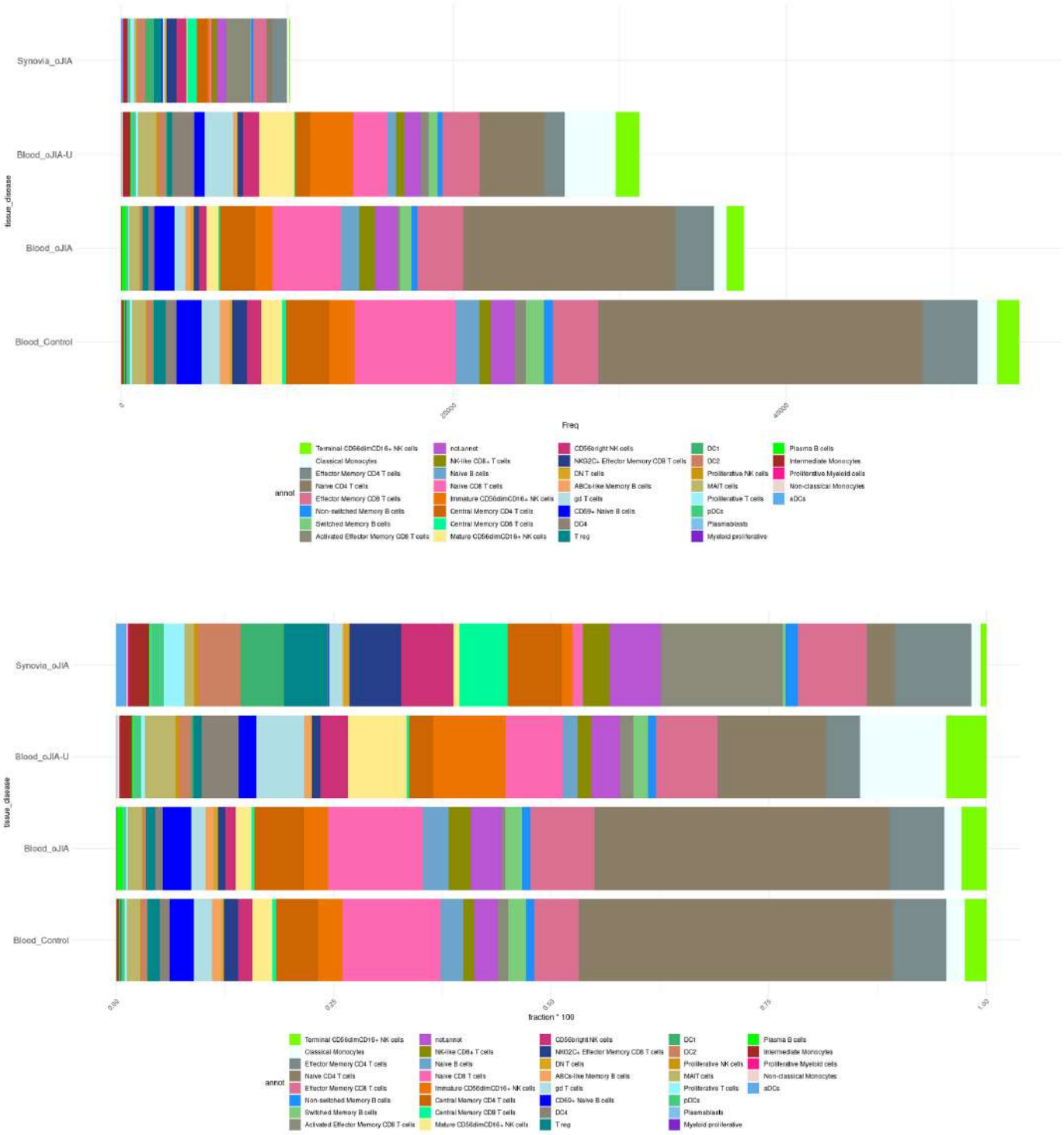

Bar plot showing the cell composition of each group based on the most accurate cell annotation. The frequency **A)** and the proportion **B)** of each population is represented.

To investigate the relationship between SF and PB in patients with two different conditions (oJIA with and without uveitis) compared to HC, we applied a t-test. A paired t-test was performed to compare cell type abundances between blood and synovial fluid from the same donor.

As there are many clusters and cells, statistically significant differences are presented globally as a first approximation (Figure 28).

Figure 28. Heatmap of the global differences in cell composition.

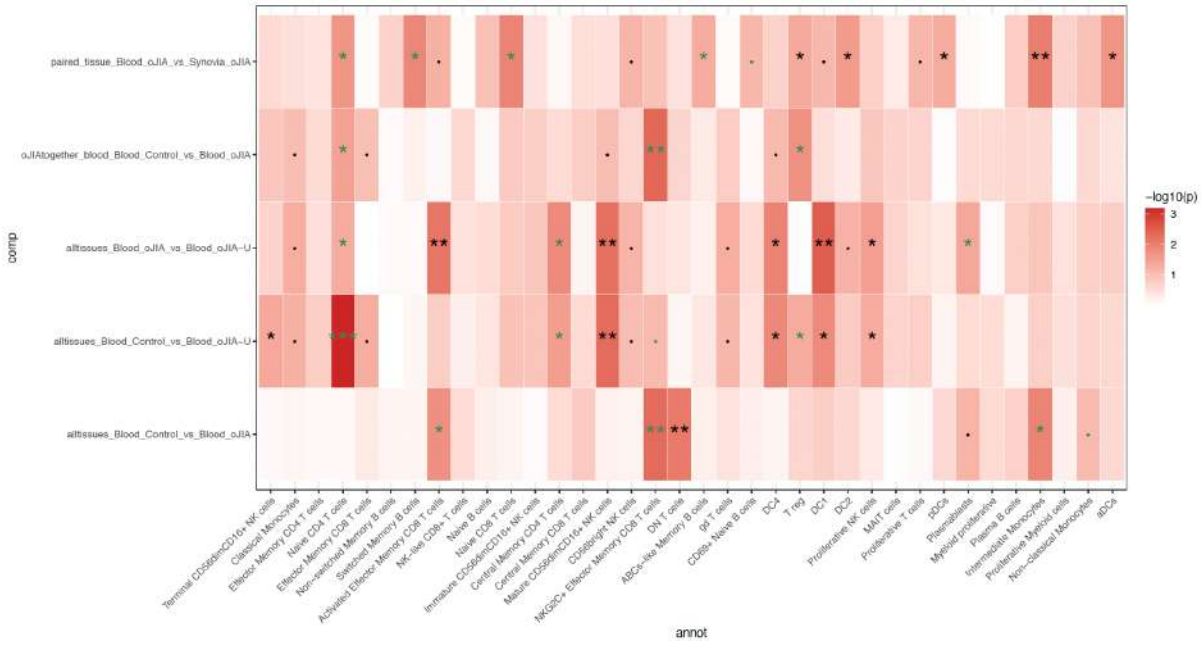

The heatmap represents the differences in cell composition in the different comparisons. Each column represents a cell subtype. Each row represents a different comparison, starting with the differences between synovial fluid and whole peripheral blood for the same patients. This is followed by comparisons in peripheral blood in different conditions. P-values <0.05 are represented with one asterisk *, p-values <0.01 with two asterisks **, and p-values <0.001 with three asterisks ***. Green asterisks represent the differences that are statistically significant, with cellular subpopulations more abundant in the first group of the comparison. Black asterisks represent the differences that are statistically significant with cellular subpopulations less abundant in the first group of the comparison.

SF: synovial fluid; PB: peripheral blood; HC: healthy control; oJIA: oligoarticular juvenile idiopathic arthritis; oJIA-U: uveitis related to oligoarticular juvenile idiopathic arthritis. DC4: dendritic cells type 4; DC1: dendritic cells type 1; DC2: dendritic cells type 2; pDCs: plasmacytoid dendritic cells; aDCs: activated dendritic cells.

The following sections detail the significant statistical cellular differences for each comparison.

5.2.3.1. Cell type abundances comparing synovial fluid to peripheral blood.

In the first analysis, a paired t-test was performed to compare cell proportions between blood and SF from the same donor (Figure 29).

Figure 29. Box plot comparing the proportion of cell types with significant differences ($p<0.05$) between SF and PB from paired samples.

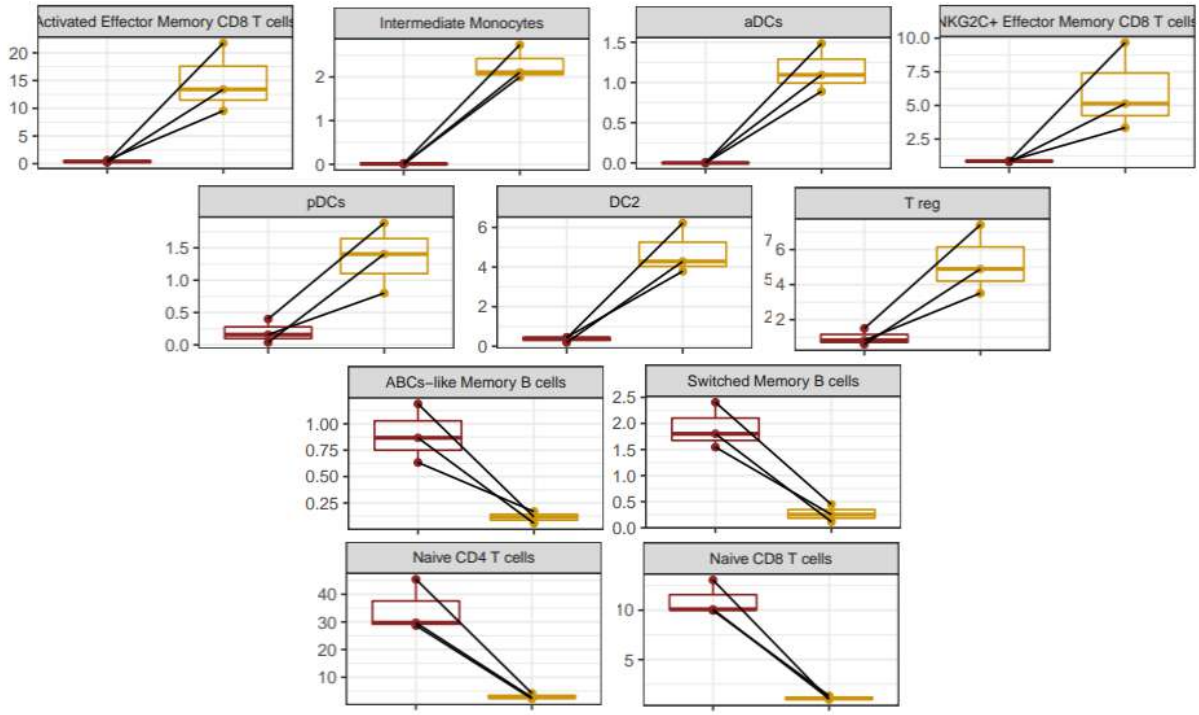

Red box plots represent peripheral blood, and the yellow boxes represent synovial fluid. ABCs-like memory B cells: age-associated B cells; DC2: dendritic cells class 2; Treg: regulatory T cells; aDCs: activated dendritic cells; pDCs: plasmacytoid dendritic cells.

A higher abundance of activated and NKG2C$^+$ effector memory CD8$^+$ T cells, intermediate monocytes, activated dendritic cells, and regulatory T cells characterizes synovial fluid. In contrast, there are more -naive CD8$^+$ and CD4$^+$ T lymphocytes, ABCs-like memory B cells, and switched B lymphocytes in peripheral blood.

These observations could indicate these cells' migration pattern from the blood to the inflamed tissue in oJIA. To assess the suggested migratory flux to the site of damage, we test the differences in cell composition among blood samples from oJIA, oJIA-U and healthy donors.

5.2.3.2. Cellular interconnection between synovial fluid and peripheral blood in different conditions

We observed a decrease in circulating naive $CD4^+$ T cells, $NKG2C^+$ effector memory $CD8^+$ T cells and T regs in oJIA and oJIA-U, compared to HCs. In turn, the relative abundance of $NKG2C^+$ effector memory $CD8^+$ T cells, and T regs was higher in SF from oJIA (Figure 30). A higher content of naive $CD4^+$ T cells in HCs suggests less exposure to antigens.
On the other hand, a higher proportion of circulating T regs and effector memory $CD8^+$ T cells in controls than in oJIA, and in SF than in oJIA blood likely indicates that these cells are migrating from blood to the inflamed tissue.

Figure 30. Box plots depicting the most significant differences in cell proportions in oJIA.

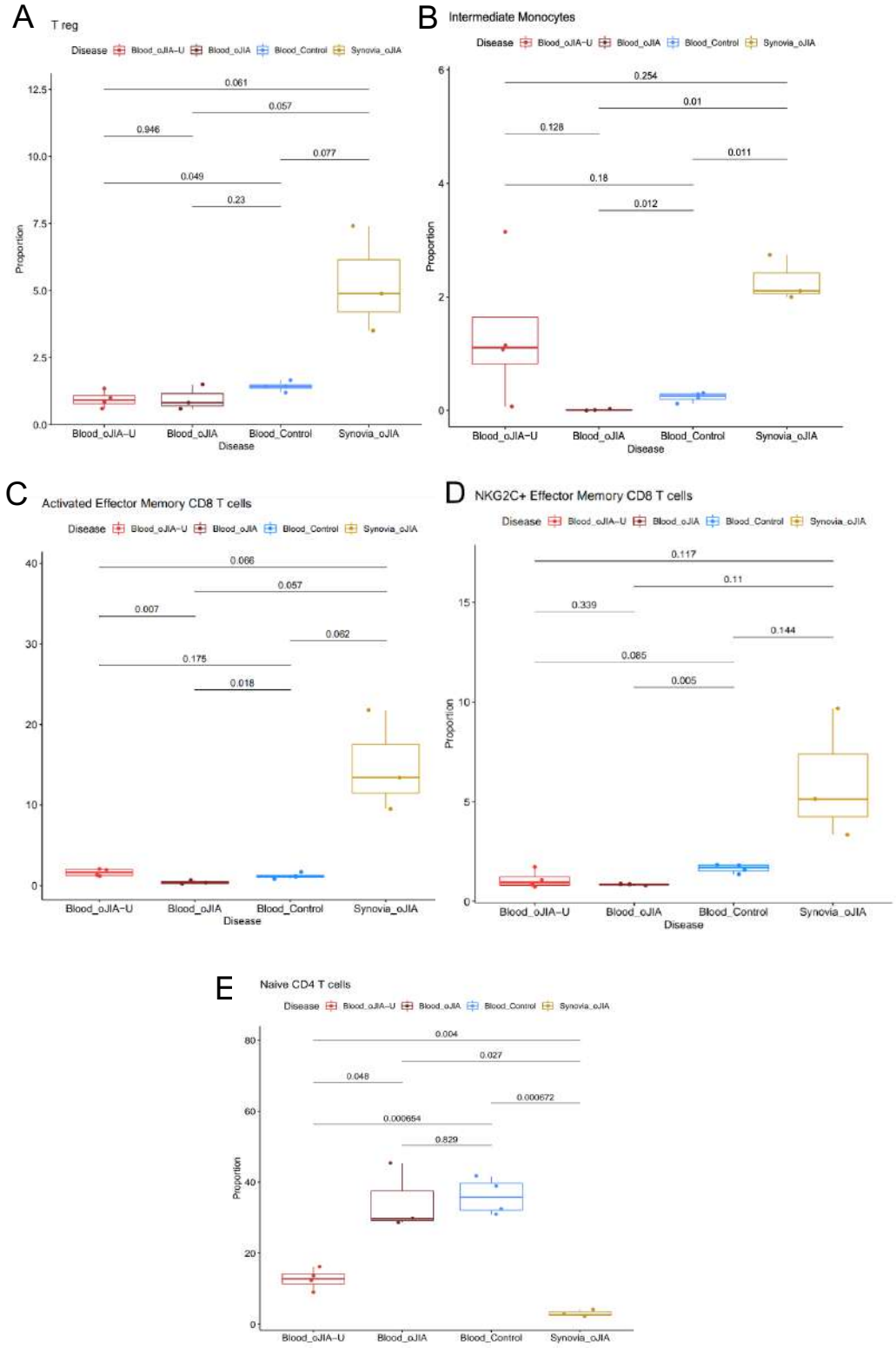

Box plots corresponding to: A) Regulatory CD4⁺ T cells. B) Intermediate monocytes. C) Activated effector memory CD8⁺ T cells. D) NKG2C⁺ effector memory CD8⁺ T cells. E) Naive CD4⁺ T cells.
In red are cells from oJIA uveitis patients, in maroon cells from oJIA patients without uveitis. In blue healthy control cells, and in yellow cells from synovial fluid.

These results yield exciting data that can help us understand the dynamics of immune cells in oJIA.

The most significant differences were observed in intermediate monocytes and NK2C$^+$ effector memory CD8$^+$ T cells. Intermediate monocytes are more abundant in the peripheral blood of healthy controls than in oJIA patients (p=0.012). If we look at SF, they are found in higher abundance than in the PB of oJIA patients (p=0.01). There are no significant differences in proportions between oJIA patients with or without uveitis (p=0.128).

Similarly, we observed a higher abundance of NKG2C$^+$ effector memory CD8$^+$ T cells in healthy controls than in oJIA patients (p=0.005). We observed a trend towards a higher proportion of these cells in SF than in peripheral blood (p=0.11). We observed no significant differences in proportions between oJIA patients with or without uveitis (p=0.339).

As for regulatory T cells, we observed a trend towards a higher proportion of these cells in HCs than in oJIA patients (p=0.23), as well as a higher abundance of these cells in SF than in the blood of oJIA patients (p=0.057).

Conversely, naive CD4$^+$ cells are less abundant in synovial fluid than peripheral blood (p=0.027), with no significant difference between the proportions in healthy controls compared to oJIA patients (p=0.829).

5.2.3.3. Differences in cell type abundance focused on uveitis condition.

In this third analysis, we profiled the blood cell composition in oJIA patients with and without uveitis, and HCs (Figure 31).

Figure 31. Box plot depicting the most significant differences in cell proportions in uveitis.

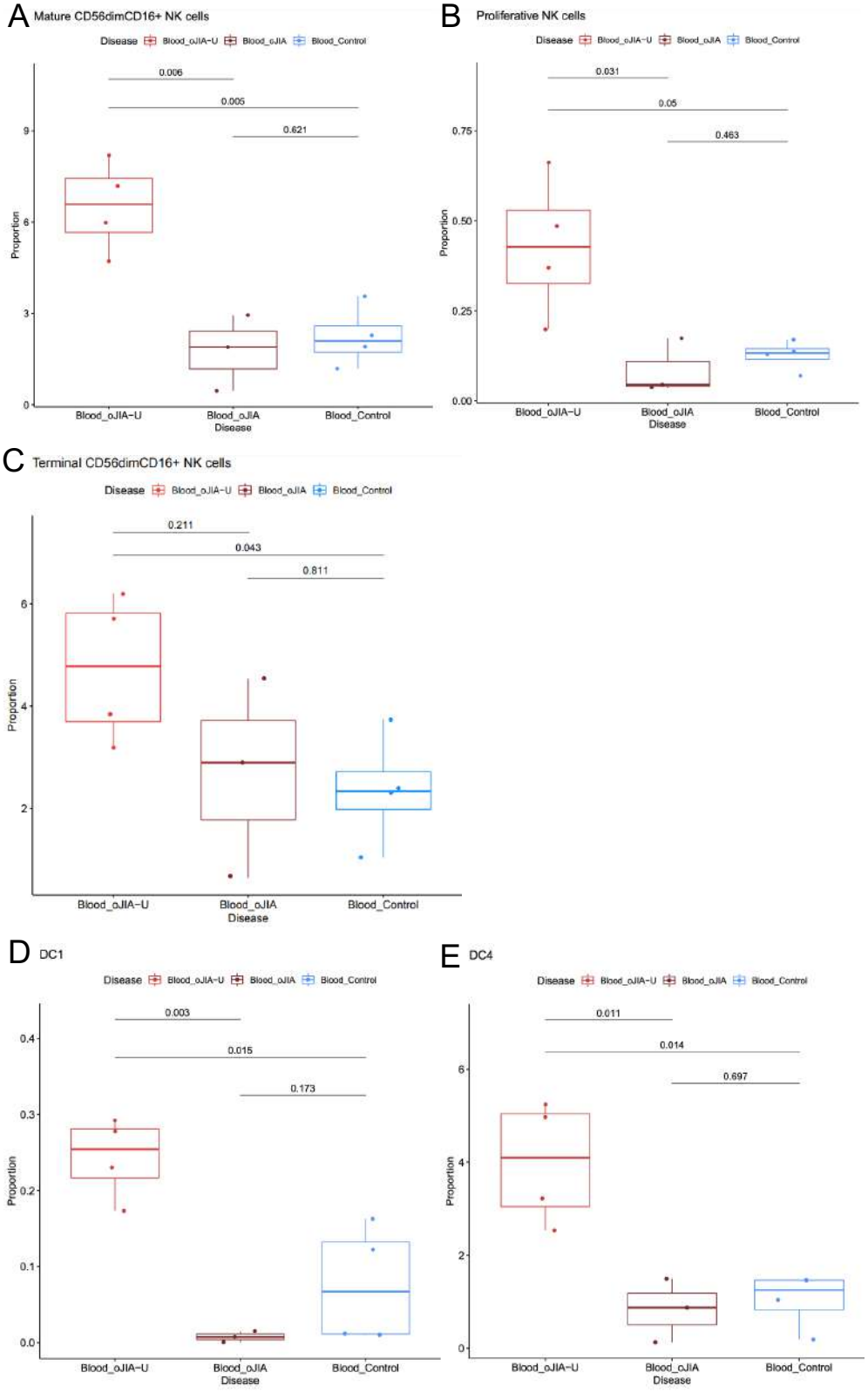

Box plot corresponding to: A) Mature CD56dim NK cells. B) Proliferative NK cells. C) Terminal CD56 dim NK cells. D) Dendritic cells type 1. E) Dendritic cells type 4. In red are cells from oJIA uveitis patients, in maroon cells from oJIA patients without uveitis. In blue healthy control cells, and in yellow cells from synovial fluid.

As for the uveitis condition, the most significant differences were observed in mature, terminal, and proliferative NK, as well as dendritic cells type 1 and 4.

Mature NK cells are significantly more abundant in the PB of patients with oJIA and uveitis than in oJIA patients without this ocular manifestation (p=0.006). They are also more abundant in oJIA-U compared to HCs (p=0.005), but no difference was found between oJIA and HCs (p=0.621), suggesting a specificity for uveitis. We also observed an expansion of terminal NK cells in uveitis, yet not statistically significant (p= 0.211).
Similarly, NK proliferating cells are more abundant in oJIA-U than in oJIA (p=0.031), as well as in comparison to HCs (p=0.05). There are no differences in the proportions of these cells between patients with oJIA and HCs (p=0.463).

Finally, type 1 and 4 dendritic cells are also differentially represented in uveitis. Type 1 dendritic cells are more abundant in oJIA-U compared to oJIA (p=0.003) and in oJIA-U compared to HCs (p=0.0015). There are no differences between oJIA and HCs (p=0.173). Similarly, type 4 dendritic cells are more abundant in oJIA-U compared to oJIA (p=0.011) and in oJIA-U compared to HCs (p=0.014). As well as Dc1, there are no differences between oJIA and HCs (p=0.697).

An overall summary of the differences in cell populations between the different tissues and conditions leads to the following conclusions:
A higher abundance of intermediate monocytes, Tregs, activated and NKG2C$^+$ effector memory CD8$^+$ T cells was observed in the SF of patients with oJIA, whereas a correspondingly lower proportion of these cells was found in the PB of patients with oJIA compared to controls. This suggests that these cells may play a key role in trafficking from the blood to the inflamed synovium in oJIA.

In patients with oJIA-U, there is a higher abundance of dendritic cells type 1 and 4 and mature NK cells than in patients with oJIA who do not have this complication. Additionally, these cells are more prevalent in oJIA-U than HCs, indicating a specific role for these cells in uveitis.

5.2.4. Differences in gene expression

To define both disease and cell type specific signatures, we tested for differentially expressed genes across all conditions.

5.2.4.1. Transcriptome deregulation in hallmark cell types of synovial fluid from oligoarticular juvenile idiopathic patients

In this first analysis, we have focused on studying the differences in the transcriptome of each cell from SF compared to PB from oJIA patients (Figure 32).

Figure 32. Differentially expressed genes in SF compared to PB.

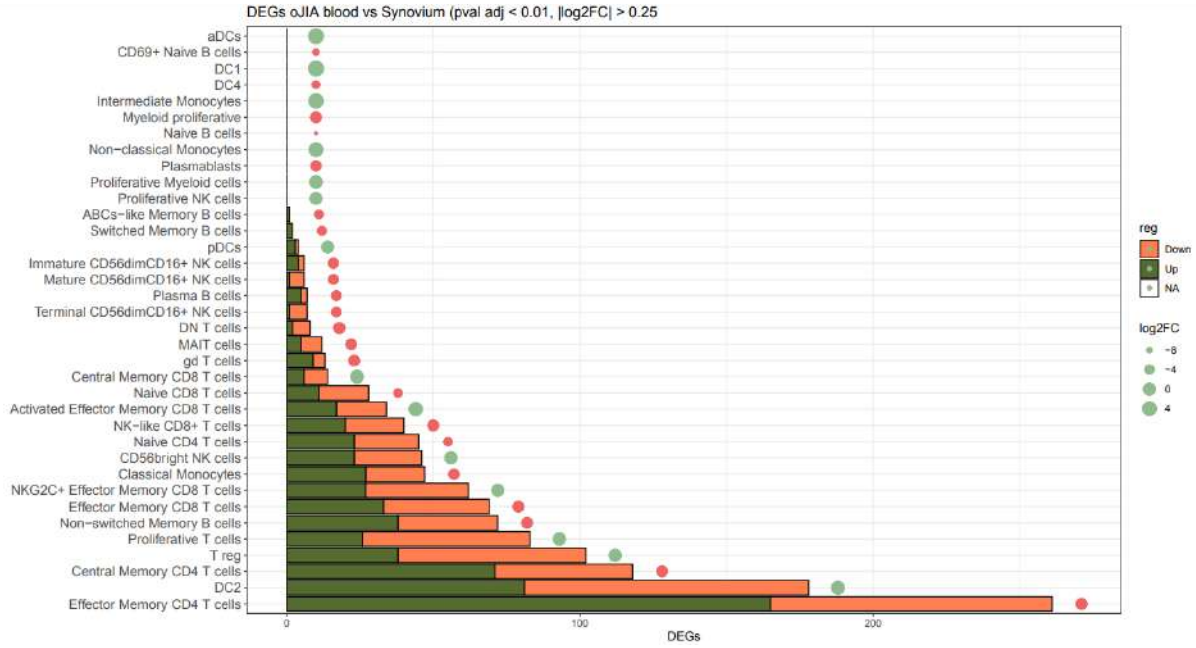

DEGs: differentially expressed genes; log2FC: log fold change; pval adj: adjusted p-value. oJIA: oligoarticular juvenile idiopathic arthritis.
Bar plot representing the number of significantly up (green) and down-regulated (orange) genes in each cell type comparing oJIA peripheral blood vs. synovial fluid. Differences with a p-value adjusted <0.01 and log2FC >0.25 were considered. Log2FC of cell proportion between oJIA PB and SF was estimated, and it is represented by a dot next to each horizontal bar. A green dot indicates that the corresponding cell type is more abundant in oJIA PB than in SF, whereas a red dot indicates that the cell type is less abundant in oJIA PB than in SF. As noted, the highest bar in each cellular type denotes major differentially expressed genes.

As can be seen, the cell population with the most abundant differential gene expression corresponds to effector memory CD4$^+$ T cells.
However, as this population was not abundant in SF, we did not conduct a more detailed transcriptomic analysis.

As for the most differentially significant cell populations in the SF, T regs have about 100 differentially expressed genes, followed by about 70 differentially expressed genes in NKG2C+ effector memory CD8+ T cells. We observed in the SF a significantly upregulated expression of genes related to effector pathways and cytotoxicity, such as CCL5, GZMA, GZMK; innate immunity such as S100A6, S100A11; and other genes related to T-B cell intercommunication such as CXCL13 and tissue residency like CXCR6, which will be explained in detail in the Discussion section.

In contrast, intermediate monocytes have no differentially expressed genes.

5.2.4.2. Transcriptome deregulation in hallmark cell types of peripheral blood oligoarticular juvenile idiopathic patients compared to healthy controls.

In the following analysis, we have compared the transcriptomic differences in each cell type from oJIA's PB compared to HCs (Figure 33).

Figure 33. Differentially expressed genes in oJIA patients compared to controls.

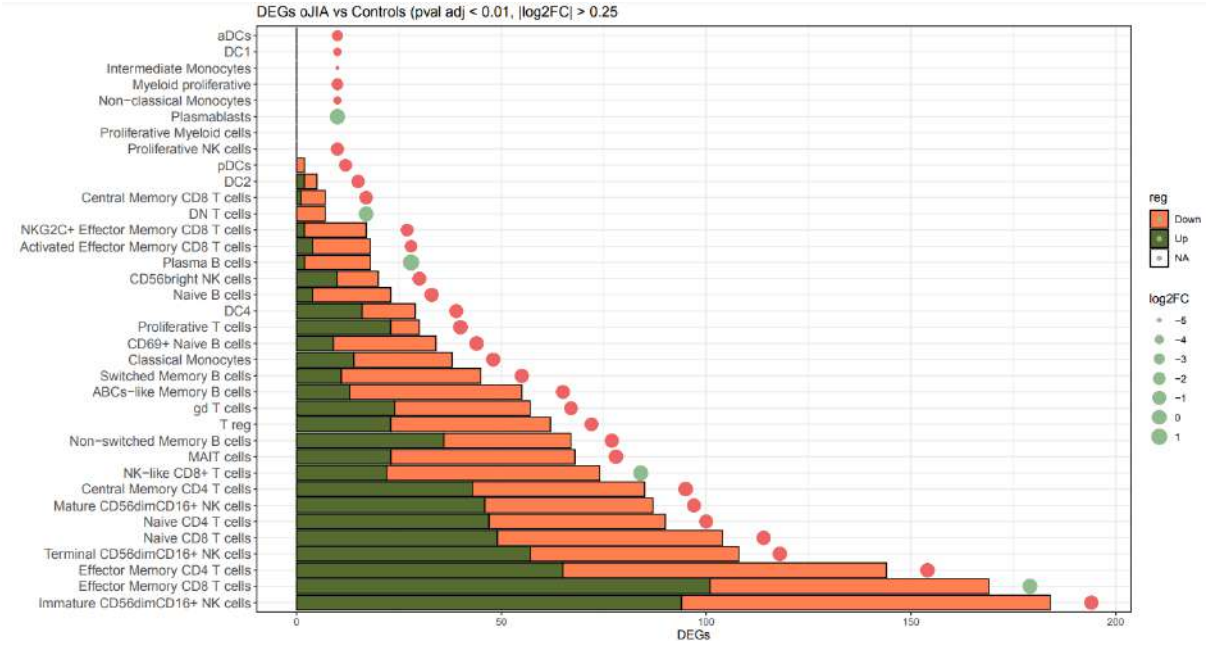

Bar plot representing the number of significantly up (green) and down-regulated (orange) genes in each cell type comparing oJIA PB vs. HCs. Differences with a p-value adjusted <0.01 and log2FC >0.25 were considered. Log2FC of cell proportion between oJIA and HCs was estimated, and it is represented by a dot next to each horizontal bar. A green dot indicates that the corresponding cell type is more abundant in oJIA than in HCs, whereas a red dot

indicates that the cell type is less abundant in oJIA than in HCs. As noted, the highest bar in each cellular type denotes major differentially expressed genes.
DEGs: differentially expressed genes; log2FC: log fold change; pval adj: adjusted p-value. oJIA: oligoarticular juvenile idiopathic arthritis

In this comparison, the cell population with the most abundant differential gene expression corresponds to immature CD56dim NK cells followed by effector memory $CD8^+$ T cells. $NKG2C^+$ effector memory $CD8^+$ T cells have less DEG in this comparison than in the previous. Similarly, intermediate monocytes do not have any differentially expressed genes.

Next, focusing on the $NKG2C^+$ effector memory $CD8^+$ T cells, since no differentially expressed genes are found in intermediate monocytes, we review those genes that are differentially expressed and up-regulated both in SF compared to oJIA PB and oJIA PB compared to HCs (Table 17).
In both comparisons, CCL5 and GZMA were the two differentially expressed and up-regulated genes in NKG2C effector memory CD8 T cells.

Table 17. $NKG2C^+$ effector memory $CD8^+$ T cells up-regulated genes.

Gene	Comparison	Avg_log2FC_oJIA_ctrl	Pct.oJIA	Pct.oJIA.ctrl	P_val_adj_oJIA_ctrl
CCL5	oJIA vs HC	0.65	0.83	0.71	6,75E-04
GZMA	oJIA vs HC	0.67	0.68	0.45	1,31E-02
Gene	Comparison	Avg_log2FC_oJIAsyn_oJIA	Pct.oJIA.syn	Pct.oJIA	P_val_adj_oJIAsyn_oJIA
CCL5	SF vs oJIA	0.82	0.92	0.83	9,51E-08
GZMA	SF vs oJIA	0.95	0.81	0.68	0.02

Avg_log2FC: log fold-change of the average expression between the two groups; CCL5: C-C Motif Chemokine Ligand 5; Ctrl: control; GZMA: Granzyme A; oJIA: oligoarticular juvenile idiopathic arthritis; P_val_adj: adjusted p-value, based on Bonferroni correction using all features in the dataset; Pct: proportion; Syn: synovial fluid.

5.2.4.3. Transcriptome deregulation in hallmark cell types of oligoarticular juvenile idiopathic arthritis-related uveitis compared to healthy controls.

Hereafter, we have compared the transcriptomic differences in each cell type from oJIA-U compared to HCs (Figure 34).

Figure 34. Differentially expressed genes oJIA-U compared to HCs.

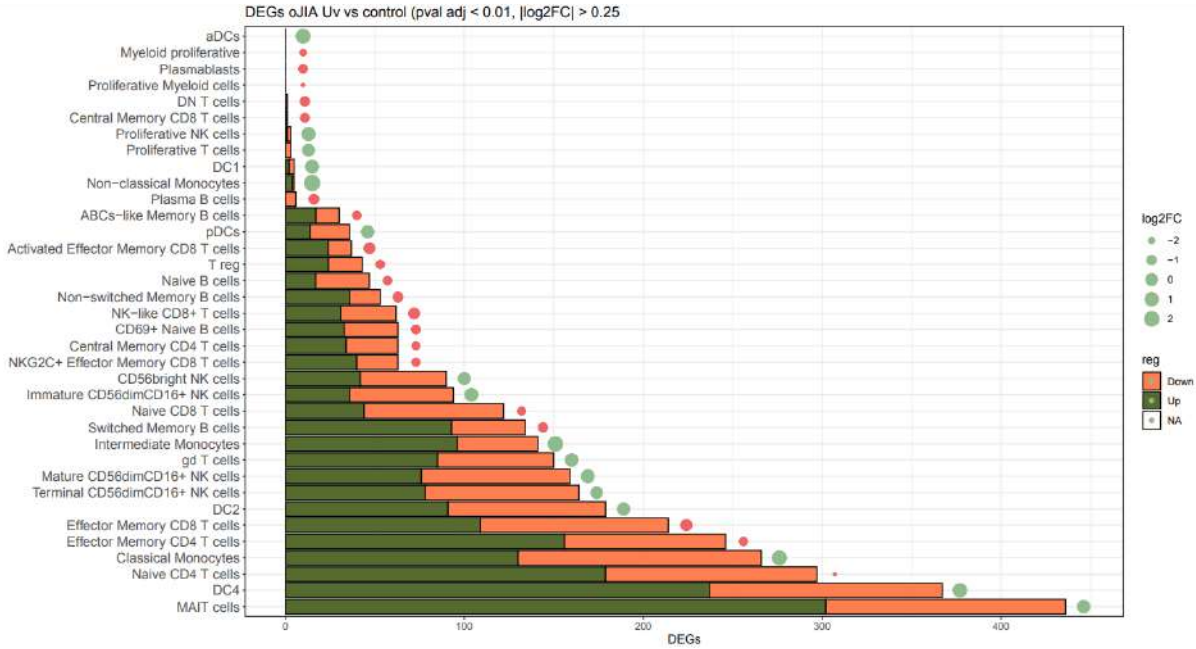

Bar plot representing the number of significantly up (green) and down-regulated (orange) genes in each cell type comparing oJIA-U PB vs. HCs. Differences with a p-value adjusted <0.01 and log2FC >0.25 were considered. Log2FC of cell proportion between oJIA PB and HCs was estimated, and it is represented by a dot next to each horizontal bar. A green dot indicates that the corresponding cell type is more abundant in oJIA-U than in HCs, whereas a red dot indicates that the cell type is less abundant in oJIA-U than in HCs. As noted, the highest bar in each cellular type denotes major differentially expressed genes.
DEGs: differentially expressed genes; log2FC: log fold change; pval adj: adjusted p-value. oJIA Uv: oligoarticular juvenile idiopathic arthritis related uveitis.

The most important transcriptional differences are found in MAIT cells, followed by Dc4 cells. With respect to the NK mature cells, which we have found to be more abundant in oJIA-U than in HCs, they have a differential expression of approximately 170 genes. In this comparison, regarding intermediate monocytes, we observed significantly upregulated expression of type I INF mediated genes: IFITM1, IFITM2, IFITM3, IFI6, ISG15S; the protein-coding gene of the S100 family 100A11; FCER1G and B2M [198] [199].

5.2.4.4. Transcriptome deregulation comparison between oligoarticular juvenile idiopathic arthritis patients with or without uveitis

Hereafter, we have analyzed the transcriptomic differences in each cell type from oJIA patients with and without uveitis (Figure 35).

Figure 35. Differentially expressed genes oJIA-U compared to oJIA without uveitis.

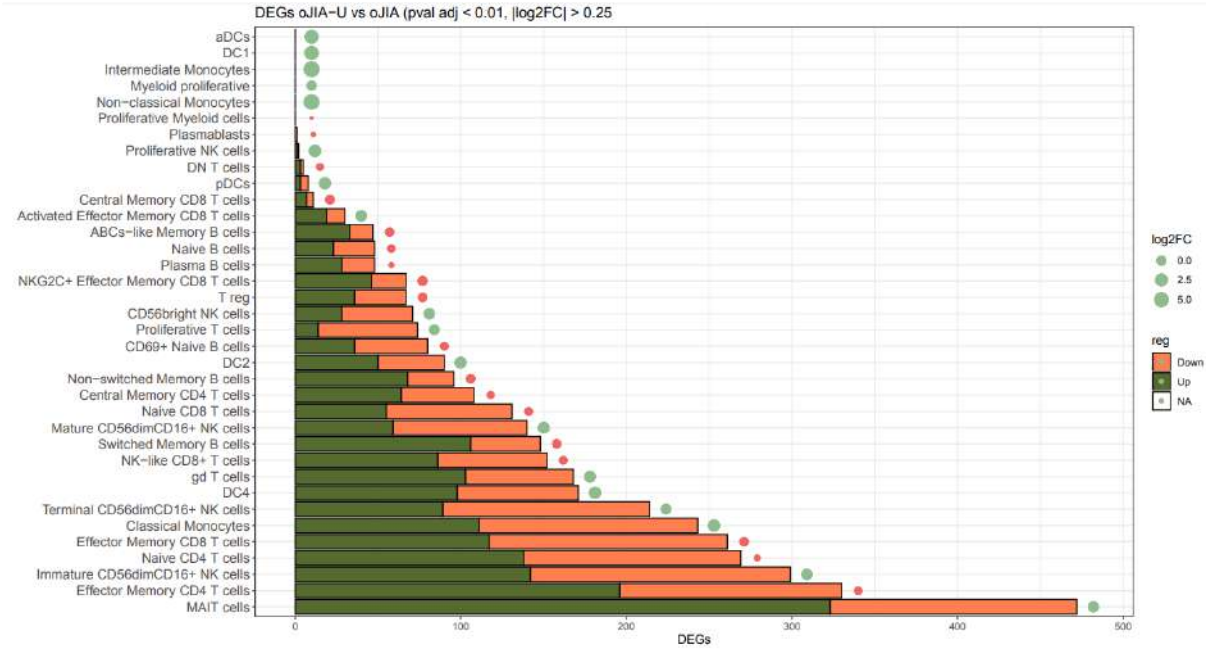

Bar plot representing the number of significantly up (green) and down-regulated (orange) genes in each cell type comparing oJIA-U PB vs. HCs. Differences with a p-value adjusted <0.01 and log2FC >0.25 were considered. Log2FC of cell proportion between oJIA-U and oJIA was estimated, and it is represented by a dot next to each horizontal bar. A green dot indicates that the corresponding cell type is more abundant in oJIA-U than in oJIA, whereas a red dot indicates that the cell type is less abundant in oJIA-U than in oJIA. As noted, the highest bar in each cellular type denotes major differentially expressed genes.
DEGs: differentially expressed genes; log2FC: log fold change; pval adj: adjusted p-value. oJIA-U: oligoarticular juvenile idiopathic arthritis related uveoJIA: oligoarticular juvenile idiopathic arthritis.

Like the previous comparison, the most notable differences are found in MAIT cells, followed by effector memory $CD4^+$ T cells. Mature NK cells and type 1 and 4 Dcs, which we found to be more abundant in oJIA-U than in oJIA without uveitis, have differential expression of approximately 150 genes.

Finally, Gene Ontology annotation was performed to understand better the biological processes associated with this set of upregulated genes in the cell populations most prevalent in uveitis compared to patients without uveitis (Figure 36).

Figure 36. Gene Ontology annotation of the top 20 biological processes enriched and up-regulated in oJIA-U per cell type.

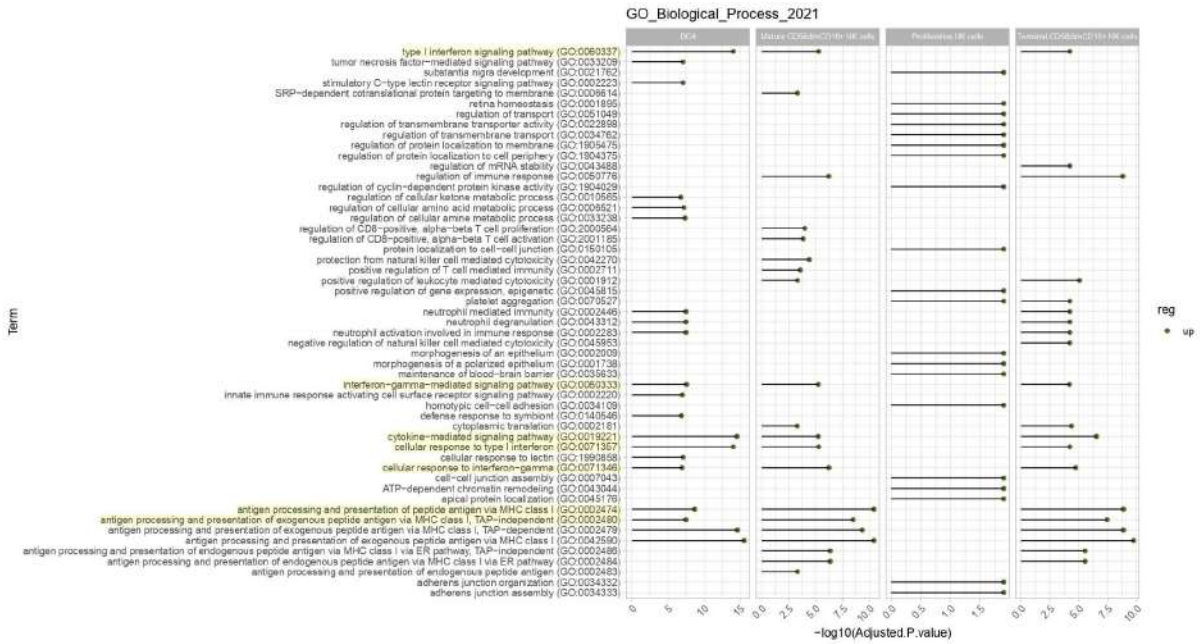

GO: gene ontology; DC4: dendritic cell type 4. Highlighted in yellow are the predominant and shared pathways between cells.

Overall, all represented cells in oJIA-U showed an upregulation of the type I interferon signaling pathway, the interferon gamma-mediated signaling pathway as well as the cytokine-mediated signaling pathway and the antigen processing and presentation of peptide antigen via MHC class I.

After this visual inspection of the DEGs and GO processes, we reviewed those genes differentially expressed and up-regulated both in oJIA-U compared to HCs and oJIA-U compared to oJIA without uveitis in PB. This review allows us to obtain a more detailed view of those genes overexpressed in the cell types most represented in uveitis and, therefore, more specific to this complication.

Specifically, we focused on genes overexpressed in mature and terminal NK (Table 18).

Table 18. Up-regulated genes in mature and terminal NK cells.

Gene	Comparison	avg_log2FC_oJIAU_ctrl	pct.oJIAU	pct.ctrl	p_val_adj_oJIAU_ctrl
B2M	oJIA-U vs HC	0.34	1	1	1,73E-46
PRF1	oJIA-U vs HC	0.88	0.43	0.27	8,36E-08
FCER1G	oJIA-U vs HC	0.37	0.70	0.54	4.28E-06
CCL4	oJIA-U vs HC	1.59	0.44	0.16	2,51E-47
Gene	Comparison	avg_log2FC_oJIAU_oJIA	pct.oJIAU	pct.oJIA	p_val_adj_oJIAU_oJIA
B2M	oJIA-U vs oJIA	0.33	1	1	4,17E-20
PRF1	oJIA-U vs oJIA	1.31	0.43	0.25	1,03E-17
FCER1G	oJIA-U vs oJIA	0.91	0.70	0.45	2,67E-17
CCL4	oJIA-U vs oJIA	0.86	0.44	0.27	3,10E-03

Avg_log2FC: log fold-change of the average expression between the two groups; B2M: beta-2-microglobulin; CCL4: C-C Motif Chemokine Ligand 4; Ctrl: control; FCER1G (Fc Epsilon Receptor Ig); oJIA: oligoarticular juvenile idiopathic arthritis; oJIA-U: oligoarticular juvenile idiopathic arthritis-related uveitis; P_val_adj: adjusted p-value, based on Bonferroni correction using all features in the dataset; Pct: proportion; PRF1: perforin 1.

For mature CD56^{+}dim NKs cells, the common up-regulated and differentially expressed genes are genes beta-2-microglobulin (B2M), perforin 1 (PRF1), Fc Epsilon Receptor Ig (FCER1G), and CCL4 C-C Motif Chemokine Ligand 4 (CCL4) also known as MIP-1β.

5.2.5. T cell receptor analysis

We also profiled the T cell receptor VDJ repertoire of the same samples through TCR single-cell sequencing to understand the clonal composition of oJIA-U, oJIA blood, and paired synovial fluid. TCR libraries were processed and filtered by quality as described in the Methods section (Table 19).

Table 19. T-cell receptor quality control. Library-specific features.

ID	Condition	Tissue	Percentage of TCRs + cells	Percentage of cells with single TCR	Percentage of cells with multiple TCR chains	Percentage of cells with only VDJ/VJ chain
oJIA1	oJIA debut	Blood	15.72	62.77	8.16	29.07
oJIA2	oJIA debut	Blood	12.39	36.47	8.38	55.12
oJIA3	oJIA debut	Blood	7.47	45.01	8.57	46.42
oJIA1	oJIA debut	SF	22.78	63.85	9.62	26.54
oJIA2	oJIA debut	SF	15.59	60.54	7.54	31.91
oJIA3	oJIA debut	SF	13.80	61.69	11.51	26.80
UV1	Uveitis flare	Blood	2.53	56.03	4.31	39.95
UV2	Uveitis flare	Blood	22.45	69.72	6.54	23.74
UV3	Uveitis flare	Blood	2.73	43.85	4.73	51.42
UV4	Uveitis flare	Blood	8.67	72.95	9.02	18.03
HC1	HC	Blood	8.89	40.09	6.59	54.33
HC2	HC	Blood	31.30	60.46	10.97	25.58
HC3	HC	Blood	8.19	41.62	2.94	55.44
HC4	HC	Blood	47.09	29.51	4.14	65.35

HC: healthy control; oJIA: oligoarticular juvenile idiopathic arthritis; SF: synovial fluid; TCR: T cell receptor; UV: uveitis flare; VDJ/VJ: gene segments which include variable (V), diversity (D), and joining (J) segments for TCRB gene and variable (V) and joining (J) for TCRA gene.

After the quality control processing, the total number of TCRs + cells analyzed was 18.786, with a mean percentage of TCR plus cells of 14%.

A TCR clonotype is a unique nucleotide sequence that arises during the gene rearrangement process for that receptor. Combining nucleotide sequences for the surface-expressed receptor pair would define the T cell clonotype.
We first looked systematically for evidence of clonal expansion defined by more than 2 clonotypes per tissue and condition (Figures 33 and 34).
The most expanded clones in SF correspond to T reg, activated effector memory $CD8^+$ T cells, and proliferative T cells. In oJIA and oJIA-U blood, we found an expansion of NK-like $CD8^+$ T and effector memory $CD8^+$ T cells. HCs had an expansion of activated effector memory $CD8^+$ T cells and effector memory $CD8^+$ T cells.

Figure 33. Clonotype distribution among tissue and conditions.

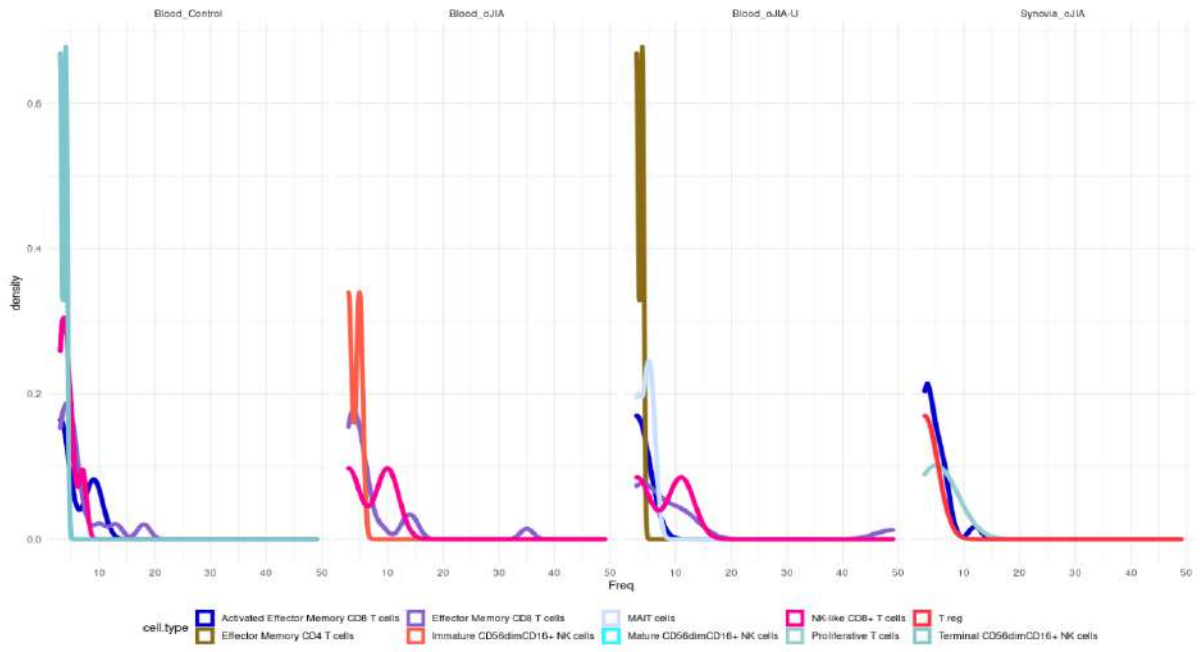

Histogram representing the distribution of clonotypes with a frequency of 2 or more in each condition and tissue. oJIA: oligoarticular juvenile idiopathic arthritis; oJIA-U: oligoarticular juvenile idiopathic arthritis-related uveitis; MAIT: Mucosal-associated invariant T cells; T reg: regulatory T cells.

Figure 34. The number of clones expanded.

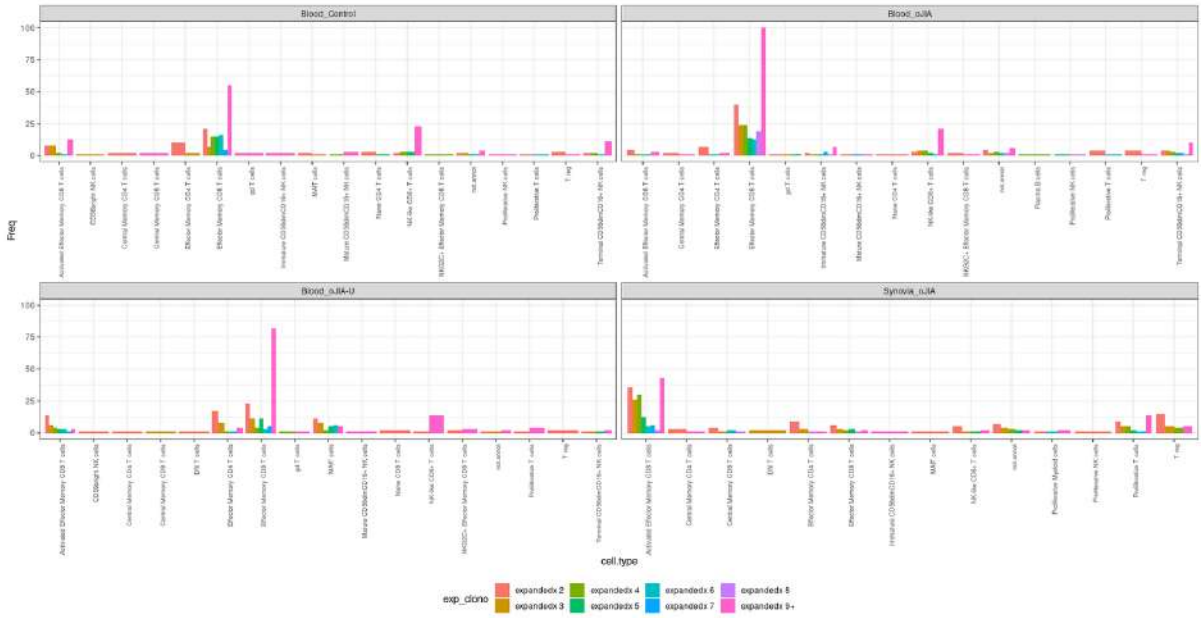

The Graph bar represents the number of clones expanded per cell type, condition, and tissue from the patients. oJIA: oligoarticular juvenile idiopathic arthritis; oJIA-U: oligoarticular juvenile idiopathic arthritis-related uveitis; MAIT: Mucosal-associated invariant T cells; T reg: regulatory T cells; DN T cells: double negative T cells.

Effector memory $CD8^+$ T cells are the cell subtype more clonally expanded, especially in blood from oJIA and oJIA-U patients with more than 9 or more clonotypes.

Analyzing in more detail the effector memory $CD8^+$ T lymphocytes, and after observing a differential expression of the CCL5 gene in this population, we have studied whether those cells clonally expanded and expressed more this protein-coding gene (Figure 35).

Figure 35. Expression of CCL5 in effector memory CD8$^+$ T cells.

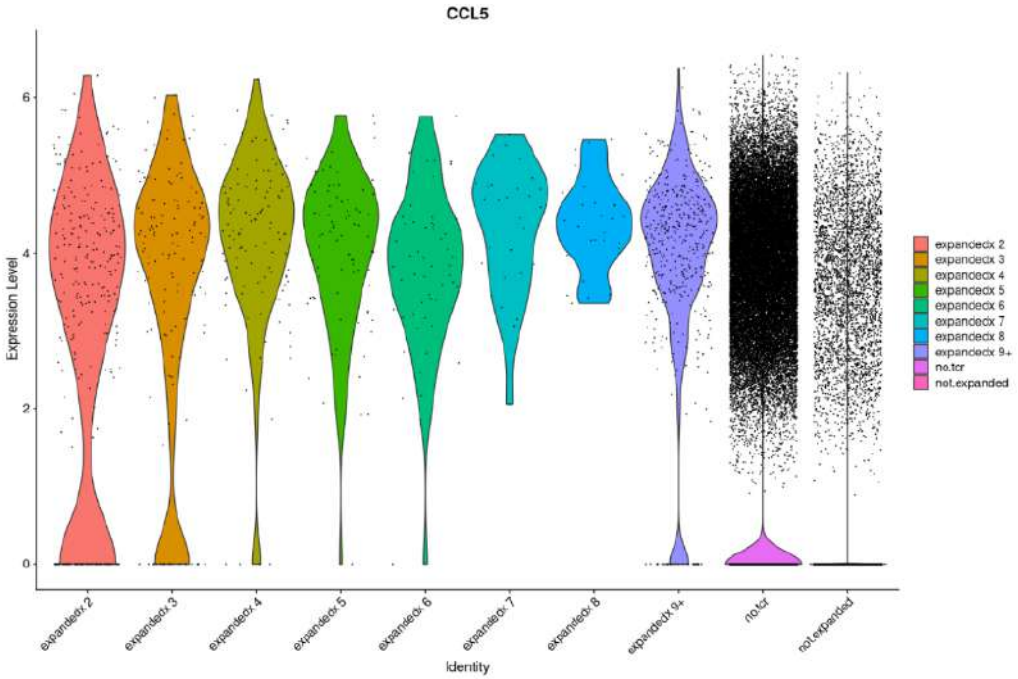

Violin plot that represents the expression of CCL5 in this CD8 T cell population and its relation to clonal expansion. X-axis represents the number of clonal expansions, and the y-axis is the expression level of CCL5.

As can be seen in the violin plot, the distribution of effector memory CD8$^+$ T cells overexpressing the CCL5 gene is less dispersed as their clonal expansion increases.

Next, following Yost *et al*. methodology, and to understand in detail the clonal expansion in the T lineage, we selected only those cell types with more than 10% sequenced TCRs, and excluded those populations composed by less than 30 cells according to scRNA-seq data [194] (Figure 36).

Figure 36. Sequenced TCR from peripheral blood and synovial fluid.

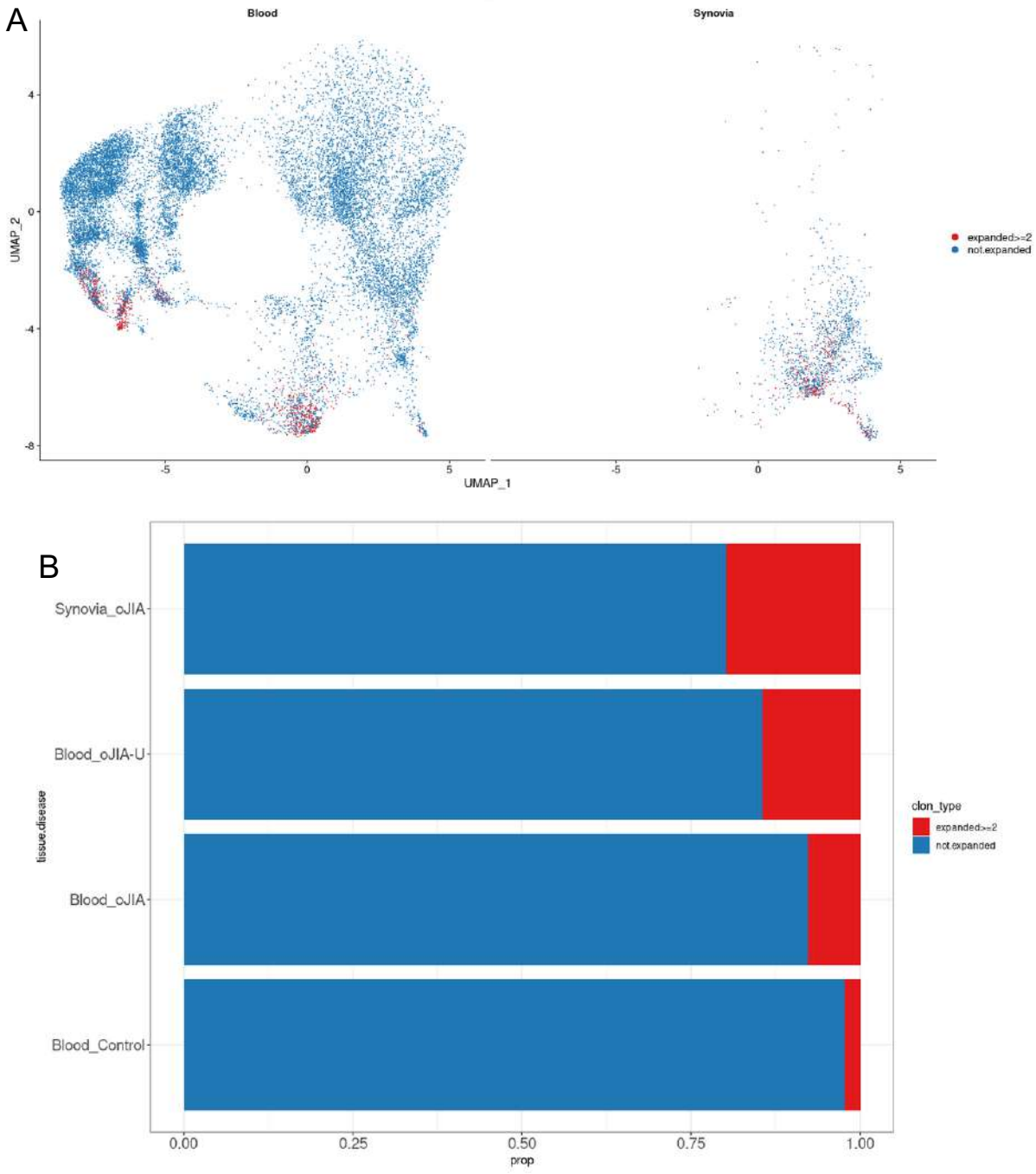

A) UMAP plot representing just those cells with sequenced TCR from PB and SF. Marked in blue are those cells without TCR expansion and those clonally expanded cells in red.
B) Graph bar representing clonal expansion among tissue and conditions.

Clonally expanded cells are more abundant in SF (proportion 0.197) compared to PB from all conditions (oJIA-U proportion 0.144, oJIA proportion 0.076, healthy control blood proportion 0.022). X-squared test 964.72, df= 3 p-value $2.2x10^{-16}$.

Finally, we studied TCR diversity in our samples. In T-cell repertoires, diversity considers the clonal composition, specifically the number of unique TCR sequences (richness) and the relative abundance of these sequences (diversity).

Several indices can be employed to study TCR diversity, and in our study, we tested the Gini coefficient (Figure 37).

This index, which ranges from 0 to 1, was originally proposed to measure inequality of income or wealth across countries. In this analysis, zero stands for total equality of clones; thus, all clones will have identical frequencies. Conserverly, one stands for total inequality, thus indicating sample oligoclonality. In other words, the higher the Gini coefficient is, the more unequal the distribution is (few clones highly expanded) [193] .

Figure 37. Representation of the Gini coefficient among tissues and clonally expanded cells.

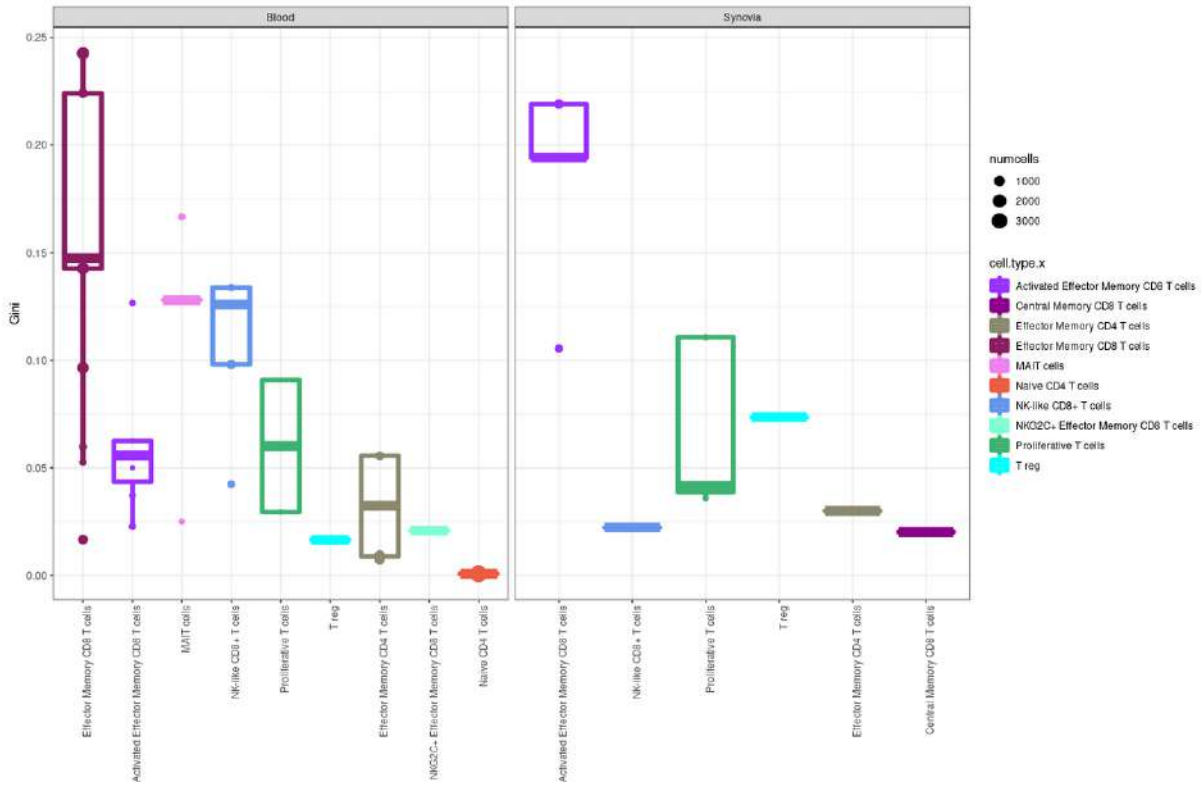

Box plot representing the Gini coefficient. MAIT: Mucosal-associated invariant T cells; T reg: regulatory T cells.

We found that the highest clonality in PB corresponded to the effector memory $CD8^+$ T cells and SF to activated effector memory $CD8^+$ T cells.

5.3. Proteomics

Based on the 235 proteins included in the analysis, different cross-sectional analyses and one paired analysis were performed to detect significant changes in protein composition between conditions.

5.3.1. Differences between oligoarticular JIA patients and healthy controls

First, a cross-sectional analysis was performed to determine which proteins are differentially represented between oJIA and HC samples.
Fifteen proteins were significantly different between oJIA (test group) and healthy controls (reference group), with fibroblast growth factor (FGF-23), tumor necrosis factor-related apoptosis-inducing ligand (TRAIL), complement component 2 (C2), interleukin-18 receptor 1 (IL-18R1), IL-6 and interleukin-13 (IL-13) being higher in oJIA than in HC. In contrast, the proteins pleiotrophin (PTN), C-C motif chemokine ligand 17 (CCL17), fibroblast growth factor 19 (FGF-19), KIT proto-oncogene receptor tyrosine kinase (KIT), uromodulin (UMOD), arginase 1 (ARG1), tumor necrosis factor receptor superfamily member 4 (TNFSF4) and Fas ligand (FAS) are higher in HCs than in oJIA (Figure 38).

Figure 38. Comparative analyses of protein levels in oJIA and HCs.

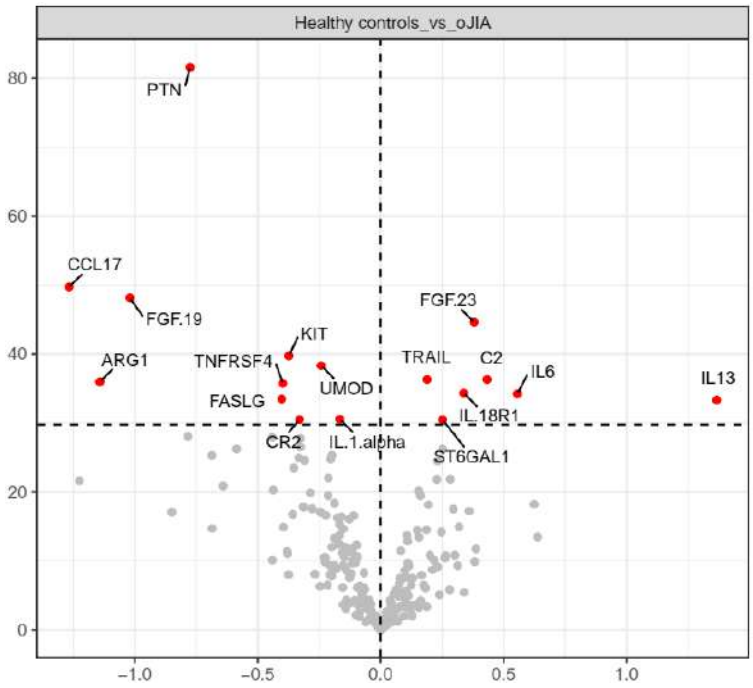

This volcano plot compares oJIA (n=14) and HC (n=8) by displaying the log fold changes and p-values. The x-axis represents the log2-fold change in protein expression between these two conditions; it is calculated as the ratio of the protein abundance in one group compared to the other. Positive log2-fold changes indicate higher protein levels in the oJIA group compared to the HC, while negative log2-fold changes indicate lower protein levels in the oJIA group compared to the HC. The y-axis represents the statistical significance of differential protein expression represented as the negative logarithm (base 10) of the p-value obtained. The red dots indicate proteins that are significantly different between the two groups.
This explanation is the same for the following volcano plots presented in the following comparisons.

5.3.2. Differences between oligoarticular JIA patients with a uveitis flare and healthy controls

Next, the protein profile between oJIA-U and HC was analyzed.

In this comparison, just three proteins were higher in UV (test group) than HC (reference group): TNF, interleukin 24 (IL-24), and matrix metalloproteinase 7 (MMP-7). Similarly, to the first comparison, HCs proteins differentially more abundant compared to UV are also CCL17, KIT, UMOD, PTN, but also matrix metalloproteinase 10 (MMP-10), C-C Motif Chemokine Ligand 18 (CCL18), cartilage oligomeric matrix protein (COMP), among other growth factor and cartilage synthesis related proteins (Figure 39).

Figure 39. Comparative analyses of protein levels in UV and HCs.

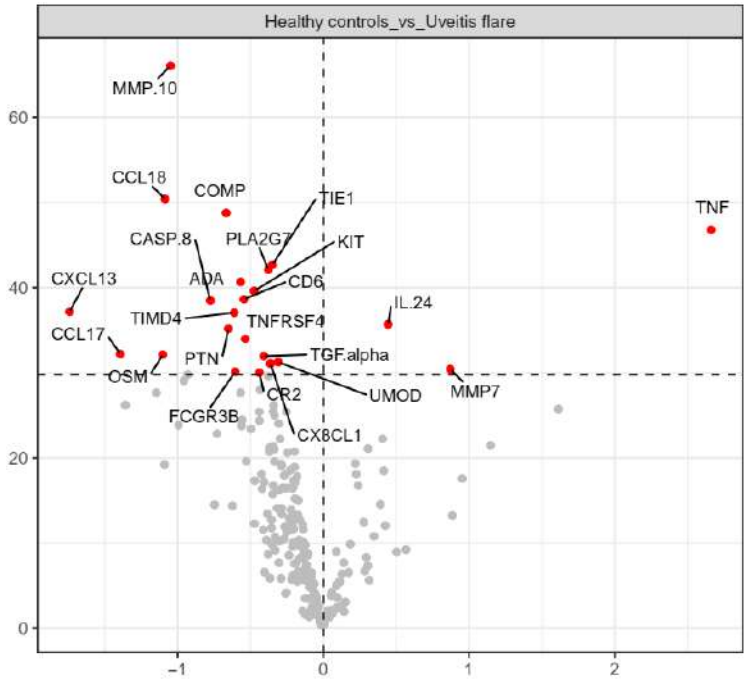

This volcano plot compares UV (n=7) and HCs (n=8) by displaying the log fold changes and p-values. The red dots indicate proteins that are significantly different between the two groups. Positive log2-fold changes indicate higher protein levels in the UV group compared to the HC, while negative log2-fold changes indicate lower protein levels in the UV group compared to the HC.

5.3.3. Differences between oligoarticular JIA patients with and without a uveitis flare

Furthermore, we compared protein profiles between patients with oJIA, both with and without uveitis, to identify protein markers associated with uveitis. Our analysis revealed twelve proteins that showed differential abundance between the two groups. Among these, TNF, regenerating islet-derived 1 alpha (REG1A), and regenerating islet-derived 3 alpha (REG3A) were found to be more abundant in patients with uveitis (test group) compared to those with oJIA alone (reference group), with TNF being the most abundant. Interestingly, a similar protein profile was observed in the oJIA group compared to the reference group (Figure 40).

Figure 40. Comparative analyses of protein levels in UV and oJIA.

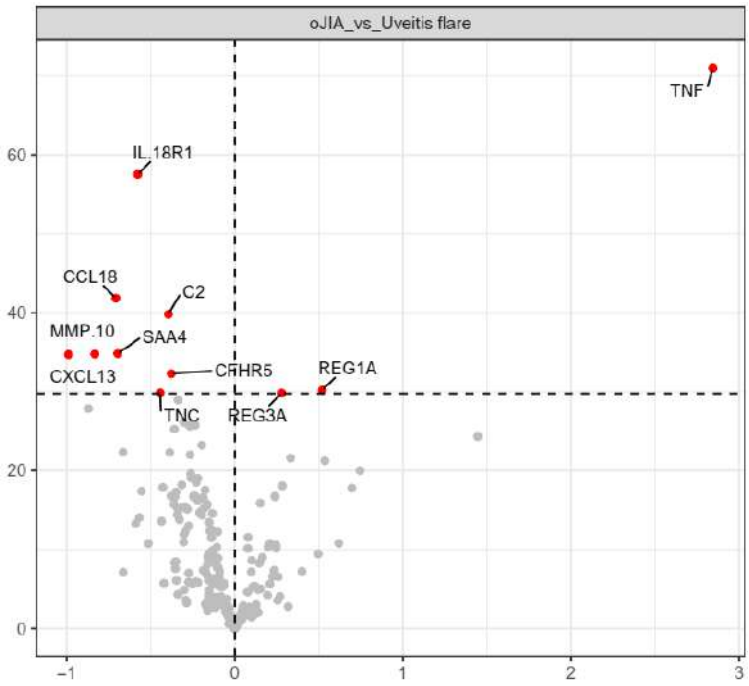

This volcano plot compares UV (n=7) and oJIA without uveitis (n=14) by displaying the log fold changes and p-values. The red dots indicate proteins that are significantly different between the two groups. Positive log2-fold changes indicate higher protein levels in the UV group compared to the HC, while negative log2-fold changes indicate lower protein levels in the UV group compared to the HC.

5.3.4. Differences between markers of disease activity in uveitis

To gain deeper insights into the pathogenic mechanisms underlying uveitis, we analyzed the proteomic profiles in patients with uveitis, distinguishing between those experiencing a more severe flare and those with a milder ocular flare. The classification of a more severe flare was based on SUN cells up to 2+ and a flare grade of 1 or 2, while a milder ocular flare was defined by SUN cells of 0.5+ and 0 flare. This comparative analysis aimed to elucidate the distinctive protein expression patterns associated with different levels of disease severity in uveitis.

Eight proteins were differentially more abundant in the most severe phenotypes than milder ones, with GZMH, killer cell immunoglobulin-like receptor (KIR3DL1), and matrix metalloproteinase 1 (MMP-1) among the most abundant proteins (Figure 41).

Figure 41. Comparative analysis of protein levels across varying patterns of uveitis severity.

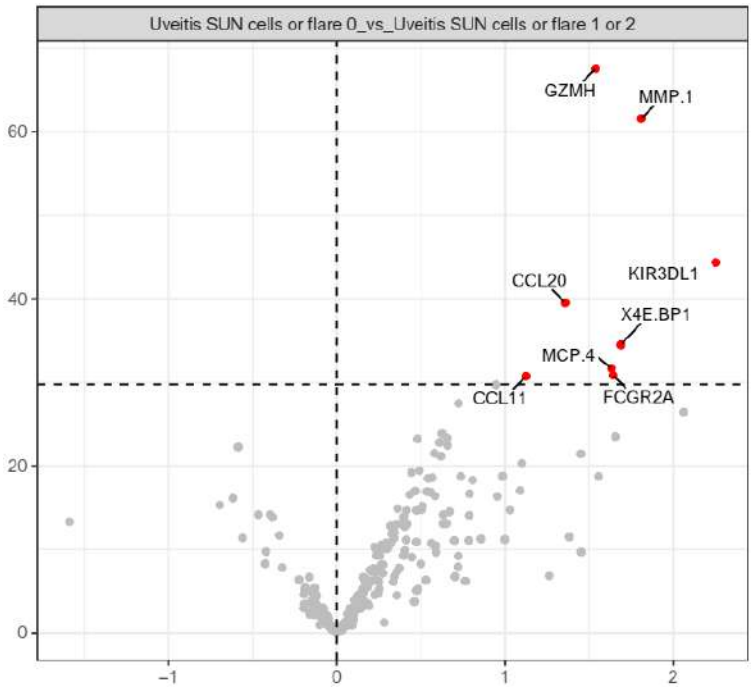

The volcano plot compares the UV severe phenotype (n=5) and mild phenotype (n=2) by displaying the log fold changes and p-values. The red dots indicate proteins that are significantly different between the two groups. Positive log2-fold changes indicate higher protein levels in the severe phenotype. Note that any proteins were significantly more abundant in the milder phenotype.

5.3.5. Paired analysis of protein levels in patients with oligoarticular JIA at week 0 and week 12 following anti-TNF alpha therapy

To comprehensively investigate the potential discriminatory proteins between active disease and remission, we conducted a paired analysis of samples obtained from three patients. These samples were collected during active disease before the initiation of anti-TNFα treatment and at week 12 after achieving remission through the treatment. Nineteen proteins were differentially abundant, with TNF and TNFB the most overrepresented at week 12 (Figure 42).

Figure 42. Paired analysis between week 0 and week 12 of anti-TNFα therapy.

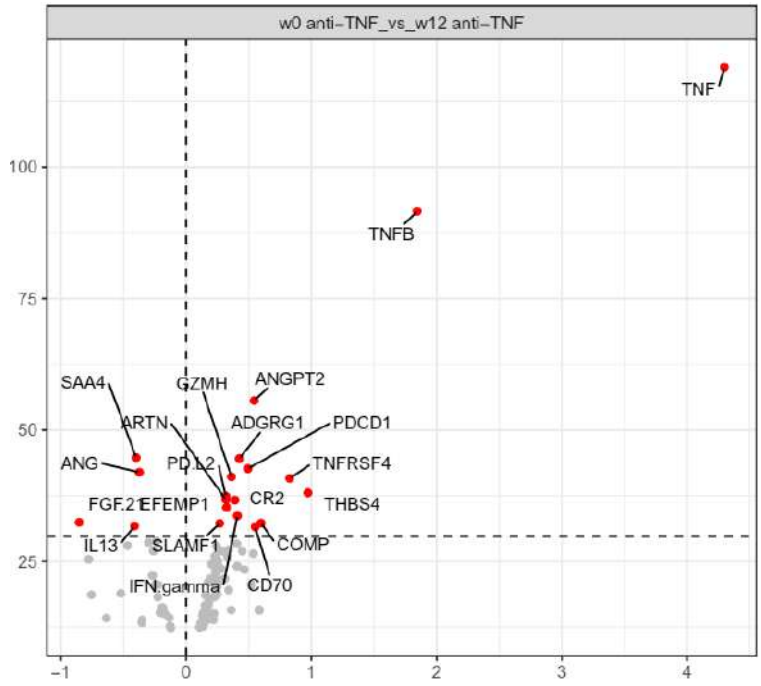

The volcano plot compares the paired samples of three patients at weeks 0 and 12 of anti-TNFα treatment. The red dots indicate proteins that are significantly different between the two groups. Positive log2-fold changes indicate higher protein levels in the week 12 of anti-TNFα treatment.

5.3.6. Differences between oligoarticular JIA and rheumatoid arthritis patients

Finally, to study whether there are differences in the protein profile of oJIA patients compared to rheumatoid arthritis patients, we compared the two groups.

Several proteins were differentially more abundant RA compared to oJIA. Among the most abundant proteins on RA are selectin L (SELL, CD62L), complement receptor 2 (CR2), KIT, protein tyrosine phosphatase, receptor type S (PTPRS), CD8A, dipeptidyl peptidase 4 (DPP4), tumor necrosis factor receptor superfamily member 9 (TNFRSF9), tenascin XB (TNXB), vascular endothelial growth factor receptor 2 (VEGFR-2), TNF-related activation-induced cytokine (TNFS11), and neural cell adhesion molecule 1 (NCAM1) (Figure 43).

Figure 43. Comparative analysis of protein levels in RA and oJIA patients.

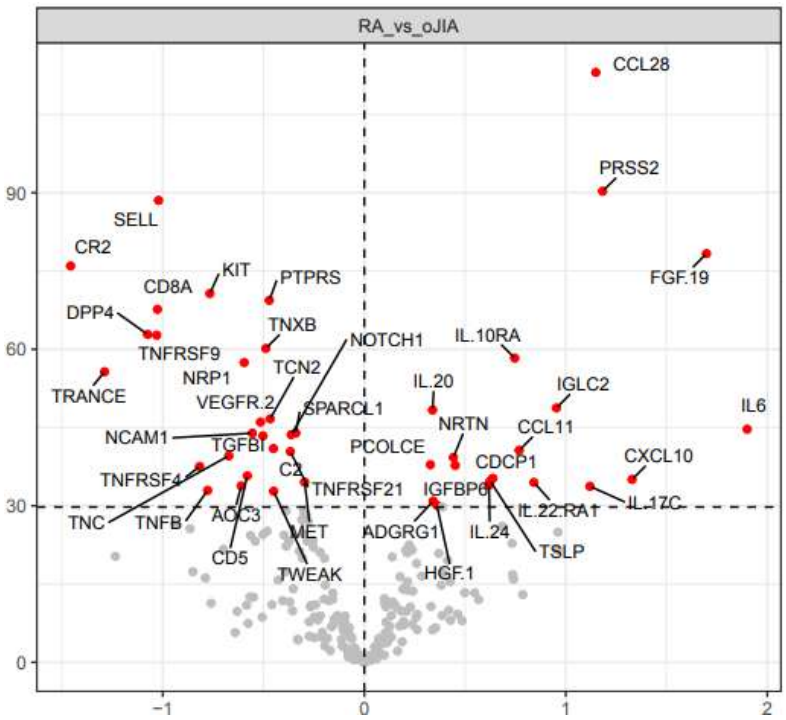

This volcano plot compares RA (n=5) and oJIA (n=14) by displaying the log fold changes and p-values. The red dots indicate proteins that are significantly different between the two groups. Positive log2-fold changes indicate higher protein levels in the UV group compared to the HC, while negative log2-fold changes indicate lower protein levels in the oJIA group compared to RA.

6. Discussion

Juvenile idiopathic oligoarticular arthritis (oJIA) represents the most prevalent form of childhood arthritis. Among the oJIA patients, there exists a subset that faces the potential risk of developing uveitis, a visually impairing condition associated with substantial morbidity. Despite its clinical significance, the etiology of oJIA-related uveitis remains inadequately understood, particularly when compared to other less common forms of JIA.

In recent years, scRNA-seq has emerged as a revolutionary tool in the realm of next-generation sequencing. This cutting-edge technology holds the promise of revolutionizing our comprehension of the pathogenic foundations underlying numerous diseases by enabling the identification of previously elusive cellular subtypes.

This research project is aimed at investigating the hypothesis that a comprehensive and personalized characterization of the immune landscape and proteome profile of patients with oJIA, utilizing the capabilities of scRNA-seq and proteomics, can lead to the identification of specific pathogenic cell populations. Furthermore, it seeks to explore the potential discovery of disease-associated biomarkers, both related to the pathogenesis of oJIA and the development of uveitis. The identified findings will subsequently be validated through replication using CyTOF, thus bolstering the reliability and robustness of the results.

By establishing a definitive connection between the pathogenic cells present in both oJIA and uveitis, this study holds significant translational potential and promises to contribute significantly to the enhancement of treatment strategies for this childhood disease.

Through the application of scRNA-seq and proteomics, this investigation endeavors to unravel the intricate molecular mechanisms that drive the development and progression of oJIA and its associated uveitis. This comprehensive molecular profiling approach has the potential to unlock novel insights into the cellular heterogeneity and regulatory networks underlying the disease pathogenesis.

Furthermore, the integration of proteomic analysis will allow for the characterization of the dynamic protein expression patterns associated with oJIA and uveitis. This multiomic approach will enable the identification of specific pathogenic cell populations and key molecular players that contribute to disease progression and the development of uveitis.

6.1. Characteristics of the cohort

Conducting studies with pediatric patients presents exciting opportunities, especially when it comes to gathering biological samples, which allows us to better understand the unique needs and characteristics of this population.
However, some dificulties have to be mentioned when working with pediatric samples, primarily due to the heightened sensitivity of this population during blood collection.

Furthermore, in the initial weeks following the diagnosis of chronic conditions like juvenile idiopathic arthritis, families often experience high levels of uncertainty and anxiety, which further complicates their participation in research studies.

Additionally, a limitation arises from the relatively small total blood volume of pediatric patients, making it difficult to perform blood draws of moderate volume. This constraint significantly impacts the feasibility of collecting an adequate amount of blood for analysis and further restricts research possibilities in this regard.

However, this study has been conducted in a satisfactory manner, demonstrating remarkable patient inclusion. The first stage of the study (discovery cohort) encompassed eleven subjects, while the subsequent second stage (validation cohort) for proteomic analysis consisted of 35 subjects. In the ongoing validation cohort for the second stage involving mass cytometry, 33 subjects have been included thus far.

The discovery cohort included three patients with debut oJIA, four patients with oJIA and a flare-up of uveitis and four healthy controls.

In the group of patients with debut oJIA, two females and one male with a mean age of 5.33 years were included, all ANA positive and with a high disease activity reflected by a JADAS27 of 15.07 points and elevation of acute phase reactants (mean ESR 67.33 mm/h and CRP 3.29 mg/dl), all variables very similar to other reported cohorts [200].

We have maintained strict adherence to the inclusion criteria for this group of patients. Despite reports suggesting that up to 30% of patients with oJIA may experience an extended course involving more than 4 joints in the early years of the disease [201], none of the patients included in our study have been classified with any other form of JIA throughout the entire duration of the doctoral project.

Regarding patients with JIA and a flare-up of uveitis, we included 4 patients, all females with a mean age of 13.75 years and in all patients the uveitis developed later than the arthritis. This is a common occurrence since anterior uveitis has been reported in a frequency ranging between 12% and 20% and among 1 to 4 years after the oJIA diagnosis, similarly to our patients [202].

Our patients exhibit ocular activity that poses a challenge to control. This is evidenced by their requirement for treatment with two drugs, cDMARDs and bDMARs (all adalimumab). It is not uncommon for children, despite receiving optimal therapy with MTX, to experience refractory uveitis, with prevalence rates ranging from 15% to 50% [203]. While the exact percentage of patients who are refractory to combination therapy with adalimumab and MTX remains unknown, the SYCAMORE study published in 2017 shed some light on this matter. It reported lower but still significant flare rates in the adalimumab plus MTX group compared to the placebo group [16 out of 60 patients (27%) versus 18 out of 60 (60%); p=0.002] [204].
Although rare, the presence of patient's refractory to this combination therapy can occur, as demonstrated in our cohort.

In the second stage of the study, we have successfully enrolled a larger cohort of patients with various conditions.

For the proteomic analysis, we collected eigth patients with debut oJIA, four females and four males with a mean age of 7.62 ± 4.5 years and not all ANA positive (5/3) and with a high disease activity. This selection of slightly older, ANA-negative patients also represents part of the clinical spectrum of oJIA.

Still not analyzed but already available for the CyTOF validation analysis, we recruited seven patients (four females and three males) with a mean age of 7.14 ± 4.36 years, all ANA positive and with a high disease activity.

Regarding the uveitis flare in oJIA patients, in the proteomics analysis we included seven female patients. These patients had a comparable age (11.85 ± 3.38) to those in the first phase of the study, and the duration from oJIA onset to uveitis development was slightly shorter (9 ± 4.56 years).
The clinical variables related to uveitis as well as the analytical variables were very similar to the first stage patients. In this cohort, 5/7 patients were on adalimumab and 6/7 were on cDMARDs.
As well, we included eight patients (all females), with a mean age of 12 ± 3.11 years and very similar duration of oJIA and uveitis. Seven patients received cDMARDs (five methotrexate; two leflunomide), and six were on adalimumab for over a year at sampling.

In this second stage, we have obtained samples that will be used for the validation phase by CyTOF in a second time. These samples have been used for the proteomic study to both discover and validate proteins found in the first stage of scRNA-seq.
Availble samples for both proteomic and cytometric analysis from all patients with all other conditions include: three patients with oJIA under cDMARDs treatment, three patients with oJIA at week 0 and week 12 after starting a bDMARD therapy, and five patients with new-onset RA.

Of note is the inclusion of three patients from whom serial samples could be obtained at week 0 prior to starting bDMARDs and at week 12. Two out of three patients were already being treated with a cDMARD. Notably, all three patients were in remission at week 12. A good response to treatment with bDMARDs is to be expected and has been reported in up to 70% of patients with oJIA [205].

In this second phase, we have also included a group of patients with RA to investigate the cellular and proteomic profile differences that may exist between oJIA and RA. Although there are similarities between inflammatory arthritis in adults and children, RA and JIA appear to be phenotypically distinct, except in the case of the older children with RF-positive polyarticular JIA [206]. This group included five patients recently diagnosed with RA, with clinical characteristics at debut that were highly representative of the disease. Four females and one male were included, with a mean age of 46.4 ± 14.04 years, a DAS28 of 6 indicating high disease activity and moderate elevation of acute phase reactants.

The healthy controls included in the first and second stages of the study were healthy children who donated for the purpose of the study, and who were selected to match for age and gender with the JIA patient group.

6.2. Characteristics of the samples

In terms of the biological characteristics of the samples, during the first stage, we collected PB and SF samples from three patients with debut oJIA. However, for the remaining eight subjects, only peripheral blood samples were obtained as the patients with a uveitis flare didn't have an arthritis flare simultaneously.

The mean volume of PB collected was 9.87 ± 2.91 cc, while the mean volume of SF was 8 cc. It's important to note that the amount of blood that can be drawn from a pediatric patient is limited by their total volume per kilogram of body weight. As for the exact mean amount of synovial fluid that can be extracted from an inflamed joint in a child, this is not contant. However, in a study conducted on a cohort of Spanish patients with debut oJIA, the mean amount of synovial fluid extracted was 2 cc, which is significantly lower than the volume collected in our study [207].

The samples were immediately transferred to the laboratory and processed with a time delay of approximately 60 minutes. The rapid processing of the samples was

constantly maintained throughout the entire dissertation project to ensure optimal sample quality of both PB and SF mononuclear cells and plasma.

Various techniques can be employed for the isolation of MCs, including density centrifugation with Ficoll, as well as isolation using cell preparation tubes and SepMate™ tubes with Lymphoprep™. In a series of experiments, these three PBMC isolation methods were compared in terms of cell recovery, viability, PBMC population composition, and cell functionality with no significant differences observed among the techniques [208]. Given our research group's prior experience in isolating mononuclear cells using the Ficoll method, this technique was implemented in our study, resulting in a high efficiency of cell isolation, as indicated in the Results section.

While the isolation of MCs is generally a straightforward process, it is important to consider the intrinsic physicochemical properties of SF in single-cell genomics studies. Therefore, when working with SF samples, a specific protocol must be employed to digest the extracellular matrix components of the synovial exudate, typically utilizing the enzyme hyaluronidase as others have conducted before [209]. In our study, we successfully implemented this protocol without any complications. As a result, we achieved a high efficiency in isolating cells from the SF (2.80E+06) (x to y millions), which aligns with findings from other relevant studies in the field [210].

It is crucial to emphasize that maintaining optimal sample processing was a priority throughout the project to ensure the highest quality of samples.
This aspect holds particular significance, especially during the initial stage of the project when implementing scRNA-seq technology.
Sample processing in scRNA-seq studies can introduce variations in gene expression profiling, for example, activating stress-related genes, or sensitive cells can be damaged during the protocol [211]. For these reasons, it is important to process samples in the shortest amount of time possible, as has been done throughout this project.

Regarding sample preservation, the first scRNA-seq protocols were initially designed based on freshly isolated cells. However, immediate sample processing can be

challenging, particularly in a clinical setting. To solve this problem, cell and tissue cryopreservation methods have been developed and have proven good results [212]. In our study, our cell isolates (SF and PBMC) were cryopreserved in liquid nitrogen at -80°C, subsequently obtaining good quality control data and good demultiplexed hashing quality control values.

6.3. Cell cluster identification

In the first stage of our study, despite including a relatively small number of patients, after filtering, 132,824 mononuclear cells from PB and SF cells were analyzed together. To our knowledge, this is the first work that has analyzed the entire cellular landscape in PB and SF of patients with oJIA. Previous studies have focused on one or few specific cellular subtypes [115,118,176,213].

The clustering process has been one of the most challenging stages of the project, due to its inherent difficulties. The lack of adequate and available references has meant that unsupervised clustering approaches had to be applied. This stragey involves manual cluster annotation. Manual annotation is a time-consuming process and places certain limits on the reproducibility of the results due to its inherent subjectivity. Cell atlases, as reference systems that systematically capture cell types and states, could help to alleviate this problem [214]. In this project, manual clustering has been carried out, but also a semi-automated annotation algorithm has also been applied.

In addition, the process of clustering presents an additional level of complexity, which is the determination of the optimal level of resolution. ScRNA-seq enables a precise delineation of cell types and states, facilitating more comprehensive characterization of cell populations compared to bulk sequencing experiments.
However, mapping cell types and states at a desired level of resolution can be difficult. Attaining the targeted level of resolution or granularity in the cellular map may necessitate significant methodological efforts and will depend on the degree of flexibility permitted by the research question in terms of resolution.

In our study, our objective was to simultaneously construct a comprehensive cellular map of both SF and PB samples obtained from patients with oJIA and oJIA-U.
To achieve this, we have adopted different levels of resolution to capture and characterize as many relevant cell populations as possible.

6.3.1. B cells

Cluster 1 comprises B cells in which we have identified seven distinct B cell subpopulations. To the best of our knowledge, it is the first time that these B cell subpopulations have been described in both PB and SF from oJIA patients. Previous research by Imbach *et al.* briefly mentions the presence of naive and memory B cell populations in oJIAs PB, but without providing further detail [213].

It is worth noting the cluster of non-switched memory B cells, wich we found in higher aundance at the SF. In the peripheral blood of humans, the B cell compartment can be divided into four major subsets on the basis of CD27 and IgD expression; naive/transitional (CD27-IgD+), double negative (CD27-IgD), switched memory B cells (CD27+IgD–) and non-switched memory B cells (CD27+IgD+) B cells. Switched memory B cells are of germinal center origin and include isotype-switched IgG, IgA, IgE and the pre-switched IgM+ only cells, whereas non-switched memory are antigen experienced B cells expressing IgM+IgD+ or the smaller subset of IgD+ only (IgM-). The non-switched memory B cell population in the literature has alternative names including ‘unswitched memory’ or ‘circulating marginal zone’ (or marginal zone-like) B cells in humans. While the ability of switched memory B cells to contribute to responses during recurrent viral infection has been demonstrated, the origin and contribution of non-switched memory B cells to humoral immunity remains controversial.
Although its role in oJIA has not been studied, a reduction of non-switching memory B cells in peripheral blood has been described in other autoimmune diseases in which the B cell plays a key role, such as Sjögren's syndrome and SLE. Feng *et al*. performed a detailed analysis of B-cell subsets by flow cytometry in 55 patients with Sjögren's syndrome and 114 adults. Memory B cells, including non-switched B cells, showed a significant reduction in peripheral blood, reflecting their

probably accumulation in exocrine glands and skin in Sjögren's patients and likely differentiation into plasma cells [215].

In oJIA, unswitched memory B cells have not been studied individually, but rather the group of memory B cells as a whole. The relationship between the production of autoantibodies such as ANAs and memory B cells has been studied.
Gregorio *et al*. studied 40 JIA patients who underwent a synovectomy and observed that 28 patients displayed T-B cell aggregates. Lymphoid organization correlate with the presence of ANA and plasma cell infiltration [101].

Plasma B cells and a cluster of plasmablasts were detected in both PB and SF of oJIA patients, in contrast to HCs. Comparably to our results, Corcione *et al.* studied the B cells from SF and peripheral blood PB of 25 JIA patients, as well as from PB of 20 controls of comparable age. By multicolor flow cytometry, the demonstrated an expansion of IgG-secreting plasma cells in the SF from oligoarticular JIA patients [216]. This highlights the importance of plasma cells in the production of ANAs, which are so characteristic of oJIA.

Finally, to conclude this cluster, we have not been able to characterize the naive B cell population in our study. In contrast, the relevant study by Orange *et al* in RA identified a naive B cluster one week prior to an arthritis flare [175]. However, it is important to acknowledge that in our study, the samples were collected after the patient had experienced a flare, making it challenging to ascertain whether a naive B-cell profile was present prior to the onset of the flare.

6.3.2. Myeloid cells

We have identified eight different cellular subtypes among this cluster.
In the bone marrow, common myeloid precursors differentiate into monocytes.
Monocytes can differentiate into inflammatory or anti-inflammatory subsets. Upon tissue damage or infection, monocytes are rapidly recruited to the tissue, where they can differentiate into macrophages or dendritic cells. Monocytes can be characterized by marker-based assays, based on a classical classification that distinguishes CD16-

positive monocytes into two subtypes: $CD14^{++}CD16^{+}$ and $CD14^{+}CD16^{++}$ monocytes. This revised classification recognizes the existence of three monocyte subsets: classical monocytes ($CD14^{++}CD16^{-}$), intermediate monocytes ($CD14^{++}CD16^{+}$), and nonclassical monocytes ($CD14^{+}CD16^{++}$) [217]. While intermediate monocytes were previously overlooked in earlier studies, they hold significant clinical relevance due to their heightened production of reactive oxygen species (ROS) and enhanced migration capacity [218].

However, classification now relies on the genes that cells express. Villani *et al*. used deep sequencing at the single-cell level and unbiased clustering to define six dendritic cell and four monocyte populations [219].

We do capture aDCs (CCR7, CD83), classical monocytes (S100A9, CD14, VCAN) and interemediate monocytes (CSTB). Macrophage cells, which have been of great interest in RA as described in the Introduction chapter, have not been captured because of the low number of cells within the myeloid lineage.

6.3.3. T-NK cells

This large cluster has been broken down into different sub-clusters applying different levels of depth.

Among effector memory $CD8^{+}$ T cells, a previously uncharacterized subtype of $NKG2C^{+}$ effector memory $CD8^{+}$ T cells in oJIA was identified. This cluster of cells is characterized by the expression of NKG2C, a marker of long-lived effector memory cell. This membrane receptor forms a heterodimer with CD94 and constitutes an activation receptor (KIR, killer cell Ig-like receptor) that binds to HLA-E. Then, $NKG2C^{+}$ $CD8^{+}$ T-cell population is endowed with NK phenotype and broad immune surveillance capacity. $CD8^{+}$ $NKG2C^{+}$ T cells have been reported to be increased with age and in diseases such as toxic epidermal necrolysis, Steven-Johnson syndrome, celiac disease, and CMV [220] [221]. These cells are characterized by the expression of granulysin, perforin, and granzymes and can be activated even in the absence of TCR stimulation, indicating that NKG2C can compensate for a weak or absent TCR signal [222]. This cell populations has not been previously described in JIA.

Among the NK cells, five different clusters were identified: immature CD56$^+$dim CD16$^+$, mature CD56$^+$dim CD16$^+$, terminal CD56$^+$dim CD16$^+$, CD56$^+$ bright NKs and NK-like CD8$^+$ T cells.

Interestingly, this level of depth makes it possible to unravel these NK subsets. Human NKs have been traditionally divided into two subsets based on the relative surface density of CD56 antigen: CD56$^+$ bright NK cells, which are preferentially located in the lymph nodes, and CD56$^+$ dim cells, which recirculate into the peripheral blood.

However, recent studies revealed functional intermediaries between these two mentioned subsets.

Using scRNA-seq technology, Yang *et al*. have identified distinct NK populations in the human bone marrow and blood. In this study, the authors discovered distinct developmental stages beyond the simple subsets of bright/dim in NK cells. They identified a genuine CD56bright NK cell population and observed a transitional population between CD56bright and CD56dim NK cells.

This supports the notion of developmental progression from CD56bright to CD56dim NK cells at the transcriptome level, as indicated by the expression of CD16 (FCGR3A). Furthermore, the authors identified mature and terminal NK cell clusters collectively representing functionally mature NK cells, with CD57$^+$ NK cells being a subset of this population. At the transcriptomic level, terminal NK cells were characterized by CX3CR1 and HAVCR2 (TIM-3) expression. However, whether there are differences in function and longevity between the mature and terminal NK cell subsets remains an open question [223]. In our cluster identification, we have characterised and differentiated between bright, mature, and terminal NKs, supporting the existence of these transitional maturation states in NK cells.

Another interesting finding in this cluster is the identification of the NK-CD8$^+$-like T cells, recently defined by the coexpression of NK markers (KIR, CD56, NKGLA, NKGLC, and CD94) and terminally differentiated effector memory CD8 markers (CD45, CD57). These cells express the transcription factor Eomesodermin (Eomes) as a lineage marker of that population of cells. EOMES belongs to the conserved T-box gene family, regulates T-cell development and function, and is a master regulator of CD8$^+$ effector memory T cells. An accumulation of EOMES-expressing CD8$^+$ T cells that show characteristics of exhausted cells has been observed in several tumors and in chronic viral infections. Based on this, a role for EOMES in T-cell dysfunction

following continuous activation of $CD8^+$ T cells was suggested. Together with their marked NK-like phenotype, a hallmark of KIR^+ $Eomes^+$ $CD8^+$ T cells is their capacity to rapidly produce large amounts of IFNγ in response to innate-like stimulation by IL-12 and IL-18 [224].

Among other less abundant T cell populations, we have described a cluster that corresponds to γδ T cells. This cell type are a unique T cell subpopulation that are rare in secondary lymphoid organs but enriched in many barrier tissues, such as the skin, intestines, and lungs [225].

We have also defined a cluster of MAIT cells, which are innate-like lymphocytes cells that typically express a $TRAV1\text{-}2^+$ semi-invariant TCRα that enables the recognition of bacterial, mycobacterial, and fungal riboflavin metabolites presented by MHC class I related molecule 1 (MR1). Human MAIT cells primarily express $CD8^+$, although a smaller subset lacks both CD4 and CD8 [226].
In a recent study conducted by Kyriakos *et al.* MAIT cells were analyzed using scRNA-seq, revealing a wide range of functional phenotypes. During early activation, MAIT cells rapidly adopt a cytotoxic phenotype characterized by high expression of GZMB, IFNγ and TNF. In contrast, prolonged stimulation induces heterogeneous states defined by proliferation, cytotoxicity, immune modulation, and exhaustion [227].
In oJIA, MAIT cells have not been previously characterised. In other autoimmune diseases such as RA and AD, circulating MAIT cells have been found to be reduced. In these patients, MAIT cells showed an increased IL-17 production capacity and the activated state of these cells correlated with disease activity in SpA [228].

In summary, in our study, we were able to identify distinct and relevant cell populations at a high level of detail, with a particular focus on T-NK cells and myeloid cells.
A notable finding is the presence of previously uncharacterised clusters such as DC1, DC2 and intermediate monocytes within the SF. These specific populations have not been described in previous studies, highlighting the novelty and significance of our findings.
Furthermore, our study provided a comprehensive characterisation of activated effector memory CD8 T cells, highlighting the subcluster represented by NKG2C effector memory CD8 T cells within the T cell compartment. This detailed

characterisation sheds light on the functional diversity and potential role of these cells in the context of the disease.
Finally, our investigation has provided an in-depth understanding of the transitional stages of NK cell development, from immature to terminal NK cells. This level of characterisation, which has not previously been described in this detail in the context of oJIA, provides valuable insights into the maturation process and functional properties of NK cells.

6.4. Differential Cell type abundance

In the first stage of the study, we used scRNA-seq analysis to determine the cellular landscape of patients with debut oJIA (n=3) from whom we were able to obtain paired PB and SF samples and PB from HCs (n=4). This allows us to study the different cellular subtypes that are more abundant in one tissue or the other and to hypothesize about the cellular dynamics of these cells.

In the paired analysis, in which the composition of the SF and PB of the same patient (n=3) was studied, we have found that, compared to PB, the SF in oJIA is characterized by a higher abundance of activated effector memory and NKG2C$^+$ effector memory CD8$^+$ T cells, intermediate monocytes, dendritic cells, and regulatory T cells. Conversely, PB from the same patients contains a larger population of naive CD8$^+$ and CD4$^+$ T lymphocytes, memory B cells with ABCs-like phenotype, and switched B lymphocytes.

The presence of CD8$^+$ T cells stand out. These findings are consistent with those of Julé *et al.* in which they found a higher proportion of effector memory CD8$^+$ and CD4$^+$ T cells expressing the Th1 cytokine INFγ in SF compared to PB from oJIA patients.
However, transcriptional differences are observed between our population of effector memory CD8$^+$ T cells and those described in the study by Julé *et al*. In our case, the effector memory CD8$^+$ T cells overexpress markers of effectornes and activation like CCL5, GZMA, GZMK as well as genes related to T-B cell intercommunication such as CXCL13 and tissue residency like CXCR6. In contrast, the effector memory CD8$^+$ T

cell population in SF from Julé's study expressed Th1-related markers such as CXCR3 and INFγ. It should be noted that the study population is clinically different from ours, as the patients included in the Julé *et al.* study had received treatment with bDMARDs or csDAMRDs at the time of sample collection. The transcriptional changes observed could be due to this factor [115].

In another landmark study by Petrelli *et al.*, in which they examined the SF and PB of 52 patients with oJIA and HCs, they found that in SF, effector memory $CD8^+$ T cells were the predominant subset compared to the PB. Terminally differentiated effector memory $CD8^+$ T cells and small fractions of naive and central memory $CD8^+$ T cells were also more abundant in SF, similar to what has been previously described in RA patients [116]. The effector memory $CD8^+$ T cells described by Petrelli *et al.* showed increased expression of the PD-1^+ marker, not detected in our cells, but they do share pathways associated with activated cells, such as cell cycle regulation and chemokine and cytokine signalling, as well as IL-12 signalling. Selected genes up-regulated in the PD-1^+ subset of the SF include chemokine receptors and ligands (e.g., CCR1, CCR2, CCR5, CXCR6, CCL4 and CCL5), IL-12-induced effector molecules (e.g., IFNG, GZMA, GZMB) and proteins directly involved in the cell cycle (e.g. TYMS, E2F2, TOP2A). In line with our findings, they also observed that $CD8^+$ T cells in SF were increased in frequency compared to those in the PB of JIA patientsat the site of inflammatory arthritis and endowed with an activated phenotype [99].

It has as been described that the SF is more heterogeneous regarding the myeloid population than PB. Our results are in line with those previously published by Schmidt *et al*. where they found a higher frequency of intermediate monocytes in SF compared to PB from oJIA paired samples (n=13) [106]. Moreover, monocytes from SF displayed features of mixed M1 (IFNγ)/M2 (IL-4), but not M2 (IL-10). The authors, to investigate the polarization pattern of synovial monocytes more thoroughly, they analyzed these monocytes at the mRNA level for 28 polarization-related genes using qPCR.
A specific pattern combined of traditional in vitro defined M1(IFNγ) (CD80, STAT1, and CXCL10) and M2(IL-4) (CD206, CCL18, and PPARγ), but not M2(IL-10)-related markers across all patients. Functionally these cells have impaired phagocytosis compared to circulating monocytes. Conversely, out intermediate monocytes display

a transcriptomic profile characterized by a stron INF signture with the upregulation of intereferon-related gene IFITM2, IFITM3, IFITM11, ISG15, and ISG20.

However, unlike in our study, HCs were not included to analyze the PB composition, so it cannot be determined whether the frequency of intermediate monocytes was lower in HCs than in oJIA. Furthermore, seven of fourteen patients included were on NSAIDs and eight of fourteen patients were not newly diagnosed patients.
Differences in the clinical characteristics of the patients could explain the transcriptional differences we observed in the intermediate monocytes, since in our study the INF signature is more pronounced.

We observed an increase in Treg cells in SF compared to PB. This finding is similar to the results of the study by De Kleer et al, in which CD25+ Treg cells were present in greater numbers in the joints of patients with persistent oJIA, which was the phenotype of our patients, compared to those with extended oJIA [95]. Their results also revealed a significantly lower number of T reg cells in PB of both subtypes of oJIA when compared to HCs. These results were corroborated by the Treg marker FOXP3 in another cohort of patients with oJIA, which described the reciprocal relationship between T regs and effector T cells at the site of inflammation. T reg in SF not only increased in proportion but also showed increased expression of FOXP3. The presence of Treg cells in SF has highlighted that the balance between effector and regulatory mechanisms may be a factor influencing disease progression [229].

In contrast, we observed an increase in naïve $CD8^+$ and $CD4^+$ T cells in PB relative to total PBMCs. There are several possible explanations for this discovery.
The inherent factor of the study population as the patients are of pediatric age. Previous studies have investigated the homeostatic control of the naive T cell compartment in children, which may be affected by both the growth of the child and changes in thymic output, which increases to a maximum over the first year of life and then declines to reach an approximately steady level by the age of about 20 years [230].
In addition, as the number of activated $CD8^+$ and $CD4^+$ T cells increases, this may have an impact on the overall distribution and availability of subsets of T cells in the immune system. This includes naïve $CD4^+$ T cells, which are responsible for

recognising and responding to new antigens that have not been encountered before. The expansion of effector $CD4^+$ T cells can lead to a relative decrease in the number of naïve $CD4^+$ T cells, as the resources and space of the immune system are occupied by the expanding effector population. Importantly, the extent of this impact may vary depending on the magnitude and duration of the immune response, as well as the specific cytokine and signalling environment present during the response. In addition, homeostatic mechanisms may also play a role in maintaining a balance between effector and naïve $CD4^+$ T cell populations over time.
Overall, the expansion of effector $CD4^+$ T cells may have consequences for the total number and availability of naïve $CD4^+$ T cells, potentially influencing the diversity and functionality of the CD4 T cell repertoire.
As expected, in our analyses, naive $CD8^+$ and $CD4^+$ T cells were not found in the SF. Also, and no differences in PB were observed in oJIA compared to HCs.

In patients with oJIA-U, we observed an elevated presence of dendritic cells type 1 and 4 and mature NK cells compared to oJIA patients without uveitis. Additionally, these cell populations were found to be more prevalent in oJIA-U cases compared to HCs, indicating their potential involvement in the development and progression of uveitis. Limited research has been conducted on the contribution of innate immune system cells to the development and progression of JIA-related uveitis. Existing studies primarily emphasize the examination of effector T cells and B cells present in the uveal tissue, with only a few investigations conducted thus far (explained in detail in the Introduction).

A recent study examined the role of innate immune cells in uveitis associated with JIA-U and SpA. Using FACS analysis, the researchers analyzed PB samples from 23 JIA-U patients, 19 SpA patients, and 16 HCs. In the SpA group, uveitis activity was correlated with a decreased frequency of $CD56^+$dim NK cells. Additionally, a constitutively activated monocyte phenotype and elevated levels of S100A8/A9 in the serum were observed. When analyzing the composition of NK cells in JIA-U patients, in crontast to SpA patients, they demonstrated increased frequencies of $CD56^+$ monocytes and $CCR7^+$ Dc, while no significant differences were found in the NK subpopulation.

This study sheds light on the distinct immune cell profiles associated with uveitis in patients with different underlying conditions, providing valuable insights into the immunopathogenesis of JIA-U and SpA-associated uveitis, where since the clinical presentation of uveitis is different, slightly different immune mechanisms are likely to underlie it [231]. Like our results, we found an increase in the number of dendritic cells in oJIA-U. In contrast, in our study we also observed an increase of NK cells in PB, which was not reported in this study.

In this regard, it should be noted that many types of non-infectious uveitis are genetically predisposed to the HLA as the region of susceptibility to the disease.
For example, uveitis strongly associated with the HLA-I region includes Behçet's disease, birdshot chorioretinopathy, and HLA-B27 positive uveitis. In contrast, uveitis that is tightly related to the HLA-II region includes Vogt-Koyanagi-Harada disease, sarcoidosis uveitis, tubulointerstitial nephritis and uveitis syndrome, and JIA-U [232].
New prospects have recently been raised regarding the pathogenesis of HLA-DRB1-related autoimmune diseases. Arase *et al.* reported that misfolded proteins complexed with HLA-II act as autoantigens for several autoimmune diseases. Misfolded proteins in the endoplasmic reticulum are usually rapidly degraded by mechanisms, such as endoplasmic reticulum-associated degeneration, and are not transported extracellularly. However, by binding to HLA-II, misfolded proteins escape proteolysis and are transported extracellularly as full-length intact proteins.
Surprisingly, these proteins presented by HLA-II include endogenous proteins, such as misfolded-IgG and misfolded-HLA-I molecules.
HLA-I molecules are essential for NK cells to distinguish between self and non-self through the activation of the KIRs. Since HLA-II molecules are not ligands for KIRs, there is no direct interaction between HLA-II and KIRs. However, many NK cells express Fc receptors that specifically bind to IgG. Since IgG can bind to Fc receptors on NK cells and regulate them, NK cells also participate in adaptive immunity.
However, APCs can present full-length misfolded intracellular proteins (then MHC-I antigens) by HLA-II [233]; these introduced intact-MHC-I molecules could interact with KIR, and therefore with the NKs, on the cell surface of APCs.
How these HLA-I ligands released by HLA-II interact with NK cells in patients with JIAo and JIA-U, which could explain the observed increase in this population in our study.

In other diseases, such as Behçet's disease (BD) uveitis, where NK cell involvement has been described, there are conflicting results.
NK cell numbers and activity have been reported previously in BD uveitis concerning disease activity and to the medication used to treat BD patients, e.g., azathioprine, cyclosporin, and corticosteroids [234]. The numbers and cytotoxic capacity of NK cells reported in BD appear to be variable, with uncertainty in the literature due to the use of different markers to phenotype NK cells and their subsets. Several studies have found increased NK cells numbers in PB of BD patients, especially during the active phases of the disease, while other studies have revealed that BD and matched healthy controls had similar NK number in PB. In contrast, other studies have revealed that BD and matched HCs had similar NK cell numbers in PB [235].
No studies have determined the abundance in peripheral blood of oJIA-U patients. Thus, our results would represent a first line of work for future studies.

6.5. Differential expression analysis

Differential gene expression analysis within each cell subtype in the pareid analysis between SF and PB, showed the greater differentially expressed genes among $CD4^+$ effector memory T cells, followed by DC2, T regs, and $NKG2C^+$ effector memory $CD8^+$ T cells.
Focusing on the likely critical role of activated effector memory CD8+ T cells and $NKG2C^+$ effector memory $CD8^+$ T cells found in abundance in the SF, we describe transcriptional differences that may characterise these cells. In pairwise analysis of PB and SF samples, we studied transcriptional differences in this cell population, showing overexpression of CCL5, GMZA, GZMK, CXCL13, CXCR6, S100A6 and S100A11 genes in SF and PB from oJIA patients compared to PB from HC.

CCL5 is chemoattractant protein, also known as regulated upon activation, normally effector T cells expressed and secreted (RANTES). CCL5 has been show to activate T cells, leading to the production of IFNγ by cytotoxic T cells and may induce the maturation of dendritic cells [236]. Thus, migrating T cells under a chemokine gradient into an inflamed tissue may lead to further T cell activation. $CD8^+$ T cells through

production of CCL5 have been shown to regulate inflammation in experimental models of arthritis. In particular $CD103^+$ $CD69^+$ $CD8^+$ Trm cells were found in elevated numbers in previously inflamed joints in RA and shown to initiate flares by recruiting circulating lymphocytes by CCL5 secretion. Inhibition of CCL5 release by these cells inhibited arthritis flares in a murine model of RA [237].

The involvement of this cytokine has been previously described in patients with JIA. Pharoah *et al*. studied the expression and production of CCL5, CXCL10, and CCL3, within the joints of oJIA and polyarticular JIA patients with matched PB, and PB HCs. All three chemokines were highly expressed at the mRNA level, with the most significant increase being demonstrated for CCL5 when compared with matched PB samples and controls. The authors investigated the source of CCL5 from inflammatory synovial cells, which were shown to be $CD8^+$ T cells with a terminally differentiated phenotype similarly to ours. These cells also contained high levels of stored intracellular CCL5, and a rapid release of CCL5 occurred under T-cell stimulation [238].

Recently, Penkava *et al.* used scRNA-seq, mass cytometry, and TCR sequencing to profile the cells involved in SF, synovial tissue, and PB from patients with psoriatic arthritis. Psoriatic arthritis can sometimes closely resemble JIA due to a clinical phenotype characterized by recurrent arthritis of large joints, such as the knees, like oJIA. In their complex and detailed analysis, they identified a significant expansion of synovial memory $CD8^+$ T cells with a significant increase in the expression of cytokines such as CCL5, CCL4, and other markers of effector function and cytotoxicity, including GZMA, GZMB, GZMH, and GZMK, which is in line with our results [239]. At present, no scRNA-seq studies have been performed in psoriatic JIA so the same conclusions cannot be drawn at this level. However, psoriatic JIA and PsA are very similar clinically. In general, peripheral joint involvement is the most common form of presentation in both adult and juvenile PsA. Enthesitis and dactylitis are hallmarks of PsA in both children and adults, with a similar reported prevalence in both groups. Therefore, in the absence of studies that analyse immunological differences in more depth, we could extrapolate the pathogenic mechanisms known so far in PsA to psoriatic JIA.

More recently, in a work that has not yet been peer-reviewed, Dunlap *et al.*, as part of the Accelerating Medicines Partnership Programme for Rheumatoid Arthritis and Systemic Lupus Erythematosus (AMP RA/SLE), have investigated clonal associations and different T and B lymphocyte subtypes in RA synovial tissue and PB by scRNA-seq. Concretely, analyzing the subcluster of $CD8^+$ T cells in both synovial tissue and PB revealed nine $CD8^+$ T cell populations that could be found across samples. Among all the populations, three were distinguished by GZMK and GZMB expression patterns. Both populations also had overexpression of GZMA and CCL5 [240]. These results would be in line with those found in our study, pointing to the role of effector memory $CD8^+$ T cells with an effector and cytotoxic phenotype in both RA and oJIA.

Both GZMA and GZMK are overexpressed on the effector memory $CD8^+$ T cells found in greater abundance in SF from oJIA patients.

GZMA and GZMK are abundant proteases that are localized in the cytosolic granules of cytotoxic T-cells and NK-cells [241]. Five human granzymes (A, B, H, K, and M) have been identified, varying among their primary substrate specificity, function, and expression in distinct cell types.

Concretely, GzmA can induce the production of different inflammatory cytokines such as TNF-α, IL1β, IL-6, or IL-8 in human cells like monocytes, macrophages, fibroblasts, endothelial and epithelial cells that might contribute to the cytokine storm observed during proinflammatory situations. Besides, one of the first described substrates for GzmA is pro-interleukin 1β, which after removal of the N-terminal part, generates the active inflammatory form IL-1β [242]. GzmK displays a similar activity but is not identical to GzmA, and it might also induce the production of proinflammatory cytokines. Nanomolar concentrations of GzmK induce the maturation and secretion of IL-1β, suggesting that GzmK may augment GzmA-induced proinflammatory processes.

Although not described in as much detail as $CD4^+$ effector T cells, Maschmeyer *et al*. also reported a cluster of $CD8^+$ T cells from JIA SF expressing GZMK and GZMH throughout the vast majority of this population [118]. This pattern seems consistent with $CD8^+$ T cells from RA and PsA, with broad GZMK expression among infiltrating T cells [239]. Moreover, these authors also reported a small cluster among synovial $CD8^+$ T cells with low expression of GZMK. These cells were characterized by the

overexpression of several markers resembling peripheral helper $CD4^+$ T cells, including CXC-chemokine ligand 13 (CXCL13), programmed cell death 1 (PDCD1), ectonucleoside triphosphate diphosphohydrolase 1 (ENTPD1), and markers of tissue-residency like C-X-C Motif Chemokine Receptor 6 (CXCR6), similar to our cluster of activated effector memory $CD8^+$ T cells [118].

Focusing on the critical role of activated effector memory $CD8^+$ T cells, including the $NKG2C^+$ subpopulation we observed transcriptional differences that distinguish these cells. Comparative analysis of SF and PB samples revealed overexpression of CXCL13, CCL5, GMZA, GZMK, CXCR6, S100A6 and S100A11 genes in both SF and PB from patients with oJIA compared to PB from HC.

CXCL13 exclusively binds to the chemokine receptor CXCR5, expressed on B cells, Tfh cells, and T follicular cytotoxic cells (Tfc), also known as $CXCR5^+$ $CD8^+$ T cells.
Described in solid cancers, Tfcs are localized similarly to CXCR5 Tfh in B-cell follicles. In the tumor microenvironment, Tfc cells maintain self-renewal capability during prolonged antigen exposure and might play an important role in sustaining antitumor immunity and responding to PD-1/PD-L1 blockade [243].
The relation between CXCL13 and Tfcs is that this chemokine helps to recruit specific B cells and Tfcs to the site of chronic inflammation to coordinate the both humoral and cell-mediated adaptative immune response. CXCL13 also influences innate immunity by shaping the character and magnitude of the inflammatory response [244].
Recently studied in ovarian cancer, Yang *et al*. described those tumors with high CXCL13 expression exhibited increased infiltration of activated and CXCR5- $CD8^+$ T cells and better survival outcomes.
Petrelli *et al.* also described an elevated expression of CXCL13 in a $PD1^+$ $CD8^+$ T cell cluster in JIA [99]. The presence of a $CXCL13^+$ $CD8^+$ T cell population appears to differ from the pattern seen in RA synovial T cells, where CXCL13 expression was only observed in $CD4^+$ T cells and raises the possibility that $CD8^+$ T cells may play a unique B cell helper role in JIA [173].

CXCR6 is another receptor chemokine overexpressed in the effector memory $CD8^+$ T cell population from our oJIA patients in both SF and PB. This is a receptor for the chemokine CXCL16, which exists as a membrane or soluble form. CXCR6 is

predominantly expressed in human memory T cells but is also detected in NK cells, NKT, DCs, and ILC [245].
Tissue-resident memory cells are usually defined by the expression of this marker, and it represents a core marker for various tumors like ovarian and lung cancer.
Barely studied in JIA, the first evidence of its role in JIA's pathogenesis was reported by Martini *et al.* In this study they investigated CXCR6 expression and functional capability in lymphocytes from SF by flow cytometry and migration assays. Furthermore, CXCR6 and CXCL16 expression in synovial tissue was analyzed by immunohistochemistry. T cells isolated from SF of patients with JIA expressed CXCR6, which was functionally active, as shown by chemotactic assays and both CXCL16 and CXCR6 were intensively expressed in the synovium cells [246].

We observed an overexpression of the S100A6 and S100A11 genes in effector memory $CD8^+$ and $NKG2C^+$ effector memory $CD8^+$ T cells in both SF and PB of oJIA patients compared to PB in HCs.
The S100 protein family comprises low molecular weight calcium-binding proteins with highly conserved amino acid sequences [247].
They regulate many activities inside and outside the cell in a calcium-dependent manner, and certain members of the S100 family are released outside the cell to regulate the proliferation of target cells.
Well described in RA during joint flares, some S100 proteins such as S100A4, S100A6-9 or S100A11 have been detected in the SF of RA patients and have been described as biomarkers of RA activity [248].

However, in oJIA, the most commonly described calcium proteins are the S100A9 and S100A8, which are expressed at high levels in the synovium and released at sites of inflammation and constitute a good biomarker of activity a relapse [249]. Overexpression of the S100 family genes have not been previously reported in $CD8^+$ T cells in oJIA.

Our study has identified a noteworthy cluster of synovial fluid $CD8^+$ effector memory T cells exhibiting distinct genetic characteristics. These cells demonstrate elevated expression levels of Tfh cell-associated genes, specifically CXCL13, and Trm cell-associated genes, particularly CXCR6. Additionally, gene transcript analysis has

revealed indications of an activated phenotype, as evidenced by granzymes and chemokines like CCL5. These findings shed light on the functional and molecular properties of this specific group of T cells within the synovial environment.

In general, oJIA-U cells displayed a marked upregulation of the type I interferon signaling pathway, interferon gamma-mediated signaling pathway, cytokine-mediated signaling pathway, and antigen processing and presentation of peptide antigens via MHC class I.

Mature CD56 $^{+}$dim NKs genes upregulated in oJIA-U compared to oJIA without uveitis were PRF1, FECR1G, CCL4 (MIP-1β) and B2M.

PRF1 is a protein-coding gene that produces perforin 1, a pore-forming protein, that plays a key role in granzyme-mediated programmed cell death. NK cells are armed with functional cytotoxic granules containing perforin and granzymes, essential effector molecules for NK-cell cytotoxicity [250]. Concretely, CD56^{+}dim NK cells express high levels of the low-affinity Fc receptor CD16, variegated display expression of several types of inhibitory receptors for MHC class I, and express high levels of perforin [251].

FCER1G (FcεRIγ) is a protein-coding gene for a signaling molecule for Fc fragment of IgE receptor and NK activating receptor complex. It is highly expressed by NK cells and involved in NK cell activity. FcεRIγ is associated with NKp46 in the transmembrane region and among the molecules which play a prominent role in NK cell activation signaling [223].
Studies utilizing animal models of chronic viral infections have provided valuable insights into the regulatory mechanism of NK cells. During viral infections, NK cells play a crucial role in eliminating hyperproliferative CD8^{+} T cells while also supporting viral persistence. Fauriat *et al*. in their investigation using a lymphocytic choriomeningitis virus model, demonstrated the essential role of FcεRIγ in maintaining the stability of NKp46, thereby ensuring its proper functioning. Through a mouse model lacking the FcεRIγ receptor, they discovered that the absence of this receptor on NK cells hampers their ability to control virus specific CD8^{+} T cell responses.

Consequently, this leads to an enhanced $CD8^+$ T cell response and rapid viral control [251].
FcεRIγ, like molecules such as PD-1, could potentially serve as a therapeutic target. Targeting FcεRIγ or its downstream signaling molecules could be a promising approach to enhance T-cell responses, and its applicability could also extend to other immune cells and other diseases.
In the case of autoimmune diseases like JIA, there is hardly any evidence for the role of this molecule in NK cell function.

CCL4, also known as MIP-1β, is an important chemokine involved in NK immune response [252]. Despite terminal and mature NKs being characterized by their cytotoxic functions, their response also involves the secretion of cytokines and chemokines, such as CCL4, being secreted in huge quantities and very fast after stimulation [251]. It has recently been shown that, contrary to the assumption that CD56 bright NK cells were the cytokine producers compared to CD56 dim NK cells, both can be prominent producers of cytokines upon target cell recognition.
Furthermore, upon both target cell recognition and exogenous cytokine stimulation, CD56 dim NK cells excelled in production of the chemokine CCL4. These experiments highlight CD56 dim NK cells as an important proinflammatory cytokine source during early immune responses [251] Our results suggest that the mature and terminal NK cells represented in higher abundance in patients with uveitis overexpress cytotoxicity markers corresponding to bright NK cells, indicating a higher degree of inflammation than theoretically expected for this cell subtype.

Finally, B2M is a gene that encodes a serum protein found in association with the MHC class I heavy chain on the surface of nearly all nucleated cells.
NK cell cytotoxicity is regulated by inhibitory receptors that bind self-MHC class I molecules. The absence of MHC class I expression causes lysis of cells, as described by the 'missing-self' hypothesis.
There are several reasons why B2M may be overexpressed in NK cells and concretely, during inflammatory responses, cytokines and other inflammatory mediators can induce the upregulation of B2M expression in NK cells. This increased expression may enhance the ability of NK cells to recognize and eliminate target cells, such as infected or tumor cells [253].

Regarding the most abundant cell type in oJIA-U, mature CD56^{+}dim NKs, we have identified notable transcriptional variances specific to this condition compared to patients with oJIA without uveitis. In particular, mature CD56^{+}dim NKs exhibit distinct gene expression profiles indicative of an activated phenotype, as evidenced by increased FCER1G, CCL4, and B2M transcription. Furthermore, these cells also display cytotoxic activity, as demonstrated by the expression of PRF1. These findings provide valuable insights into the unique molecular characteristics of mature NK cells in oJIA-U, highlighting their potential role in the pathogenesis of uveitis in this patient population.

6.6. T-cell receptor analysis

The use of T-cell receptor VDJ sequencing in this study allowed us to understand the clonal architecture of oJIA with a level of detail not previously possible.

Our study observed a high degree of clonal expansion of activated effector memory CD8^{+} T cells in SF and effector memory CD8^{+} T cells in PB of oJIA and oJIA-U patients. This finding agrees with previous data in oJIA showing that CD8^{+} T cells are generally more expanded than CD4^{+} T cells [254]. We have also observed that effector memory CD8^{+} T cells contain the highest number of expanded clones in both SF and PB from both oJIA and oJIA-U patients. During clonal expansion, the activated T cell undergoes multiple rounds of cell division, resulting in the generation of a larger population of T cells with identical TCR sequences. This expansion allows for an amplified and coordinated immune response against the antigen. Clonal expansion is a fundamental mechanism by which the immune system can generate a robust and specific response to combat pathogens or respond to other immune challenges.
The simultaneous analysis of PB and SF from the same individual revealed overlapping clones, suggesting that CD8^{+} effector memory T cells that came from periphery and locally expanded at sites of inflammation.

In line with our results is the study by Vanni *et al*. in which they reanalyzed publicly available scRNA-seq and TCR repertoire data of memory $CD4^+$ and $CD8^+$ T cells derived from six SF and six PB samples of oJIA patients. Dissecting the diversity of $CD8^+$ T cells, most derived from both tissues, PB and SF, and expressed high levels of granzymes and cytotoxic genes as our results. Also, they performed a trajectory analysis and could identify terminal $CD8^+$ T cell clusters characterized by the expression of CXCR3, not overexpressed in our cells, and INF-related genes [118,255].

Upon closer analysis of the effector memory $CD8^+$ T cell clusters, we found a unique observation regarding the differential expression of the CCL5 gene within this population. Similarly, to our results, Penkava F *et al.*, sequencing of paired T cells receptor alpha and beta sequences, also observed a pronounced $CD8^+$ T cell clonal expansion within the SF of psoriatic arthritis patients. This cluster was defined by transcripts indicating an activated phenotype with upregulation of granzyme-related genes (GZMA, GZMB, GZMH, GZMK) and chemokines CCL4 and CCL5.

While the role of $CD8^+$ T cells and their clonal expansion in oJIA has received limited attention in previous studies, T regs, another cell population we found to undergo clonal expansion in SF, have been more extensively investigated by various research groups.
Rossetti *et al.* compared Treg cells of patients with oJIA responding or not to therapy with cDMARDs by using TCR sequencing to identify clonotypes shared between PB and SF. They also investigated FOXP3 Treg cell-specific demethylated region DNA methylation assays, to investigate their stability. The authors found a subset of synovial Treg cells that expanded and proliferated during active disease and displayed a reduced TCR diversity as we also found [114]

Further research is needed to fully explore the contribution and importance of clonally expanded $CD8^+$ T cells in the pathogenesis of oligoarticular oJIA. This research complements existing knowledge on clonally expanded Tregs. By bridging this research gap, we can improve our understanding of the intricate immune mechanisms involved in oJIA and potentially reveal new therapeutic targets for intervention.

6.7. Proteomic analysis

In our proteomics study, our primary objective was to elucidate the inflammatory mediators and pathways implicated in oJIA, oJIA-U, and related conditions. We aimed to identify potential biomarkers that could enhance disease diagnosis, aid in uveitis detection, and provide insights into uveitis severity and response to anti-TNFα treatment.

We adopted a comprehensive approach, combining cross-sectional and paired analysis strategies to immune profile the cohort. This approach enabled us to discern distinct sets of mediators exhibiting varying plasma levels across different conditions. By employing this methodology, we have successfully identified candidate biomarkers that hold promise for diagnostic and prognostic applications in the context of oJIA and uveitis. Furthermore, our findings offer valuable insights into the underlying mechanisms contributing to uveitis severity and the potential impact of anti-TNFα treatment response.

Compared to HCs, six proteins were significantly different in the plasma of oJIA patients, including FGF-23, TRAIL, C2, IL-18R1, IL-6, and IL-13.

FGF-23 is a fibroblast growth factor family member, which participates in phosphate and vitamin D metabolism and regulation. It is also implicated in chronic kidney disease associated mineral bone disorder, which increases progressively with declining renal function. FGF-23 is associated with left ventricular hypertrophy, impaired left ventricular function, endothelial dysfunction, and heart failure. Studied previously in RA, an association between circulating FGF-23 and dislipemia en RA patients has been reported [256].

While FGF-23 may not have a direct link to JIA, it's important to note that JIA affects bone metabolism inducing osteoclastogenesis and therefore regulating the production of FGF-23 in osteoblasts [257]. Previously studied in systemic JIA, a study by Qu H *et al.*, using the same protein determination technique as ours, found that FGF-23, among other proinflammatory proteins, could discern between patients with systemic JIA and HCs [258].

TRAIL is a proinflammatory cytokine that belongs to the TNF ligand family that induces apoptosis in transformed and tumor cells but does not appear to kill normal cells. However, it is expressed at a significant level in most normal tissues. This protein binds to several members of the TNF receptor superfamily. It is also an IFN-inducible protein and has been described in systemic JIA, with increased levels in anakinra-treated patients [259]. No previously studied in oJIA, it has been reported to bé elevated in RA. Interestingly, TRAIL has been implicated in impairing the function of Treg cells in RA. Maintenance of the appropriate levels and biological activity of circulating Treg cells are required for maintaining immune tolerance. In that regard, Xiao *et al*. showed that Treg cells recovered from RA patients exhibited an impaired capacity to limit the proliferation and cytokine production of autologous T-effector cells which appeared to be due to an intrinsic defect in RA Treg cells [260]. Thus, RA T-effector cells had an elevated expression of membrane-associated TRAIL. These cells also released soluble TRAIL which was considered important because soluble TRAIL could induce apoptosis in Treg cells.
In line with our results, although we have not examined the transcriptional profile of Tregs in SF or PB, the presence of this protein in a more abundant form in oJIA than in HCs could be related to the higher abundance of TRAIL in plasma.

Component C2 is an essential protein of the complement system, which is a part of the immune system responsible for host defense against pathogens. C2 plays a crucial role in the classical pathway of complement activation. The function of C2 is to serve as a precursor to the protease C2a. During complement activation, C2 is cleaved by the enzyme C1s (activated form of C1) to generate C2a and C2b fragments. The C2a fragment remains bound to the C4b fragment, forming the C3 convertase enzyme (C4b2a). This enzyme then cleaves C3 into C3a and C3b, initiating a cascade of reactions that lead to opsonization, chemotaxis, inflammation, and the formation of the membrane attack complex (MAC) for pathogen destruction.
In summary, C2 plays a critical role in the initiation of the classical pathway by forming the C3 convertase enzyme, which leads to the activation of downstream complement components and various immune responses against pathogens. Complement is a key component of the innate immune system, and there is evidence of high turnover of C3, C4, and C5 in inflamed joints of RA patients [261].

However, the role of the complement system in the pathogenesis of oJIA is unclear. Our study detected high levels of C2, a protein part of the classical pathway. Previous studies have observed a high consumption of C2 in the SF, but, to our knowledge, no studies evaluate the classical complement pathway in PB plasma from oJIA patients [262].

IL-18R1, also known as interleukin-18 receptor 1, is a protein that serves as a receptor for the cytokine interleukin-18 (IL-18). IL-18R1 is expressed on the surface of various immune cells, including T cells, B cells, NK cells, and macrophages.
In the context of JIA pathogenesis, IL-18, and its receptor IL-18R1 have been implicated in the dysregulated immune responses observed in the disease. Studies have shown that IL-18 levels are elevated in the serum and SF of JIA patients, particularly in those with the systemic subtype. Increased IL-18 production can promote inflammation and contribute to the pathogenesis of JIA.
IL-18R1 plays a crucial role in transmitting the signals initiated by IL-18, leading to the activation of downstream signaling pathways involved in inflammation and immune responses. The binding of IL-18 to IL-18R1 triggers the recruitment of another protein called IL-18R accessory protein, forming a functional receptor complex. This complex initiate signaling cascades, including the activation of NF-κB and MAPK pathways, which mediate the production of pro-inflammatory cytokines and chemokines.
The dysregulation of IL-18 and its receptor in JIA suggests their potential involvement in driving the inflammatory processes and immune dysfunctions observed in the disease. Targeting the IL-18/IL-18R1 axis has emerged as a potential therapeutic approach for modulating the immune response and reducing inflammation in JIA. However, further research is needed to fully understand the specific role of IL-18R1 and its contribution to JIA pathogenesis.
IFN-alpha and IL12 are reported to induce the expression of this receptor in NK and T cells. Studied in detail in sJIA, IL-18 has been described as one of the top contributing proteins that differentiate between active and inactive JIA [258].
However, there is little information about the involvement of this protein in other forms of non-systemic JIA.

Similarly, to IL-18, IL-6 is a pleiotropic cytokine that mediates the production of acute phase proteins, stimulates collagen production from fibroblasts, and exerts vascular

endothelial activation and osteoclast differentiation. Mainly studied in sJIA, the involvement of IL-6 is supported by the clinical finding that treatment with IL-6 inhibitors restores NK cytotoxic activity impaired in this disease subtype [263]. However, the role of IL-6 in oJIA has also been considered, as Th17 from SF could be differentiated by IL-6, and also IL-6 inhibitors can improve the inhibitory function of Tregs [90].
In addition, a recent, not yet peer-reviewed paper highlights the crucial role of IL-6 in the pathogenesis of oJIA, emphasizing its importance in disease progression [264]. The study investigates the impact of synovial monocytes on oJIA and employs various functional assays to demonstrate their heightened capacity to induce T-cell activation. The study reveals that SF can confer regulatory properties onto healthy monocytes through an IL-6/JAK/STAT mechanism.
The research findings suggest that the level of IL-6-driven activation in monocytes within the synovium is reflected in the circulating cytokine levels, providing valuable insights into the systemic effects of IL-6 in oJIA. With these results, the authors point out that although oJIA has not traditionally been associated with systemic inflammation, their findings support that future studies may identify synovial or circulating markers predicting treatment response and stratifying patients with more IL-6-prominent disease.

In contrast, the proteins most significantly downregulated in oJIA in comparison to healthy controls were proteins related to T-cell homeostasis, growth development, or glucose uptake in adipocytes: PTN, CCL17, FGF-19, UMOD, ARG1, FASLG and KIT.

Focusing on the differences in the protein profile between oJIA-U patients and HCs, we found a higher abundance of TNFα, IL-24, and MMP-7 in uveitis patients.

TNFα is an important cytokine involved in the pathogenesis of JIA and can induce the expression of other proinflammatory cytokines, including IL-6, IL-18, or IL-1β. Several studies have attempted to characterize cytokine expression patterns in SF and plasma or plasma from JIA patients, with variable results. Some studies found increased levels of TNFα in children with different subtypes of JIA compared to HCs, although other studies reported only mild increases in patients with active disease [137,265].

All patients with a flare of uveitis included in this study phase received treatment with adalimumab. This is an important limitation of the study since the proteomic results could be biased by the treatment's effect.
The elevation of TNFα in this comparison, in the comparison of anti-TNFα treatment (week 0 and week 12), and in the comparison of patients with oJIA with and without uveitis corresponds to the treatment effect since the cytokine is not elevated in patients with oJIA without treatment.

Previous studies have determined the levels of TNFα as a biomarker of favorable outcomes of anti-TNFα treatment, as documented in a cohort of 41 non-systemic JIA patients with a follow-up for more than 7 years. Patients who experienced a good response to anti-TNFα (etanercept) increased TNFα levels at 6 weeks post-treatment compared to patients who did not respond [266].
TNF-α was detected in serum as complexes between etanercept and soluble TNFα. Still, this increase is due to the detection of inactive TNF sequestered by etanercept and therefore does not reflect the biologically active TNFα.
Similar results have been reported using a competition enzyme-linked immunosorbent assay that quantifies TNFα in the presence of large amounts of anti-TNFα inhibitors. In 193 consecutive adalimumab-treated patients with RA, the circulating TNFα increased an average of >50-fold upon treatment. This implies that TNFα in circulation during anti-TNFα treatment is not primarily associated with disease activity [267].
Therefore, our results align with previous studies linking elevated TNF levels with treatment, without having a translation to the disease mechanisms of action.

Apart from TNFα, we have observed that other relevant cytokines are increased in oJIA-U compared to HCs and in more severe forms of uveitis, such as MMPs 7 and 1, respectively.
MMPs are present in virtually all areas of the eye. They are responsible for maintaining and remodeling ocular architecture by influencing processes such as basement membrane remodeling, blood–retinal barrier integrity, wound healing, debris clearance, neovascularization, and fibrotic repair tissue deposition. Their role has been described in several common eye diseases, such as age-related macular degeneration, diabetic retinopathy, or glaucoma, but little is known about their involvement in oJIA-U [268].

However, little is known about the role of these proteins in oJIA-U.
Animal models of autoimmune uveitis have been studied at the tissue, cellular, and protein level without the potential confounding effects of immunosuppressive treatment and the role of different cytokines. Concretely, Di Girolamo *et al*. examined the presence of MMPs in the AH of uveitis patients and rabbits with endotoxin-induced uveitis. The analysis of AH samples from uveitis patients revealed elevated levels of MMPs, suggesting their contribution to tissue destruction and repair processes [269].

IL-24 was found to be elevated in oJIA-U compared to controls. Recently, IL-24 has been involved in Th17 cell regulation. The most targeted Th17 cytokine is IL-17A, which has shown good results in treating psoriasis and SpA. However, it has not been effective in diseases such as RA or Behçet's disease uveitis. It has not been yet studied in JIA-uveitis. In the case of uveitis, the lack of efficacy is attributed to the involvement of other cytokines from the Th17 lineage. Blocking IL-17A leads to the increased secretion of other Th17-lineage pro-inflammatory cytokines like IL-17F and GM-CSF. Nevertheless, compensatory mechanisms have been described, wherein the autocrine secretion of IL-24 by Th17 cells regulates the secretion of these cytokines. TNFα was complex with adalimumab during treatment with oJIA-U. This increase could be attributed to either the impact of anti-TNFα therapy or the intrinsic regulatory mechanism of Th17 cells [270,271].
Thus, IL-17A limits the pathogensis of Th17 cells by inducing IL-24. Treatments focus on enhancing the secrection of this anti-inflammatory cytokine could be of interest.

6.8. CyTOF validation stage

Although we have not been able to complete the second stage of the study by validating the results obtained by the scRNA-seq study, we have designed the antibody panel for this purpose. At the time of submission of this PhD thesis project, the correct conjugation of some previously unconjugated antibodies is being finalised (see Methods section).

The following membrane markers have been selected for the correct characterisation of CD8 T cells: CD3, CD4, CD8a, CD45, CD45RA, CD45RO, CD27, CCL5, CX3CR1 CXCR6 (CD186), GZMA, CCR7. Canonical markets of T cells are CD3, CD4 and CD8a. As well, CD45 is a canonical marker for effector memory $CD8^+$ T cells. CD45RA is highly expressed in naïve T cells. With CD45RA and CD45RO it could be differentiated between naïve and memory T cells. We also selected negative markers for effector memory CD8 T cells like CD27 and CXCR1 to correctly characterize this population.

We have also included CCR7 because the CCR7 expression discriminates between T cells with effector function that can migrate to inflamed tissues (CCR7-) vs. T cells that require a secondary stimulus prior to displaying effector functions.

CXCR6 was selected to characterize activated and memory T cells involved in the recruitment of cells during the inflammatory response. It is a marker differentially expressed in activated effector memory $CD8^+$ T cells from scRNA-seq data.

CCL5 has been selected, as it is a marker differentially expressed in activated effector memory $CD8^+$ T cells from scRNA-seq data. An intracellular marker must be previously stimulated. Like CCL5, GZMA has also been selected, as it is a marker DEG in activated effector memory CD8 T cells from scRNA-seq data.

The markers selected for a comprehensive characterisation of the NK population were CD16, CD56, CD57, CD7, FceRI, MIP-1β (CCL4), CD62L, CD335 (NKp46), CD161 (KLRB1/NKR-P1A), CD314 (NKG2D), CD159a (NKG2A), B2M, CD94 and Perforin.

CD16 is an important marker for NK characterisation, as it is low in bright NKs and positive or high in dim NKs. CD56 is a canonical marker of NKs, and it exists in two isoforms: dim and bright. Other related markers helpful to NKs correct characterization are CD57, CD7 (which is positive in NKs and negative in monocytes), and CD62L.

We have also selected several markers of NK activation and inhibition such as CD335, CD161, CD314, CD159a, and CD94.

Perforin, B2M, FceRI, and MIP-1β have been selected as they are differentially expressed in NK from scRNA-seq data.

Finally, the markers selected for a comprehensive characterization of monocytes have been CD14 as it is a positive marker for monocytes, CD33 that help to differentiate between monocytes and NKs, and HLA-DR which is expressed in activated monocytes.

6.8. Clinical applications of our results

Childhood chronic inflammatory arthritis exhibits a diverse range of presentations and courses of evolution. While most forms share clinical and genetic similarities with adult-onset arthritis, at least one phenotype appears to be exclusive to children. Unfortunately, pediatric, and adult rheumatologists, resulting in JIA not being classified in a cohesive manner, have traditionally approached the classification of the disease separately. This lack of terminological overlap between JIA and adult-onset arthritis highlights the need for a new approach to defining the biological categories of JIA. Over the years, efforts have been made to establish a more representative nomenclature for each subtype of JIA that aligns with the underlying pathogenic mechanisms. Among the seven subtypes currently defined by the ILAR classification, only oJIA, does not have a counterpart in adults. It is also associated with a high risk of developing chronic anterior uveitis, a feature not found in other forms of arthritis in children or adults.

In recent years, two models, namely the PRINTO model and the four-cluster model, have been proposed for classifying JIA. The latter aims to simplify the subtypes into different "biological fault lines" based on synovitis versus enthesitis forms of JIA, autoantibody-related versus autoantibody-independent, and autoimmune versus autoinflammatory disease. This conceptual model provides a broader understanding of JIA, allowing for some clinical manifestations to overlap between different domains [15].

While stronger evidence is still needed, early-onset JIA (which refers to the currently known oJIA) falls within the seronegative/autoimmune/synovitis “line” form of JIA. However, our findings suggest that multiple pathogenic pathways may be involved in oJIA. Specifically, we have identified a population of oligoclonal effector memory $CD8^+$ T cells with increased expression of genes related to effector pathways, cytotoxicity, innate immunity, T-B cell intercommunication, and tissue residence. These cells are potentially crucial in the development of synovitis, as they are recruited from PB to SF. Similar results have been observed in PsA, an adult form of arthritis characterized by

recurrent arthritis in large joints of the lower extremities, like oJIA. Recent studies have described pronounced clonal expansion of $CD8^+$ T cells within joints in psoriatic arthritis, indicating their involvement in the disease. Transcriptome analyses of these expanded synovial $CD8^+$ T cells reveal markers of cycling, activation, tissue localisation and tissue residence. These characteristics contribute to the better characterisation of these cells and to a deeper understanding of the transcriptomic mechanisms that confer their pathogenicity [239].

Our study also suggests a role for innate immune system cells, such as NK cells, in the development of uveitis in oJIA. This finding has not been previously reported in oJIA-related uveitis. In other entities causing uveitis, such as Behçet's disease, the involvement of NK cells has been previously described. These results contribute to the understanding of this dreaded ocular complication of oJIA and may lead to future studies that further investigate the role of NK cells in uveitis.
We have also identified several cytokines associated with the innate immune system that are more abundant in the plasma of oJIA patients compared to healthy controls. Additionally, we have discovered some cytokines that have received limited previous attention, indicating the need for further investigation.

This PhD project presents the first single-cell atlas of mononuclear cells from synovial fluid and peripheral blood of patients with oligoarticular juvenile idiopathic arthritis (oJIA) and uveitis (oJIA-U), providing insights into the cellular composition and pathogenic mechanisms of the disease. In oJIA, specific cell types are actively recruited to the synovial joint, while oJIA-U is associated with an increased abundance of mature NK cells in peripheral blood. Transcriptional profiling reveals gene expression patterns related to effector pathways, cytotoxicity, innate immunity, and antigen processing. Proinflammatory proteins and elevated levels of matrix metalloproteinases are identified, underlining the role of innate immunity in oJIA and uveitis. With these results, we can help to understand the underlying pathogenic mechanisms of this subtype of JIA, oJIA, hitherto categorised as a form of JIA in which adaptive innate immunity plays a key role. However, in our study we found pathogenic mechanisms related to innate immunity and the more cytotoxic pathway of adaptive immunity. There is probably no single correct approach to classify every patient with JIA or JIAo. Instead, a thorough analysis of each patient is needed, using available

omics techniques, as not all patients with oJIA will have the same cellular profile involved.

6.9. Limitations

The cohort selection in this study has some inherent limitations, primarily due to the small sample size. While the high-resolution technologies employed in the dissertation project can yield valuable insights from a small cohort, recruiting more patients experiencing debut oJIA and uveitis flares would be highly advantageous to compare. Additionally, it would be worthwhile to include longitudinal data from patients with untreated uveitis flares and those in remission with treatment to obtain a more comprehensive understanding of the condition.
Furthermore, it would be relevant to include patients undergoing treatment with bDMARDs, encompassing responders and non-responders. This broader inclusion would enable a more comprehensive evaluation of the therapeutic effectiveness of these treatments.

Relative to the high-resolution technology used in the first stage, scRNA-seq is a powerful method; however, it does have its limitations, most of which are currently being actively addressed. Regarding the analysis methodology, clustering poses a significant challenge as it raises the question of what defines a cell subset. The typical approach involves initially identifying a cell based on the expression of a defining phenotype. For instance, human NK cells can be characterized as lymphocytes that lack CD3 on their cell surface while expressing CD56.
Then, the subset is further refined by determining the presence or absence of other markers, such as CD94, inhibitory immune killer receptors, and chemokine receptors. As more markers are added, the subsets become progressively smaller [272].
However, at what point can we truly consider a subset? Each cell is unique. Therefore, the challenge lies in comprehending the physiological significance of this remarkable phenotypic diversity and understanding how it relates to the immune function of these cells.

In our study, we have invested much time in ensuring correct cell annotation and understanding the physiological significance of a determined cluster.

Despite analyzing many cells, we were limited in identifying less abundant cell populations such as Th1, Th2, Th17, or T regs in further detail, T peripheral helper, T follicular helper, innate lymphoid cells, macrophages, and fibroblasts. This may be partly explained by the fact that the type of tissue analyzed, SF, confers certain limitations because the cellular landscape is less representative than synovial tissue.

Few studies have investigated the cellular landscape and discrepancies between synovial fluid and synovial tissue in inflammatory arthritis. Penkava *et al*. investigated the cellular profile of oligoarticular psoriatic arthritis using scRNAseq and mass cytometry in synovial fluid, synovial tissue, and peripheral blood. While the $CD3^+$ T cell compartment of the synovial fluid was similar in SF and synovial tissue, B cells, and plasma cells were absent in SF but abundant in synovial tissue. This suggests a possible differential ability of lymphocytes to move from tissue to synovial fluid, or a selective survival advantage of B cell lineages in the tissue microenvironment [239]. In addition to not having synovial tissue as a target site where most cell interactions occur, we do not have uveal tissue, due to the high invasiveness of obtaining this type of sample.

Regarding the scRNA-seq technique, integrating other genomics methods within the single-cell study is another challenge that needs to be tackled. This integration would provide insights into the regulation of gene expression through the interaction between the epigenome and transcriptome, or the integration of scRNA-seq with single-cell proteomics.

When considering the integration of scRNA-seq and proteomics, it is important to acknowledge that scRNA-seq assumes that information from the mRNA message is accurately translated into proteins. Combining scRNA-seq with single-cell proteomics data will make it possible to determine the extent to which this assumption holds.

Our study does not use a technique that can integrate transcriptomic and proteomic information at the single-cell level, such as CITE-Seq, which uses DNA-encoded antibodies to convert protein detection into a quantitative, sequenceable readout [273].

However, we have used high-throughput technology to measure many proteins in peripheral blood from a larger cohort of patients with relevant results.

Referring to TCR sequencing, it is important to note that it is impossible to directly measure total TCR diversity in each sample. Since the TCR repertoire is extraordinarily diverse and the distributions of individual TCR can be heavily skewed, the whole diversity cannot be evaluated from experimental samples alone [274]. Furthermore, we have not analyzed the BCR repertoire or the TCR gamma delta.
Studying both the TCR and BCR repertoires provides a more complete picture of the immune response in conditions such as JIA.The study of the BCR repertoire may identify B-cell clonotypes that produce specific autoantibodies and better understand their contribution to disease. Besides, a combined analysis of the TCR and BCR repertoires could detect specific immunological patterns, such as clonal expansions or restricted repertoires, which may indicate abnormal or dysfunctional immune responses [275].

Other more general limitations of working in a scRNA-seq study include computational and analytical challenges and translation into the clinical setting.
The analysis of scRNA-seq data involves complex computational and bioinformatic methods, and the choice of analysis algorithms and parameters can affect the results. Translating scRNA-seq findings into clinical applications, such as diagnostic biomarkers or targeted therapies, requires extensive validation and integration with other clinical data. The translation process from research to clinical practice is complex and time-consuming.

The main limitation of the proteomic study is the small sample size, which limits the ability to draw robust conclusions. Therefore, it will be essential for future studies to include patients with untreated oJIA-U. Including more patients with uveitic involvement in more severe stages and with a higher inflammatory burden will also be necessary.
The proteomic profile was determined in plasma and not in aqueous humor, which would be the most representative fluid for uveal inflammatory activity. However, aqueous humor sampling in pediatrics is an invasive technique associated with some complications. Although progress has been made in the study of protein biomarkers

by detecting proteins in the tears of patients with autoimmune diseases such as Sjögren's syndrome, it is not yet clear that the biomarkers found in tears are fully representative of the inflammatory activity of the uvea and aqueous humor due to the variety of layers that make up the tears [276].

Finally, it should be noted that the panels selected for the proteomic study did not include two key proteins involved in several pathogenic mechanisms, such as IL-1β and INFα, which will be determined by another technique in a next step of this research project.

7. Conclusions

1. This project describes the first single-cell atlas of mononuclear cells obtained from synovial fluid and peripheral blood of patients diagnosed with oligoarticular juvenile idiopathic arthritis (oJIA) and uveitis (oJIA-U). This comprehensive study provides a detailed and unprecedented understanding of the cellular composition within these biological fluids, shedding new light on the pathogenic mechanisms of this disease.

2. Patients with oJIA exhibited more activated and NKG2C$^+$ effector memory CD8$^+$ T cells, intermediate monocytes, dendritic cells, and regulatory T cells in their synovial fluid than in peripheral blood. A lower abundance of these cells was observed in the peripheral blood of oJIA patients compared to controls. This intriguing finding suggests that these specific cell types may play a crucial role in migrating from the bloodstream to the inflamed synovium, thereby contributing to the development of oJIA.

3. In patients with oJIA-U, mature NK cells were found in higher abundance in the peripheral blood compared to patients with oJIA without uveitis and healthy controls. Therefore, the higher prevalence of mature NK cells, specifically in oJIA-U, suggests their involvement in developing this condition.

4. Transcriptional differences in NKG2C$^+$ effector memory CD8$^+$ T cells in the oJIA synovial fluid were found, with significantly increased expression of genes related to effector pathways and cytotoxicity, genes related to T-B cell intercommunication, and tissue residence. The transcriptional profiling of the cells mainly represented in oJIA-U, primarily mature CD56$^+$ dim NKs cells, showed an up-regulation of type I and III interferon signaling pathway and, peptide antigen presentation through MHC class I.

5. Single-cell RNA sequencing of paired T cell receptor alpha and beta chain sequences showed a clonal expansion of activated effector memory CD8$^+$ T in synovial fluid in oJIA expressing the CCL5 activation marker. In peripheral blood of oJIA and oJIA-U patients a clonal expansion of effector memory CD8$^+$ T cells has been observed.

6. We identified a specific set of proteins in plasma that are differentially overrepresented in oJIA compared to healthy controls. Notably, our findings emphasize the presence of the proinflammatory proteins FGF-23, IL-6, TRAIL, and IL-18R1, highlighting the role of innate immunity in oJIA's pathogenesis. Additionally, in the context of uveitis, we observed elevated levels of matrix metalloproteinases and IL-24, suggesting increased extracellular matrix turnover and Th17 activation in the disease.

8. Future steps

The doctoral thesis project has made significant progress in advancing our understanding of the disease, despite encountering a limitation in completing the second stage of the project. Notably, substantial strides have been made in the refinement of the mass cytometry technique, overcoming various challenges along the way.

The forthcoming availability of mass cytometry data presents a promising opportunity to validate and reinforce the robustness of the results obtained in the initial stage of scRNA-seq. This validation phase will provide highly reliable and trustworthy evidence to support the findings.

Moreover, this groundbreaking research project represents a significant milestone in the field. It marks the first time that the entire immune landscape of both peripheral blood and synovial fluid has been comprehensively analyzed in this disease. Previous studies have predominantly focused on limited subsets of cellular populations, whereas this study provides a holistic perspective.

Furthermore, the project has fostered valuable collaborations with other basic researchers, creating a platform for future partnerships and collaborative endeavors. This collaboration opens doors to explore and embark on new projects together, maximizing the potential for advancing knowledge in the field.

My long-term goal is to generate an extensive collection of clinical and molecular data that will contribute to a deeper understanding of the pathogenic mechanisms underlying juvenile idiopathic arthritis. To address unresolved hypotheses, I am actively recruiting JIA patients with diverse conditions and healthy controls. Additionally, in collaboration with IMID-Biobank, a growing repository of high-quality biological samples will serve as a foundation for future studies in this field.

It is worth emphasizing the transformative impact of the technology employed in this project. The utilization of scRNA-seq analysis, with its ability to examine cellular dynamics at an unprecedented level, is revolutionizing the field of immunology. This powerful technique continues to uncover new cellular states and processes,

suggesting that immunology will undergo significant paradigm shifts and emerge as one of the foremost areas of fundamental knowledge in the years to come.

An emerging technique complementary to scRNA-seq is spatial transcriptomics. By integrating spatial information with transcriptomic data, this innovative approach enables the examination of gene expression patterns within their anatomical context.

In rheumatic diseases, such as RA and SLE, understanding the spatial organization of cell types and their interactions within affected tissues is crucial for deciphering disease mechanisms and identifying potential therapeutic targets. By visualizing gene expression patterns in situ, spatial transcriptomics offers insights into the local microenvironment, highlighting key cellular players and molecular pathways driving disease progression. This approach not only enhances our understanding of the spatial relationships between different cell types but also enables the identification of novel cell populations that may have previously gone unnoticed using traditional bulk RNA sequencing.

As the field of spatial transcriptomics continues to advance, it holds the potential to guide the development of targeted therapies by identifying spatially restricted therapeutic targets and evaluating treatment responses within specific tissue compartments.

Ultimately, the integration of spatial transcriptomics into the study of sinovial tissue in JIA will improve our understanding of this complex condition and pave the way for more precise and effective interventions.

9. Bibliography

1. Prakken B, Albani S, Martini A. Juvenile idiopathic arthritis. Lancet. 2011;377: 2138–2149.

2. Petty RE, Southwood TR, Manners P, Baum J, Glass DN, Goldenberg J, et al. International League of Associations for Rheumatology classification of juvenile idiopathic arthritis: second revision, Edmonton, 2001. J Rheumatol. 2004;31: 390–392.

3. Thierry S, Fautrel B, Lemelle I, Guillemin F. Prevalence and incidence of juvenile idiopathic arthritis: a systematic review. Joint Bone Spine. 2014;81: 112–117.

4. Modesto C, Antón J, Rodriguez B, Bou R, Arnal C, Ros J, et al. Incidence and prevalence of juvenile idiopathic arthritis in Catalonia (Spain). Scand J Rheumatol. 2010;39: 472–479.

5. Ravelli A, Martini A. Juvenile idiopathic arthritis. Lancet. 2007;369: 767–778.

6. Kuhlmann A, Schmidt T, Treskova M, López-Bastida J, Linertová R, Oliva-Moreno J, et al. Social/economic costs and health-related quality of life in patients with juvenile idiopathic arthritis in Europe. Eur J Health Econ. 2016;17 Suppl 1: 79–87.

7. Martini A, Lovell DJ, Albani S, Brunner HI, Hyrich KL, Thompson SD, et al. Juvenile idiopathic arthritis. Nat Rev Dis Primers. 2022;8: 5.

8. MacRae VE, Farquharson C, Ahmed SF. The pathophysiology of the growth plate in juvenile idiopathic arthritis. Rheumatology. 2006;45: 11–19.

9. Martini A. It is time to rethink juvenile idiopathic arthritis classification and nomenclature. Ann Rheum Dis. 2012;71: 1437–1439.

10. Martini A, Ravelli A, Avcin T, Beresford MW, Burgos-Vargas R, Cuttica R, et al. Toward New Classification Criteria for Juvenile Idiopathic Arthritis: First Steps, Pediatric Rheumatology International Trials Organization International Consensus. J Rheumatol. 2019;46: 190–197.

11. Rumsey DG, Laxer RM. The Challenges and Opportunities of Classifying Childhood Arthritis. Curr Rheumatol Rep. 2020;22: 4.

12. Beukelman T, Nigrovic PA. Juvenile Idiopathic Arthritis: An Idea Whose Time Has Gone? The Journal of rheumatology. 2019. pp. 124–126.

13. Nigrovic PA, Mannion M, Prince FHM, Zeft A, Rabinovich CE, van Rossum MAJ, et al. Anakinra as first-line disease-modifying therapy in systemic juvenile idiopathic arthritis: report of forty-six patients from an international multicenter series. Arthritis Rheum. 2011;63: 545–555.

14. Guzmán J, Burgos-Vargas R, Duarte-Salazar C, Gómez-Mora P. Reliability of the articular examination in children with juvenile rheumatoid arthritis: interobserver agreement and sources of disagreement. J Rheumatol. 1995;22: 2331–2336.

15. Nigrovic PA, Colbert RA, Holers VM, Ozen S, Ruperto N, Thompson SD, et al. Biological classification of childhood arthritis: roadmap to a molecular nomenclature. Nat Rev Rheumatol. 2021;17: 257–269.

16. Frisell T, Holmqvist M, Källberg H, Klareskog L, Alfredsson L, Askling J. Familial risks and heritability of rheumatoid arthritis: role of rheumatoid factor/anti-citrullinated protein antibody status, number and type of affected relatives, sex, and age. Arthritis Rheum. 2013;65: 2773–2782.

17. Kahn PJ. Juvenile idiopathic arthritis - what the clinician needs to know. Bull Hosp Jt Dis. 2013;71: 194–199.

18. d'Angelo DM, Di Donato G, Breda L, Chiarelli F. Growth and puberty in children with juvenile idiopathic arthritis. Pediatr Rheumatol Online J. 2021;19: 28.

19. Felici E, Novarini C, Magni-Manzoni S, Pistorio A, Magnani A, Bozzola E, et al. Course of joint disease in patients with antinuclear antibody-positive juvenile idiopathic arthritis. J Rheumatol. 2005;32: 1805–1810.

20. Sen ES, Dick AD, Ramanan AV. Uveitis associated with juvenile idiopathic arthritis. Nat Rev Rheumatol. 2015;11: 338–348.

21. Jabs DA, Nussenblatt RB, Rosenbaum JT, Standardization of Uveitis Nomenclature (SUN) Working Group. Standardization of uveitis nomenclature for reporting clinical data. Results of the First International Workshop. Am J Ophthalmol. 2005;140: 509–516.

22. Sabri K, Saurenmann RK, Silverman ED, Levin AV. Course, complications, and outcome of juvenile arthritis-related uveitis. Journal of AAPOS: the official publication of the American Association for Pediatric Ophthalmology and Strabismus / American Association for Pediatric Ophthalmology and Strabismus. 2008. pp. 539–545.

23. Moradi A, Amin RM, Thorne JE. The role of gender in juvenile idiopathic arthritis-associated uveitis. J Ophthalmol. 2014;2014: 461078.

24. Angeles-Han ST, McCracken C, Yeh S, Jenkins K, Stryker D, Rouster-Stevens K, et al. Characteristics of a cohort of children with Juvenile Idiopathic Arthritis and JIA-associated Uveitis. Pediatr Rheumatol Online J. 2015;13: 19.

25. Nordal E, Rypdal V, Christoffersen T, Aalto K, Berntson L, Fasth A, et al. Incidence and predictors of Uveitis in juvenile idiopathic arthritis in a Nordic long-term cohort study. Pediatr Rheumatol Online J. 2017;15: 66.

26. Hoeve M, Kalinina Ayuso V, Schalij-Delfos NE, Los LI, Rothova A, de Boer JH. The clinical course of juvenile idiopathic arthritis-associated uveitis in childhood and puberty. Br J Ophthalmol. 2012;96: 852–856.

27. Consolaro A, Giancane G, Schiappapietra B, Davì S, Calandra S, Lanni S, et al. Clinical outcome measures in juvenile idiopathic arthritis. Pediatr Rheumatol Online J. 2016;14: 23.

28. Consolaro A, Ruperto N, Bazso A, Pistorio A, Magni-Manzoni S, Filocamo G, et al. Development and validation of a composite disease activity score for juvenile idiopathic arthritis. Arthritis Rheum. 2009;61: 658–666.

29. Bazso A, Consolaro A, Ruperto N, Pistorio A, Viola S, Magni-Manzoni S, et al. Development and testing of reduced joint counts in juvenile idiopathic arthritis. J Rheumatol. 2009;36: 183–190.

30. Wallace CA, Ruperto N, Giannini E, Childhood Arthritis and Rheumatology Research

Alliance, Pediatric Rheumatology International Trials Organization, Pediatric Rheumatology Collaborative Study Group. Preliminary criteria for clinical remission for select categories of juvenile idiopathic arthritis. J Rheumatol. 2004;31: 2290–2294.

31. Wallace CA, Giannini EH, Huang B, Itert L, Ruperto N, Childhood Arthritis Rheumatology Research Alliance, et al. American College of Rheumatology provisional criteria for defining clinical inactive disease in select categories of juvenile idiopathic arthritis. Arthritis Care Res . 2011;63: 929–936.

32. Tappeiner C, Heinz C, Roesel M, Heiligenhaus A. Elevated laser flare values correlate with complicated course of anterior uveitis in patients with juvenile idiopathic arthritis. Acta Ophthalmol. 2011;89: e521-7.

33. Trusko B, Thorne J, Jabs D, Belfort R, Dick A, Gangaputra S, et al. The Standardization of Uveitis Nomenclature (SUN) Project. Development of a clinical evidence base utilizing informatics tools and techniques. Methods Inf Med. 2013;52: 259–65, S1-6.

34. Bou R, Adán A, Borrás F, Bravo B, Calvo I, De Inocencio J, et al. Clinical management algorithm of uveitis associated with juvenile idiopathic arthritis: interdisciplinary panel consensus. Rheumatol Int. 2015;35: 777–785.

35. Giannini EH, Ruperto N, Ravelli A, Lovell DJ, Felson DT, Martini A. Preliminary definition of improvement in juvenile arthritis. Arthritis Rheum. 1997;40: 1202–1209.

36. Lovell DJ, Ruperto N, Giannini EH, Martini A. Advances from clinical trials in juvenile idiopathic arthritis. Nat Rev Rheumatol. 2013;9: 557–563.

37. McErlane F, Beresford MW, Baildam EM, Chieng SEA, Davidson JE, Foster HE, et al. Validity of a three-variable Juvenile Arthritis Disease Activity Score in children with new-onset juvenile idiopathic arthritis. Ann Rheum Dis. 2013;72: 1983–1988.

38. Zulian F, Martini G, Gobber D, Plebani M, Zacchello F, Manners P. Triamcinolone acetonide and hexacetonide intra-articular treatment of symmetrical joints in juvenile idiopathic arthritis: a double-blind trial. Rheumatology . 2004;43: 1288–1291.

39. Zaripova LN, Midgley A, Christmas SE, Beresford MW, Baildam EM, Oldershaw RA. Juvenile idiopathic arthritis: from aetiopathogenesis to therapeutic approaches. Pediatr Rheumatol Online J. 2021;19: 135.

40. Lovell DJ, Giannini EH, Reiff A, Cawkwell GD, Silverman ED, Nocton JJ, et al. Etanercept in children with polyarticular juvenile rheumatoid arthritis. Pediatric Rheumatology Collaborative Study Group. N Engl J Med. 2000;342: 763–769.

41. Ruperto N, Brunner HI, Pacheco-Tena C, Louw I, Vega-Cornejo G, Spindler AJ, et al. Open-label phase 3 study of intravenous golimumab in patients with polyarticular juvenile idiopathic arthritis. Rheumatology . 2021;60: 4495–4507.

42. Balevic SJ, Rabinovich CE. Profile of adalimumab and its potential in the treatment of uveitis. Drug Des Devel Ther. 2016;10: 2997–3003.

43. Brunner HI, Ruperto N, Zuber Z, Cuttica R, Keltsev V, Xavier RM, et al. Efficacy and Safety of Tocilizumab for Polyarticular-Course Juvenile Idiopathic Arthritis in the Open-Label Two-Year Extension of a Phase III Trial. Arthritis Rheumatol. 2021;73: 530–541.

44. Brunner HI, Tzaribachev N, Vega-Cornejo G, Louw I, Berman A, Calvo Penadés I, et al.

Subcutaneous Abatacept in Patients With Polyarticular-Course Juvenile Idiopathic Arthritis: Results From a Phase III Open-Label Study. Arthritis Rheumatol. 2018;70: 1144–1154.

45. Clarke SLN, Ramanan AV. Tofacitinib in juvenile idiopathic arthritis. The Lancet. 2021. pp. 1943–1945.

46. Ruperto N, Brunner HI, Synoverska O, Ting TV, Mendoza CA, Spindler A, et al. Tofacitinib in juvenile idiopathic arthritis: a double-blind, placebo-controlled, withdrawal phase 3 randomised trial. Lancet. 2021;398: 1984–1996.

47. Saurenmann RK, Levin AV, Feldman BM, Laxer RM, Schneider R, Silverman ED. Risk of new-onset uveitis in patients with juvenile idiopathic arthritis treated with anti-TNFalpha agents. J Pediatr. 2006;149: 833–836.

48. Ramanan AV, Dick AD, Guly C, McKay A, Jones AP, Hardwick B, et al. Tocilizumab in patients with anti-TNF refractory juvenile idiopathic arthritis-associated uveitis (APTITUDE): a multicentre, single-arm, phase 2 trial. Lancet Rheumatol. 2020;2: e135–e141.

49. Tappeiner C, Miserocchi E, Bodaghi B, Kotaniemi K, Mackensen F, Gerloni V, et al. Abatacept in the treatment of severe, longstanding, and refractory uveitis associated with juvenile idiopathic arthritis. J Rheumatol. 2015;42: 706–711.

50. Giancane G, Consolaro A, Lanni S, Davì S, Schiappapietra B, Ravelli A. Juvenile Idiopathic Arthritis: Diagnosis and Treatment. Rheumatol Ther. 2016;3: 187–207.

51. Häfner R, Truckenbrodt H, Spamer M. Rehabilitation in children with juvenile chronic arthritis. Baillieres Clin Rheumatol. 1998;12: 329–361.

52. Selvaag AM, Aulie HA, Lilleby V, Flatø B. Disease progression into adulthood and predictors of long-term active disease in juvenile idiopathic arthritis. Ann Rheum Dis. 2016;75: 190–195.

53. Barišić Kutija M, Perić S, Knežević J, Juratovac Z, Vukojević N. Complication and prognosis of juvenile idiopathic arthritis associated uveitis in the era of modern immunomodulatory treatment. Psychiatr Danub. 2019;31: 44–49.

54. Kindgren E, Fredrikson M, Ludvigsson J. Early feeding and risk of Juvenile idiopathic arthritis: a case control study in a prospective birth cohort. Pediatr Rheumatol Online J. 2017;15: 46.

55. Sevelsted A, Stokholm J, Bønnelykke K, Bisgaard H. Cesarean section and chronic immune disorders. Pediatrics. 2015;135: e92-8.

56. Kristensen K, Henriksen L. Cesarean section and disease associated with immune function. J Allergy Clin Immunol. 2016;137: 587–590.

57. Lehmann HW, Plentz A, von Landenberg P, Küster R-M, Modrow S. Different patterns of disease manifestations of parvovirus B19-associated reactive juvenile arthritis and the induction of antiphospholipid-antibodies. Clin Rheumatol. 2008;27: 333–338.

58. Von Landenberg P, Lehmann HW, Knöll A, Dorsch S, Modrow S. Antiphospholipid antibodies in pediatric and adult patients with rheumatic disease are associated with parvovirus B19 infection. Arthritis Rheum. 2003;48: 1939–1947.

59. Gonzalez B, Larrañaga C, León O, Díaz P, Miranda M, Barría M, et al. Parvovirus B19 may have a role in the pathogenesis of juvenile idiopathic arthritis. J Rheumatol. 2007;34: 1336–1340.

60. Massa M, Mazzoli F, Pignatti P, De Benedetti F, Passalia M, Viola S, et al. Proinflammatory responses to self HLA epitopes are triggered by molecular mimicry to Epstein-Barr virus proteins in oligoarticular juvenile idiopathic arthritis. Arthritis Rheum. 2002;46: 2721–2729.

61. Sun G, Hazlewood G, Bernatsky S, Kaplan GG, Eksteen B, Barnabe C. Association between Air Pollution and the Development of Rheumatic Disease: A Systematic Review. Int J Rheumatol. 2016;2016: 5356307.

62. Mauldin J, Cameron HD, Jeanotte D, Solomon G, Jarvis JN. Chronic arthritis in children and adolescents in two Indian health service user populations. BMC Musculoskelet Disord. 2004;5: 30.

63. Uffelmann E, Huang QQ, Munung NS, de Vries J, Okada Y, Martin AR, et al. Genome-wide association studies. Nature Reviews Methods Primers. 2021;1: 1–21.

64. Cobb JE, Hinks A, Thomson W. The genetics of juvenile idiopathic arthritis: current understanding and future prospects. Rheumatology . 2014;53: 592–599.

65. Hinks A, Cobb J, Sudman M, Eyre S, Martin P, Flynn E, et al. Investigation of rheumatoid arthritis susceptibility loci in juvenile idiopathic arthritis confirms high degree of overlap. Ann Rheum Dis. 2012;71: 1117–1121.

66. Hinks A, Martin P, Flynn E, Eyre S, Packham J, Barton A, et al. Investigation of type 1 diabetes and coeliac disease susceptibility loci for association with juvenile idiopathic arthritis. Ann Rheum Dis. 2010;69: 2169–2172.

67. Hollenbach JA, Thompson SD, Bugawan TL, Ryan M, Sudman M, Marion M, et al. Juvenile idiopathic arthritis and HLA class I and class II interactions and age-at-onset effects. Arthritis Rheum. 2010;62: 1781–1791.

68. Murray KJ, Moroldo MB, Donnelly P, Prahalad S, Passo MH, Giannini EH, et al. Age-specific effects of juvenile rheumatoid arthritis-associated HLA alleles. Arthritis Rheum. 1999;42: 1843–1853.

69. Cortes A, Brown MA. Promise and pitfalls of the Immunochip. Arthritis Res Ther. 2011;13: 101.

70. Hinks A, Cobb J, Marion MC, Prahalad S, Sudman M, Bowes J, et al. Dense genotyping of immune-related disease regions identifies 14 new susceptibility loci for juvenile idiopathic arthritis. Nat Genet. 2013;45: 664–669.

71. Hinks A, Bowes J, Cobb J, Ainsworth HC, Marion MC, Comeau ME, et al. Fine-mapping the MHC locus in juvenile idiopathic arthritis (JIA) reveals genetic heterogeneity corresponding to distinct adult inflammatory arthritic diseases. Ann Rheum Dis. 2017;76: 765–772.

72. Haasnoot A-MJW, Schilham MW, Kamphuis S, Hissink Muller PC, Heiligenhaus A, Foell D, et al. Identification of an Amino Acid Motif in HLA-DRβ1 That Distinguishes Uveitis in Patients With Juvenile Idiopathic Arthritis. Arthritis & Rheumatology. 2018. pp. 1155–1165.

73. Hinks A, Barton A, John S, Bruce I, Hawkins C, Griffiths CEM, et al. Association between the PTPN22 gene and rheumatoid arthritis and juvenile idiopathic arthritis in a UK population: further support that PTPN22 is an autoimmunity gene. Arthritis Rheum. 2005;52: 1694–1699.

74. Prahalad S, Hansen S, Whiting A, Guthery SL, Clifford B, McNally B, et al. Variants in TNFAIP3, STAT4, and C12orf30 loci associated with multiple autoimmune diseases are also associated with juvenile idiopathic arthritis. Arthritis Rheum. 2009;60: 2124–2130.

75. Li YR, Zhao SD, Li J, Bradfield JP, Mohebnasab M, Steel L, et al. Genetic sharing and heritability of paediatric age of onset autoimmune diseases. Nat Commun. 2015;6: 8442.

76. International Multiple Sclerosis Genetics Consortium (IMSGC), Beecham AH, Patsopoulos NA, Xifara DK, Davis MF, Kemppinen A, et al. Analysis of immune-related loci identifies 48 new susceptibility variants for multiple sclerosis. Nat Genet. 2013;45: 1353–1360.

77. Trynka G, Hunt KA, Bockett NA, Romanos J, Mistry V, Szperl A, et al. Dense genotyping identifies and localizes multiple common and rare variant association signals in celiac disease. Nat Genet. 2011;43: 1193–1201.

78. Yang W, Tang H, Zhang Y, Tang X, Zhang J, Sun L, et al. Meta-analysis followed by replication identifies loci in or near CDKN1B, TET3, CD80, DRAM1, and ARID5B as associated with systemic lupus erythematosus in Asians. Am J Hum Genet. 2013;92: 41–51.

79. McIntosh LA, Marion MC, Sudman M, Comeau ME, Becker ML, Bohnsack JF, et al. Genome-wide association meta-analysis reveals novel juvenile idiopathic arthritis susceptibility loci. Arthritis rheumatol. 2017;69: 2222–2232.

80. López-Isac E, Smith SL, Marion MC, Wood A, Sudman M, Yarwood A, et al. Combined genetic analysis of juvenile idiopathic arthritis clinical subtypes identifies novel risk loci, target genes and key regulatory mechanisms. Ann Rheum Dis. 2021;80: 321–328.

81. Wang, Wang. B7-H4, a promising target for immunotherapy. Cell Immunol. 2020.

82. Alberdi-Saugstrup M, Enevold C, Zak M, Nielsen S, Nordal E, Berntson L, et al. Non-HLA gene polymorphisms in juvenile idiopathic arthritis: associations with disease outcome. Scand J Rheumatol. 2017;46: 369–376.

83. Prahalad S, Thompson SD, Conneely KN, Jiang Y, Leong T, Prozonic J, et al. Hierarchy of risk of childhood-onset rheumatoid arthritis conferred by HLA-DRB1 alleles encoding the shared epitope. Arthritis Rheum. 2012;64: 925–930.

84. Ombrello MJ, Arthur VL, Remmers EF, Hinks A, Tachmazidou I, Grom AA, et al. Genetic architecture distinguishes systemic juvenile idiopathic arthritis from other forms of juvenile idiopathic arthritis: clinical and therapeutic implications. Ann Rheum Dis. 2017;76: 906–913.

85. Wakil SM, Monies DM, Abouelhoda M, Al-Tassan N, Al-Dusery H, Naim EA, et al. Association of a mutation in LACC1 with a monogenic form of systemic juvenile idiopathic arthritis. Arthritis Rheumatol. 2015;67: 288–295.

86. Stock CJW, Ogilvie EM, Samuel JM, Fife M, Lewis CM, Woo P. Comprehensive association study of genetic variants in the IL-1 gene family in systemic juvenile idiopathic

arthritis. Genes Immun. 2008;9: 349–357.

87. Thomson W, Barrett JH, Donn R, Pepper L, Kennedy LJ, Ollier WER, et al. Juvenile idiopathic arthritis classified by the ILAR criteria: HLA associations in UK patients. Rheumatology. 2002;41: 1183–1189.

88. Hinks A, Martin P, Flynn E, Eyre S, Packham J, Childhood Arthritis Prospective Study-CAPS, et al. Subtype specific genetic associations for juvenile idiopathic arthritis: ERAP1 with the enthesitis related arthritis subtype and IL23R with juvenile psoriatic arthritis. Arthritis Res Ther. 2011;13: R12.

89. Day TG, Ramanan AV, Hinks A, Lamb R, Packham J, Wise C, et al. Autoinflammatory genes and susceptibility to psoriatic juvenile idiopathic arthritis. Arthritis Rheum. 2008;58: 2142–2146.

90. Mahendra A, Misra R, Aggarwal A. Th1 and Th17 Predominance in the Enthesitis-related Arthritis Form of Juvenile Idiopathic Arthritis. J Rheumatol. 2009;36: 1730–1736.

91. Patrick AE, Shoaff K, Esmond T, Patrick DM, Flaherty DK, Graham TB, et al. Increased Development of Th1, Th17, and Th1.17 Cells Under T1 Polarizing Conditions in Juvenile Idiopathic Arthritis. Front Immunol. 2022;13: 848168.

92. Amadi-Obi A, Yu C-R, Liu X, Mahdi RM, Clarke GL, Nussenblatt RB, et al. TH17 cells contribute to uveitis and scleritis and are expanded by IL-2 and inhibited by IL-27/STAT1. Nat Med. 2007;13: 711–718.

93. Zhu L, Chen B, Su W. A Review of the Various Roles and Participation Levels of B-Cells in Non-Infectious Uveitis. Front Immunol. 2021;12: 676046.

94. Miyara M, Yoshioka Y, Kitoh A, Shima T, Wing K, Niwa A, et al. Functional delineation and differentiation dynamics of human CD4+ T cells expressing the FoxP3 transcription factor. Immunity. 2009;30: 899–911.

95. de Kleer IM, Wedderburn LR, Taams LS, Patel A, Varsani H, Klein M, et al. CD4+CD25bright regulatory T cells actively regulate inflammation in the joints of patients with the remitting form of juvenile idiopathic arthritis. J Immunol. 2004;172: 6435–6443.

96. Olivito B, Simonini G, Ciullini S, Moriondo M, Betti L, Gambineri E, et al. Th17 transcription factor RORC2 is inversely correlated with FOXP3 expression in the joints of children with juvenile idiopathic arthritis. J Rheumatol. 2009;36: 2017–2024.

97. Bending D, Giannakopoulou E, Lom H, Wedderburn LR. Synovial Regulatory T Cells Occupy a Discrete TCR Niche in Human Arthritis and Require Local Signals To Stabilize FOXP3 Protein Expression. J Immunol. 2015;195: 5616–5624.

98. Hunter PJ, Nistala K, Jina N, Eddaoudi A, Thomson W, Hubank M, et al. Biologic predictors of extension of oligoarticular juvenile idiopathic arthritis as determined from synovial fluid cellular composition and gene expression. Arthritis Rheum. 2010;62: 896–907.

99. Petrelli A, Mijnheer G, Hoytema van Konijnenburg DP, van der Wal MM, Giovannone B, Mocholi E, et al. PD-1+CD8+ T cells are clonally expanding effectors in human chronic inflammation. J Clin Invest. 2018;128: 4669–4681.

100. Amsen D, van Gisbergen KPJM, Hombrink P, van Lier RAW. Tissue-resident memory T

cells at the center of immunity to solid tumors. Nat Immunol. 2018;19: 538–546.

101. Gregorio A, Gambini C, Gerloni V, Parafioriti A, Sormani MP, Gregorio S, et al. Lymphoid neogenesis in juvenile idiopathic arthritis correlates with ANA positivity and plasma cells infiltration. Rheumatology . 2007;46: 308–313.

102. Carlsson E, Beresford MW, Ramanan AV, Dick AD, Hedrich CM. Juvenile Idiopathic Arthritis Associated Uveitis. Children. 2021;8.

103. Parikh JG, Tawansy KA, Rao NA. Immunohistochemical study of chronic nongranulomatous anterior uveitis in juvenile idiopathic arthritis. Ophthalmology. 2008;115: 1833–1836.

104. Wildschütz L, Ackermann D, Witten A, Kasper M, Busch M, Glander S, et al. Transcriptomic and proteomic analysis of iris tissue and aqueous humor in juvenile idiopathic arthritis-associated uveitis. J Autoimmun. 2019;100: 75–83.

105. Petty RE, Laxer RM, Lindsley C, Wedderburn L, Fuhlbrigge RC, Mellins ED. Textbook of Pediatric Rheumatology E-Book. Elsevier Health Sciences; 2020.

106. Schmidt T, Berthold E, Arve-Butler S, Gullstrand B, Mossberg A, Kahn F, et al. Children with oligoarticular juvenile idiopathic arthritis have skewed synovial monocyte polarization pattern with functional impairment-a distinct inflammatory pattern for oligoarticular juvenile arthritis. Arthritis Res Ther. 2020;22: 186.

107. Arve-Butler S, Schmidt T, Mossberg A, Berthold E, Gullstrand B, Bengtsson AA, et al. Synovial fluid neutrophils in oligoarticular juvenile idiopathic arthritis have an altered phenotype and impaired effector functions. Arthritis Res Ther. 2021;23: 109.

108. De Simone M, Rossetti G, Pagani M. Single Cell T Cell Receptor Sequencing: Techniques and Future Challenges. Front Immunol. 2018;9: 1638.

109. Schatz DG, Ji Y. Recombination centres and the orchestration of V(D)J recombination. Nature Reviews Immunology. 2011. pp. 251–263.

110. Davis MM, Boniface JJ, Reich Z, Lyons D. Ligand recognition by (alpha)(beta) T cell receptors. Annual Review of Immunology; Palo Alto Tomo. 1998. pp. 523–544.

111. Arstila TP, Petteri Arstila T, Casrouge A, Baron V, Even J, Kanellopoulos J, et al. A Direct Estimate of the Human αβ T Cell Receptor Diversity. Science. 1999. pp. 958–961. doi:10.1126/science.286.5441.958

112. Pai JA, Satpathy AT. High-throughput and single-cell T cell receptor sequencing technologies. Nat Methods. 2021;18: 881–892.

113. Spreafico R, Rossetti M, van Loosdregt J, Wallace CA, Massa M, Magni-Manzoni S, et al. A circulating reservoir of pathogenic-like CD4+ T cells shares a genetic and phenotypic signature with the inflamed synovial micro-environment. Ann Rheum Dis. 2016;75: 459–465.

114. Rossetti M, Spreafico R, Consolaro A, Leong JY, Chua C, Massa M, et al. TCR repertoire sequencing identifies synovial Treg cell clonotypes in the bloodstream during active inflammation in human arthritis. Ann Rheum Dis. 2017;76: 435–441.

115. Julé AM, Hoyt KJ, Wei K, Gutierrez-Arcelus M, Taylor ML, Ng J, et al. Th1 polarization

defines the synovial fluid T cell compartment in oligoarticular juvenile idiopathic arthritis. JCI Insight. 2021;6.

116. Cho B-A, Sim JH, Park JA, Kim HW, Yoo W-H, Lee S-H, et al. Characterization of effector memory CD8+ T cells in the synovial fluid of rheumatoid arthritis. J Clin Immunol. 2012;32: 709–720.

117. Couzi L, Merville P, Deminière C, Moreau J-F, Combe C, Pellegrin J-L, et al. Predominance of CD8 T lymphocytes among periglomerular infiltrating cells and link to the prognosis of class III and class IV lupus nephritis. Arthritis & Rheumatism. 2007. pp. 2362–2370.

118. Maschmeyer P, Heinz GA, Skopnik CM. Antigen-driven PD-1+ TOX+ BHLHE40+ and PD-1+ TOX+ EOMES+ T lymphocytes regulate juvenile idiopathic arthritis in situ. European Journal of. 2021.

119. Giannopoulou EG, Elemento O, Ivashkiv LB. Use of RNA sequencing to evaluate rheumatic disease patients. Arthritis Res Ther. 2015;17: 167.

120. van Hal NL, Vorst O, van Houwelingen AM, Kok EJ, Peijnenburg A, Aharoni A, et al. The application of DNA microarrays in gene expression analysis. J Biotechnol. 2000;78: 271–280.

121. Peeters JGC, de Graeff N, Lotz M, Albani S, de Roock S, van Loosdregt J. Increased autophagy contributes to the inflammatory phenotype of juvenile idiopathic arthritis synovial fluid T cells. Rheumatology . 2017;56: 1694–1699.

122. Moncrieffe H, Bennett MF, Tsoras M, Luyrink LK, Johnson AL, Xu H, et al. Transcriptional profiles of JIA patient blood with subsequent poor response to methotrexate. Rheumatology . 2017;56: 1542–1551.

123. Mahmoud L, Al-Enezi F, Al-Saif M, Warsy A, Khabar KSA, Hitti EG. Sustained stabilization of Interleukin-8 mRNA in human macrophages. RNA Biol. 2014;11: 124–133.

124. Kalinina Ayuso V, van Dijk MR, de Boer JH. Infiltration of Plasma Cells in the Iris of Children With ANA-Positive Anterior Uveitis. Invest Ophthalmol Vis Sci. 2015;56: 6770–6778.

125. Wennink RAW, Pandit A, Haasnoot A-MJW, Hiddingh S, Kalinina Ayuso V, Wulffraat NM, et al. Whole Transcriptome Analysis Reveals Heterogeneity in B Cell Memory Populations in Patients With Juvenile Idiopathic Arthritis-Associated Uveitis. Front Immunol. 2020;11: 2170.

126. Shao Y, Kim SY, Shin D, Kim MS, Suh H-W, Piao Z-H, et al. TXNIP regulates germinal center generation by suppressing BCL-6 expression. Immunol Lett. 2010;129: 78–84.

127. Numata M, Yener MD, Ekmekçi SS, Aydın M, Grosveld G, Cardone M, et al. High MN1 expression increases the in vitro clonogenic activity of primary mouse B-cells. Leuk Res. 2015;39: 906–912.

128. Wong L, Jiang K, Chen Y, Hennon T, Holmes L, Wallace CA, et al. Limits of Peripheral Blood Mononuclear Cells for Gene Expression-Based Biomarkers in Juvenile Idiopathic Arthritis. Sci Rep. 2016;6: 29477.

129. Camafeita E, Lamas JR, Calvo E, López JA, Fernández-Gutiérrez B. Proteomics: New insights into rheumatic diseases. Proteomics Clin Appl. 2009;3: 226–241.

130. Rifai N, Gillette MA, Carr SA. Protein biomarker discovery and validation: the long and uncertain path to clinical utility. Nat Biotechnol. 2006;24: 971–983.

131. Lequin RM. Enzyme immunoassay (EIA)/enzyme-linked immunosorbent assay (ELISA). Clin Chem. 2005;51: 2415–2418.

132. Tighe PJ, Ryder RR, Todd I, Fairclough LC. ELISA in the multiplex era: potentials and pitfalls. Proteomics Clin Appl. 2015;9: 406–422.

133. Dayon L, Cominetti O, Affolter M. Proteomics of human biological fluids for biomarker discoveries: technical advances and recent applications. Expert Rev Proteomics. 2022;19: 131–151.

134. The promise of proteomics. In: Olink [Internet]. 28 Jul 2021 [cited 5 Sep 2022]. Available: https://www.olink.com/our-platform/promise-of-proteomics/

135. Foell, Däbritz. Biomarkers in Juvenile Idiopathic Arthritis: Translating Disease Mechanisms into Diagnostic Tools. Int J High Risk Behav Addict. 2011.

136. Gibson DS, Finnegan S, Jordan G, Scaife C, Brockbank S, Curry J, et al. Stratification and monitoring of juvenile idiopathic arthritis patients by synovial proteome analysis. J Proteome Res. 2009;8: 5601–5609.

137. de Jager W, Hoppenreijs EPAH, Wulffraat NM, Wedderburn LR, Kuis W, Prakken BJ. Blood and synovial fluid cytokine signatures in patients with juvenile idiopathic arthritis: a cross-sectional study. Ann Rheum Dis. 2007;66: 589–598.

138. Ganeva M, Fuehner S, Kessel C, Klotsche J, Niewerth M, Minden K, et al. Trajectories of disease courses in the inception cohort of newly diagnosed patients with JIA (ICON-JIA): the potential of serum biomarkers at baseline. Pediatr Rheumatol Online J. 2021;19: 64.

139. Cattalini M, Maduskuie V, Fawcett PT, Brescia AM, Rosé CD. Predicting duration of beneficial effect of joint injection among children with chronic arthritis by measuring biomarkers concentration in synovial fluid at the time of injection. Clin Exp Rheumatol. 2008;26: 1153–1160.

140. Moncrieffe H, Ursu S, Holzinger D, Patrick F, Kassoumeri L, Wade A, et al. A subgroup of juvenile idiopathic arthritis patients who respond well to methotrexate are identified by the serum biomarker MRP8/14 protein. Rheumatology. 2013;52: 1467–1476.

141. Gerss J, Tedy M, Klein A, Horneff G, Miranda-Garcia M, Kessel C, et al. Prevention of disease flares by risk-adapted stratification of therapy withdrawal in juvenile idiopathic arthritis: results from the PREVENT-JIA trial. Ann Rheum Dis. 2022;81: 990–997.

142. Walscheid K, Heiligenhaus A, Holzinger D, Roth J, Heinz C, Tappeiner C, et al. Elevated S100A8/A9 and S100A12 Serum Levels Reflect Intraocular Inflammation in Juvenile Idiopathic Arthritis-Associated Uveitis: Results From a Pilot Study. Invest Ophthalmol Vis Sci. 2015;56: 7653–7660.

143. Angeles-Han ST, Ringold S, Beukelman T, Lovell D, Cuello CA, Becker ML, et al. 2019 American College of Rheumatology/Arthritis Foundation Guideline for the Screening,

Monitoring, and Treatment of Juvenile Idiopathic Arthritis-Associated Uveitis. Arthritis Care Res. 2019;71: 703–716.

144. Yasumura J, Yashiro M, Okamoto N, Shabana K, Umebayashi H, Iwata N, et al. Clinical features and characteristics of uveitis associated with juvenile idiopathic arthritis in Japan: first report of the pediatric rheumatology association of Japan (PRAJ). Pediatr Rheumatol Online J. 2019;17: 15.

145. Tappeiner C, Klotsche J, Sengler C, Niewerth M, Liedmann I, Walscheid K, et al. Risk Factors and Biomarkers for the Occurrence of Uveitis in Juvenile Idiopathic Arthritis: Data From the Inception Cohort of Newly Diagnosed Patients With Juvenile Idiopathic Arthritis Study. Arthritis Rheumatol. 2018;70: 1685–1694.

146. Haasnoot AJW, van Tent-Hoeve M, Wulffraat NM, Schalij-Delfos NE, Los LI, Armbrust W, et al. Erythrocyte sedimentation rate as baseline predictor for the development of uveitis in children with juvenile idiopathic arthritis. Am J Ophthalmol. 2015;159: 372–7.e1.

147. de Groot-Mijnes JDF, Dekkers J, de Visser L, Rothova A, van Loon AM, de Boer JH. Antibody Production against B19 Virus in Ocular Fluid of JIA-Associated Uveitis Patients. Ophthalmology. 2015;122: 1270-1272.e1.

148. Kalinina Ayuso V, de Boer JH, Byers HL, Coulton GR, Dekkers J, de Visser L, et al. Intraocular biomarker identification in uveitis associated with juvenile idiopathic arthritis. Invest Ophthalmol Vis Sci. 2013;54: 3709–3720.

149. Bauer D, Kasper M, Walscheid K, Koch JM, Müther PS, Kirchhof B, et al. Multiplex Cytokine Analysis of Aqueous Humor in Juvenile Idiopathic Arthritis-Associated Anterior Uveitis With or Without Secondary Glaucoma. Front Immunol. 2018;9: 708.

150. Angeles-Han ST, Utz VM, Thornton S, Schulert G, Rodriguez-Smith J, Kauffman A, et al. S100 proteins, cytokines, and chemokines as tear biomarkers in children with juvenile idiopathic arthritis-associated uveitis. Ocul Immunol Inflamm. 2021;29: 1616–1620.

151. Rosina S, Natoli V, Santaniello S, Trincianti C, Consolaro A, Ravelli A. Novel biomarkers for prediction of outcome and therapeutic response in juvenile idiopathic arthritis. Expert Rev Clin Immunol. 2021;17: 853–870.

152. Bandura DR, Baranov VI, Ornatsky OI, Antonov A, Kinach R, Lou X, et al. Mass cytometry: technique for real time single cell multitarget immunoassay based on inductively coupled plasma time-of-flight mass spectrometry. Anal Chem. 2009;81: 6813–6822.

153. Hartmann FJ, Bendall SC. Immune monitoring using mass cytometry and related high-dimensional imaging approaches. Nat Rev Rheumatol. 2020;16: 87–99.

154. Iyer A, Hamers AAJ, Pillai AB. CyTOF® for the Masses. Front Immunol. 2022;13: 815828.

155. Finck R, Simonds EF, Jager A, Krishnaswamy S, Sachs K, Fantl W, et al. Normalization of mass cytometry data with bead standards. Cytometry A. 2013;83: 483–494.

156. Miao Q, Wang F, Dou J, Iqbal R, Muftuoglu M, Basar R, et al. Ab initio spillover compensation in mass cytometry data. Cytometry A. 2021;99: 899–909.

157. Weber LM, Robinson MD. Comparison of clustering methods for high-dimensional single-cell flow and mass cytometry data. Cytometry A. 2016;89: 1084–1096.

158. McInnes L. umap: Uniform Manifold Approximation and Projection. Github; Available: https://github.com/lmcinnes/umap

159. Jaitin DA, Kenigsberg E, Keren-Shaul H, Elefant N, Paul F, Zaretsky I, et al. Massively parallel single-cell RNA-seq for marker-free decomposition of tissues into cell types. Science. 2014;343: 776–779.

160. Trapnell C, Cacchiarelli D, Grimsby J, Pokharel P, Li S, Morse M, et al. The dynamics and regulators of cell fate decisions are revealed by pseudotemporal ordering of single cells. Nat Biotechnol. 2014;32: 381–386.

161. Kim JK, Marioni JC. Inferring the kinetics of stochastic gene expression from single-cell RNA-sequencing data. Genome Biol. 2013;14: R7.

162. Padovan-Merhar O, Raj A. Using variability in gene expression as a tool for studying gene regulation. Wiley Interdiscip Rev Syst Biol Med. 2013;5: 751–759.

163. Liu S, Trapnell C. Single-cell transcriptome sequencing: recent advances and remaining challenges. F1000Res. 2016;5.

164. Haque A, Engel J, Teichmann SA, Lönnberg T. A practical guide to single-cell RNA-sequencing for biomedical research and clinical applications. Genome Med. 2017;9: 75.

165. Jiang P, Thomson JA, Stewart R. Quality control of single-cell RNA-seq by SinQC. Bioinformatics. 2016;32: 2514–2516.

166. Lun ATL, McCarthy DJ, Marioni JC. A step-by-step workflow for low-level analysis of single-cell RNA-seq data with Bioconductor. F1000Res. 2016;5: 2122.

167. Satija R, Farrell JA, Gennert D, Schier AF, Regev A. Spatial reconstruction of single-cell gene expression data. Nat Biotechnol. 2015;33: 495–502.

168. Ji Z, Ji H. TSCAN: Pseudo-time reconstruction and evaluation in single-cell RNA-seq analysis. Nucleic Acids Res. 2016;44: e117–e117.

169. Clough E, Barrett T. The Gene Expression Omnibus Database. Methods Mol Biol. 2016;1418: 93–110.

170. Dabbish L, Stuart C, Tsay J, Herbsleb J. Social coding in GitHub: transparency and collaboration in an open software repository. Proceedings of the ACM 2012 conference on Computer Supported Cooperative Work. New York, NY, USA: Association for Computing Machinery; 2012. pp. 1277–1286.

171. Stephenson W, Donlin LT, Butler A, Rozo C, Bracken B, Rashidfarrokhi A, et al. Single-cell RNA-seq of rheumatoid arthritis synovial tissue using low-cost microfluidic instrumentation. Nat Commun. 2018;9: 1–10.

172. Mizoguchi F, Slowikowski K, Wei K, Marshall JL, Rao DA, Chang SK, et al. Functionally distinct disease-associated fibroblast subsets in rheumatoid arthritis. Nat Commun. 2018;9: 789.

173. Zhang F, Wei K, Slowikowski K, Fonseka CY, Rao DA, Kelly S, et al. Defining inflammatory cell states in rheumatoid arthritis joint synovial tissues by integrating single-cell transcriptomics and mass cytometry. Nat Immunol. 2019;20: 928–942.

174. Alivernini S, MacDonald L, Elmesmari A, Finlay S, Tolusso B, Gigante MR, et al. Distinct synovial tissue macrophage subsets regulate inflammation and remission in rheumatoid arthritis. Nat Med. 2020;26: 1295–1306.

175. Orange DE, Yao V, Sawicka K, Fak J, Frank MO, Parveen S, et al. RNA Identification of PRIME Cells Predicting Rheumatoid Arthritis Flares. N Engl J Med. 2020;383: 218–228.

176. Del Castillo Velasco-Herrera M, Young MD, Vieira Braga FA, Rosser EC, Miranda E, Marshall L, et al. A novel innate lymphoid cell delineates childhood autoimmune arthritis. bioRxiv. 2018. p. 416784.

177. Perrotti PP, Aterido A, Fernández-Nebro A, Cañete JD, Ferrándiz C, Tornero J, et al. Genetic variation associated with cardiovascular risk in autoimmune diseases. PLoS One. 2017;12: e0185889.

178. Julià A, López-Longo FJ, Pérez Venegas JJ, Bonàs-Guarch S, Olivé À, Andreu JL, et al. Genome-wide association study meta-analysis identifies five new loci for systemic lupus erythematosus. Arthritis Res Ther. 2018;20: 100.

179. Aterido A, Cañete JD, Tornero J, Ferrándiz C, Pinto JA, Gratacós J, et al. Genetic variation at the glycosaminoglycan metabolism pathway contributes to the risk of psoriatic arthritis but not psoriasis. Ann Rheum Dis. 2019;78.

180. Julià A, Pinto JA, Gratacós J, Queiró R, Ferrándiz C, Fonseca E, et al. A deletion at ADAMTS9-MAGI1 locus is associated with psoriatic arthritis risk. Ann Rheum Dis. 2015;74: 1875–1881.

181. Masachs, Estefanía. (2017). *Diferencias inmunológicas en la Artritis Idiopática Juvenil en relación a la actividad y la respuesta al tratamiento anti-TNF alpha entre población pediátrica y adulta joven*. Universitat Autònoma de Barcelona.

182. Bethencourt-Baute JJ, Montero N, Zacarias AM, Nieto JC, López-Corbeto M, Boteanu A, et al. Artritis idiopática juvenil en el adulto joven. Metodología, objetivos y datos iniciales del registro JUVENSER. Reumatología Clínica. 2023.

183. Bustaffa M, Koné-Paut I, Ozen S, Amaryan G, Papadopoulou-Alataki E, Gallizzi R, et al. The impact of the Eurofever criteria and the new InFevers MEFV classification in real life: Results from a large international FMF cohort. Semin Arthritis Rheum. 2022;52: 151957.

184. Aletaha D, Neogi T, Silman AJ, Funovits J, Felson DT, Bingham CO 3rd, et al. 2010 Rheumatoid arthritis classification criteria: an American College of Rheumatology/European League Against Rheumatism collaborative initiative. Arthritis Rheum. 2010;62: 2569–2581.

185. Assarsson E, Lundberg M, Holmquist G, Björkesten J, Thorsen SB, Ekman D, et al. Homogenous 96-plex PEA immunoassay exhibiting high sensitivity, specificity, and excellent scalability. PLoS One. 2014;9: e95192.

186. Sallusto F, Lenig D, Förster R, Lipp M, Lanzavecchia A. Two subsets of memory T lymphocytes with distinct homing potentials and effector functions. Nature. 1999;401: 708–712.

187. van Vreden C, Niewold P, McGuire HM, Fazekas de St Groth B. Titration of Mass Cytometry Reagents. Methods Mol Biol. 2019;1989: 83–92.

188. Leipold MD. Another step on the path to mass cytometry standardization. Cytometry. Part A: the journal of the International Society for Analytical Cytology. 2015. pp. 380–382.

189. Stoeckius M, Zheng S, Houck-Loomis B, Hao S, Yeung BZ, Mauck WM 3rd, et al. Cell Hashing with barcoded antibodies enables multiplexing and doublet detection for single cell genomics. Genome Biol. 2018;19: 224.

190. Luecken MD, Theis FJ. Current best practices in single-cell RNA-seq analysis: a tutorial. Mol Syst Biol. 2019;15: e8746.

191. Stuart T, Butler A, Hoffman P, Hafemeister C, Papalexi E, Mauck WM 3rd, et al. Comprehensive Integration of Single-Cell Data. Cell. 2019;177: 1888-1902.e21.

192. Domínguez Conde C, Xu C, Jarvis LB, Rainbow DB, Wells SB, Gomes T, et al. Cross-tissue immune cell analysis reveals tissue-specific features in humans. Science. 2022;376: eabl5197.

193. Chiffelle J, Genolet R, Perez MA, Coukos G, Zoete V, Harari A. T-cell repertoire analysis and metrics of diversity and clonality. Curr Opin Biotechnol. 2020;65: 284–295.

194. Yost KE, Satpathy AT, Wells DK, Qi Y, Wang C, Kageyama R, et al. Clonal replacement of tumor-specific T cells following PD-1 blockade. Nat Med. 2019;25: 1251–1259.

195. Sturm G, Szabo T, Fotakis G, Haider M, Rieder D, Trajanoski Z, et al. Scirpy: a Scanpy extension for analyzing single-cell T-cell receptor-sequencing data. Bioinformatics. 2020;36: 4817–4818.

196. Bagwell CB, Inokuma M, Hunsberger B, Herbert D, Bray C, Hill B, et al. Automated Data Cleanup for Mass Cytometry. Cytometry A. 2020;97: 184–198.

197. Korsunsky I, Millard N, Fan J, Slowikowski K, Zhang F, Wei K, et al. Fast, sensitive and accurate integration of single-cell data with Harmony. Nat Methods. 2019;16: 1289–1296.

198. Narayana SK, Helbig KJ, McCartney EM, Eyre NS, Bull RA, Eltahla A, et al. The Interferon-induced Transmembrane Proteins, IFITM1, IFITM2, and IFITM3 Inhibit Hepatitis C Virus Entry. J Biol Chem. 2015;290: 25946–25959.

199. D'Cunha J, Knight E Jr, Haas AL, Truitt RL, Borden EC. Immunoregulatory properties of ISG15, an interferon-induced cytokine. Proc Natl Acad Sci U S A. 1996;93: 211–215.

200. Padeh S, Pinhas-Hamiel O, Zimmermann-Sloutskis D, Berkun Y. Children with oligoarticular juvenile idiopathic arthritis are at considerable risk for growth retardation. J Pediatr. 2011;159: 832-837.e1–2.

201. Al-Matar MJ, Petty RE, Tucker LB, Malleson PN, Schroeder M-L, Cabral DA. The early pattern of joint involvement predicts disease progression in children with oligoarticular (pauciarticular) juvenile rheumatoid arthritis. Arthritis Rheum. 2002;46: 2708–2715.

202. Zannin ME, Buscain I, Vittadello F, Martini G, Alessio M, Orsoni JG, et al. Timing of uveitis onset in oligoarticular juvenile idiopathic arthritis (JIA) is the main predictor of severe course uveitis. Acta Ophthalmol. 2012;90: 91–95.

203. Foeldvari I, Wierk A. Methotrexate is an effective treatment for chronic uveitis associated with juvenile idiopathic arthritis. J Rheumatol. 2005;32: 362–365.

204. Ramanan AV, Dick AD, Jones AP, Hughes DA, McKay A, Rosala-Hallas A, et al. Adalimumab in combination with methotrexate for refractory uveitis associated with juvenile idiopathic arthritis: a RCT. Health Technol Assess. 2019;23: 1–140.

205. Castillo-Vilella M, Giménez N, Tandaipan JL, Quintana S, Modesto C. Clinical remission and subsequent relapse in patients with juvenile idiopathic arthritis: predictive factors according to therapeutic approach. Pediatr Rheumatol Online J. 2021;19: 130.

206. Prahalad S, Glass DN. Is juvenile rheumatoid arthritis/juvenile idiopathic arthritis different from rheumatoid arthritis? Arthritis Res. 2002;4: 303.

207. Martínez del Val E, Rodríguez Martínez A, Sánchez Becerra V, Cruz Rojo J, Enríquez Merayo E, Barral Mena E, et al. Characteristics of synovial fluid in patients with juvenile idiopathic arthritis. Anales de Pediatría (English Edition). 2019;91: 244–250.

208. Grievink HW, Luisman T, Kluft C, Moerland M, Malone KE. Comparison of Three Isolation Techniques for Human Peripheral Blood Mononuclear Cells: Cell Recovery and Viability, Population Composition, and Cell Functionality. Biopreserv Biobank. 2016;14: 410–415.

209. Lutter L, van der Wal MM, Brand EC, Maschmeyer P, Vastert S, Mashreghi M-F, et al. Human regulatory T cells locally differentiate and are functionally heterogeneous within the inflamed arthritic joint. Clin Transl Immunology. 2022;11: e1420.

210. Boere J, van de Lest CHA, Libregts SFWM, Arkesteijn GJA, Geerts WJC, Nolte-'t Hoen ENM, et al. Synovial fluid pretreatment with hyaluronidase facilitates isolation of CD44+ extracellular vesicles. J Extracell Vesicles. 2016;5: 31751.

211. van den Brink SC, Sage F, Vértesy Á, Spanjaard B, Peterson-Maduro J, Baron CS, et al. Single-cell sequencing reveals dissociation-induced gene expression in tissue subpopulations. Nat Methods. 2017;14: 935–936.

212. Guillaumet-Adkins A, Rodríguez-Esteban G, Mereu E, Mendez-Lago M, Jaitin DA, Villanueva A, et al. Single-cell transcriptome conservation in cryopreserved cells and tissues. Genome Biol. 2017;18: 45.

213. Imbach KJ, Treadway NJ, Prahalad V, Kosters A, Arafat D, Duan M, et al. Profiling the peripheral immune response to ex vivo TNF stimulation in untreated juvenile idiopathic arthritis using single cell RNA sequencing. Pediatr Rheumatoll Online. 2023; 21: 17.

214. Schiller HB, Montoro DT, Simon LM, Rawlins EL, Meyer KB, Strunz M, et al. The Human Lung Cell Atlas: A High-Resolution Reference Map of the Human Lung in Health and Disease. Am J Respir Cell Mol Biol. 2019;61: 31–41.

215. Feng R, Zhao J, Sun F, Miao M, Sun X, He J, et al. Comparison of the deep immune profiling of B cell subsets between healthy adults and Sjögren's syndrome. Ann Med. 2022;54: 472–483.

216. Corcione A, Ferlito F, Gattorno M, Gregorio A, Pistorio A, Gastaldi R, et al. Phenotypic and functional characterization of switch memory B cells from patients with oligoarticular juvenile idiopathic arthritis. Arthritis Res Ther. 2009;11: R150.

217. Ziegler-Heitbrock L, Ancuta P, Crowe S, Dalod M, Grau V, Hart DN, et al. Nomenclature of monocytes and dendritic cells in blood. Blood. 2010;116: e74-80.

218. Rogacev KS, Seiler S, Zawada AM, Reichart B, Herath E, Roth D, et al. CD14++CD16+

monocytes and cardiovascular outcome in patients with chronic kidney disease. Eur Heart J. 2011;32: 84–92.

219. Villani A-C, Satija R, Reynolds G, Sarkizova S, Shekhar K, Fletcher J, et al. Single-cell RNA-seq reveals new types of human blood dendritic cells, monocytes, and progenitors. Science. 2017;356.

220. Caillat-Zucman S. How NKG2D Ligands Trigger Autoimmunity? Hum Immunol. 2006;67: 204–207.

221. Koh J-Y, Kim D-U, Moon B-H, Shin E-C. Human CD8+ T-Cell Populations That Express Natural Killer Receptors. Immune Netw. 2023;23: e8.

222. Gumá M, Busch LK, Salazar-Fontana LI, Bellosillo B, Morte C, García P, et al. The CD94/NKG2C killer lectin-like receptor constitutes an alternative activation pathway for a subset of CD8+ T cells. Eur J Immunol. 2005;35: 2071–2080.

223. Yang C, Siebert JR, Burns R, Gerbec ZJ, Bonacci B, Rymaszewski A, et al. Heterogeneity of human bone marrow and blood natural killer cells defined by single-cell transcriptome. Nat Commun. 2019;10: 3931.

224. Barbarin A, Cayssials E, Jacomet F, Nunez NG, Basbous S, Lefèvre L, et al. Phenotype of NK-Like CD8(+) T Cells with Innate Features in Humans and Their Relevance in Cancer Diseases. Front Immunol. 2017;8: 316.

225. Ribot JC, Lopes N, Silva-Santos B. γδ T cells in tissue physiology and surveillance. Nat Rev Immunol. 2020;21: 221–232.

226. Godfrey DI, Koay H-F, McCluskey J, Gherardin NA. The biology and functional importance of MAIT cells. Nat Immunol. 2019;20: 1110–1128.

227. Vorkas CK, Krishna C, Li K, Aubé J, Fitzgerald DW, Mazutis L, et al. Single-Cell Transcriptional Profiling Reveals Signatures of Helper, Effector, and Regulatory MAIT Cells during Homeostasis and Activation. J Immunol. 2022;208: 1042–1056.

228. Hayashi E, Chiba A, Tada K, Haga K, Kitagaichi M, Nakajima S, et al. Involvement of Mucosal-associated Invariant T cells in Ankylosing Spondylitis. J Rheumatol. 2016;43: 1695–1703.

229. Nistala K, Moncrieffe H, Newton KR, Varsani H, Hunter P, Wedderburn LR. Interleukin-17-producing T cells are enriched in the joints of children with arthritis, but have a reciprocal relationship to regulatory T cell numbers. Arthritis Rheum. 2008;58: 875–887.

230. Bains I, Antia R, Callard R, Yates AJ. Quantifying the development of the peripheral naive CD4+ T-cell pool in humans. Blood. 2009;113: 5480–5487.

231. Kasper M, Walscheid K, Laffer B, Bauer D, Busch M, Loser K, et al. Phenotype of Innate Immune Cells in Uveitis Associated with Axial Spondyloarthritis- and Juvenile Idiopathic Arthritis-associated Uveitis. Ocul Immunol Inflamm. 2021;29: 1080–1089.

232. Nakamura J, Takeuchi M, Ota M, Mizuki N, Ohno S. Does the Interaction of KIR and HLA Affect the Development of Non-Infectious Uveitis? Curr Mol Med. 2022;22: 703–716.

233. Jiang Y, Arase N, Kohyama M, Hirayasu K, Suenaga T, Jin H, et al. Transport of misfolded endoplasmic reticulum proteins to the cell surface by MHC class II molecules.

Int Immunol. 2013;25: 235–246.

234. van der Houwen TB, van Hagen PM, van Laar JAM. Immunopathogenesis of Behçet's disease and treatment modalities. Semin Arthritis Rheum. 2022;52: 151956.

235. Cosan F, Aktas Cetin E, Akdeniz N, Emrence Z, Cefle A, Deniz G. Natural killer cell subsets and their functional activity in Behçet's disease. Immunol Invest. 2017;46: 419–432.

236. Hinrichs AC, Blokland SLM, Kruize AA, Lafeber FPJ, Leavis HL, van Roon JAG. CCL5 Release by CCR9+ CD8 T Cells: A Potential Contributor to Immunopathology of Primary Sjögren's Syndrome. Front Immunol. 2022;13: 887972.

237. Chang MH, Levescot A, Nelson-Maney N, Blaustein RB, Winden KD, Morris A, et al. Arthritis flares mediated by tissue-resident memory T cells in the joint. Cell Rep. 2021;37: 109902.

238. Pharoah DS, Varsani H, Tatham RW, Newton KR, de Jager W, Prakken BJ, et al. Expression of the inflammatory chemokines CCL5, CCL3 and CXCL10 in juvenile idiopathic arthritis, and demonstration of CCL5 production by an atypical subset of CD8+ T cells. Arthritis Res Ther. 2006;8: R50.

239. Penkava F, Del Castillo Velasco-Herrera M, Young MD, Yager N, Nwosu LN, Pratt AG, et al. Single-cell sequencing reveals clonal expansions of pro-inflammatory synovial CD8 T cells expressing tissue-homing receptors in psoriatic arthritis. Nature Communications. 2020; 21:11(1):4767.

240. Dunlap G, Wagner A, Meednu N, Zhang F, Jonsson AH, Wei K, et al. Clonal associations of lymphocyte subsets and functional states revealed by single cell antigen receptor profiling of T and B cells in rheumatoid arthritis synovium. bioRxiv. 2023.

241. Trapani JA. Granzymes: a family of lymphocyte granule serine proteases. Genome Biol. 2001;2(12).

242. Irmler M, Hertig S, MacDonald HR, Sadoul R, Becherer JD, Proudfoot A, et al. Granzyme A is an interleukin 1 beta-converting enzyme. J Exp Med. 1995;181: 1917–1922.

243. E J, Yan F, Kang Z, Zhu L, Xing J, Yu E. CD8+CXCR5+ T cells in tumor-draining lymph nodes are highly activated and predict better prognosis in colorectal cancer. Hum Immunol. 2018;79: 446–452.

244. Havenar-Daughton C, Lindqvist M, Heit A, Wu JE, Reiss SM, Kendric K, et al. CXCL13 is a plasma biomarker of germinal center activity. Proc Natl Acad Sci U S A. 2016;113: 2702–2707.

245. Mabrouk N, Tran T, Sam I, Pourmir I, Gruel N, Granier C, et al. CXCR6 expressing T cells: Functions and role in the control of tumors. Front Immunol. 2022;13: 1022136.

246. Martini G, Cabrelle A, Calabrese F, Carraro S, Scquizzato E, Teramo A, et al. CXCR6-CXCL16 interaction in the pathogenesis of Juvenile Idiopathic Arthritis. Clin Immunol. 2008;129: 268–276.

247. Wu Y-Y, Li X-F, Wu S, Niu X-N, Yin S-Q, Huang C, et al. Role of the S100 protein family in rheumatoid arthritis. Arthritis Res Ther. 2022;24: 35.

248. Nys G, Cobraiville G, Servais A-C, Malaise MG, de Seny D, Fillet M. Targeted proteomics reveals serum amyloid A variants and alarmins S100A8-S100A9 as key plasma biomarkers of rheumatoid arthritis. Talanta. 2019;204: 507–517.

249. Mariani A, Marsili M, Nozzi M, Faricelli R, Chiarelli F, Breda L. Serum calprotectin: review of its usefulness and validity in paediatric rheumatic diseases. Clin Exp Rheumatol. 2015;33: 109–114.

250. Huang Q, Ding J, Gong M, Wei M, Zhao Q, Yang J. Effect of miR-30e regulating NK cell activities on immune tolerance of maternal-fetal interface by targeting PRF1. Biomed Pharmacother. 2019;109: 1478–1487.

251. Fauriat C, Long EO, Ljunggren H-G, Bryceson YT. Regulation of human NK-cell cytokine and chemokine production by target cell recognition. Blood. 2010;115: 2167–2176.

252. Maghazachi AA. Role of chemokines in the biology of natural killer cells. Curr Top Microbiol Immunol. 2010;341: 37–58.

253. Bern MD, Parikh BA, Yang L, Beckman DL, Poursine-Laurent J, Yokoyama WM. Inducible down-regulation of MHC class I results in natural killer cell tolerance. J Exp Med. 2019;216: 99–116.

254. Qi Q, Liu Y, Cheng Y, Glanville J, Zhang D, Lee J-Y, et al. Diversity and clonal selection in the human T-cell repertoire. Proc Natl Acad Sci U S A. 2014;111: 13139–13144.

255. Vanni A, Mazzoni A, Semeraro R, Capone M, Maschmeyer P, Lamacchia G, et al. Clonally expanded PD-1-expressing T cells are enriched in synovial fluid of juvenile idiopathic arthritis patients. Eur J Immunol. 2023; e2250162.

256. de Cienfuegos AA, Cantero-Nieto L, García-Gómez JA, Robledo G, Trigo M, Ibanez JM, et al. THU0121 Circulating fibroblast growth factor-23 is associated with dyslipidemia in rheumatoid arthritis patients. Ann Rheum Dis. 2019;78: 332–333.

257. Wu C-Y, Yang H-Y, Luo S-F, Huang J-L, Lai J-H. Vitamin D Supplementation in Patients with Juvenile Idiopathic Arthritis. Nutrients. 2022;14.

258. Qu H, Sundberg E, Aulin C, Neog M, Palmblad K, Horne AC, et al. Immunoprofiling of active and inactive systemic juvenile idiopathic arthritis reveals distinct biomarkers: a single-center study. Pediatr Rheumatol Online J. 2021;19: 173.

259. Quartier P, Allantaz F, Cimaz R, Pillet P, Messiaen C, Bardin C, et al. A multicentre, randomised, double-blind, placebo-controlled trial with the interleukin-1 receptor antagonist anakinra in patients with systemic-onset juvenile idiopathic arthritis (ANAJIS trial). Ann Rheum Dis. 2011;70: 747–754.

260. J Malemud C. Dysfunctional immune-mediated inflammation in rheumatoid arthritis dictates that development of anti-rheumatic disease drugs target multiple intracellular signaling pathways. Antiinflamm Antiallergy Agents Med Chem. 2011;10: 78–84.

261. Okroj M, Heinegård D, Holmdahl R, Blom AM. Rheumatoid arthritis and the complement system. Ann Med. 2007;39: 517–530.

262. Brunner J, Prelog M, Riedl M, Giner T, Hofer J, Würzner R, et al. Analysis of the classical, alternative, and mannose binding lectin pathway of the complement system in the pathogenesis of oligoarticular juvenile idiopathic arthritis. Rheumatol Int. 2012;32: 1815–

1818.

263. Akioka S. Interleukin-6 in juvenile idiopathic arthritis. Mod Rheumatol. 2019;29: 275–286.

264. Schmidt T, Dahlberg A, Berthold E, Król P, Arve-Butler S, Rydén E, et al. Synovial monocytes drive the pathogenesis in oligoarticular juvenile idiopathic arthritis via IL-6/JAK/STAT signalling and cell-cell interactions. bioRxiv. 2023.

265. van den Ham H-J, de Jager W, Bijlsma JWJ, Prakken BJ, de Boer RJ. Differential cytokine profiles in juvenile idiopathic arthritis subtypes revealed by cluster analysis. Rheumatology . 2009;48: 899–905.

266. Choida V, Hall-Craggs M, Jebson BR, Fisher C, Leandro M, Wedderburn LR, et al. Biomarkers of Response to Biologic Therapy in Juvenile Idiopathic Arthritis. Front Pharmacol. 2020;11: 635823.

267. Bourgonje AR, Wichers SJ, Hu S, van Dullemen HM, Visschedijk MC, Faber KN, et al. Proteomic analyses do not reveal subclinical inflammation in fatigued patients with clinically quiescent inflammatory bowel disease. Sci Rep. 2022;12: 14581.

268. Sivak JM, Fini ME. MMPs in the eye: emerging roles for matrix metalloproteinases in ocular physiology. Prog Retin Eye Res. 2002;21: 1–14.

269. Di Girolamo N, Verma MJ, McCluskey PJ, Lloyd A, Wakefield D. Increased matrix metalloproteinases in the aqueous humor of patients and experimental animals with uveitis. Curr Eye Res. 1996;15: 1060–1068.

270. Chong WP, Mattapallil MJ, Raychaudhuri K, Bing SJ, Wu S, Zhong Y, et al. The Cytokine IL-17A Limits Th17 Pathogenicity via a Negative Feedback Loop Driven by Autocrine Induction of IL-24. Immunity. 2020;53: 384-397.e5.

271. Chong WP, Mattapallil M, Raychaudhuri K, Silver PB, Jittayasothorn Y, Chan C-C, et al. A novel self-regulatory mechanism of Th17 cells controls autoimmune uveitis through interleukin-24. J Immunol. 2020;204: 142.5-142.5.

272. Lanier LL. Of snowflakes and natural killer cell subsets. Nature biotechnology. 2014. pp. 140–142.

273. Stoeckius M, Hafemeister C, Stephenson W, Houck-Loomis B, Chattopadhyay PK, Swerdlow H, et al. Simultaneous epitope and transcriptome measurement in single cells. Nat Methods. 2017;14: 865–868.

274. Arunkumar M, Zielinski CE. T-Cell Receptor Repertoire Analysis with Computational Tools-An Immunologist's Perspective. Cells. 2021; Dec 18;10(12):3582.

275. Zheng B, Yang Y, Chen L, Wu M, Zhou S. B-cell receptor repertoire sequencing: Deeper digging into the mechanisms and clinical aspects of immune-mediated diseases. iScience. 2022;25: 105002.

276. Zhan X, Li J, Guo Y, Golubnitschaja O. Mass spectrometry analysis of human tear fluid biomarkers specific for ocular and systemic diseases in the context of 3P medicine. EPMA J. 2021;12: 449–475.

10. Annexes

10.1. Funding

The project has been supported by AES from Instituto Carlos III, grant number PI19/00225, PI Prof. Sara Marsal, and Moving4 in juvenile idiopathic arthritis 2022 research grant from the Spanish Society of Pediatric Rheumatology.

10.2. Supplementary Tables

Supplementary Table 1. Complete list of all 276 investigated plasma biomarkers.

Immuno-oncology panel		**Inflammation panel**		**Cardiometabolic panel**	
Gene Abbreviation	Gene name	Gene Abbreviation	Gene name	Gene Abbreviation	Gene name
ADA	Adenosine deaminase	ADA	Adenosine Deaminase	ANG	Angiogenin
MCP-3	C-C motif chemokine 7	CXCL9	C-X-C motif chemokine 9	F7	Coagulation factor VII
CX3CL1	Fractalkine	IL-2RB	Interleukin-2 receptor subunit beta	GAS6	Growth arrest-specific protein 6
IL2	Interleukin-2	IL-22 RA1	Interleukin-22 receptor subunit alpha-1	FCGR2A	Low affinity immunoglobulin gamma Fc region receptor II-a
CD244	Natural killer cell receptor 2B4	PD-L1	Programmed cell death 1 ligand 1	NRP1	Neuropilin-1
PGF	Placenta growth factor	TNFRSF9	Tumor necrosis factor receptor superfamily member 9	SAA4	Serum amyloid A-4 protein
ADGRG1	Adhesion G-protein coupled receptor G1	ARTN	Artemin	ANGPTL3	Angiopoietin-related protein 3
MCP-2	C-C motif chemokine 8	CXCL10	C-X-C motif chemokine 10	F11	Coagulation factor XI
Gal-1	Galectin-1	IL-4	Interleukin-4	MET	Hepatocyte growth factor receptor
IL33	Interleukin-33	IL-24	Interleukin-24	FCGR3B	Low affinity immunoglobulin gamma Fc region receptor III-B
KLRD1	Natural killer cells antigen CD94	EN-RAGE	Protein S100-A12	DEFA1	Neutrophil defensin 1
PDGF subunit B	Platelet-derived growth factor subunit B	uPA	Urokinase-type plasminogen activator	SPARCL1	SPARC-like protein 1
ANGPT1	Angiopoietin-1	AXIN1	Axin-1	APOM	Apolipoprotein M

CD27	CD27 antigen	CXCL11	C-X-C motif chemokine 11	COL18A1	Collagen alpha-1(XVIII) chain
Gal-9	Galectin-9	IL5	Interleukin-5	IGLC2	Ig lambda-2 chain C regions
IL4	Interleukin-4	IL-33	Interleukin-33	SELL	L-selectin
NOS3	Nitric oxide synthase, endothelial	SLAMF1	Signaling lymphocytic activation molecule	LCN2	Neutrophil gelatinase-associated lipocalin
PTN	Pleiotrophin	VEGF-A	Vascular endothelial growth factor A	SOD1	Superoxide dismutase [Cu-Zn]
TIE2	Angiopoietin-1 receptor	Beta-NGF	Beta-nerve growth factor	CNDP1	Beta-Ala-His dipeptidase
CD40-L	CD40 ligand	CST5	Cystatin D	C1QTNF1	Complement C1q tumor necrosis factor-related protein 1
GZMA	Granzyme A	IL6	Interleukin-6	IGFBP3	Insulin-like growth factor-binding protein 3
IL5	Interleukin-5	LAP TGF-beta-1	Latency-associated peptide transforming growth factor beta-1	LYVE1	Lymphatic vessel endothelial hyaluronic acid receptor 1
Pro-EGF	Pro-epidermal growth factor	SIRT2	SIR2-like protein 2	NID1	Nidogen-1
ANGPT2	Angiopoietin-2	CASP-8	Caspase-8	TIMD4	T-cell immunoglobulin and mucin domain-containing protein 4
CD40	CD40L receptor	DNER	Delta and Notch-like epidermal growth factor-related receptor	ST6GAL1	Beta-galactoside alpha-2,6-sialyltransferase 1
GZMB	Granzyme B	IL-7	Interleukin-7	C2	Complement C2
IL6	Interleukin-6	LIF	Leukemia inhibitory factor	IGFBP6	Insulin-like growth factor-binding protein 6
PD-L1	Programmed cell death 1 ligand 1	STAMBP	STAM-binding protein	PRCP	Lysosomal Pro-X carboxypeptidase
ARG1	Arginase-1	CCL3	C-C motif chemokine 3	OSMR	Oncostatin-M-specific receptor subunit beta
CD70	CD70 antigen	CCL11	Eotaxin	TNC	Tenascin
GZMH	Granzyme H	IL-8	Interleukin-8	CDH1	Cadherin-1
IL7	Interleukin-7	LIF-R	Leukemia inhibitory factor receptor	CFHR5	Complement factor H-related protein 5
PDCD1	Programmed cell death protein 1	SCF	Stem cell factor	ITGAM	Integrin alpha-M

CASP-8	Caspase-8	CCL4	C-C motif chemokine 4	MBL2	Mannose-binding protein C
CXCL1	C-X-C motif chemokine 1	4E-BP1	Eukaryotic translation initiation factor 4E-binding protein 1	PAM	Peptidyl-glycine alpha-amidating monooxygenase
HGF	Hepatocyte growth factor	IL10	Interleukin-10	TNXB	Tenascin-X
KIR3DL1	Killer cell immunoglobulin-like receptor 3DL1	CSF-1	Macrophage colony-stimulating factor 1	CA1	Carbonic anhydrase 1
PD-L1	Programmed cell death 1 ligand 1	ST1A1	Sulfotransferase 1A1	CR2	Complement receptor type 2
CXCL12	Stromal cell-derived factor 1	CCL19	C-C motif chemokine 19	ICAM1	Intercellular adhesion molecule 1
MCP-4	C-C motif chemokine 13	FGF-21	Fibroblast growth factor 21	KIT	Mast/stem cell growth factor receptor Kit
CXCL10	C-X-C motif chemokine 10	IL-10RA	Interleukin-10 receptor subunit alpha	PLTP	Phospholipid transfer protein
ICOSLG	ICOS ligand	MMP-1	Matrix metalloproteinase -1	THBS4	Thrombospondin-4
LAP TGF- beta-1	Latency-associated peptide transforming growth factor beta-1	CD6	T cell surface glycoprotein CD6 isoform	CA3	Carbonic anhydrase 3
PD-L2	Programmed cell death 1 ligand 2	CCL20	C-C motif chemokine 20	CST3	Cystatin-C
CD4	T-cell surface glycoprotein CD4	FGF-23	Fibroblast growth factor 23	ICAM3	Intercellular adhesion molecule 3
CCL17	C-C motif chemokine 17	IL-10RB	Interleukin-10 receptor subunit beta	CD46	Membrane cofactor protein
CXCL11	C-X-C motif chemokine 11	MMP-10	Matrix metalloproteinase -10	SERPINA5	Plasma serine protease inhibitor
IFN-gamma	Interferon gamma	CD5	T-cell surface glycoprotein CD5	SERPINA7	Thyroxine-binding globulin
LAG3	Lymphocyte activation gene 3 protein	CCL23	C-C motif chemokine 23	CA4	Carbonic anhydrase 4
PDCD1	Programmed cell death protein 1	FGF-5	Fibroblast growth factor 5	DPP4	Dipeptidyl peptidase 4
CD5	T-cell surface glycoprotein CD5	IL-12B	Interleukin-12 subunit beta	IL7R	Interleukin-7 receptor subunit alpha
CCL19	C-C motif chemokine 19	MCP-1	Monocyte chemotactic protein 1	AOC3	Membrane primary amine oxidase

CXCL13	C-X-C motif chemokine 13	CD8A	T-cell surface glycoprotein CD8 alpha chain	GP1BA	Platelet glycoprotein Ib alpha chain
IL-1 alpha	Interleukin-1 alpha	CCL25	C-C motif chemokine 25	TCN2	Transcobalamin-2
LAMP3	Lysosome-associated membrane glycoprotein 3	FGF-19	Fibroblast growth factor 19	CRTAC1	Cartilage acidic protein 1
CXCL12	Stromal cell-derived factor 1	IL-13	Interleukin-13	EFEMP1	EGF-containing fibulin-like extracellular matrix protein 1
CD8A	T-cell surface glycoprotein CD8 alpha chain	MCP-2	Monocyte chemotactic protein 2	LTBP2	Latent-transforming growth factor beta-binding protein 2
MCP-1	C-C motif chemokine 2	TSLP	Thymic stromal lymphopoietin	TIMP1	Metalloproteinase inhibitor 1
CXCL5	C-X-C motif chemokine 5	CCL28	C-C motif chemokine 28	PLA2G7	Platelet-activating factor acetylhydrolase
IL10	Interleukin-10	Flt3L	Fms-related tyrosine kinase 3 ligand	TGFBR3	Transforming growth factor beta receptor type 3
CSF-1	Macrophage colony-stimulating factor 1	IL-15RA	Interleukin-15 receptor subunit alpha	COMP	Cartilage oligomeric matrix protein
CD4	T-cell surface glycoprotein CD4	MCP-3	Monocyte chemotactic protein 3	ENG	Endoglin
CD28	T-cell-specific surface glycoprotein CD28	TNFB	TNF-beta	LILRB1	Leukocyte immunoglobulin-like receptor subfamily B member 1
CCL20	C-C motif chemokine 20	CD40	CD40L receptor	MFAP5	Microfibrillar-associated protein 5
CXCL9	C-X-C motif chemokine 9	CX3CL1	Fractalkine	PLXNB2	Plexin-B2
IL12	Interleukin-12	IL-17A	Interleukin-17A	TGFBI	Transforming growth factor-beta-induced protein ig-h3
MMP12	Macrophage metalloproteinase -12	MCP-4	Monocyte chemotactic protein 4	CCL5	C-C motif chemokine 5
CD5	T-cell surface glycoprotein CD5	TRANCE	TNF-related activation-induced cytokine	FETUB	Fetuin-B
TRAIL	TNF-related apoptosis-inducing ligand	CDCP1	CUB domain-containing protein 1	LILRB2	Leukocyte immunoglobulin-like receptor subfamily B member 2

CCL23	C-C motif chemokine 23	GDNF	Glial cell line-derived neurotrophic factor	MEGF9	Multiple epidermal growth factor-like domains protein 9
CRTAM	Cytotoxic and regulatory T-cell molecule	IL-17C	Interleukin-17C	PCOLCE	Procollagen C-endopeptidase enhancer 1
IL12RB1	Interleukin-12 receptor subunit beta-1	CD244	Natural killer cell receptor 2B4	PRSS2	Trypsin-2
MMP7	Matrix metalloproteinase -7	TRAIL	TNF-related apoptosis-inducing ligand	CCL14	C-C motif chemokine 14
CD8A	T-cell surface glycoprotein CD8 alpha chain	CDCP1	CUB domain-containing protein 1	FCN2	Ficolin-2
TNF	Tumor necrosis factor	HGF	Hepatocyte growth factor	LILRB5	Leukocyte immunoglobulin-like receptor subfamily B member 5
CCL3	C-C motif chemokine 3	IL-18	Interleukin-18	NCAM1	Neural cell adhesion molecule 1
DCN	Decorin	NT-3	Neurotrophin-3	FAP	Prolyl endopeptidase FAP
IL13	Interleukin-13	TGF-alpha	Transforming growth factor alpha	TIE1	Tyrosine-protein kinase receptor Tie-1
MIC-A/B Q2998	MHC class I polypeptide-related sequence A/B	CXCL1	C-X-C motif chemokine 1	CCL18	C-C motif chemokine 18
CD244	Natural killer cell receptor 2B4	IFN-gamma	Interferon gamma	QPCT	Glutaminyl-peptide cyclotransferase
TWEAK	Tumor necrosis factor ligand superfamily member 12	IL-18R1	Interleukin-18 receptor 1	REG1A	Lithostathine-1-alpha
CCL4	C-C motif chemokine 4	NRTN	Neurturin	CHL1	Neural cell adhesion molecule L1-like protein
FGF2	Fibroblast growth factor 2	TWEAK	Tumor necrosis factor (Ligand) superfamily, member 12	PTPRS	Receptor-type tyrosine-protein phosphatase S
IL15	Interleukin-15	CXCL5	C-X-C motif chemokine 5	UMOD	Uromodulin
MUC-16	Mucin-16	IL-1 alpha	Interleukin-1 alpha	CD59	CD59 glycoprotein
KLRD1	Natural killer cells antigen CD94	IL-20	Interleukin-20	GNLY	Granulysin
TNFSF14	Tumor necrosis factor ligand superfamily member 14	OSM	Oncostatin-M	CES1	Liver carboxylesterase 1

TNFRSF21	Tumor necrosis factor receptor superfamily member 21	TNF	Tumor necrosis factor	NOTCH1	Neurogenic locus notch homolog protein 1
TNFRSF4	Tumor necrosis factor receptor superfamily member 4	CXCL6	C-X-C motif chemokine 6	REG3A	Regenerating islet-derived protein 3-alpha
IL18	Interleukin-18	IL-2	Interleukin-2		
NCR1	Natural cytotoxicity triggering receptor	IL-20RA	Interleukin-20 receptor subunit alpha		
NOS3	Nitric oxide synthase, endothelial	OPG	Osteoprotegerin		
FASLG	Tumor necrosis factor ligand superfamily member 6	TNFSF14	Tumor necrosis factor ligand superfamily member 14 (TNFSF14)		
TNFRSF12A	Tumor necrosis factor receptor superfamily member 12A				
TNFRSF9	Tumor necrosis factor receptor superfamily member 9				
VEGFA	Vascular endothelial growth factor A				
VEGFR-2	Vascular endothelial growth factor receptor 2				

Supplementary Table 2. Additional material for CyTOF experiments

Product	Supplier	SOP Product Code	Buy from	Product Code
Pierce™ 16% Formaldehyde (w/v), Methanol-free	Thermo Fisher	28906	Thermo Fisher	28906
Human TruStain FcX (Fc Receptor Blocking Solution)	BioLegend	422302	Palex Medical	
Polypropylene round-bottom tubes, 5 mL capacity, 12 x 75 mm	Falcon	352063	Fisher Scientific	10314791

Polypropylene round-bottom tubes with 35 µm cell-strainer cap, 5 mL capacity, 12 x 75 mm	Falcon	352235	Fisher Scientific	10585801
1 mL Norm-Ject® latex-free syringes and compatible 0.1 µm syringe filters	VWR	53548-001	VWR	613-2001
0.1 µm syringe filters	VWR		VWR	514-4125
Tris(2-carboxyethyl)phosphine hydrochloride (TCEP) solution, pH 7.0, 0.5M	MilliporeSigma	646547	Merck	646547-10X1ML
HRP-Protector™ peroxidase stabilizer	Candor	222 050	Inycom	222 050
Amicon® Ultra-0.5 Centrifugal Filter Unit, 0.5 mL, V-bottom	MilliporeSigma	UFC500308 (3 kDa) UFC505008 (50 kDa) UFC510008 (100 kDa)	Merck	UFC500308 UFC505008 UFC510008
Eppendorf® Protein LoBind Tubes, 1.5 mL	Eppendorf	22431081	Eppendorf	30108116
Monesin	BioLegend	420701	Palex Medical	
Brefeldin A	BioLegend	420601	Palex Medical	
Benzonase Nuclease, Purity > 90%	Millipore	70746-3	Merck	70746-3
Anti-human CD8a mAb, clone RPA-T8	BioLegend (Palex Medical)	301053	Palex Medical	
Anti-human CD19 mAb, clone HIB19	BioLegend (Palex Medical)	302247	Palex Medical	
Anti-human FcεRI mAb, clone AER-37 (CRA-1)	BioLegend (Palex Medical)	334602	Palex Medical	
Anti-human FcεRI mAb, clone AER-37 (CRA-1)	eBioscience	14-5899-82	ThermoFisher	14-5899-82
Anti-human CCL5/RANTES mAb, clone VL1	BioLegend (Palex Medical)	515502	Palex Medical	
Anti-human CCL5/RANTES mAb, clone 2D5	BD Biosciences	550420	BD Biosciences	550420
Anti-human Granzyme A mAb, clone CB9	BioLegend (Palex Medical)	507202	Palex Medical	

Anti-human Granzyme A mAb, clone CB9	BD Biosciences	557449	BD Biosciences	557449
Anti-human CX3CR1 mAb, 2A9-1	BioLegend (Palex Medical)	341602	Palex Medical	
Cell-ID Cisplatin	Fluidigm	201064	Izasa Scientific	
Vacuum aspirator	VWR		VWR	181-0270

Supplementary Table 3. Frequencies and proportions of B cell populations.

Cell type	SF	oJIA	oJIA-UV	HC
Naive B cells	3 (0.03%)	1117 (2.98%)	524 (1.68%)	1418 (2.63%)
Switched memory B cells	29 (0.29%)	707 (1.89%)	543 (1.74%)	1091 (2.02%)
CD69+ naive B cells	8 (0.08%)	1227 (3.27%)	622 (1.99%)	1498 (2.77%)
Non-switched B cells	143 (1.41%)	344 (0.92%)	300 (0.96%)	541 (1.00%)
ABCs-like B cells	11 (0.11%)	329 (0.88%)	218 (0.70%)	600 (1.11%)
Plasma B cells	20 (0.20%)	284 (0.76%)	66 (0.21%)	109 (0.20%)
Plasmablasts	8 (0.08%)	36 (0.10%)	8 (0.03%)	18 (0.03%)

Supplementary Table 4. Frequencies and proportions of myeloid cell populations.

Cell type	SF	oJIA	oJIA-UV	HC
Classical monocytes	10 (1.08%)	752 (2.01%)	3075 (9.86%)	1174 (2.17%)
DC4	6 (0.06%)	328 (0.88%)	1374 (4.32%)	626 (1.16%)
DC2	491 (4.84%)	136 (0.36%)	421 (1.35%)	353 (0.65%)
DC1	509 (5.01%)	3 (0.01%)	80 (0.26%)	51 (0.09%)
pDCs	145 (1.43%)	78 (0.21%)	263 (0.84%)	211 (0.39%)
Intermediate monocytes	225 (2.25%)	4 (0.01%)	449 (1.44%)	129 (0.24%)
Non-classical monocytes	21 (0.21%)	1 (0%)	93 (0.30%)	18 (0.03%)
aDC	116 (1.14%)	1 (0%)	17 (0.05%)	6 (0.01%)

Supplementary Table 5. Frequencies and proportions of CD8 T cell populations.

Cell type	SF	oJIA	oJIA-UV	HC
Effector memory CD8	806 (7.94%)	2768 (7.39%)	2191 (7.03%)	2734 (5.06%)
Activated effector memory CD8	1424 (14.03%)	163 (0.43%)	465 (1.49%)	640 (1.18%)
NKG2C effector memory CD8	604 (5.95%)	317 (0.85%)	316 (1.01%)	897 (1.66%)
Central memory CD8	556 (5.48%)	115 (0.31%)	93 (0.30%)	218 (0.40%)

Supplementary Table 6. Frequencies and proportions of NK cell populations.

Cell type	SF	oJIA	oJIA-UV	HC
Immature CD56 Dim NK	126 (1.22%)	1029 (2.75%)	2610 (8.37%)	1544 (2.86%)
Mature CD56 Dim NK	69 (0.68%)	690 (1.84%)	2087 (6.69%)	1239 (2.29%)
Terminal CD56 Dim NK	68 (0.67%)	1056 (2.82%)	1451 (4.65%)	1345 (2.49%)
CD56 Bright NK	612 (6.03%)	454 (1.21%)	986 (3.16%)	891 (1.65%)
NK-like CD8 T cells	317 (3.12%)	954 (2.55%)	488 (1.56%)	681 (1.26%)

Supplementary Table 7. Frequencies and proportions of naive T cells, CD4 T cells, and other less abundant cellular populations.

Cell type	SF	oJIA	oJIA-UV	HC
Naive CD4 T cells	320 (3.15%)	12720 (33.94%)	3876 (12.43%)	19506 (36.11%)
Naive CD8 T cells	116 (1.11%)	4089 (10.91%)	2050 (6.57%)	6072 (11.24%)
MAIT cells	118 (1.16%)	624 (1.67%)	1110 (3.56%)	846 (1.57%)
Gamma-delta T cells	162 (1.60%)	643 (1.72%)	1713 (5.49%)	1100 (2.04%)
Double-negative T cells	66 (0.65%)	174 (0.46%)	66 (0.21%)	133 (0.25%)
Regulatory T cells	508 (5%)	373 (1%)	277 (0.89%)	746 (1.38%)
Effector memory CD4 T cells	897 (8.84%)	2335 (6.28%)	1232 (3.95%)	3283 (6.08%)
Central memory CD4 T cells	640 (6.31%)	2143 (5.72%)	858 (2.75%)	2608 (4.83%)

Supplementary Table 8. Frequencies and proportions of proliferative cells.

Cell type	SF	oJIA	oJIA-UV	HC
Proliferative NK	50 (0.49%)	33 (0.06%)	138 (0.44%)	71 (0.13%)
Proliferative T cells	237 (2.33%)	88 (0.23%)	120 (0.38%)	104 (0.19%)
Proliferative myeloid cells	21 (0.21%)	14 (0.04%)	12 (0.04%)	47 (0.09%)

10.3. Supplementary Graphs

Supplementary Figure 1. Universal mass cytometry panel titration and validation workflow.

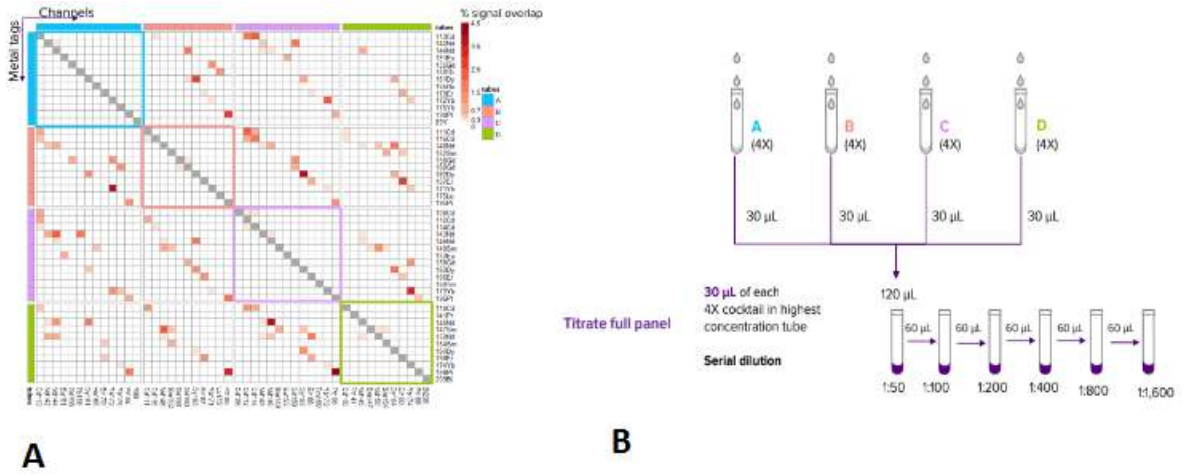

A) Matrix that helps to distribute the metals in groups based of their signal overlap. **B)** Titration strategy: it is recommended to titrate 4 metals in each tube for a maximum of 4 tubes to assess signal overlap and 6 additional tubes for titrating the full panel in serial dilutions.

Supplementary Figure 2. Typical gating strategy using Gaussian parameters for Mass Cytometry.

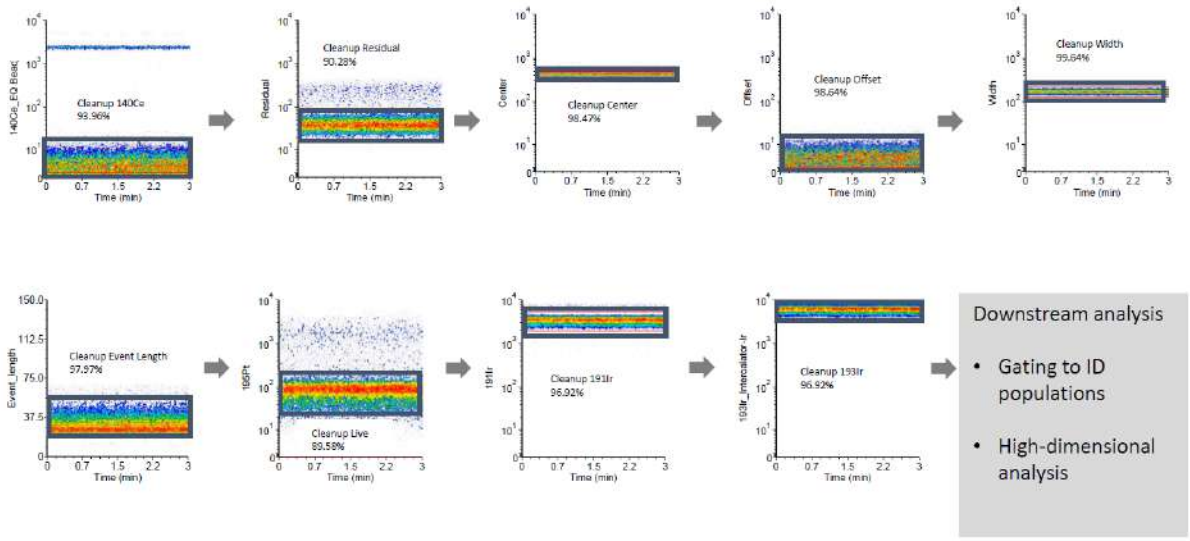

Supplementary Figure 3. Scree plot of PCA proteomic analysis.

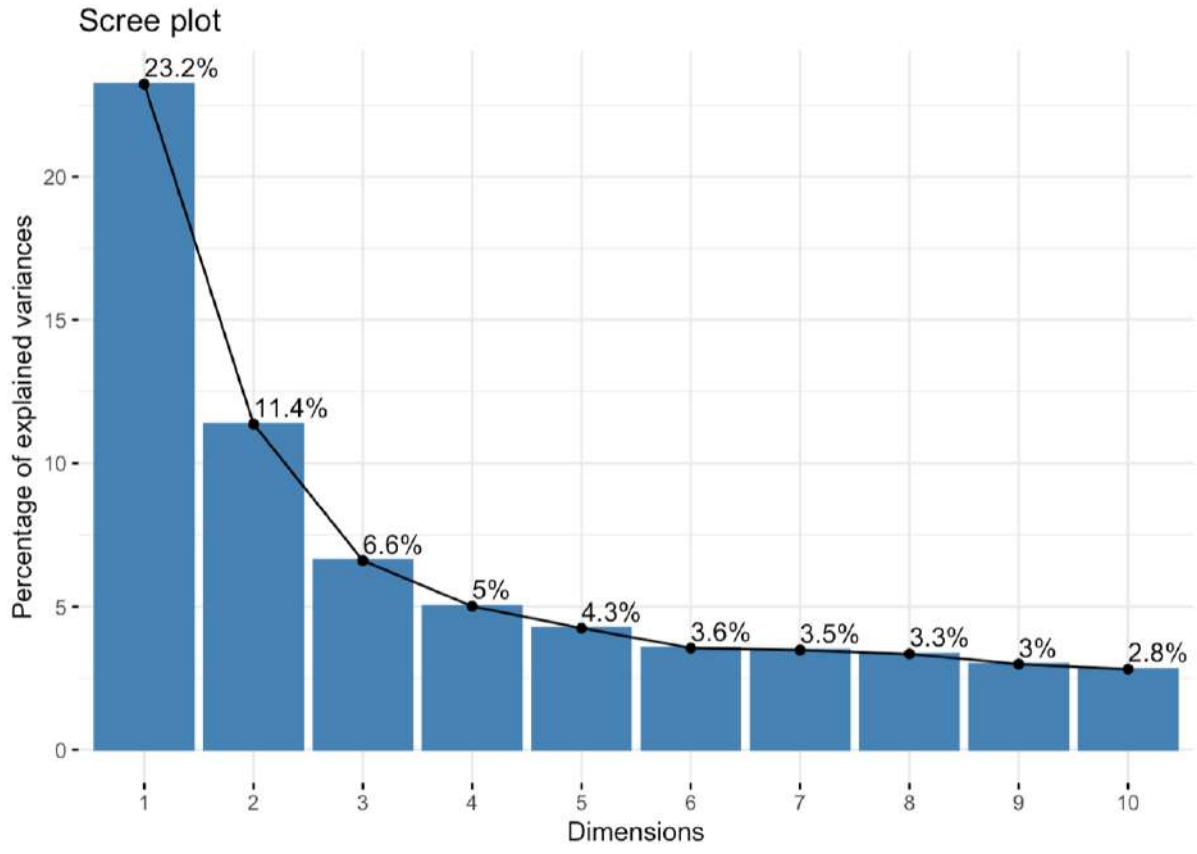

X-axis represent the number of principal components for the PCA and the y-axis is the percentage of explained variances. PC1 harbors almost 25% of the total sample variance.